Title
THE INTERACTI0N BETWEEN A LAMINAR FLAME AND ITS SELF-GENERATED FLOW

Author
Dunn-Rankin, D.

Publication Date
1985-04-01

Lawrence Berkeley Laboratory
UNIVERSITY OF CALIFORNIA

APPLIED SCIENCE DIVISION

THE INTERACTION BETWEEN A LAMINAR FLAME AND ITS SELF-GENERATED FLOW

D. Dunn-Rankin
(Ph.D. Thesis)

April 1985

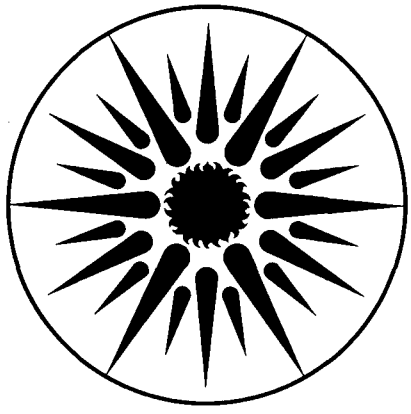

APPLIED SCIENCE DIVISION

Prepared for the U.S. Department of Energy under Contract DE-AC03-76SF00098

DISCLAIMER

THE INTERACTION BETWEEN A LAMINAR FLAME AND ITS SELF-GENERATED FLOW

Derek Dunn-Rankin

Ph.D. Thesis

April 1985

University of California, Department of Mechanical Engineering
Lawrence Berkeley Laboratory, Applied Science Division
Berkeley, California 94720

Research Advisor: R.F. Sawyer

This work was supported by the Assistant Secretary for Conservation and Renewable Energy, Office of Transportation Programs, Division of Transportation Energy of the U.S. Department of Energy under contract DE-AC03-76SF00098.

The Interaction Between a Laminar Flame and Its Self-Generated Flow

Derek Dunn-Rankin

Abstract

The interaction between a premixed laminar flame and its self-generated flow is experimentally studied in a closed duct. The simple geometry of the duct allows fundamental understanding of the mechanisms involved in the flame/flow interaction. This understanding is applicable to more complex combustion situations.

A laser Doppler anemometer measures two components of the enclosed gas velocity during the flame propagation. The measurements provide a complete vector velocity map of the flame generated flow. High-speed schlieren cinematography is used to observe changes in flame shape and location. Pressure records correlate with the qualitative schlieren movies and help quantify the progress of the combustion process. The experimental results are interpreted using a one-dimensional flame model and a two-dimensional description of flow deflection through an oblique flame sheet.

The one-dimensional model accurately predicts the unburned gas motion. The flow in the burned gas is rotational because of vorticity generated from flow deflection through the curved flame front. The density difference between the burned and unburned gas requires a velocity jump at the flame front to maintain

continuity of mass flux. The measured velocity jump corresponds to this predicted value.

A large flame cusp, called a "tulip" flame appears during the flame propagation. Flame instability, pressure wave/flame interaction, and large scale circulation in the unburned gas are suggested explanations for the "tulip" flame. Velocity measurements of this work show that no large scale circulation exists in the unburned gas. Instead, the measurements suggest another likely mechanism for the "tulip" formation. The onset of the "tulip" process coincides with the quench of part of the flame at the sidewalls of the combustion vessel. The velocity decrease in the unburned gas and the curved flame shape at the time of quench combine to generate a vortex in the burned gas. The vortex remains in the proximity of the flame and modifies the flame shape and unburned gas field such that the flame cusp or "tulip" is formed.

.....

Thesis Committee Chairperson

ACKNOWLEDGEMENTS

There are many people who contributed to the successful completion of this thesis:

My fellow graduate combustion researchers, Diana Brehob, John Cavolowski, Chris Edwards, Janet Elzey, Richard Joklik, and Terry Parker, provided useful exchanges of ideas on both experimental techniques and interpretation of the results.

Professor John Daily and Professor William Webster, as members of my thesis committee, contributed useful suggestions to clarify the presentation of the work.

Dr. Donald Lucas and visiting scholar Dr. Wolfram Steinert helped shape the approach of this work with discussions of research technique and philosophy.

Dick Jensen and Horton Stewert gave expert and cheerful assistance in mechanical design and fabrication of the experimental apparatus.

Gary Hubbard, whose Graphical Display and Analysis software prepared the figures contained in this work, also assisted in the development of data acquisition software used in the research.

Professor Antoni K. Oppenheim helped motivate the work with his energetic interest and ideas.

Ken Hom contributed selfless assistance in the electronic and photographic facets of the research. His unquenchable good spirit and expertise eliminated many difficulties.

Dr. Robert K. Cheng suggested the laser Doppler anemometry technique as the primary research tool in the study. His patient and masterful introduction to this technique, as well as his discussions of the experimental results helped the research considerably.

Professor Robert F. Sawyer, as research advisor, provided the necessary encouragement for the completion of this work. His suggestions, both for the research and its presentation, were extremely helpful. His flexibility allowed the pursuit of the thesis work, and his generous approach to graduate researchers produced a fruitful research atmosphere.

The research was supported by the Assistant Secretary for Conservation and Renewable Energy, Office of Transportation Programs, Division of Transportation Energy of the U.S. Department of Energy under contract number DE-AC03-76SF00098. The program manager is Marvin Gunn.

TABLE OF CONTENTS

NOMENCLATURE

α - thermal diffusivity of unburned gas

a_c - cross-sectional area of combustion vessel

a_f - area of the flame

A_f - non-dimensional flame area = a_f/a_c

c - speed of sound

d - width of flame preheat zone

γ - ratio of specific heats of unburned gas

L - combustion vessel length

m - mass

M - Mach number

ν - kinematic viscosity of unburned gas

p - pressure inside combustion vessel

p_f - final pressure after combustion

P - ratio of pressure to initial pressure

ρ - gas density

σ - expansion ratio (density unburned/density burned)

S - speed of gas relative to the flame front

θ_d - angle between unburned and burned gas velocity vector

θ_i - angle between flame and unburned gas velocity vector

t - time

t_m - representative convective mixing time

t_t - representative thermal diffusion time

t_v - representative viscous diffusion time

T_c - total combustion time

T_{cr} - time of velocity zero crossing at a fixed location

T_{vmax} - time of maximum velocity

U - representative velocity in system

V - gas velocity in laboratory reference frame

V_{max} - maximum velocity at a fixed location

X - axial coordinate

X^* - non-dimensional axial coordinate (X/L)

Y - radial coordinate

Subscripts:

b - burned gas

o - initial conditions

u - unburned gas

INTRODUCTION

I.1 Motivation and discussion

Considerable research has been conducted on the subject of the influence of fluid flow on a flame front, but very little is known about the reverse relationship - the influence of the flame on the flow field. This flame influence is often an important contributor to the combustion process. Interest in the reverse relationship grew out of research on flame propagation in an internal combustion (IC) engine simulator (Steinert et al., 1982, Dunn-Rankin and Sawyer, 1983). Flame phenomenon, apparently related to combustion induced flow, appeared during the course of these studies. It seems likely, therefore, that combustion induced flow plays a role in IC engine combustion. In the present work, the interaction between a laminar flame and its self-generated flow in a closed duct is experimentally investigated using laser Doppler anemometry and high-speed schlieren cinematography. The understanding of the interaction in the simple duct geometry is applicable in the complex IC engine combustion environment.

It is well known that flame propagation through premixed gases is influenced significantly by the surrounding flow field. In fact, premixed flame fronts are commonly visualized as reaction interfaces which are shaped by the surrounding flow, without considering the effect of the flame on the fluid motion. Shadowgraph photographs of flames in swirling internal

combustion (IC) engine flows (Witze and Vilchis, 1981) suggest this passive flame behavior, as the bulk swirl appears to simply sweep the flame around the cylinder. However, Witze et al. (1983) investigated the influence of the combustion process on a slightly turbulent IC engine flow using laser Doppler anemometry, and found substantial differences between the flow field with combustion and the motored flow field. Unfortunately, the complexity of the flow field, cycle-to-cycle variations and low data rates in the burned gas made complete interpretation of the flow difficult. Their results do suggest, however, that the passive flame interpretation of flame movement, although useful in many descriptive discussions, neglects the significant active participation of the flame front in the generation of the surrounding flow field. The interaction of the flame with its self-generated flow creates a combustion feedback mechanism that is not well understood. This feedback, if it is significant, requires a reassessment of the correlation of motored IC engine flow studies (for example, Morse et al., 1979 and Liou and Santavicca, 1982) to actual firing situations. Experimental investigation of the feedback mechanism in internal combustion engines is difficult because of the complex combustion environment. Consequently, the present investigation uses a simple constant volume combustion vessel to allow experimental determination of the mechanisms associated with the interaction between a laminar flame and its self-generated flow. The understanding of this interaction in the simple constant volume

geometry is applicable to flame propagation in internal combustion engines.

The combustion vessel is a closed rectangular duct (30 mm < L < 200 mm) with square cross-section (38 mm x 38 mm). A spark initiates combustion at one end of the closed tube or duct. Despite the apparent simplicity of this combustion vessel, a very interesting flame behavior appears. The flame begins propagating with a shape convex toward the unburned gas. Then the flame inverts, a sharp cusp appears at its center, and the flame forms a vee-shape which is concave toward the unburned gas. An example of the vee-shaped flame is shown in Figure I-1. The photograph is a composite of several frames extracted from a high-speed schlieren movie of a stoichiometric methane/air flame propagating in a closed duct. Below the photograph is the digitized flame shape history from the same high-speed movie. The cusp shaped flame has also been named "tulip" flame, and it is described in detail in Chapter 2. The "tulip" flame has been noted by researchers for nearly sixty years and several explanations for the sudden shape change have been proposed. However, quantitative measurements in support of these explanations are rare. It is likely that the "tulip" formation is a result of the feedback mechanism between the flame and its self-generated flow.

The present study experimentally investigates both the interaction between a premixed laminar flame and its self-generated flow and the feedback hypothesis for the "tulip" formation. The laser Doppler anemometer measures the combustion

(a)

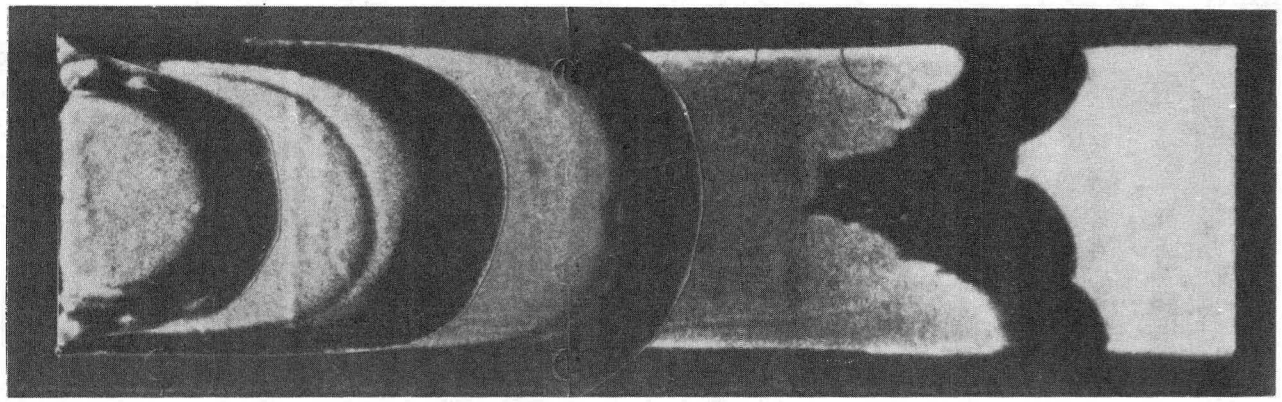

(b)

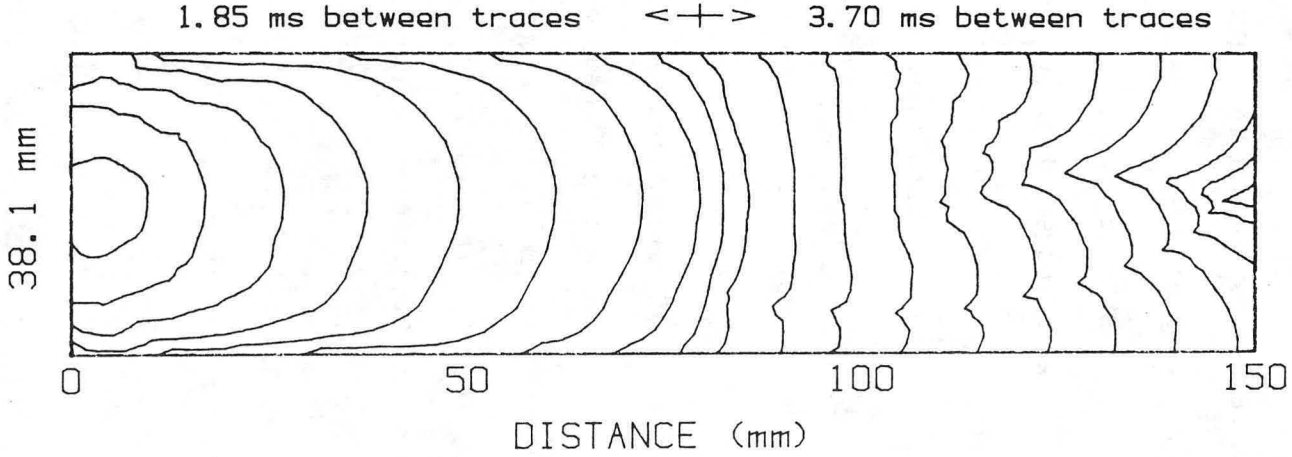

Figure I-1. An example of the "tulip" flame formation during closed tube combustion. Stoichiometric methane/air mixture initiated by a line igniter.
a) Composite of frames from a schlieren movie
b) Digitized flame history from the same movie

generated flow and the high-speed schlieren cinematographic system records the flame shape and position. A one-dimensional flame model and a two-dimensional description of flow deflection through an oblique flame sheet help interpret the experimental results.

I.2 Thesis outline

Chapter 1 presents background information on flame generated flow and combustion in tubes. This chapter contains a survey of experiments concerned with the interaction between a flame and its self-generated flow. A short history of the various flame propagation problems which have been studied in open and closed tubes is also presented. The subjects include: determination of laminar flame speed, vibratory flame propagation, transition to detonation, and flame shape stability.

Chapter 2 contains a description of the "tulip" flame followed by a survey of previous studies that presented this flame shape. The proposed mechanisms leading to the "tulip" formation are also presented.

Chapter 3 presents the flame sheet model adopted in this thesis to assist in interpretation of the results. Justification of the model assumptions, and some nomenclature definitions appear here as well.

Chapter 4 is an experimental, but primarily qualitative, study of the "tulip" flame. High-speed schlieren movies coupled with pressure records of the closed vessel combustion help determine the influence of chamber length, fuel type, equivalence

ratio, and ignition source on the qualitative features of the "tulip" shape.

Chapter 5 is an analytical discussion relating the rate of chamber pressure rise to the instantaneous flame area. The experimental results of Chapter 4 are compared to the findings of the analysis.

Chapter 6 is an experimental investigation of the flow field generated during non-steady flame propagation through premixed gases in a closed duct. Laser Doppler anemometry is used to make the velocity measurements. The measurements explore the possibility of large scale recirculation flows in the combustion vessel, and describe flow characteristics which correspond to changes in flame shape during the transition to the "tulip" flame.

Chapter 7 is an expanded investigation of the flow field described in Chapter 6. The measurements provide a complete vector velocity map of the flow field in a closed duct during nonsteady flame propagation. The chapter also includes a discussion of the vector velocity characteristics of the flow field and their relationship to the "tulip" flame.

Chapter 8 consists of an analytical discussion of simple correlations between the flame and the flow which became apparent during experimental observations. The chapter presents a one-dimensional model for the unburned gas motion and compares the predictions based on this model to the velocity measurements.

Chapter 9 is also an analytical discussion. The subject of this chapter is the deflection of flow by a flame sheet. Again the predictions of the analysis are compared to the experimental results.

Chapter 10 proposes a new fluid mechanical explanation for the formation of "tulip" flames. Both the experimental results and the analytical discussions suggest that the new explanation is more likely than those previously proposed.

Chapter 11 is a recapitulation of the significant conclusions. It provides a unified view of the flame/flow interactions during combustion in closed tubes.

The appendix contains data acquisition software written for the research. The software is written in the Pascal programming language.

CHAPTER 1

Review of Previous Studies

1.1 Flame generated flow

The fluid motion generated by a flame is a consequence of mass flux conservation across the flame front. The mass flow of unburned gas into the flame must be balanced by the mass flow of burned gas out of the flame,

$$\rho_u S_u = \rho_b S_b, \qquad (1.1)$$

where ρ is the density, and S is the velocity of the gas relative to the flame front. The subscripts u and b represent the unburned and burned gas respectively. Because the combustion process is exothermic, the burned gas has higher temperature and lower density than the unburned gas. Consequently, the burned gas velocity relative to the flame front is larger than the velocity of unburned gas relative to the flame front, Figure 1-1. The increase in velocity, which quantifies the flame generated flow, results from expansion of the gas as it passes from the unburned side to the burned side of the flame.

The geometric constraints of the combustion vessel dictate the influence that the expanding burned gas has on the entire flow field, and the subsequent interaction of this flow field with the flame. For example, when a flame propagates in a tube closed at the ignition end and open at the opposite end, the closed end and tube walls confine the expanding burned gas. This expanding gas drives toward the open end of the tube pushing the

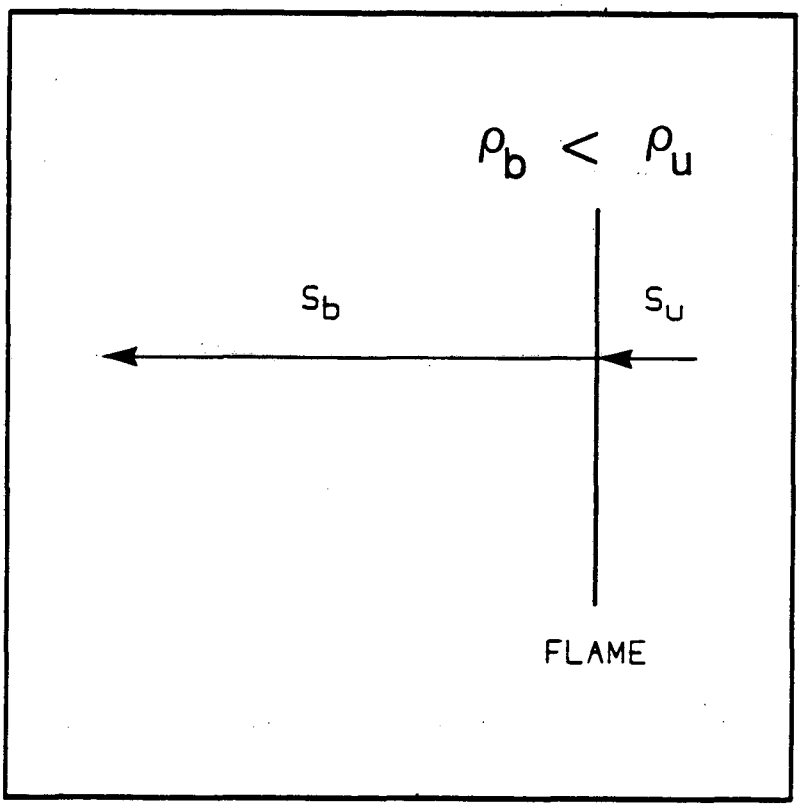

Figure 1-1. Mass continuity through a premixed flame sheet requires an increase in burned gas velocity.

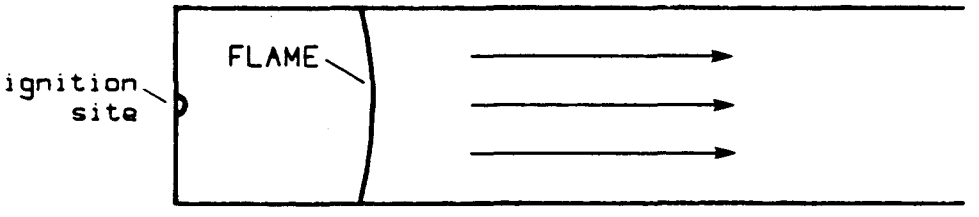

Figure 1-2. Expanding burned gas pushes the flame and the unburned gas ahead of it.

unburned gas and flame ahead of it, Figure 1-2. The flow of unburned gas is parallel, and gradually forms a parabolic velocity profile (Cho and Jeung, 1983) just as in classical developing tube flow, except that the source of the motion is the expanding burned gas behind the flame. The unburned gas flow which develops for very fast burning mixtures is turbulent. The flame interaction with the turbulent flow can lead to the detonation phenomenon which is discussed briefly in the next section.

There are two dramatic examples of the interaction of a flame with the fluid flow produced by expanding burned gas. The first example occurs when the combustion tube, described in the previous paragraph, contains obstacles, Figure 1-3a. The obstacles disrupt the parallel unburned gas flow by serving as vortex generators. When the flame is entrained into these vortices, its area increases rapidly and it accelerates at remarkable velocity down the tube (Lee et al., 1983). The second example occurs during premixed combustion in a divided chamber vessel. An orifice separates a small prechamber from a main chamber which also contains combustible gas, Figure 1-3b. Combustion begins in the prechamber, and the expanding burned gas forces unburned fluid through the orifice. The exiting fluid forms a ring vortex in the main chamber. Once the flame arrives, the ring vortex quickly rolls the flame up, greatly increasing the combustion rate. The interaction between the flame and its prechamber generated flow has been studied extensively by Shimizu

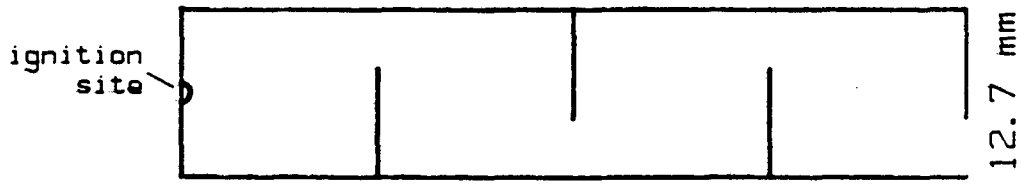

a) Lee et al. (1983) 60 mm

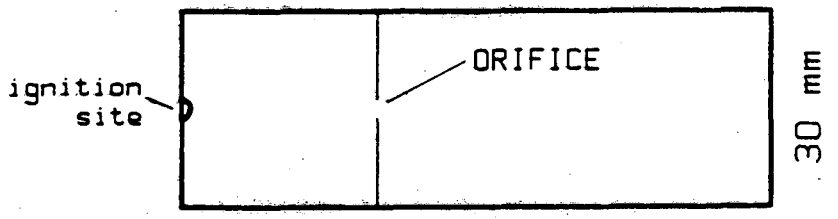

b) Shimizu et al. (1983) 90 mm

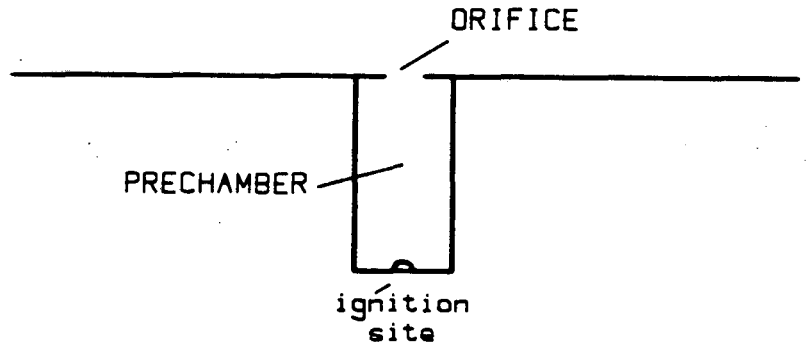

c) Cattolica and Vosen (1984)

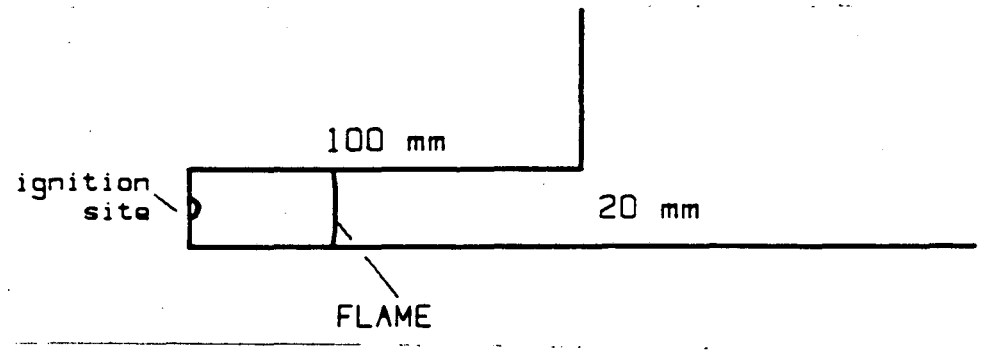

d) Yip et al. (1984)

Figure 1-3. Enclosures used by various researchers to investigate interactions between a flame and flame generated flow.

et al. (1983). A similar investigation using two-dimensional mapping of OH concentration in a prechamber combustion configuration was presented by Cattolica and Vosen (1984). The main chamber was unconfined and did not contain combustible gas in this study, Figure 1-3c. The interaction between a flame and a combustion generated vortex in another divided chamber configuration, Figure 1-3d, was studied experimentally by Yip et al. (1984) and numerically by Barr (1984). The flame was initiated in a narrow tube closed at the ignition end, and the vortex appeared as the expanding burned gas pushed unburned gas out of the tube into a large plenum. Combustion generated flow clearly plays an active role in determining the flame behavior in the above cases, but it is primarily vessel constraints (either obstacles or orifices) which are responsible for the vortex generation and dramatic flame influence.

The present study concentrates on the interaction between the flame and the flame induced fluid motion, where the only external modification of the fluid motion comes from the constraints of the vessel walls. In particular, the flame/flow interaction is studied during spark initiated combustion of premixed gas in closed tubes without obstacles and without orifices. The tubes or ducts have square cross-section and are relatively short (30 mm < L < 200 mm). The contained gas is motionless before ignition so that the combustion process is entirely responsible for any fluid motion. The tube geometry has been used for fundamental studies of premixed flame propagation

for many years. The results of these studies comprise an information base that provides a useful perspective on the present study. The next section discusses some combustion topics which have been investigated in tubes.

1.2 Flame propagation in tubes

Tubes and ducts have been used from the advent of combustion research (Mallard and LeChatlier, 1883) as an experimentally tractable environment for studying fundamental properties of premixed flames. The early researchers studied a flame property, introduced by Mallard and LeChatlier (1883), known as "la vitesse normale" or "the normal velocity." Streak photographs, taken on a revolving drum camera, indicated that a flame propagates at a nearly constant velocity in a tube which is open at the ignition end and closed at the opposite end. Mallard and LeChatlier suggested that the constant (or "normal") velocity represented the propagation speed of a flame normal to itself by heat conduction alone. However, when their experiments were repeated with tubes of different diameter (Haward and Sastry, 1917), "the normal velocity" measured was much different. The dependence of "the normal velocity" (also known as "the speed of uniform movement") on the tube diameter was explored more thoroughly by Mason and Wheeler (1919), but it was Coward and Hartwell (1932), employing improved photographic techniques, who determined that the dependence on tube diameter arose from variations in flame shapes with different tubes. The dependence on flame shape meant

that the "speed of uniform movement" was not a fundamental property of the combustible gas, and consequently the "speed of uniform movement" was replaced by Coward and Payman (1937), when they changed the earlier translation of "la vitesse normale" to "the fundamental flame speed." The fundamental flame speed is defined by these authors as,

$$S_u = (S_f - V_u)(a_c/a_f), \qquad (1.2)$$

where S_f is the observed flame speed, V_u is the velocity of the unburned gas, a_c is the cross-sectional area of the tube, and a_f is the flame area. This definition is equivalent to the modern definition of laminar flame speed (see for example Glassman, 1977) averaged over the flame surface.

Based on Equation (1.2), determination of the fundamental flame speed in tubes requires measurement of both the flame area and the speed of the unburned gas ahead of the flame. The measurement of the flame area is complicated because the flame shape is three-dimensional and nonsteady. Fortunately, it was theoretically and experimentally shown (Guenoche et al., 1948) that an orifice placed at the open end of the combustion tube improves flame shape steadiness. The steady flames made an estimation of flame area possible, and the fundamental flame speeds of many mixtures were determined using combustion in tubes (see for example Gerstein et al., 1951, and the survey paper by Linnet, 1952). However, the three-dimensionality of the flame made precise flame area determination from two-dimensional

photographic images of the flame very difficult. In fact, Guenoche and Juoy (1954) showed that the flame area could not be accurately reconstructed even if three orthogonal projections of the flame were available. The imprecision in flame area measurements and the consequent imprecision in flame speed calculations (recently reviewed by Andrews and Bradley, 1972 and Rallis and Garforth, 1980) eventually eliminated the use of tubes for flame speed determination. Interestingly, it was precisely the flame shape fluctuation difficulties in using tubes for flame speed determination which became the focus for new areas of tube combustion research.

One of these areas was the vibratory propagation of flames in tubes. Evidence of this phenomenon first appeared in the streak photograph records of Mallard and LeChatlier (1883). Flames propagating in relatively long tubes show a small oscillation superimposed on their normal burning speed. After a considerable research effort, the vibratory motion has now been conclusively shown to arise from the influence of combustion generated longitudinal acoustic fluctuations on the flame (for the early work see the review paper by Guenoche, 1964, and more recently, Leyer and Manson, 1971, Starke and Roth, 1984).

The transition to detonation is another phenomenon which appeared during the early flame speed studies of tube combustion. For some combustible mixtures in long tubes, the vibratory motion described above is followed by a transition to detonation. The flow ahead of fast burning flames in long tubes generates a

turbulent boundary layer. When the flame enters the turbulent zone the rate of combustion and the flame velocity increase, generating pressure waves (Chu, 1952). The pressure waves eventually merge into a shock wave. The unburned gas between the shock front and the flame is heated by the shock passage until, after a delay period, it spontaneously ignites, or detonates. Extensive photographic studies (Oppenheim et al., 1962, Laderman et al., 1963, Urtiew and Oppenheim, 1966,1968) clearly illustrate the transition to detonation process.

The tube geometry has also been used extensively in both experimental and theoretical studies of flame shape stability. Landau (1944) and Darrieus (1938) predicted by a linear analysis that a planar flame is inherently unstable to disturbances of all wavelengths. Consequently they surmised that stable laminar premixed flames should not exist, as they would become spontaneously turbulent. Experimental evidence, however, showed the existence of stable laminar flames propagating in tubes. Markstein (1951) eliminated the discrepancy by modifying the analysis of Darrieus and Landau to include the stabilizing effect of flame curvature for small wavelength disturbances. Markstein (1957) studied the instability of a flame front after interaction with a shock wave. The shock wave creates a funnel in the center of the initially smooth laminar flame front. After the shock passes, the funnel breaks up, and the flame quickly becomes turbulent. The instability of an interface between fluids of different density to accelerations toward the lighter fluid, or

the Taylor (1950) instability, is the accepted explanation for this phenomenon. Tube combustion was also used for investigations of cellular flame instability, vibration induced cell structure, and the stability of flames propagating near their lean limit (see the review papers by Markstein, 1953, 1964). The instabilities noted in these early experiments have been the subject of more recent analytical (Sivashinsky, 1977) and numerical (Michelson and Sivashinsky, 1977) treatments. Sivashinsky (1983) has reviewed the modern asymptotic approach to cellular flame instability. However, the recent work in cellular structure does not employ the tube geometry.

Combustion in open tubes has also been used to study the hydrodynamics of flame propagation, and the influence of the hydrodynamics on the flame shape. It has been widely accepted that the hydrodynamics cause a laminar flame propagating in an open tube to assume a stable domed shape (for photographs of the dome see Maxworthy, 1962, or Strehlow, 1984). Jost (1939) presents a qualitative description of the flow field associated with the domed shape, and Ball (1951) presents a numerical calculation in qualitative agreement with the observations of Jost. Uberoi (1959) used a channel to create an approximately two-dimensional flame front, and experimentally demonstrated some shortcomings of Ball's treatment. In particular, Uberoi pointed out the existence of a stagnation region behind the flame near the walls of the channel. The flow field and the stagnation region associated with curved flames has been the focus of recent

investigations. Zeldovich et al. (1980) described a general analytical approach to combustion in open tubes. The approach of Zeldovich et al. has subsequently been extended by Clavin and Pelce (1982) to demonstrate the theoretical existence of slow burning stable planar laminar flames. This result is contrary to the predictions of previous stability analyses. Clavin and Pelce have shown that, because of the coupling between the hydrodynamic field and the flame front, planar laminar flames can be stabilized in tubes if the effects of gravity are included in the analysis. They have also shown the existence of such flames experimentally. The effect of the hydrodynamics on the shape and stability of laminar flames is treated extensively in a recent review article by Clavin (1985).

The analyses and experiments concerning the flame shape/flow interactions mentioned above are limited to steady, open tube configurations because the closed tube, nonsteady case is not analytically convenient. While some analytical open tube results are applicable to closed tube combustion, flames propagating in short closed tubes have specific peculiarities which separate them from flames propagating in long closed tubes or open tubes. One of these peculiarities is a flame cusping phenomenon known as "tulip" flame formation. The history of the "tulip" flame and its proposed causes are presented in the next chapter. The complication of nonsteadiness and the enclosed volume boundary conditions which manifest in the "tulip" flame have thus far prevented analytical solutions to the closed tube combustion

problem. Even numerical solutions to this problem have yet to appear in the literature. Cloutman (1982) successfully reproduced the early flame behavior using a version of the CONCHAS combustion computer code (1982) developed at Los Alamos National Laboratory, but he admitted that the need for excessive manipulation of the available parameters made the result unsatisfying. Several other attempts at modeling closed tube combustion are in progress (Barr, 1985 and Shin Lu, 1985), but have not yet been fruitful. Experimental investigations, such as the work presented here, will be valuable as an aid to the development of suitable theoretical models for flame propagation in closed tubes.

CHAPTER 2

The "Tulip" Flame

2.1 Description of a "tulip" flame

The occurrence of a single-cusped (or "tulip") flame in relatively short (L < 0.5 m) closed tubes and ducts has been documented for nearly sixty years (Ellis, 1928). One example of the "tulip" flame was shown in Figure I-1. A larger sequence of frames from the schlieren movie of the same "tulip" flame is shown in Figure 2-1. The combustion vessel is a closed rectangular duct (38 mm x 38 mm x 150 mm). A line spark ignition source, oriented perpendicular to the viewing plane, initiates an approximately two-dimensional flame front. The combustible gas is a stoichiometric mixture of methane (CH_4) and air. There are three general phases of flame propagation: (1) an initial phase, where the flame propagates away from the igniter with a shape dictated by the geometry of the ignition source (in the case shown, the initial phase is approximately an extended semi-cylinder), (2) a transition stage, where the flame flattens into a nearly planar front and begins to cusp at the center, (3) a fully developed "tulip" phase, where the flame has formed a distinct cusp, which is maintained for the remainder of the flame propagation. All cases of closed tube combustion in which "tulip" flames appear demonstrate the above three phases.

The "tulip" name was first used by scientists from the Soviet Union to describe the cusp shape which formed in flames propagating in long closed tubes (Salamandra et al., 1959).

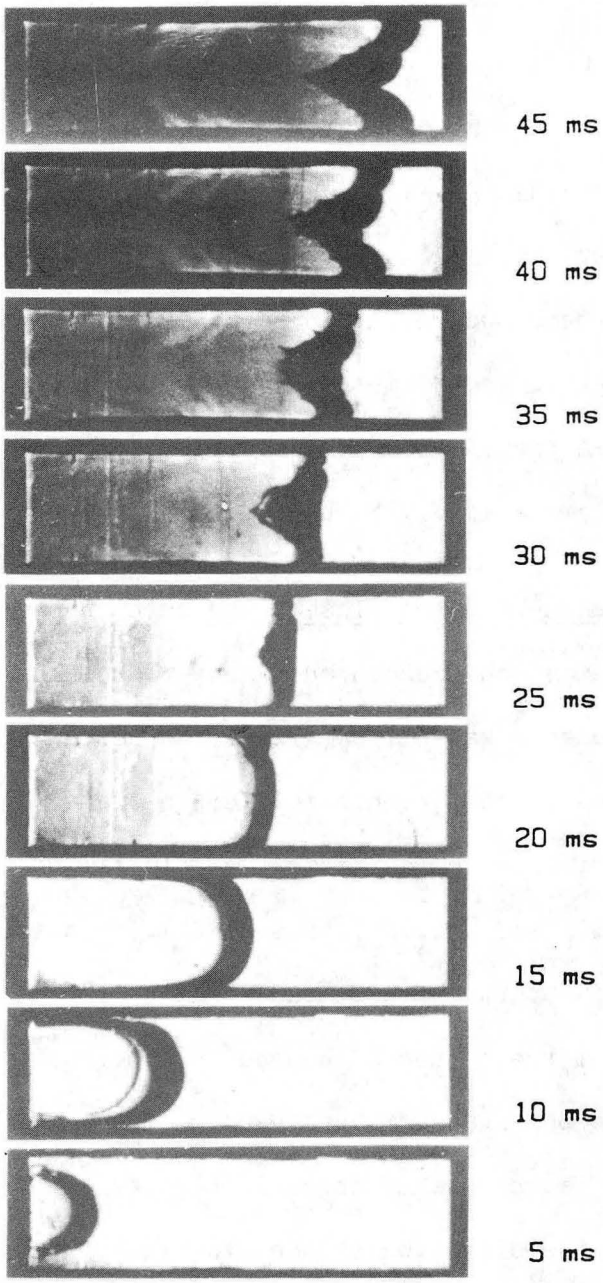

Figure 2-1. An example of the "tulip" flame formation. Stoichiometric methane/air flame initiated by a line igniter. Square cross-section chamber (38 mm x 38 mm x 150 mm).

Flame propagation in long tubes was studied because of interest in the transition to detonation discussed in Chapter 1. The transition to "tulip" in long tubes is slightly different than in short closed tubes, and more closely resembles the tulip flower, hence the name. Professor A.K. Oppenheim, of the University of California, Berkeley, is credited with suggesting the "tulip" name for cusped flames propagating in short closed tubes. Although the shape of these flames does not resemble the tulip flower as closely as the flames described by Salamandra et al. (1959), the mechanism is likely to be the same.

2.2 Previous research on short closed tube phenomenon

The first and most referenced researcher to explore the "tulip" flame phenomenon was Ellis (1928). He conducted extensive stroboscopic photographic studies of flames in tubes using the flame luminescence to expose the film (Ellis and Robinson, 1925, Ellis and Wheeler, 1925, 1928). His study included: the effect of tube length and diameter on the "tulip" flame, ignition from the center of a tube so that two "tulips" formed as the flame propagated toward each of two endwalls, and the use of tracer flames, placed at various distances along the tube, to determine the direction of the flow inside the chamber. A short list of the tube lengths and diameters for which Ellis obtained stroboscopic photographs appears in Table 2-1. All of the tubes were glass with circular cross-section. Ellis suggests that a 10CO + O2 flame has a speed similar to a stoichiometric

TABLE 2-1

Closed Tube Combustion Experiments Performed by Ellis (1928)

mixture	tube length	tube diameter
10CO + 02	203 mm	25 mm
10CO + 02	195 mm	50 mm
10CO + 02	170 mm	50 mm
10CO + 02	120 mm	50 mm
10CO + 02	95 mm	50 mm
10CO + 02	400 mm	20 mm
13CO + 02	320 mm	40 mm

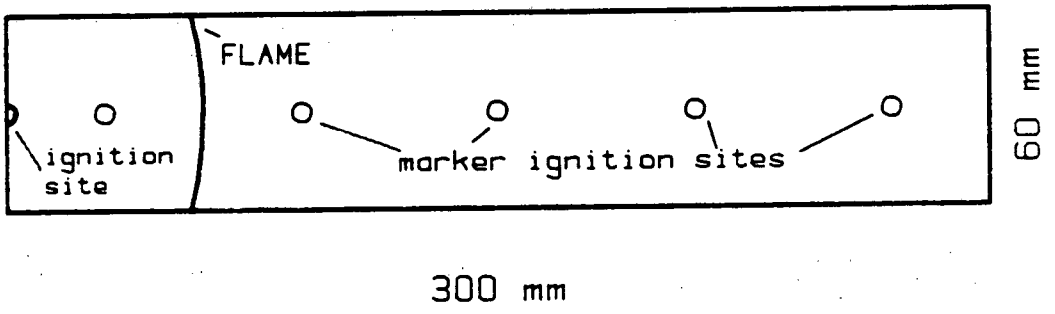

Figure 2-2. Geometry of cylindrical combustion vessel and marker flames used by Ellis (1928) to investigate flame generated flow during closed tube combustion.

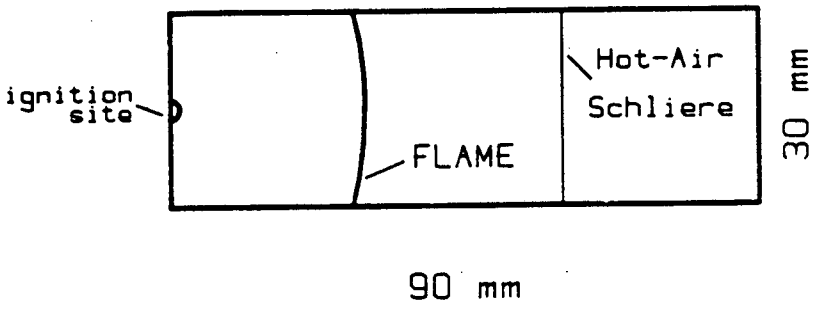

Figure 2-3. Schematic of rectangular combustion vessel and the hot-air schlieren technique employed by Shimizu et al. (1983) to investigate flame generated flow during closed tube combustion.

methane/air flame, but the carbon monoxide/oxygen flames have the additional advantage of sufficient luminosity to expose the photographic film. A "tulip" flame was noted in all of the cases listed in Table 2-1. Flames in the shorter tubes (L = 95 mm and L = 120 mm) showed a much less pronounced "tulip" formation. Flames in the longer tubes (L > 200 mm) showed definite signs of buoyancy during the latter stages of flame propagation. Ellis noticed the correlation between the time of flame quench at the side walls and the formation of the "tulip" shape. He attributed the "tulip" cusp to a reverse flow generated when the heat loss from the burned gas dropped the pressure there below the pressure in the unburned gas. He tried to show this reverse flow by igniting the mixture at several locations in front of the primary flame, Figure 2-2. The direction of motion of the marker flames then represented the direction of the flow. Unfortunately, the combustion from the marker flames created their own flow which obscured any other flow in the combustion tube. The stroboscopic photographs of Ellis have appeared subsequently in many text books on combustion (Lewis and Von Elbe, 1961, Guenoche, 1964, Strehlow, 1984).

A second extensive study of flames propagating in closed tubes was presented by Guenoche (1964). This work reviews most of the literature on the subject, but is, by the author's admission, mainly descriptive. The problem statement from

Guenoche summarizes the state of closed tube deflagration research in 1964,

> "A quantitative interpretation of the way a flame develops in a tube is not easy to make, as it is a question of following the nonsteady development of a surface at which the fresh gases, with velocity varying in time and in space, are changed into burned gases. Since plane or spherical approximations are inconsistent with this case, it does not appear possible to tackle the problem without introducing simplifications and assumptions which may well deprive the results obtained of any real meaning. We must therefore be content with a qualitative interpretation of the flame propagation based on the available experimental results."

Guenoche separates the flame propagation in a closed tube into two phases. The first phase corresponds to phase (1) described in the opening section of this chapter. He notes that the radial motion of the flame during this phase is essentially independent of tube length. The second phase corresponds to phases (2) and (3) described in Section 2.1. During this period the flame decelerates and inverts into a "tulip" flame. Guenoche also notes that if the tube is long enough the "tulip" will crumble and the flame will assume an approximately hemispherical shape again. Evidence of this behavior appears in the schlieren photographs of Schmidt et al. (1952) and Egerton et al. (1952). The crumbling behavior occurs due to turbulence generated ahead of the flame as described in the transition to detonation section of Chapter 1. The turbulence is not likely to be responsible for the "tulip" flame because the cusp appears even in short tubes, where the turbulence has no time to develop.

Guenoche opposes a commonly held view that the "tulip" flame results from a compression wave hitting the flame front after

being reflected off of the closed downstream end. Instead, he proposes that a rarefaction wave, generated when the flame quenches at the side-walls, reflects off of the ignition end of the tube and interacts with the flame front. The rarefaction draws the flame center back toward the ignition end causing the "tulip" shape.

Fairly recently, the "tulip" flame has appeared as simply an "interesting phenomenon" in several works which focused on other subjects. For example, Smith (1977), noted the "tulip" flame, but was concerned primarily with bulk-quenching of lean mixtures by an expanding piston. Woodard et al. (1981) recorded "tulip" flames with high-speed schlieren cinematography, but this work was concerned primarily with heat transfer during closed tube combustion. Steinert et al. (1982) conducted experiments similar to those reported by Ellis (1928) and mentioned changes in "tulip" flames with equivalence ratio, fuel type, and chamber length. Their work, however, was concerned primarily with combustion parameters such as total combustion time, peak pressure, calculated flame speeds and mass burning rates. These works, as the works of Ellis and Guenoche, were only descriptive in regards to the "tulip" flame.

The accurate determination of the flow field during nonsteady flame propagation in a closed duct would provide quantitative information about the "tulip" phenomenon. Unfortunately, though particle track methods have been applied quite successfully in burner studies (Lewis and Von Elbe, 1943

and Maxworthy, 1961) and open channel propagation studies (Uberoi, 1959), closed tube combustion presents the difficulty of an initially quiescent environment. Particles of a size suitable for photography will not remain in suspension, making particle track photographs difficult. With the development of laser techniques the particle size difficulty is somewhat alleviated. Laser Doppler anemometry (LDA) employs particles small enough to remain in suspension before ignition of the initially quiescent combustible gas. Laser Doppler anemometry provides an accurate quantitative measure of the non-steady velocity at a single point in the combustion vessel.

In 1984 two very similar works were presented on the application of laser Doppler anemometry to the measurement of fluid motion generated by flame propagation in a closed duct (Dunn-Rankin et al., 1984, Starke and Roth, 1984). These are the first quantitative measurements available to help understand the propagation of flames in closed tubes. The study of Starke and Roth used somewhat longer tubes than were used in the study of Dunn-Rankin et al., and it concentrated on vibratory motion of the gases in the tube. Both studies were incomplete in their mapping of the flow field, and consequently, they could not produce conclusive evidence as to the influence of fluid motion on the "tulip" flame. However, they did provide quantitative information previously lacking in the study of closed tube flame propagation. The results of these works are similar to some of

the results obtained in this thesis, and consequently, a detailed discussion of these results is reserved for later chapters.

Recently, Wakai and Shimizu (1984) and Wakai et al. (1984) have presented both qualitative and quantitative discussions of "tulip" flames. These studies were prompted by their observation of the "tulip" flame during research on divided chamber combustion mentioned in Chapter 1 (Shimizu et al., 1983). These authors used laser Doppler velocimetry and a technique named "the hot air method" to determine the flow field. The laser Doppler velocimetry results are discussed in later chapters. The "hot air method" uses a fine wire which spans two opposing vessel walls. An electric pulse through the wire heats the surrounding air. The hot-air gives rise to a schliere in photographs. The thin hot-air schliere follows the gas motion giving unburned gas flow information. A schematic of the combustion vessel, hot air schliere, and flame front is shown in Figure 2-3. Their chamber measured 28 mm x 30 mm x 90 mm. The advantage of the hot-air-method is its ability to give the flow field across the entire chamber cross-section. Unfortunately, near the flame front the combustion schliere swamps the hot-air schliere and no further flow information can be obtained. Similarly the hot-air schliere cannot survive the flame passage and so no information on the flow in the burned gas is available. Again the quantitative information describing the flow field during the flame propagation is incomplete, and consequently the "tulip" flame cannot be conclusively explained.

2.3 Theories on the cause of "tulip" flames

Several theories on the cause of "tulip" flames have been proposed. The proposed theories are based on the above mentioned qualitative observations of the "tulip" flame formation.

1) Spontaneous instability - It has been shown that under certain circumstances a smooth flame front will spontaneously break down into a cellular structure (Markstein, 1951, Sivashinsky, 1977). The cellular structure is the result of an inherent instability of the flame interface. The "tulip" flame has been suggested as a single cell of the cellular structure.

2) Pressure wave/flame interaction - Taylor (1950) has shown that an interface between two fluids of different density is unstable to accelerations in the direction of the more dense to the less dense medium. Further, Markstein (1957) has demonstrated experimentally that a funnel, vaguely reminiscent of a "tulip", is formed in flames after the passage of a shock wave. The origin of the shock (or in this case the pressure wave) during closed tube combustion is the rapid deceleration of the flame when it quenches at the side walls of the vessel. The instability of the flame interface to the deceleration is suggested as the cause of the "tulip" shape (see Strehlow, 1984).

3) Reverse flow - A combustion generated flow at the duct centerline toward the igniter causes the center of the flame to be retarded relative to the flame near the walls, forming the

"tulip" shape. Heat transfer effects have been suggested as the source of the reverse flow (Ellis, 1928, Salamandra et al. 1959, Wakai and Shimizu, 1984).

There is no conclusive evidence which eliminates any of the above explanations for the formation of "tulip" flames, and in fact, a combination of them may be responsible. The experiments in this thesis concentrate on determining the validity of the fluid mechanical or third explanation.

CHAPTER 3

Premixed Flame Sheet Approximation

3.1 Introduction

Many combustion texts discuss the modeling of a premixed combustion wave as an interface between burned and unburned gas (Lewis and Von Elbe, 1961, Williams, 1964, Glassman, 1977, Strehlow, 1984). Consequently, only a brief description of the interface model with particular additional assumptions and nomenclature adopted for this thesis is presented here.

3.2 Assumptions

The term "premixed" actually refers to the state of the unburned combustible mixture into which the flame propagates. The fuel and oxidizer are "premixed" so that, given an ignition source, any location in the unburned gas can sustain combustion. The internal structure of premixed flames is fairly well understood (Fristrom and Westenberg, 1965). At atmospheric pressure the reaction zone of these flames is very thin (except if the mixture is near the lean or rich limit) because the combustion reactions are extremely sensitive to temperature. Outside the thin reaction zone the excess thermal energy from the reaction does not heat the unburned gas sufficiently for significant chemical reaction to occur. This narrowly confined flame zone allows the internal structure of the flame to be disregarded because the flame thickness is much smaller than any representative dimension of the combustion vessel. Consequently, for this study, a flame

front is an infinitesimally thin reaction interface where unburned gas instantaneously and irreversibly converts to higher temperature, lower density burned gas.

The flame interface moves both by self-advancement and convection, Figure 3-1. The self-advancement step propagates the interface, in the normal direction, at the laminar flame speed (or fundamental flame speed) of the combustible mixture. The convective step moves the interface in the direction of the existing flow. Although the laminar flame speed may not be uniform everywhere on the flame front (Clavin, 1985), the variations are small, and a constant, average laminar flame speed, S_u, can be defined by the rate at which unburned gas converts to burned gas,

$$S_u = (dm_b/dt)/(a_f \rho_u). \qquad (3.1)$$

The mass of burned gas is m_b; a_f denotes the flame area; and ρ_u represents the unburned gas density. Separation of flame motion into a self-advancement step and a convective step has been a successful approach in numerical modeling of flame propagation through premixed gases (Chorin, 1980, and Ghoneim et al., 1982)

The gases in the combustion vessel are dynamically incompressible (zero Mach number). Therefore the pressure is uniform throughout the system. Actually, the pressure has only leading order uniformity because pressure variations on the order required for velocity gradients must be present. A pressure drop

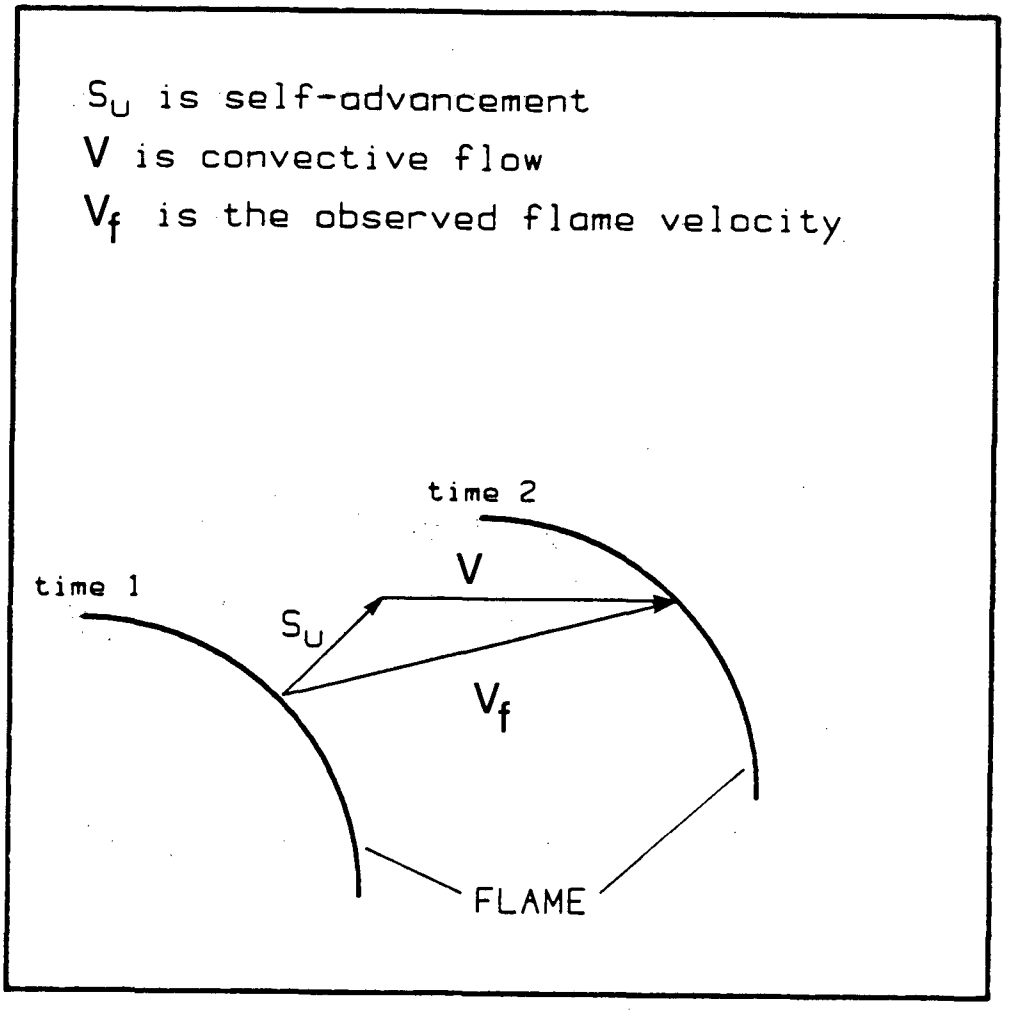

Figure 3-1. Separation of observed flame motion into a self-advancement step at the laminar flame speed and a convective step at the velocity of the flow field.

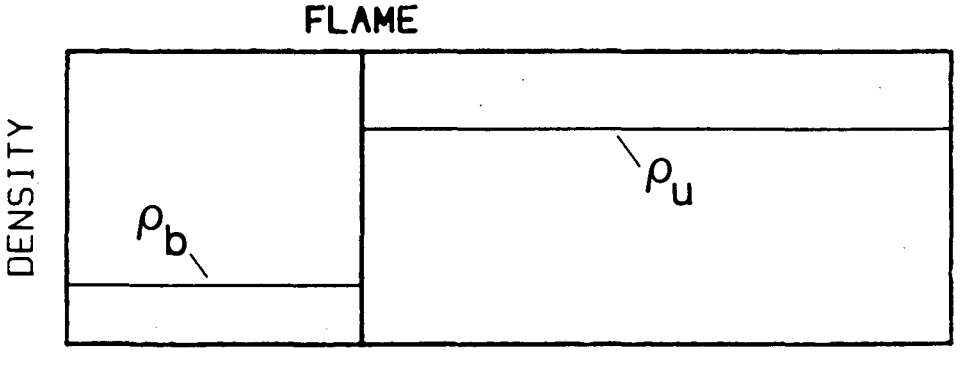

Figure 3-2. Assumption of spatially uniform density in the burned and unburned gas with a jump in density at the flame sheet.

across the flame is also necessary to maintain momentum continuity there. These pressure variations are negligibly small.

The flame behaves as an active semi-permeable interface which separates the unburned gas from the burned gas. The density (or equivalently, the temperature) in the unburned gas is spatially uniform; then, at the flame there is a jump discontinuity from the density of the unburned gas to the density of the burned gas; and in the burned gas the density is again spatially uniform, Figure 3-2. Actually, it was expermentally demonstrated by Hopkinson (1906) that successive compression of burned gas layers creates a temperature and density gradient in the burned gas. The temperature gradient occurs, however, only if no mixing occurs. Velocity measurements and high-speed schlieren movies during flame propagation in closed ducts presented in later chapters indicate that significant mixing of burned gas is likely. Consequently, the burned gas temperature is assumed uniform.

Both the burned and unburned gas behave ideally, and they have different but fixed composition. Both gases are inviscid and they do not transfer heat to the vessel walls.

3-3 Justification of assumptions

A brief discussion of the validity of the above assumptions follows:

1) Infinitesimally thin flame front-

The flame consists of a preheat zone and a reaction zone. The reaction zone is much smaller than the preheat zone, and consequently the flame thickness is the width of the preheat zone (Lewis and Von Elbe, 1961),

$$d = \alpha/S_u, \tag{3.2}$$

where d is the flame thickness, α is the thermal diffusivity of the unburned gas. Taking $S_u \approx 0.4$ m/s (which is a value common for hydrocarbon fuels) and $\alpha \approx 3.0 \times 10^{-5}$ m^2/s (the value for air around 350 K), the flame thickness is approximately 0.1 mm. The smallest physical dimension of the combustion vessels used in this study is 38 mm. Therefore, assumption of an infinitesimally thin flame front is reasonable.

2) Dynamic incompressibility (zero mach number)-

The Mach number is,

$$M = U/c \tag{3.3}$$

where U is a representative velocity in the flow, and c is the velocity of sound in the medium. The highest velocity achieved in the system is approximately 6 m/s. The velocity of sound in

air at 350 K is approximately 370 m/s. The Mach number is then 0.016. Compressible effects are negligible at this Mach number.

3) Viscosity and heat transfer neglected-

A time scale argument justifies neglecting viscosity and heat transfer. A representative time for viscous diffusion is,

$$t_v = L^2/\nu, \tag{3.4}$$

where L is an appropriate length scale and ν is the viscous diffusivity. Similarly, a representative time for thermal diffusion is,

$$t_t = L^2/\alpha, \tag{3.5}$$

where α is the thermal diffusivity. An appropriate length scale for the combustion vessel is on the order of L = 0.01 m. Taking the thermal diffusivity of 3×10^{-5} m^2/s, as before, and a viscous diffusivity of 2×10^{-5} m^2/s, then $t_v \approx 5$ s and $t_t \approx$ 3.3 s. A typical combustion event takes only 0.05 s, therefore it is unlikely that viscosity or heat transfer are important factors in the global fluid flow.

4) Uniform density of the burned gas -

The temperature gradient generated by a centrally ignited methane/air flame in a spherical combustion vessel with no mixing in the burned gas has been calculated numerically by Garforth and Rallis (1976) and Bradley and Mitcheson (1976). The former researchers found the temperature variation at the time of peak

pressure to be substantial (approximately 30 percent, or 1000 K for a vessel with 80 mm radius). The latter researchers found the variation at peak pressure to be somewhat less (approximately 17 percent, or 500 K for a vessel with 100 mm radius). However, measured velocities in the burned gas during flame propagation in a closed duct (Chapter 7) show significant mixing of the burned fluid. The convective time scale of this mixing is approximately,

$$t_m = L/U, \tag{3.6}$$

with L and U defined above. U is approximately 5 m/s and L is approximately 0.15 m. The convective time scale is therefore 30 ms. This time is smaller than the total combustion time (approximately 50 ms), and consequently, there is sufficient time for significant mixing to occur. It seems likely that the density field is much more uniform than the numerical calculations predict. Furthermore, the assumption of uniform burned gas density is used only in the one-dimensional description for the fluid motion (Chapter 8), and this description is shown to be invalid from a fluid mechanical viewpoint in the burned gas.

CHAPTER 4

Qualitative Investigation of "Tulip" Flames

4.1 Introduction

A summary of the experiments presented in this and later chapters is provided for reference in Table 4-1. The first set of experiments, which is the subject of the present chapter, uses high-speed schlieren movies of the flame and in-chamber pressure records to investigate the effects of various boundary conditions and initial conditions on flame propagation in closed ducts. The photographic results are necessarily qualitative because the line-of-sight integration inherent in the schlieren technique (Guenoche and Juoy, 1954) prevents quantitative determination of the flame area. The pressure/time records of closed tube combustion show distinct features which correlate with flame shape changes during the transition to "tulip".

4.2 Apparatus

The experimental set-up, Figure 4-1, consists of a high-speed schlieren cinematography system, a pressure recording system, a gas mixing device, a constant volume combustion vessel, and a high-voltage spark ignition system.

The schlieren system, Figure 4-2, consists of two spherical mirrors (3.93 m focal length), a point light source (Oriel xenon lamp, model 6140, with a 2 mm aperture), a vertical schlieren knife edge stop, and a high-speed 16 mm movie camera (Hycam Model 41-0004, approximately 5000 frames/s, Kodak Tri-X-Reversal film).

TABLE 4-1
SUMMARY OF CLOSED TUBE EXPERIMENTS

TYPE	CHAPTER	FUEL	EQUIVALENCE RATIO	LENGTH	IGNITER	VELOCITY MEASUREMENTS
qualitative photographic flame shape	4	CH4 CH4 C2H4	1.0 1.0 0.6-1.1	30-150 mm 150-155 mm 150 mm	line line, 2pt, 1pt line	NONE
pressure/flame relationship	5	C2H4 CH4	0.6-1.1 1.0	150 mm 30-150 mm	line line	NONE
axial centerline velocity	6	CH4	1.0	150 mm	2 point	LDA, X-centerline only
velocity field	7	CH4	1.0	155 mm	1 point	LDA, two components / two dimensions

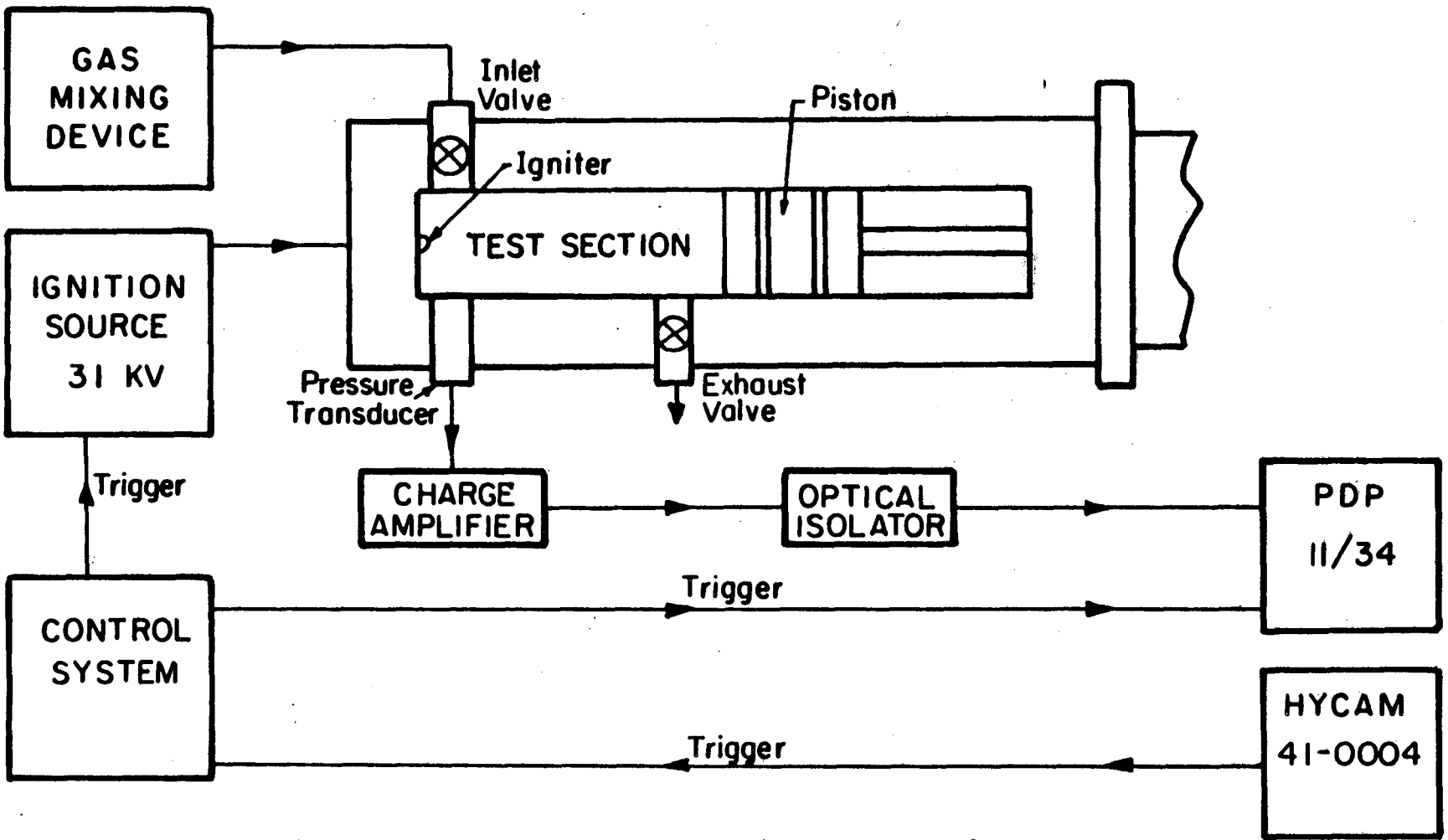

Figure 4-1. Schematic of experimental apparatus used for qualitative observations of the "tulip" flame formation.

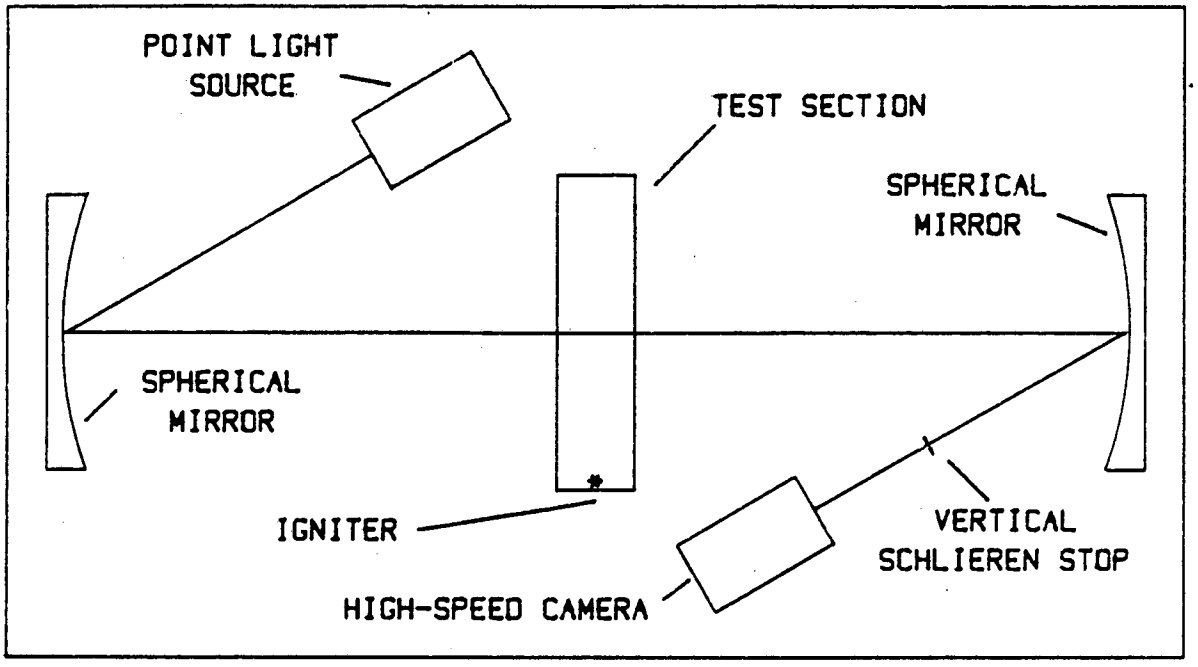

Figure 4-2. Schematic of the high-speed schlieren cinematographic system used to observe flame propagation.

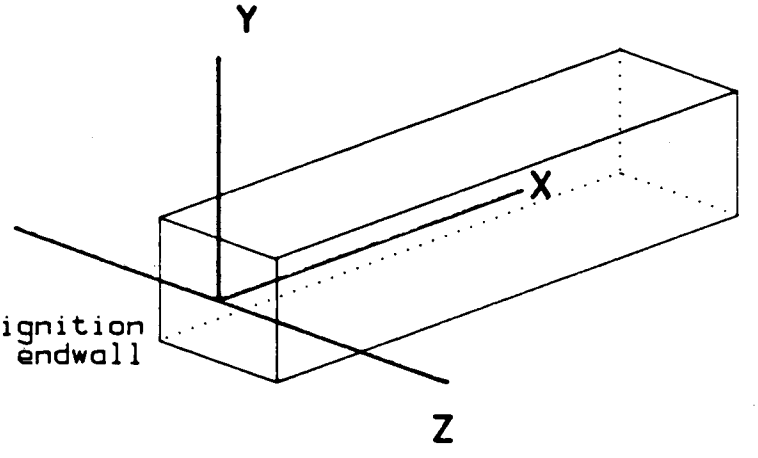

Figure 4-3. Coordinate convention adopted for the flame propagation studies.

The schlieren system is arranged in a standard Z-configuration. Further information on the schlieren technique (Weinberg, 1963), and on the particular implementation of the technique used in this work can be found in the literature (Smith, 1977, Steinert et al., 1982).

A piezoelectric transducer (AVL 120p300 cvk#1402, sensitivity 42.04 pc/bar) measures the chamber pressure during the combustion process. A charge amplifier (Kistler 5004E) amplifies the transducer signal, and the amplified signal is then recorded either by a data acquisition minicomputer or an oscilloscope equipped with a polaroid camera. The computer (PDP 11/34 with an AR-11 analog to digital converter) samples and stores the pressure signal every 0.2 ms. When the oscilloscope and camera are used, the pressure/time trace is digitized (using an HP7470A graphics plotter) for computational flexibility. The calibration of the transducer/amplifier combination was dynamically verified in a shock tube and statically verified with a dead weight tester.

Two combustion vessels are used in the study. Both vessels are rectangular with square cross-section (38 mm x 38 mm). Parallel side walls are necessary for schlieren cinematography and facilitate laser Doppler anemometry access as well. However, circular cross-section tubes were used in most of the closed tube combustion work described in Chapter 2. Previous investigations have shown that there is little qualitative difference between the "tulip" flame in circular cross-section tubes and square

cross-section tubes. The coordinate convention adopted for the combustion vessels is shown in Figure 4-3. One of the combustion vessels, Figure 4-4a, has two borosilicate glass side windows for optical viewing of the X-Y plane. The top and bottom walls of the vessel are stainless steel. A moveable end-wall allows a variable chamber length (from 20 mm to 200 mm). The second closed duct, Figure 4-4b, is constructed entirely of 12.7 mm plexiglas to allow optical viewing of two orthogonal planes (X-Y and X-Z). The access from both directions helps remove the ambiguity which arises from the line-of-sight integrated schlieren records. The plexiglas vessel has a fixed length of 155 mm.

The gas mixing device controls the equivalence ratio of the fuel/air combustible premixture by flow rotameters. Calibration of the rotameters with a soap bubble meter indicates that the uncertainty in the equivalence ratio of the gas delivered by the mixing device is approximately 5%. To insure negligible residual gas effects, the combustion vessel is purged for a time sufficient for twenty complete changes of mixture between each experiment.

Three types of spark igniters, Figure 4-5, are used: 1) a line igniter, for a continuous line source of ignition, 2) a two point igniter, for ignition at each of the side walls, 3) a single point igniter, for axial ignition near one endwall. The single point ignition is the igniter configuration most commonly reported in the literature.

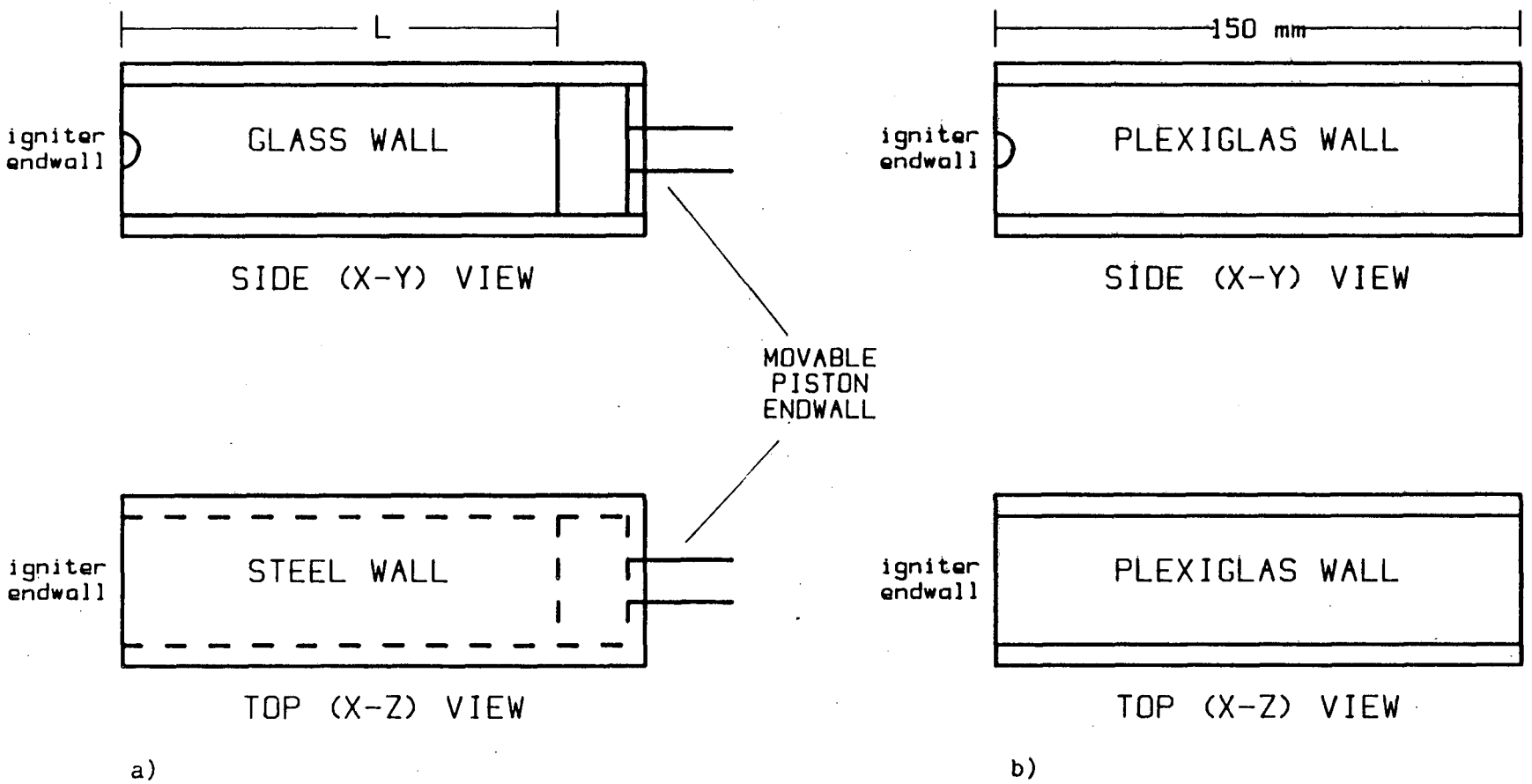

Figure 4-4. The combustion vessels employed in the research.
a) Steel/glass vessel
b) All plexiglas vessel

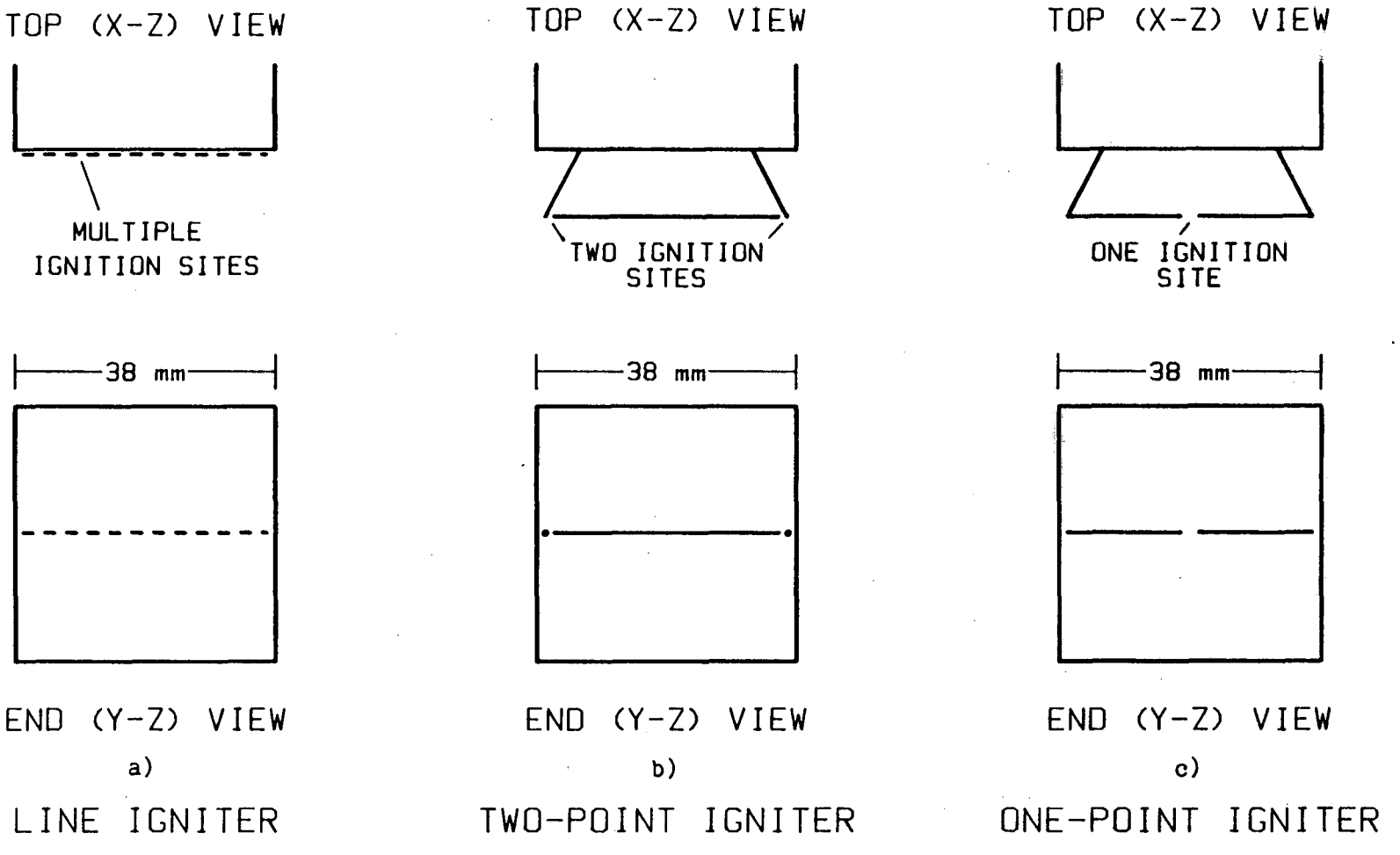

Figure 4-5. The spark igniters employed in the research.
a) Multi-point line igniter
b) Two-point igniter for ignition near sidewalls
c) Single point igniter for central ignition

The spark energy is obtained from a high voltage (30 kV) ignition source. Three ignition sources are used. All three sources are capacitive discharge devices. The first ignition source, which is used with the line igniter, is described in detail by Smith (1977) and Steinert et al. (1982). The second ignition source, which is used with the two-point igniter is described in detail by Edwards and Oppenheim (1983). The third ignition source, which is used with the single-point igniter is a commercial trigger transformer (EG&G TM11A). The stored ignition energy in all three devices is approximately equal to 100 mj. The actual energy delivered to the combustible gas is not known, but de Soete (1981) has shown that the ignition energy affects only the early flame propagation (2 ms). In this study the combustion process is sufficiently long to insure that the ignition energy effects are not significant.

4.3 Methodology

First, the chamber is purged with the desired combustible gas for a time sufficient for twenty complete changes of gas contents. The chamber is then sealed and the gas motion induced by the purging process subsides. Various settling times were used (from 30 seconds to 10 minutes) with no noticeable effect. Next, the high-speed camera is started. When the camera reaches operating speed (approximately 5000 frames/s), it sends a trigger pulse simultaneously to the data acquisition computer and to the spark ignition source. Consequently, time zero of the pressure record corresponds to ignition. The pressure is recorded for

100 ms beyond the end of combustion. The decay in pressure after combustion gives an approximate measure of the heat and leak losses from the combustion vessel.

4.4 Results

High-speed movies and pressure records are available for the conditions described in Table 4-2. Representative sequences from the high-speed movies and the corresponding pressure/time records are shown for the various conditions in Figures 4-6 to 4-10 and Figures 4-12 to 4-15. High-speed movies without accompanying pressure traces are available for several miscellaneous conditions, Table 4-3. Representative sequences from the schlieren movies taken at these conditions are shown in Figures 4-17 to 4-21.

The first group of schlieren sequences, Figures 4-6 to 4-10, show the effect of chamber length on the "tulip" flame. The line igniter initiates the combustion in this group of sequences. The photographs show an increasing "tulip" effect with increasing chamber length. In fact, if the chamber is too short the "tulip" does not form at all. This effect can also be seen in the stroboscopic photographs of CO-O2 closed tube flames made by Ellis (1928). If the flame reaches the endwall of the combustion vessel at approximately the same time that it reaches the side walls of the vessel a "tulip" flame does not form. Therefore, the "tulip" appears connected closely with the rapid reduction in flame area due to wall quench.

Table 4-2

Schlieren Sequences in Steel/Glass Vessel : X-Y Projection Plane

FIGURE NO.	LENGTH	IGNITER	EQUIVALENCE RATIO	FUEL
4-6	30 mm	line	1.0	CH4
4-7	60 mm	line	1.0	CH4
4-8	90 mm	line	1.0	CH4
4-9	120 mm	line	1.0	CH4
4-10	150 mm	line	1.0	CH4
4-12	150 mm	line	1.1	C2H4
4-13	150 mm	line	0.9	C2H4
4-14	150 mm	line	0.7	C2H4
4-15	150 mm	line	0.6	C2H4

Table 4-3

Miscellaneous Schlieren Sequences

FIGURE NO.	LENGTH	IGNITER	EQUIVALENCE RATIO	FUEL	PROJECTION PLANE	VESSEL	NOTES
4-17	150 mm	line	1.0	CH4	X-Z	plexiglas	top view of line ignited flame
4-18	150 mm	2-point	1.0	CH4	X-Y,X-Z	plexiglas	two views of two point ignited flame
4-19	155 mm	1-point	1.0	CH4	X-Y	plexiglas	
4-20	150 mm	line	0.9	C2H4	X-Y	steel/glass	open exhaust valve in chamber
4-21	180 mm	line	1.0	CH4	X-Y	steel/glass	non-planar endwall

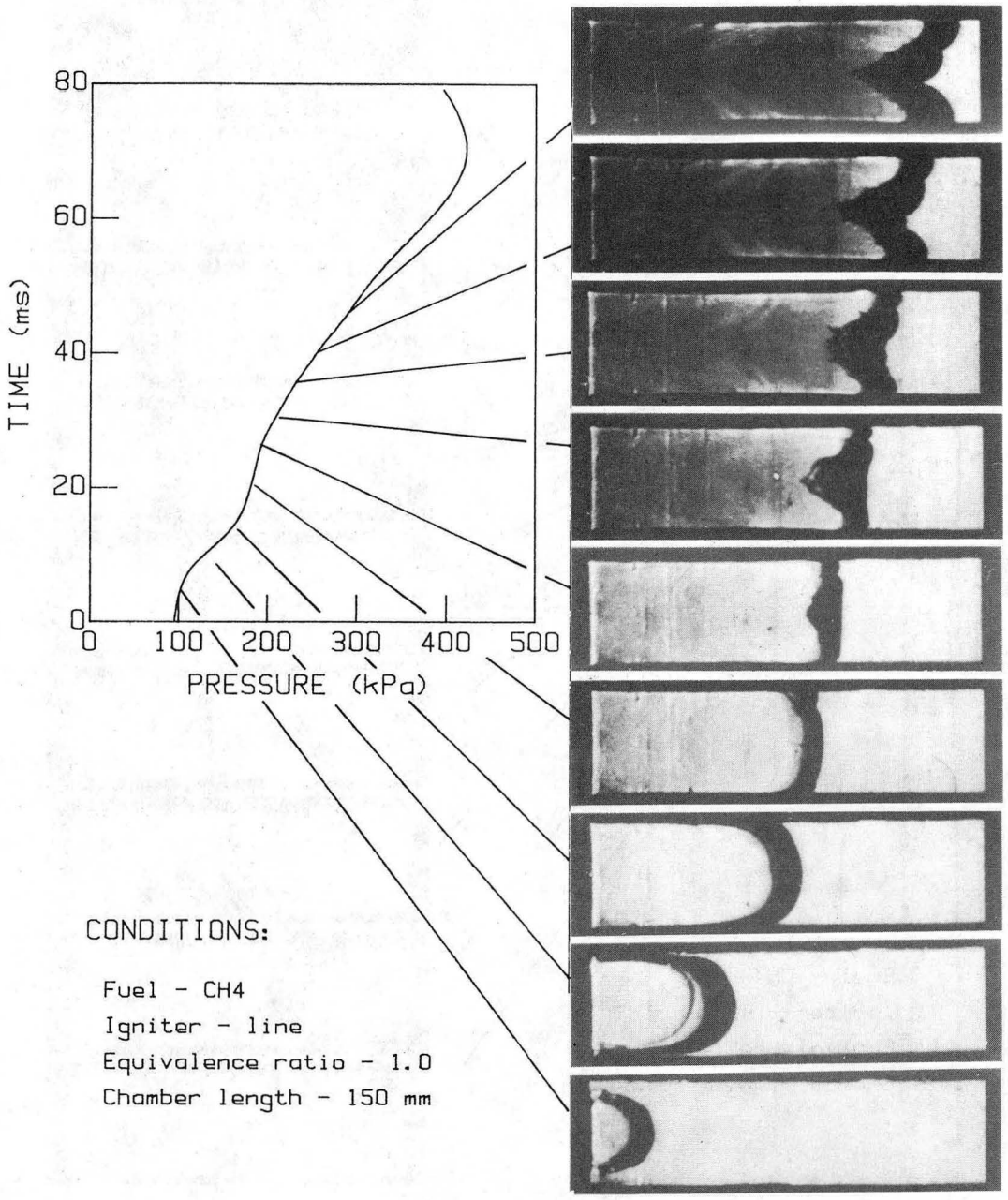

Figure 4-10. Flame shape and pressure history during constant volume combustion. Chamber length = 150 mm.

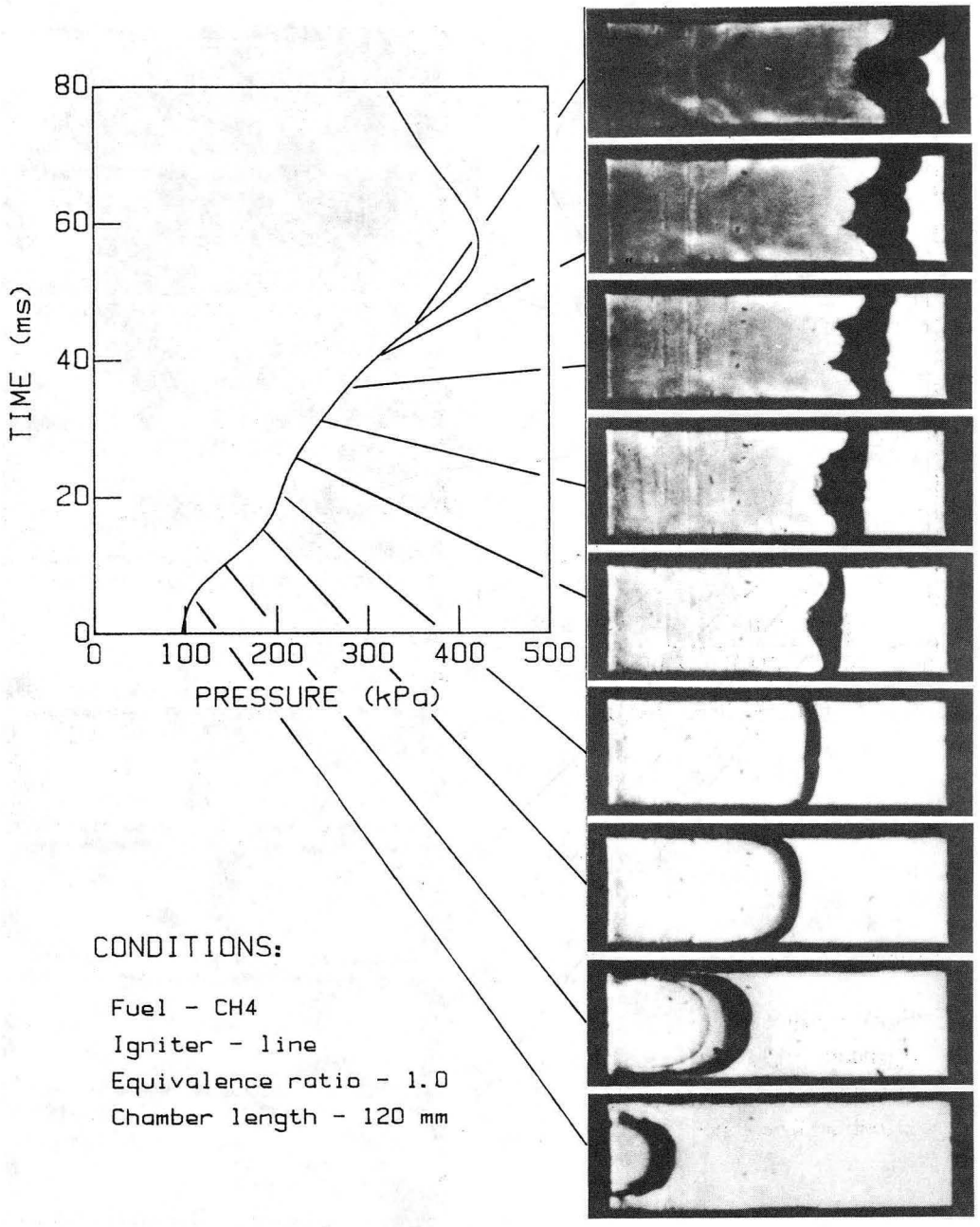

Figure 4-9. Flame shape and pressure history during constant volume combustion. Chamber length = 120 mm.

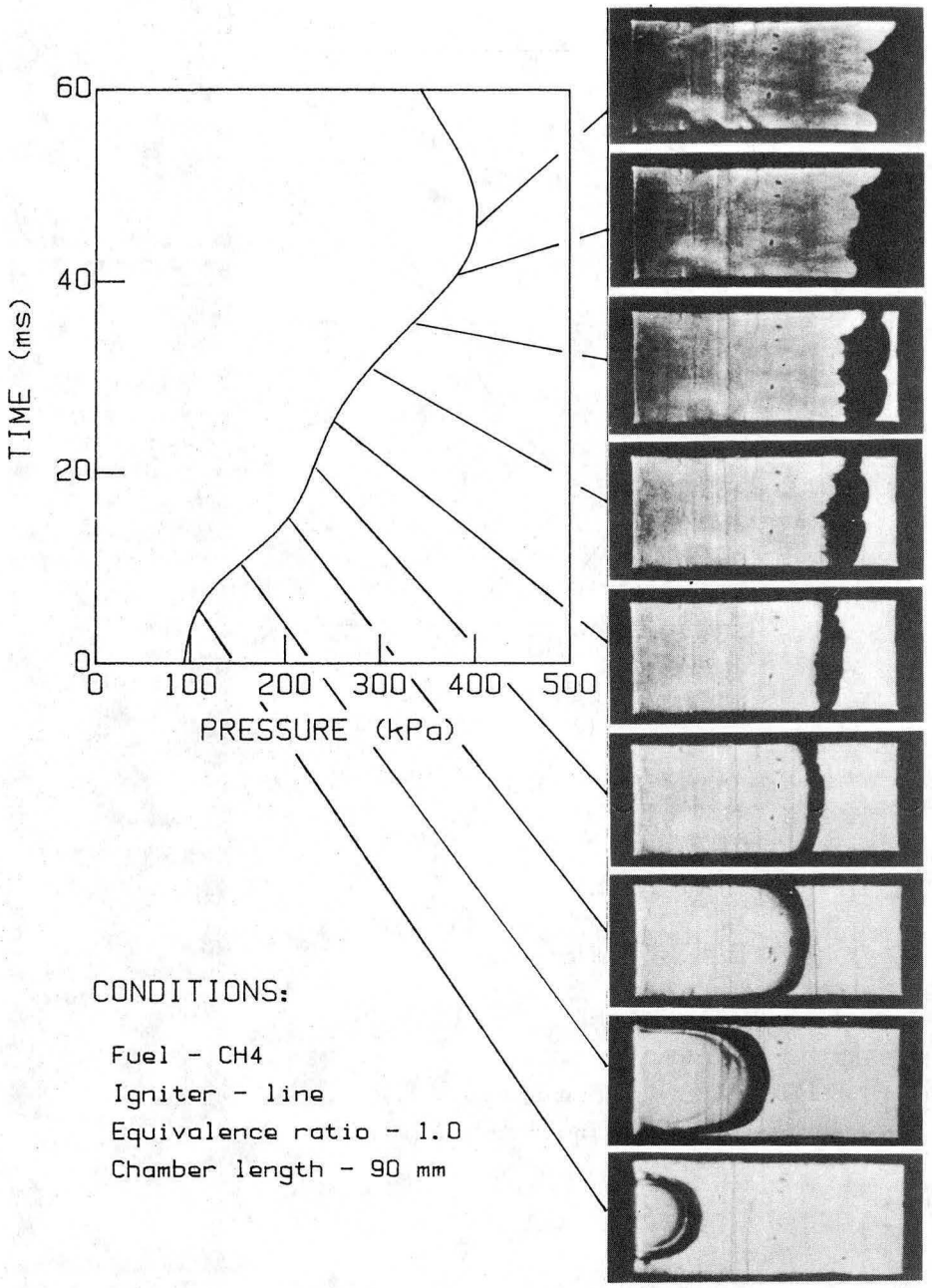

Figure 4-8. Flame shape and pressure history during constant volume combustion. Chamber length = 90 mm.

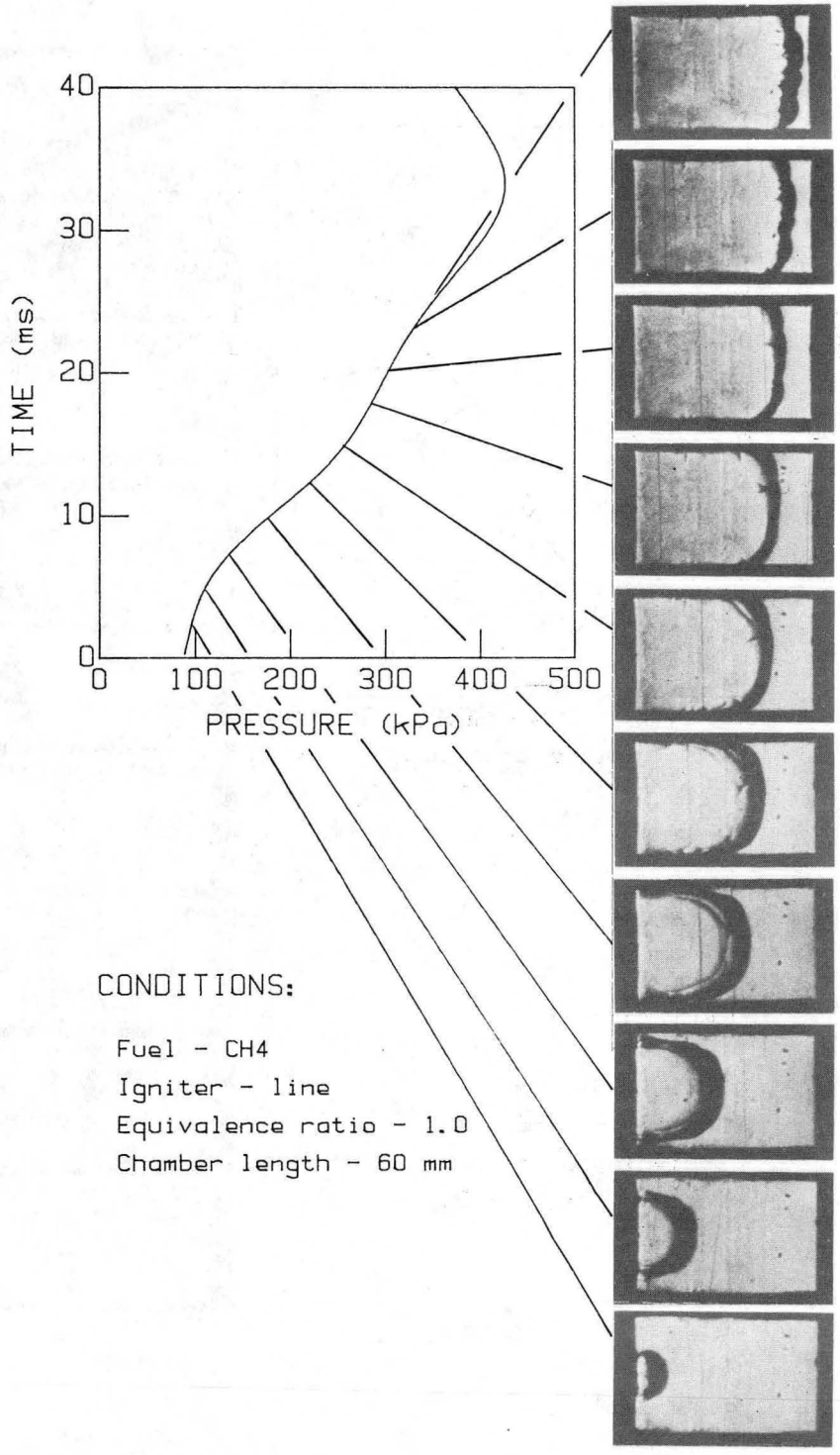

Figure 4-7. Flame shape and pressure history during constant volume combustion. Chamber length = 60 mm.

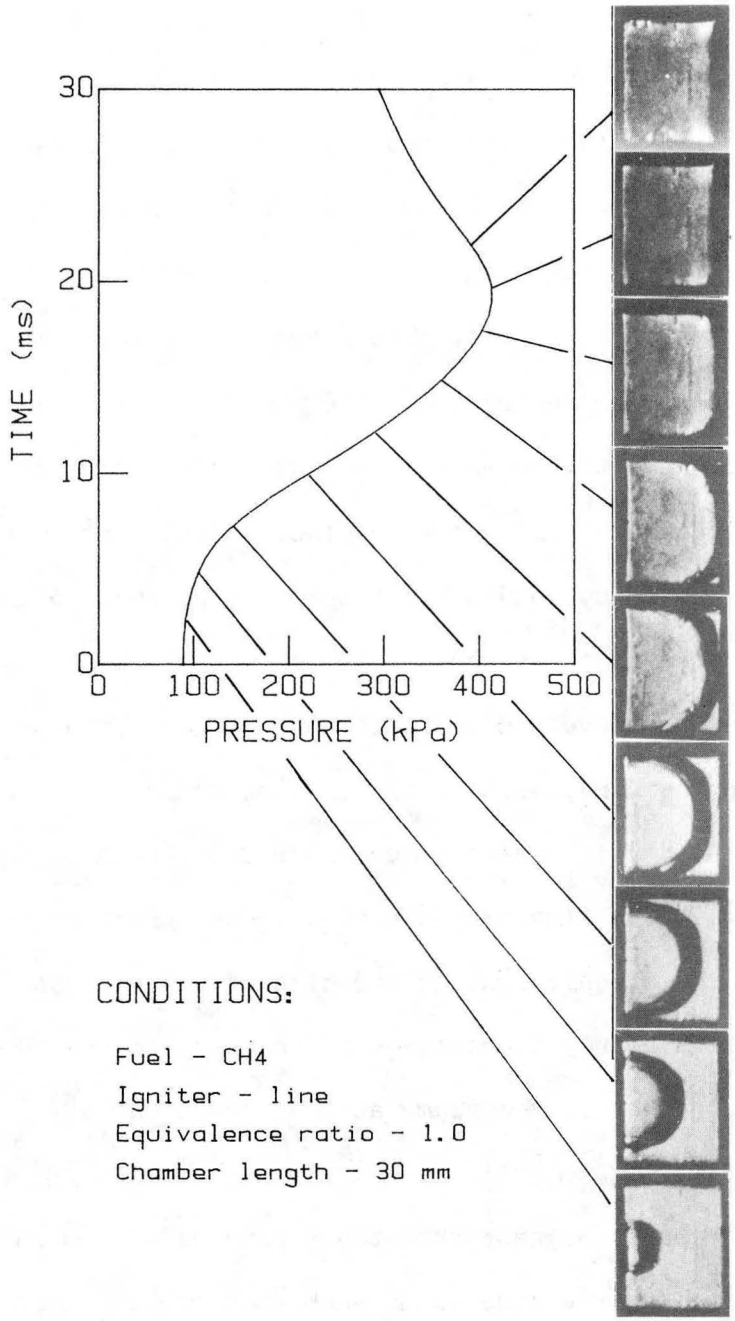

Figure 4-6. Flame shape and pressure history during constant volume combustion. Chamber length = 30 mm.

The pressure traces also reflect the wall quench behavior. The inflection in the pressure trace, which appears at approximately t = 15 ms (Figures 4-8 to 4-10), correlates very closely with the "tulip" flame. The inflection occurs as the flame burns out at the side walls of the chamber just prior to the flattening of the flame. The flame flattening immediately precedes the "tulip" formation. The rapid reduction in flame area associated with the wall quench causes the dramatic reduction in the rate of pressure rise, dp/dt. The more pronounced the reduction in dp/dt the more pronounced the "tulip" effect. In the shortest chamber (30 mm) there is no visible kink in the pressure curve and no noticeable "tulip" effect. As the chamber length increases both the inflection in the pressure curve and the "tulip" shape become more pronounced. Interestingly, the time that the kink in the pressure curve occurs, which is equivalent to the time of flame quench at the side walls, is nearly independent of chamber length. However, the axial location of the flame at the quench varies significantly, Figure 4-11.

These results suggest that the expansion of the burned gas is constricted by the side walls such that the expansion carries primarily the portions of the flame parallel to the endwall forward. The flame parallel to the side walls burns outward at much lower speed. The combustion toward the side walls is approximately independent of the axial motion of the flame and chamber length. Based on the convective plus self-advancement

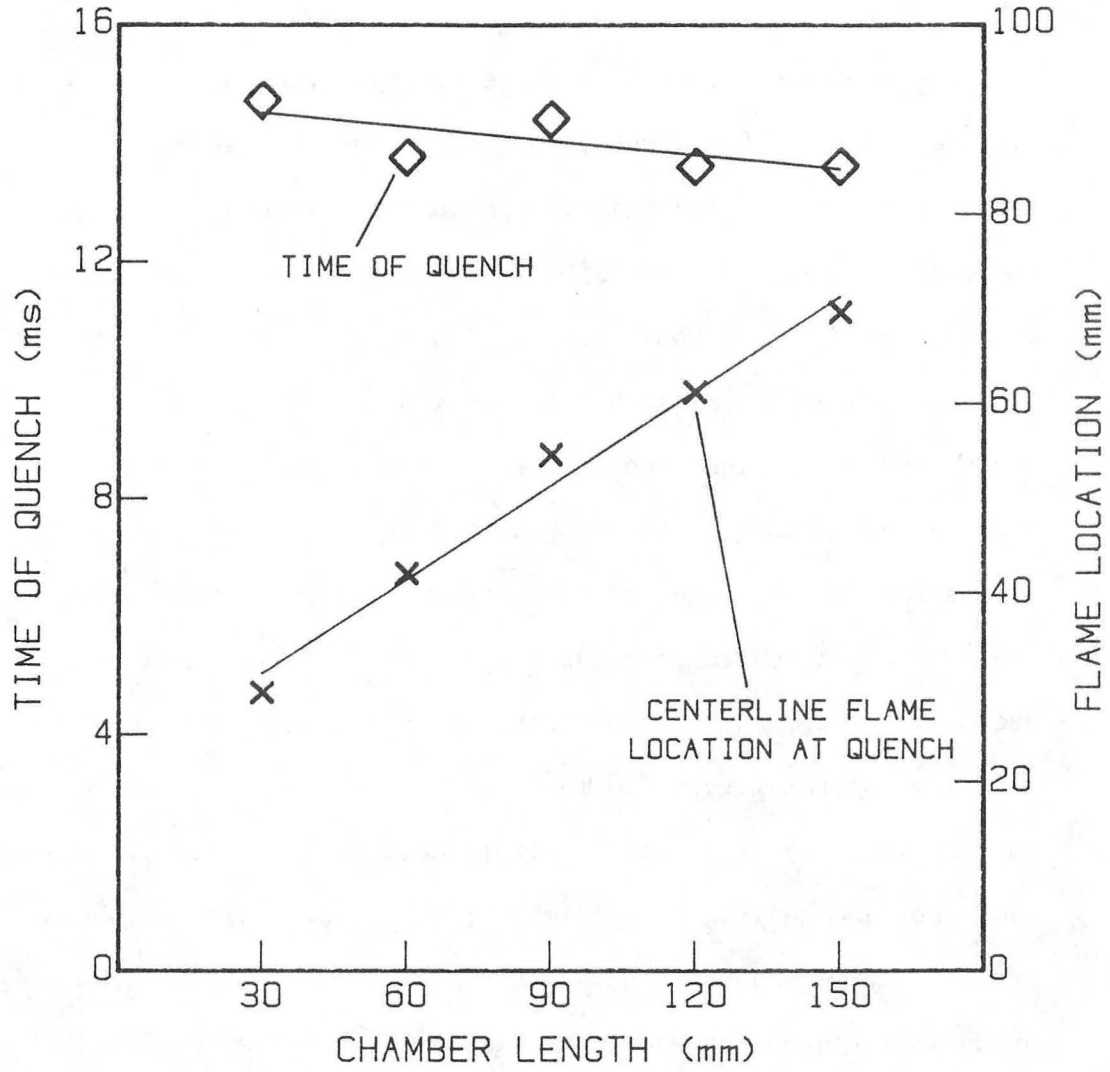

Figure 4-11. Relationship between the time of flame quench at the vessel sidewalls and the chamber length. Also the effect of chamber length on the axial flame location at the time of quench.

flame motion model described in Chapter 3, the unburned gas flow inside the closed tube must be primarily axial to account for this behavior.

The second set of schlieren sequences, Figures 4-12 to 4-15, explores the effect of equivalence ratio and laminar burning velocity on the "tulip" flame. Ethylene/air is used as the combustible gas. The laminar flame speed varies with changing equivalence ratio of the mixture. The combustion vessel in this series of experiments has a fixed length, and the line igniter is again used as the ignition source. A comparison of the ethylene/air flames to the methane/air flames provides an indication of the effect of fuel type on the combustion.

The first schlieren sequence, Figure 4-12, is a stoichiometric mixture of ethylene and air with a laminar burning velocity (approximately 0.8 m/s) more than twice the laminar burning velocity of a stoichiometric methane/air mixture. The two cases are qualitatively similar; both show a kink in the pressure curve and a strong "tulip" formation. The ethylene burns much faster, however, and displays considerably greater turbulization of the flame front. The "tulip" forms in about half the time it takes for a methane/air mixture in the same length combustion vessel, but the location of the flame when the "tulip" occurs is nearly the same in both cases.

The laminar flame speed of the ethylene/air flame is reduced by lowering the equivalence ratio. As before, the kink in the pressure curve gives a good indication of the "tulip" formation.

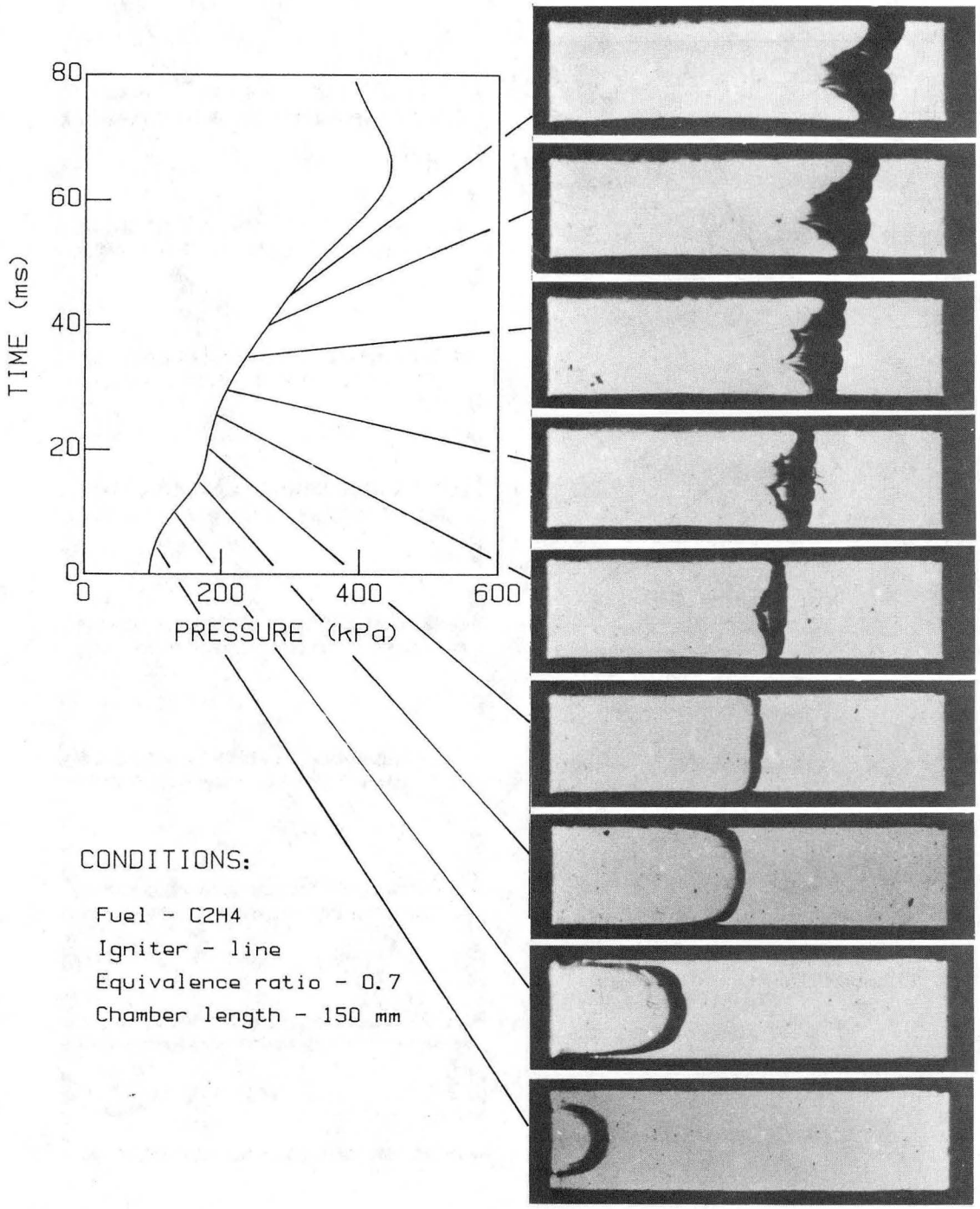

Figure 4-14. Flame shape and pressure history during constant volume combustion. Equivalence ratio = 0.7.

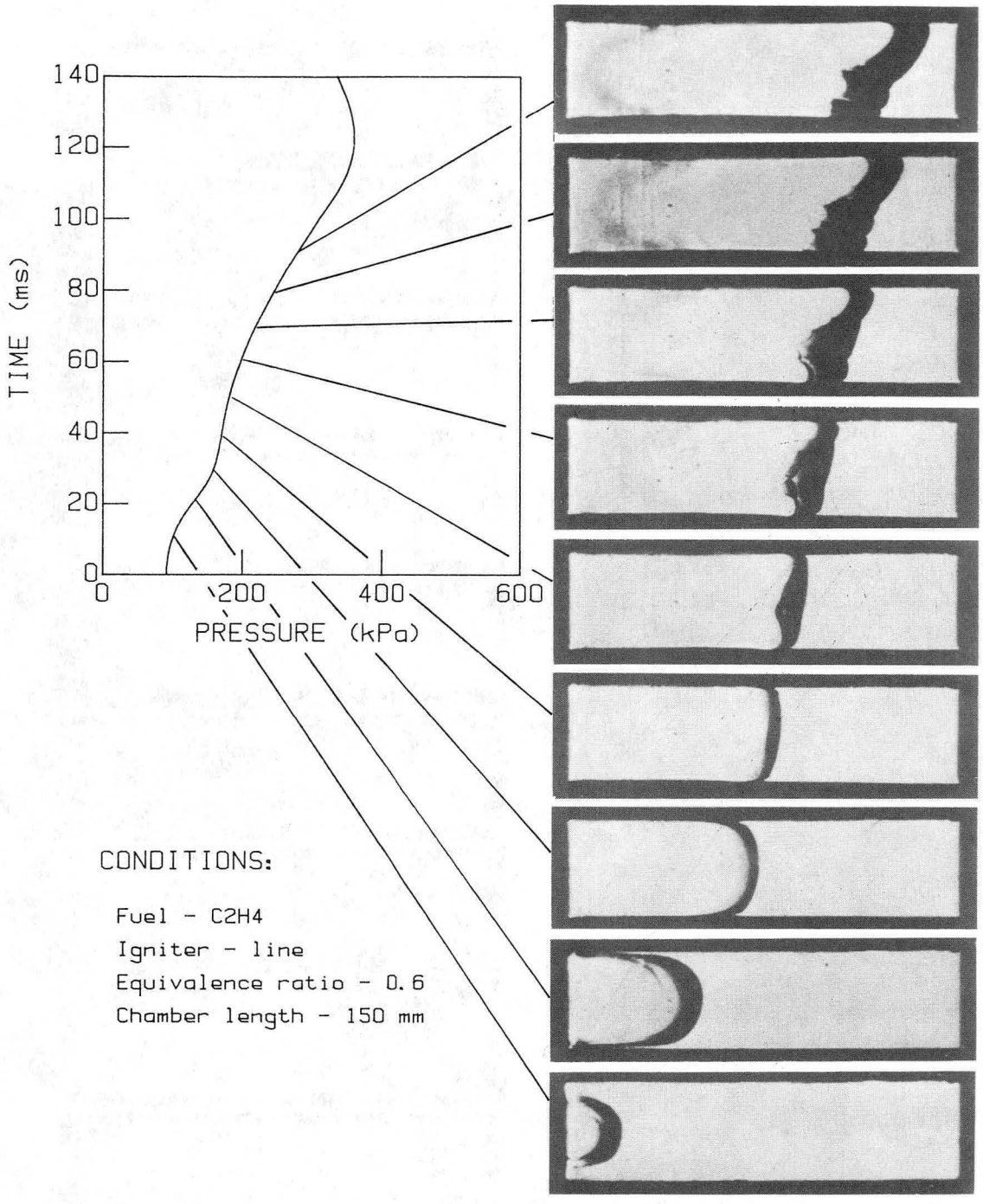

Figure 4-15. Flame shape and pressure history during constant volume combustion. Equivalence ratio = 0.6.

For leaner mixtures, both the kink in the pressure curve and the "tulip" formation occurs later in time and is spread over a longer period, appearing less pronounced. The basic "tulip" shape, however, is unaffected. There is more small scale turbulent structure in the faster burning, higher equivalence ratio ethylene/air flames, Figures 4-12 and 4-13. In the very slow burning mixture, Figure 4-15 (equivalence ratio = 0.6), the effects of buoyancy become apparent, as the flame billows toward the top of the combustion vessel during the latter stages of the propagation. The equivalence ratio has a significant effect on the time scale of the combustion process and "tulip" phenomenon. The general behavior of the "tulip" flame formation, however, shows little dependence on equivalence ratio or, equivalently, laminar flame speed.

A comparison between a methane/air flame and an ethylene/air flame with an equivalent laminar burning speed helps separate the effect of laminar flame speed from the effect of fuel type. An ethylene/air flame with equivalence ratio 0.7 has a laminar flame speed comparable to the laminar flame speed of a stoichiometric methane/air flame. The pressure traces from the two cases are shown in Figure 4-16 and are very similar. Both cases show the the kink indicative of "tulip" formation at nearly the same time and pressure. The actual "tulip" in the methane/air case, Figure 4-6, is slightly more pronounced than the "tulip" in the ethylene/air flame, Figure 4-14. The ethylene/air flame has more small scale structure suggestive of the spontaneous instabilities

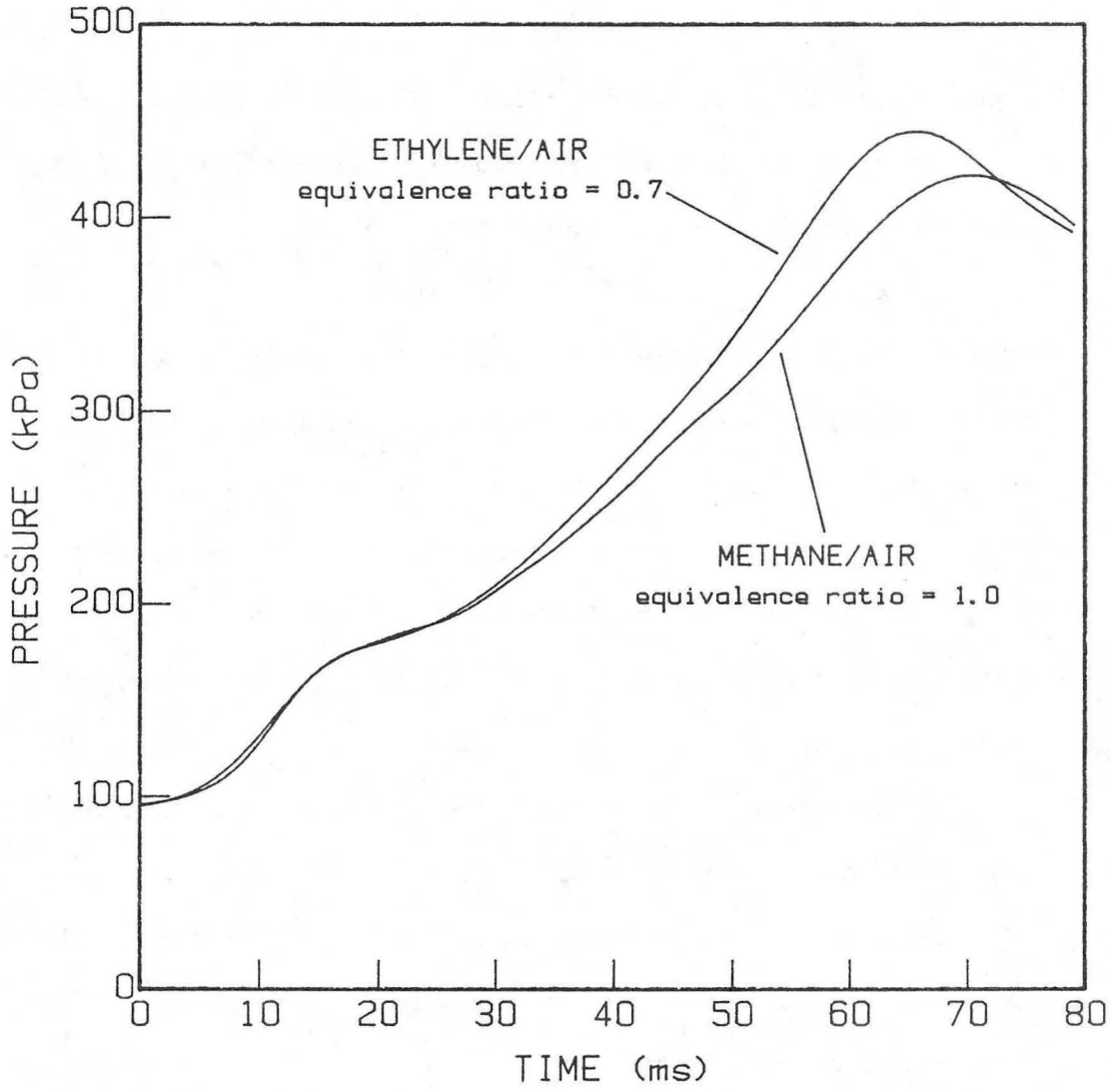

Figure 4-16. Comparison between pressure histories of methane/air combustion (equivalence ratio = 1.0) and ethylene/air combustion (equivalence ratio = 0.7) with similar laminar flame speeds.

described in Chapter 1. The small scale flame regions have orientations which generate strong schlieren effects. These effects obscure the forward edge of the "tulip" cusp. The "tulip" phenomenon is still apparent, however, from the trailing edge of the flame. Except for these slight differences, there is little effect of fuel type on the "tulip" flame formation. This result, and the results of Ellis (1928) with carbon monoxide/oxygen flames, suggest that the "tulip" flame formation is virtually independent of chemistry.

The third group of schlieren sequences, Figure 4-17 to Figure 4-20, consists of further qualitative observations of the "tulip" flame. The first sequence, Figure 4-17, shows a top view (X-Z) of a line ignited methane/air flame. The ignition is fairly uniform except for the region very near the wall. Despite the uniform shape just after ignition, the flame assumes a "tulip" form from this orientation just as when viewed in the X-Y plane. In this case the cusping begins near the vessel sidewalls, and the "tulip" grows from these smaller cusps. The second sequence, Figure 4-18, shows both views of a two-point ignited methane/air flame. In the X-Z projection, two flame kernels are distinguishable. The kernels grow together until they join at the centerline of the duct. The rapid flame area reduction accompanying the "tulip" occurs in part due to the coalescing of the two individual flame fronts rather than due to only a wall quench phenomenon. A "tulip" forms following the rapid reduction in flame area as before. In the X-Y projection

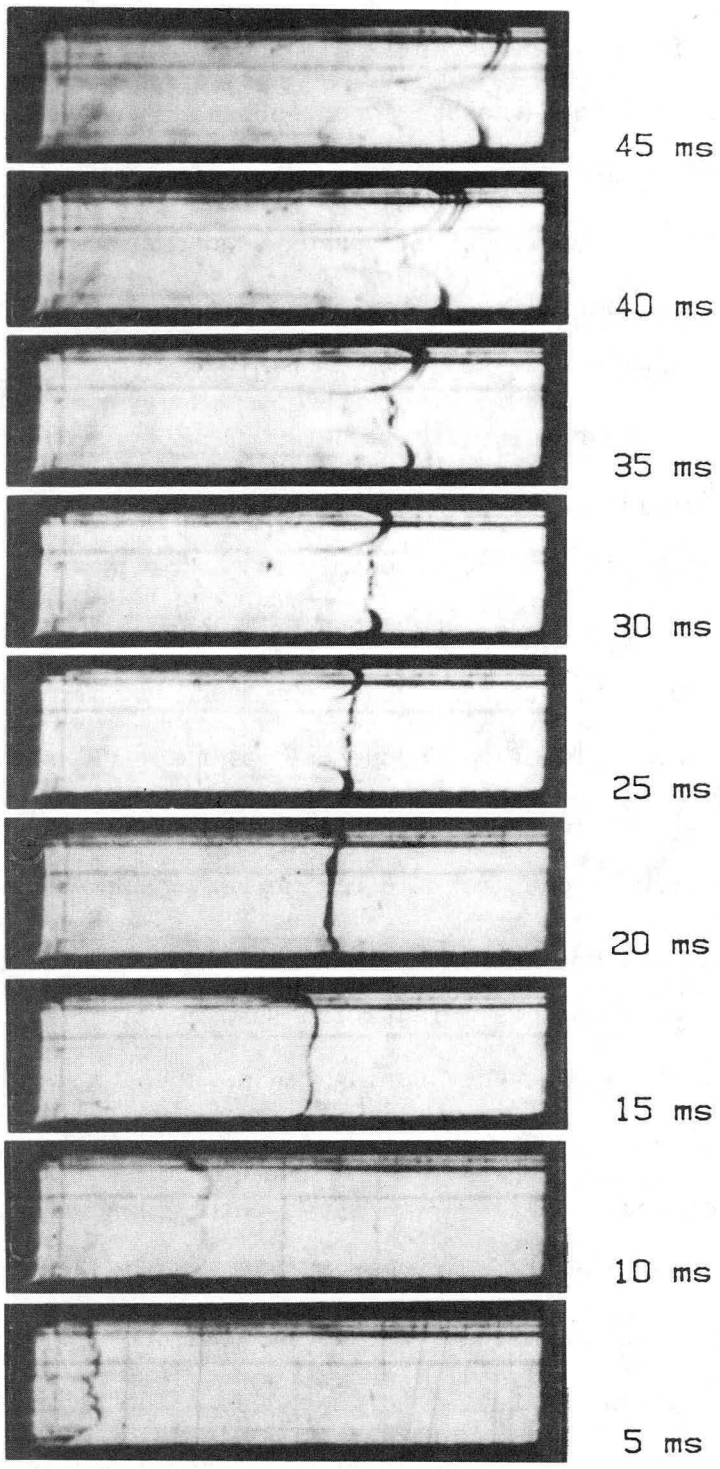

Figure 4-17. Top (X-Z) view of stoichiometric methane/flame initiated by a line igniter in a plexiglas combustion vessel. Despite the early nearly planar form, the "tulip" still forms during the latter stages of combustion.

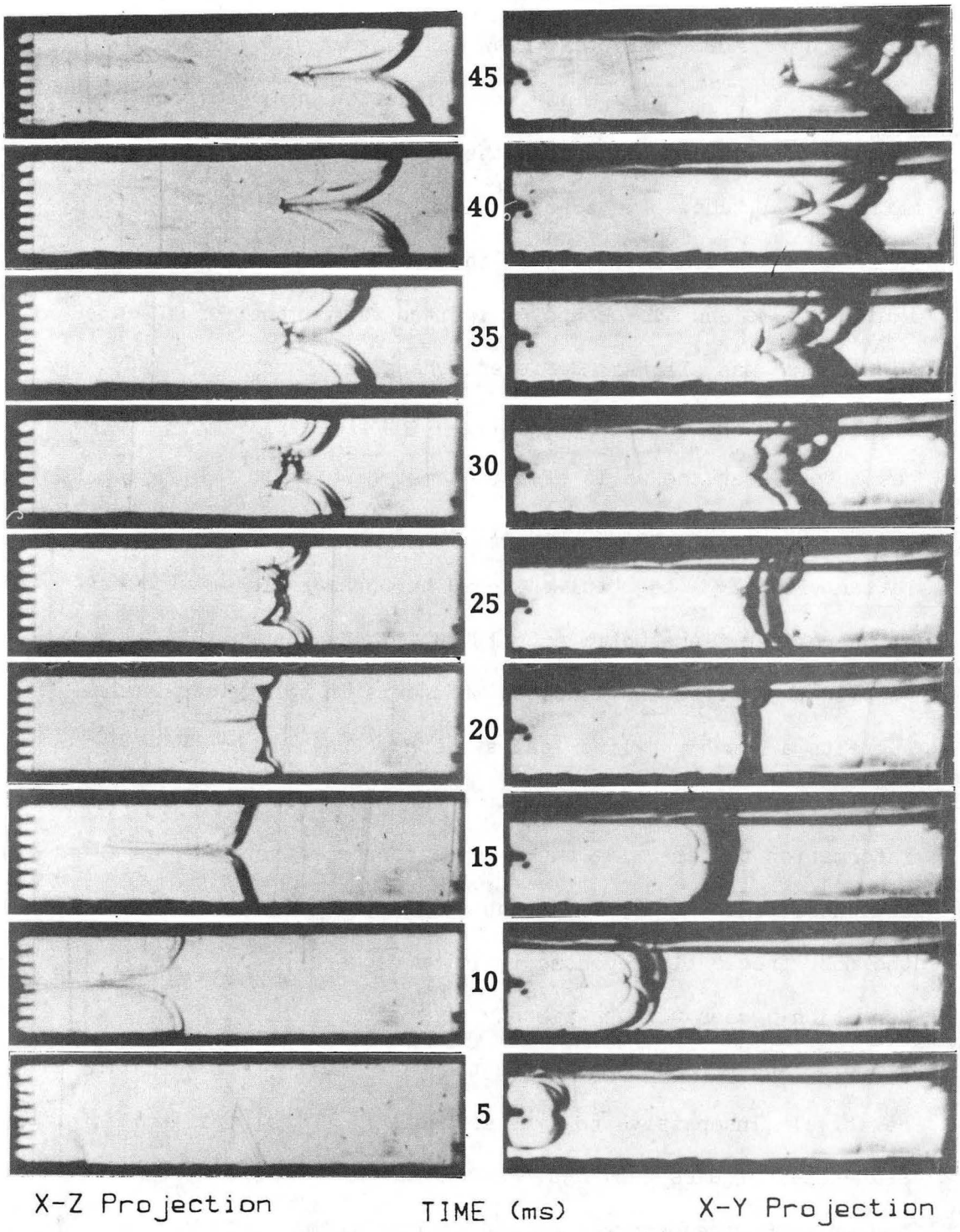

Figure 4-18. Two views (X-Z and X-Y) of two point initiated stoichiometric methane/air flame in a plexiglas combustion vessel. The "tulip" forms in both views.

the two-point ignited flame behaves nearly identically with the line ignited flame. In this view wall quench is clearly responsible for a rapid flame area reduction prior to the "tulip" formation. The dark line near the top of the vessel is the fresh mixture fill tube. The tube has little effect on the flame and is left in for convenience. In the X-Z view of both the line ignited flame and the two-point ignited flame, the formation of the "tulip" has slightly different character than the "tulip" formation in the X-Y projection. In the former view, two small cusps form near the walls of the chamber, which then burn toward the center of the chamber finally forming a full "tulip". In the latter view (X-Y) the "tulip" seems to be drawn from the center of the planar flame until a full "tulip" cusp is achieved. Despite this difference the "tulip" forms in both views, which suggests a roughly cylindrical symmetry (the duct corners complicate the shape to some extent but there is insufficient information to determine the precise corner effects). The third sequence, Figure 4-19, shows the single point ignition, which is the most frequently reported ignition geometry. The "tulip" formation agrees with previously reported results.

The above results indicate that the "tulip" formation is relatively insensitive to igniter geometry. The final schlieren sequences, Figures 4-20 and 4-21, show the effect of a large leak and an odd-shaped endwall on the "tulip" formation. The exhaust valve is left open during the ethylene/air (equivalence ratio = 0.9) flame propagation shown in Figure 4-20. The "tulip" forms

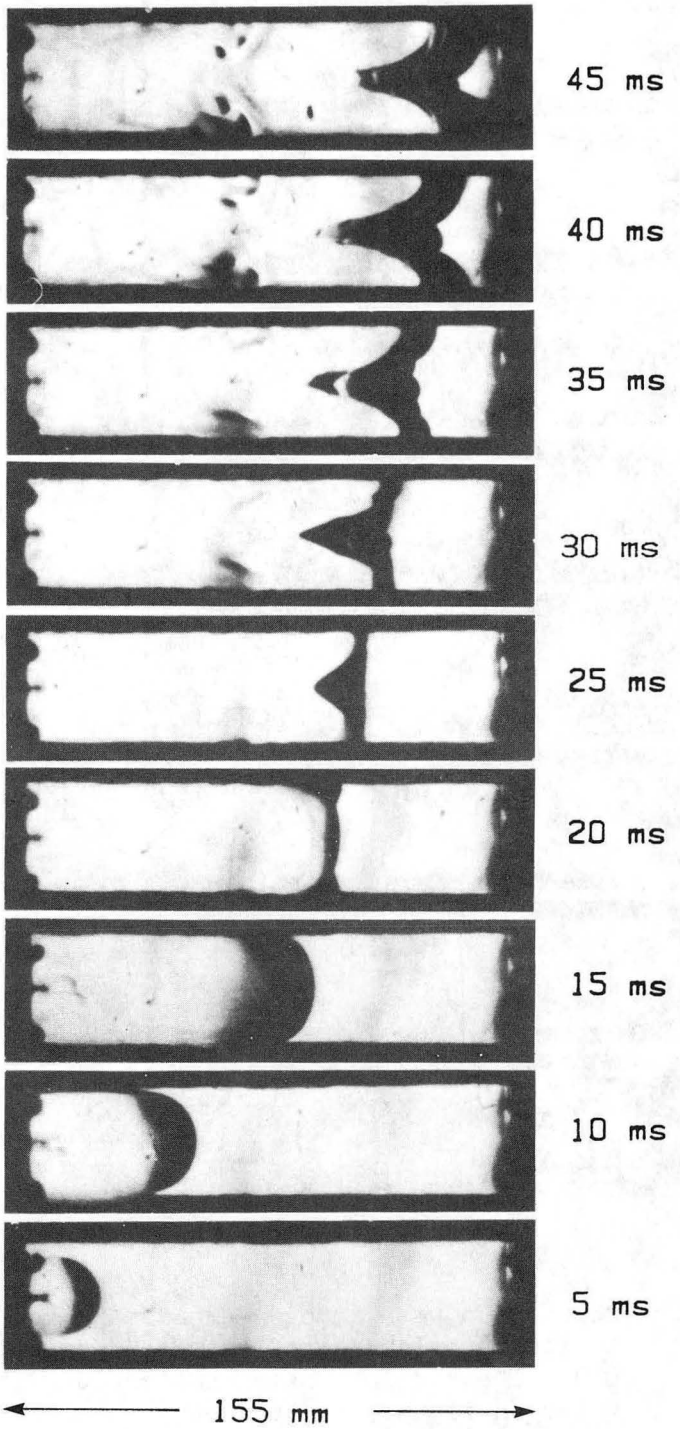

Figure 4-19. "Tulip" flame formation in a single-point ignited stoichometric methane/air flame in a plexiglas combustion vessel.

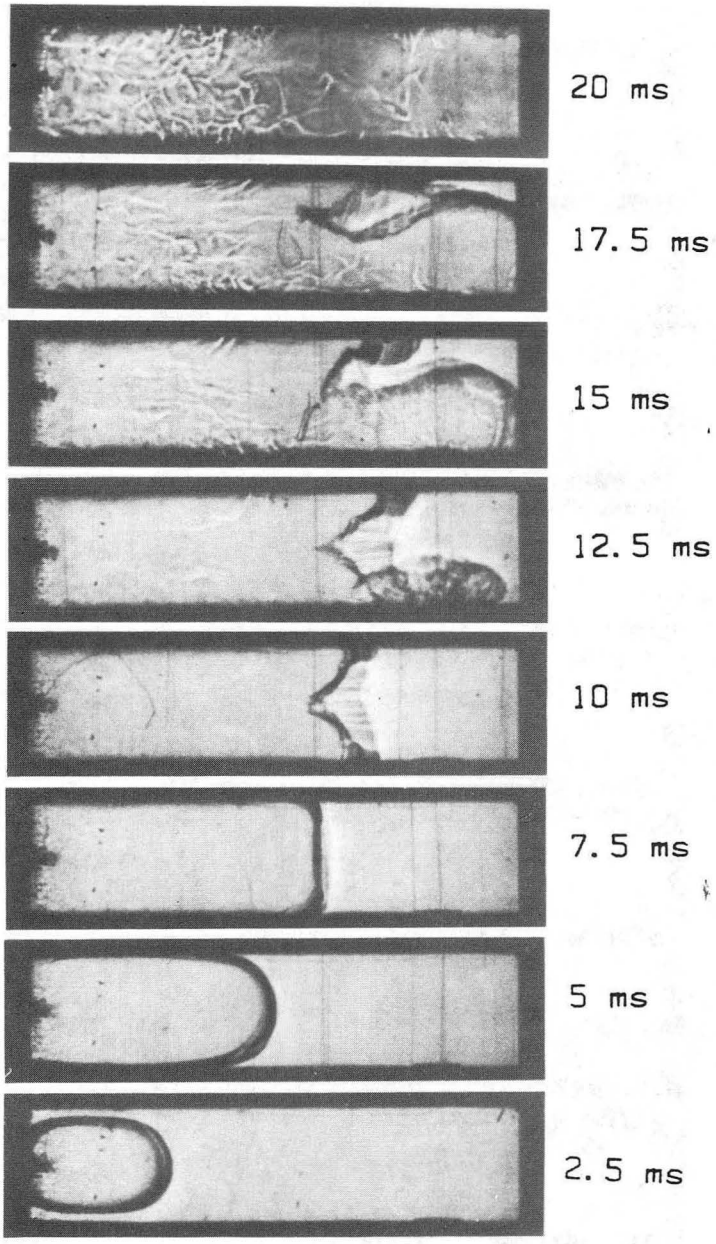

Figure 4-20. Combustion with an open exhaust valve. Line ignited ethylene/air flame with equivalence ratio 0.9. The "tulip" forms unaffected by the open valve until the "tulip" petal burns into the valve generating a combustion jet.

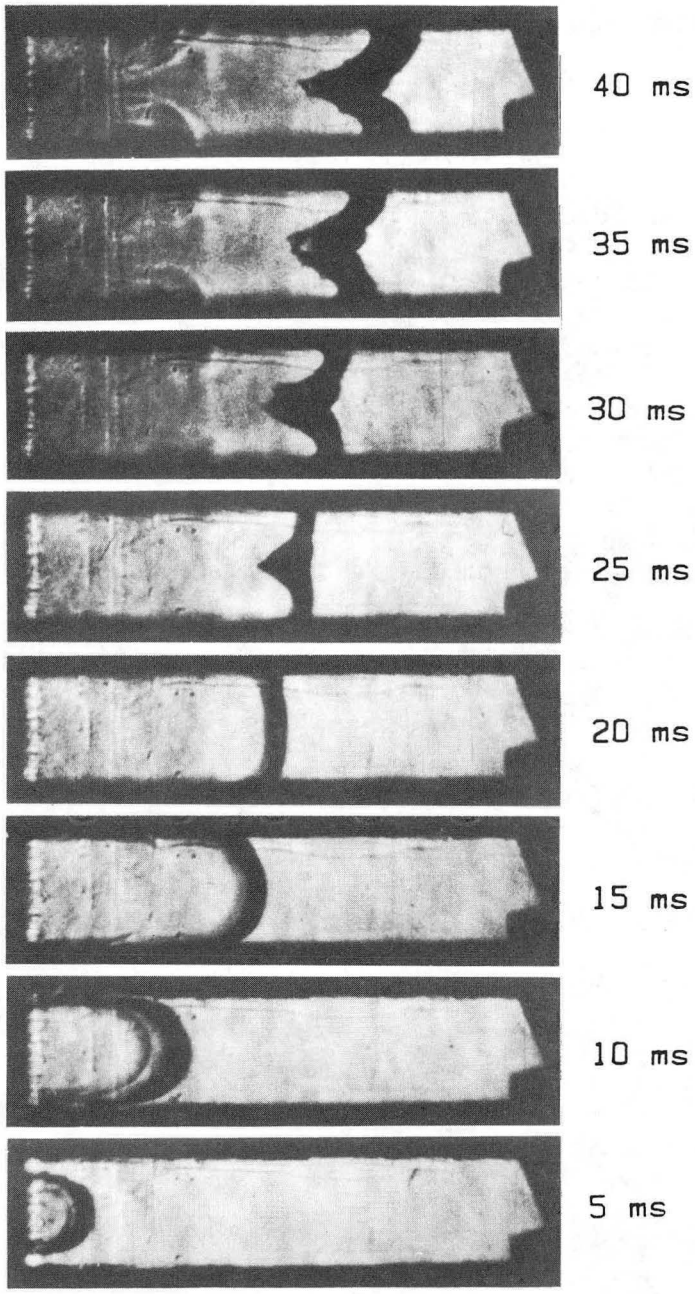

Figure 4-21. Stoichiometric methane/air flame initiated by a line igniter. Combustion vessel has a non-planar endwall (length of vessel = 185 mm). The "tulip" forms as in planar endwall cases.

just as in the completely sealed case until the flame reaches the open valve. Once the lip of the "tulip" burns into the valve, a turbulent combustion jet is formed there, and a turbulent combustion front explodes into the unburned gas. The non-planar endwall has no noticeable effect on the stoichiometric methane/air flame shown in Figure 4-21. The endwall geometry and mass loss do not appear to affect the "tulip" formation.

4.5 Summary

The results obtained from qualitative observations of the "tulip" formation and concurrent pressure measurements are summarized below:

1) The "tulip" formation begins simultaneously with the rapid decrease in flame area (and the coincident drop in rate of pressure rise, dp/dt) as the flame quenches at the sidewalls of the combustion vessel.

2) As the drop in dp/dt becomes more pronounced, the "tulip" shape also becomes more pronounced.

3) The "tulip" is less pronounced in shorter combustion vessels.

4) The time of the flame quench at the sidewalls of the chamber and of "tulip" formation depends on the equivalence ratio (or equivalently the laminar flame speed) of the mixture and is nearly independent of the length of the chamber.

5) Ethylene/air flames have more small scale turbulent structure than methane/air flames.

6) The "tulip" flame has roughly cylindrical symmetry (except in the duct corners where the flame shape is uncertain).

7) For very slowly burning mixtures buoyancy noticeably affects the flame shape.

8) The formation of a "tulip" flame is independent of igniter geometry.

9) The formation of the "tulip" is not noticeably affected by mass loss or endwall geometry.

The qualitative aspects of "tulip" flames in closed tubes described above are in accord with the discussions of cusp (or "tulip") flames found in the literature. Unfortunately, the qualitative results do not provide the cause of the "tulip" formation. The results indicate a strong connection between the pressure inside the combustion vessel and the flame shape, but there appears to be no causal relationship between the pressure and the "tulip" formation. The connection is, however, discussed in the next chapter.

CHAPTER 5

The Relationship Between the Chamber Pressure and the Flame

5.1 Analytical discussion

Closed volume combustion is particularly convenient for exploiting the relationship between the pressure rise in the vessel and the dynamics of the flame propagation. In closed volume combustion it is reasonable to assume a linear relationship between pressure rise and mass burned (Lewis and Von Elbe, 1961),

$$(p - p_o)/(p_f - p_o) = m_b/m_o, \tag{5.1}$$

where m is the mass and p represents the chamber pressure. The subscripts o, f, b represent initial conditions, final conditions, and burned gas respectively. Differentiating the above equation with time leads to,

$$(1/(p_f - p_o))(dp/dt) = (1/m_o)(dm_b/dt). \tag{5.2}$$

A second relationship between the mass burning rate and the pressure in the combustion vessel is obtained by rearranging the definition of the laminar flame speed (Equation 1 from Chapter 3),

$$dm_b/dt = \rho_u S_u a_f. \tag{5.3}$$

The assumption of isentropic compression of the unburned gas,

$$p/p_o = (\rho/\rho_o)^{\gamma}, \tag{5.4}$$

allows the chamber pressure to replace the unburned gas density in Equation 5.3,

$$dm_b/dt = \rho_o(p/p_o)^{(1/\gamma)}S_u a_f. \tag{5.5}$$

A relationship between the flame area and the pressure can be found by equating and rearranging the two above equations for mass burning rate,

$$a_f = [(m_o/\rho_o)(1/(p_f - p_o))S_u](p/p_o)^{(-1/\gamma)}(dp/dt). \tag{5.6}$$

If the flame speed is constant, the entire bracketed term is constant, and the flame area can be determined from the rate of pressure rise and the instantaneous pressure in the vessel.

5.2 Universal pressure scaling

The qualitative similarity in shape of the pressure curves of the ethylene/air flames and the methane/air flame in the 150 mm vessel with line ignition (Chapter 4) suggests that a time scaling law may be appropriate. Figure 5-1 shows dimensional and non-dimensional pressure/time traces for six ethylene/air flames and one methane/air flame. The pressure rise $(p - p_o)$ is scaled by the total pressure rise $(p_f - p_o)$ and the time is scaled by the time to maximum pressure. The time to maximum pressure is approximately the total combustion time, T_c. The ordinate is simply the mass burned fraction as defined in

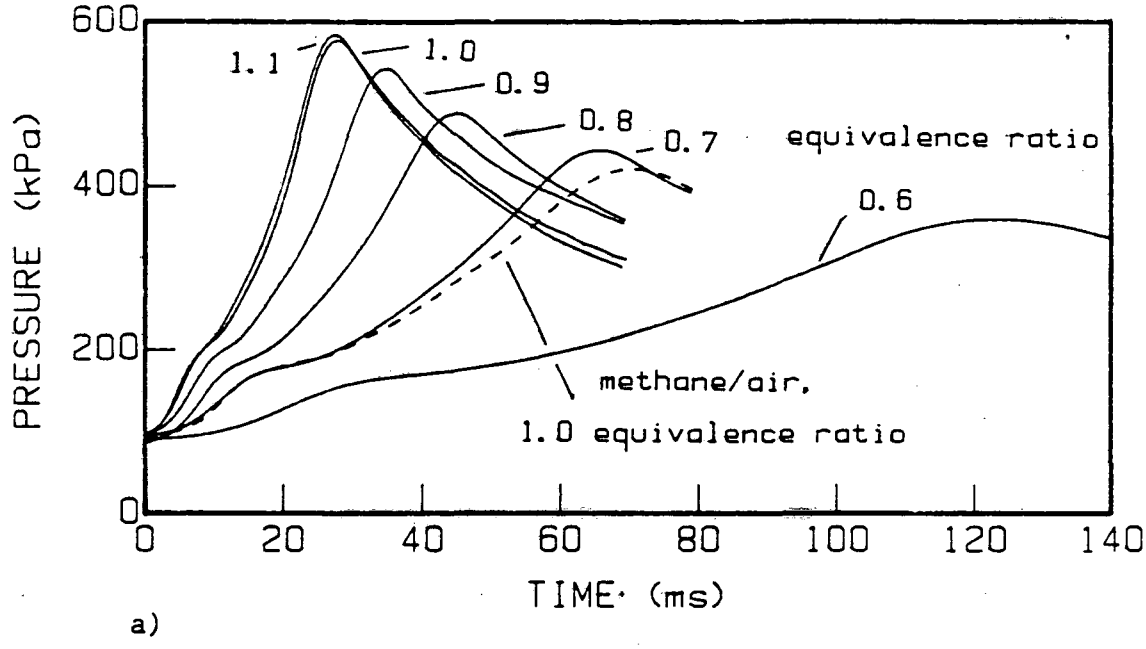

a)

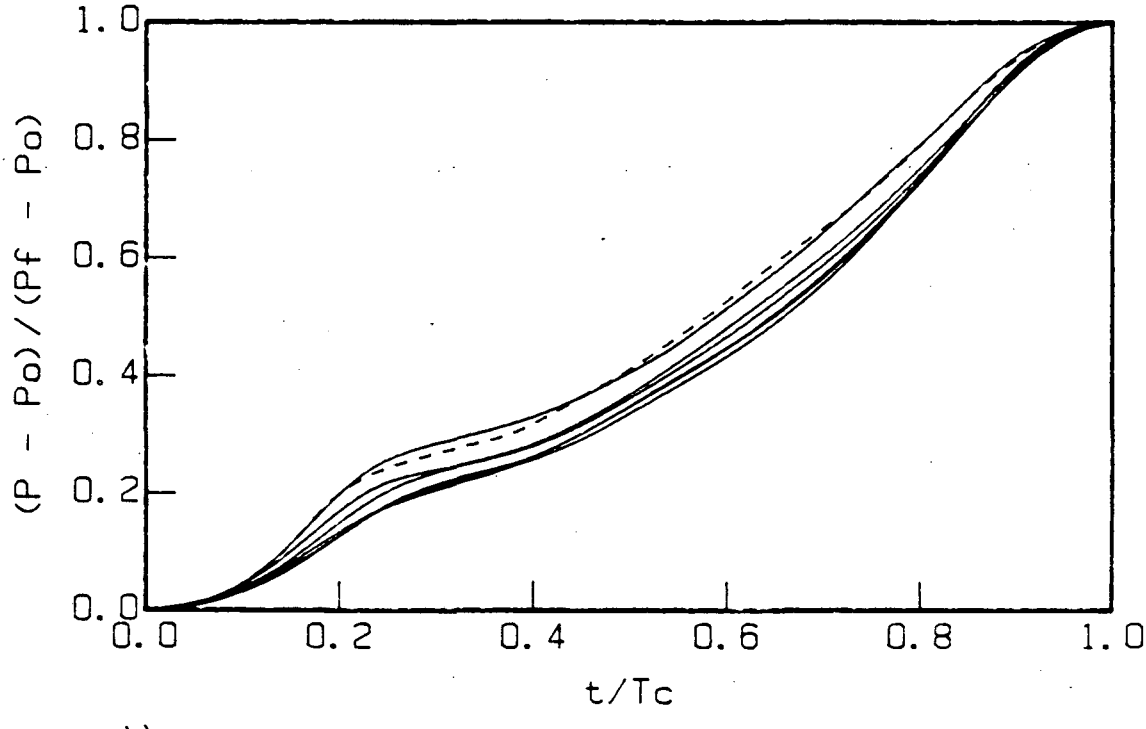

b)

Figure 5-1. Comparison between dimensional and non-dimensional pressure histories of closed tube combustion in 150 mm length chamber. Mixtures have different equivalence ratios and laminar flame speeds.
a) Dimensional pressure histories
b) Non-dimensional pressure histories

Equation 5.1. The laminar flame speed, S_u, is the most influential physical property associated with the total combustion time. Normalizing by the laminar flame speed can be justified as follows:

$$(1/m_o)(dm_b/dt) = (1/(p_f - p_o))(dp/dt) = (\rho_u/\rho_o)S_u a_f/V_o, \quad (5.7)$$

where V_o is the volume of the combustion vessel. The time derivative when non-dimensionalized by the total combustion time is,

$$(1/(p_f - p_o))(dp/d(t/T_c)) = [\rho_u/\rho_o]T_c S_u a_f/V_o. \quad (5.8)$$

The left side of the equation is simply the slope of the curves shown in Figure 5-1. From the similarity of these curves the left side of the equation does not change between cases. Consequently the right side of the equation must not change between cases either. The term (ρ_u/ρ_o) as a function of reduced time (t/T_c) is approximately constant between cases. This term actually varies by a maximum of 30 percent. S_u and T_c vary for the different cases but their product must be constant to produce the universal scaling shown in the figure,

$$S_u T_c = \text{constant}. \quad (5.9)$$

The product of the laminar flame speed and the total combustion time for several ethylene/air flames with different equivalence ratios are shown in Figure 5-2. The laminar flame

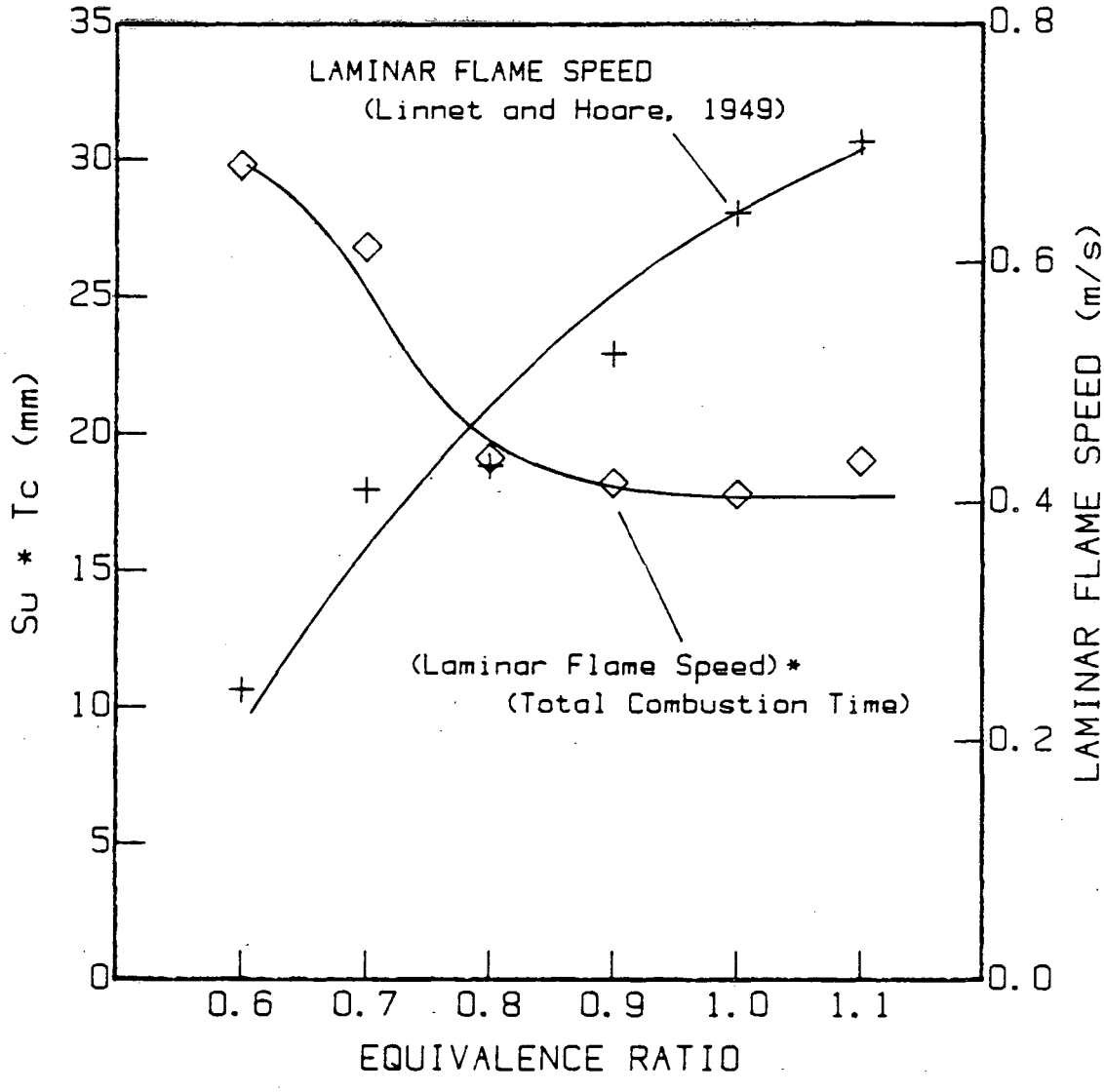

Figure 5-2. Variation of the product (laminar flame speed x total combustion time) with equivalence ratio in ethylene/air flames. Also shown is the laminar flame speed from Linnet and Hoare (1949).

speed for the ethylene/air mixtures comes from Linnet and Hoare (1949). The assumption of a constant value for the product appears reasonable except for the leaner mixtures (equivalence ratio = 0.6 and 0.7). Based on the above analysis, the flame area as a function of reduced time for equivalence ratios greater than 0.7 must not change between cases. The discrepancy for equivalence ratios 0.6 and 0.7 is not large (approximately 25%), and may be due to inaccuracies in the flame speed measurements for these slower burning mixtures. It is not uncommon for the scatter in flame speed measurements to exceed 30% (Andrews and Bradley, 1972). The approximately constant value for $S_u T_c$ suggests that the flame passes through similar shapes for all equivalence ratios, and that the absolute time of the shape changes varies according to the laminar flame speed of the mixture. Mixtures with similar laminar flame speeds should show the same flame shape histories as well as pressure/time histories. The similarity between flame shape histories of a methane/air flame (equivalence ratio = 1.0, $S_u \approx 0.35$ m/s, Figure 4-6) and an ethylene/air flame (equivalence ratio = 0.7, $S_u \approx 0.40$ m/s, Figure 4-14) with similar laminar flame speed was shown in Chapter 4. The similarity of the pressure traces for these two cases was shown in Figure 4-16.

When the scaling described above is applied to the methane/air flames in chambers of different lengths, there is no apparent similarity between the scaled pressure/time

curves, Figure 5-3. The chamber length, contrary to fuel type, and equivalence ratio, has a significant effect both on the time scale of the combustion and on the basic flame shape history of an enclosed tube flame. The effect on the flame shape history is clearly shown in the schlieren sequences of Figures 4-6 to 4-10. The universal scaling of pressure and flame shape is limited to combustion vessels of the same length. The geometry of the combustion vessel, therefore, plays a significant role in the formation of the "tulip" flame. The vessel geometry may act on the flame through the modification of the in-chamber flow field. The next chapters explore the role of combustion generated flow on the "tulip" formation.

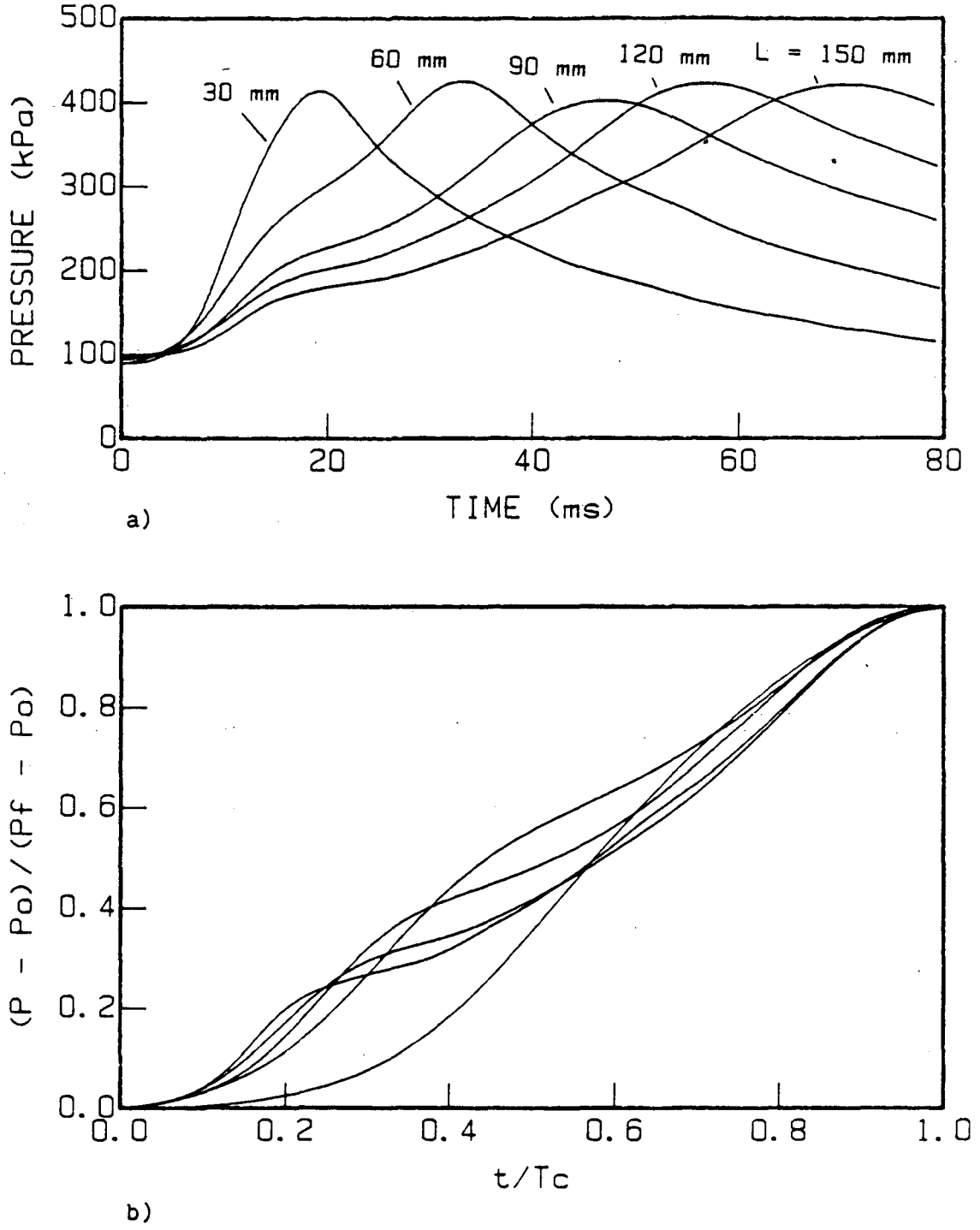

Figure 5-3. Comparison between dimensional and non-dimensional pressure histories of closed tube combustion in different length chambers. All cases are stoichiometric methane/air.
a) Dimensional pressure histories
b) Non-dimensional pressure histories

CHAPTER 6

Gas Velocity During Closed Tube Combustion

6.1 Introduction

The qualitative experiments discussed in Chapter 4 are unable to determine conclusively the cause of the "tulip" flame. The second set of experiments, using laser Doppler anemometry, examines combustion driven flow during nonsteady flame propagation in a closed duct. Further, the role, if any, of combustion driven circulation in the formation of the "tulip" flame is explored.

6.2 Apparatus

The experiment, Figure 6-1, uses the plexiglas combustion vessel, Figure 4-4b and the two-point igniter, Figure 4-5b, described previously. The combustible gas is restricted to a stoichiometric mixture of methane/air. A laser Doppler anemometer (LDA) measures the axial component of velocity (X-direction) at various points along the duct centerline during the combustion event. A modification of the rotameter gas mixing device used in the qualitative experiments allows the introduction of LDA seed particles into the combustion vessel along with the combustible premixture.

The LDA set-up is similar to that described by Cheng and Ng (1983). A 4-watt argon-ion laser operated at 514 nm is used. The LDA probe is formed with a beam splitter of 50 mm fixed separation and a 250 mm focal length lens. It is arranged to

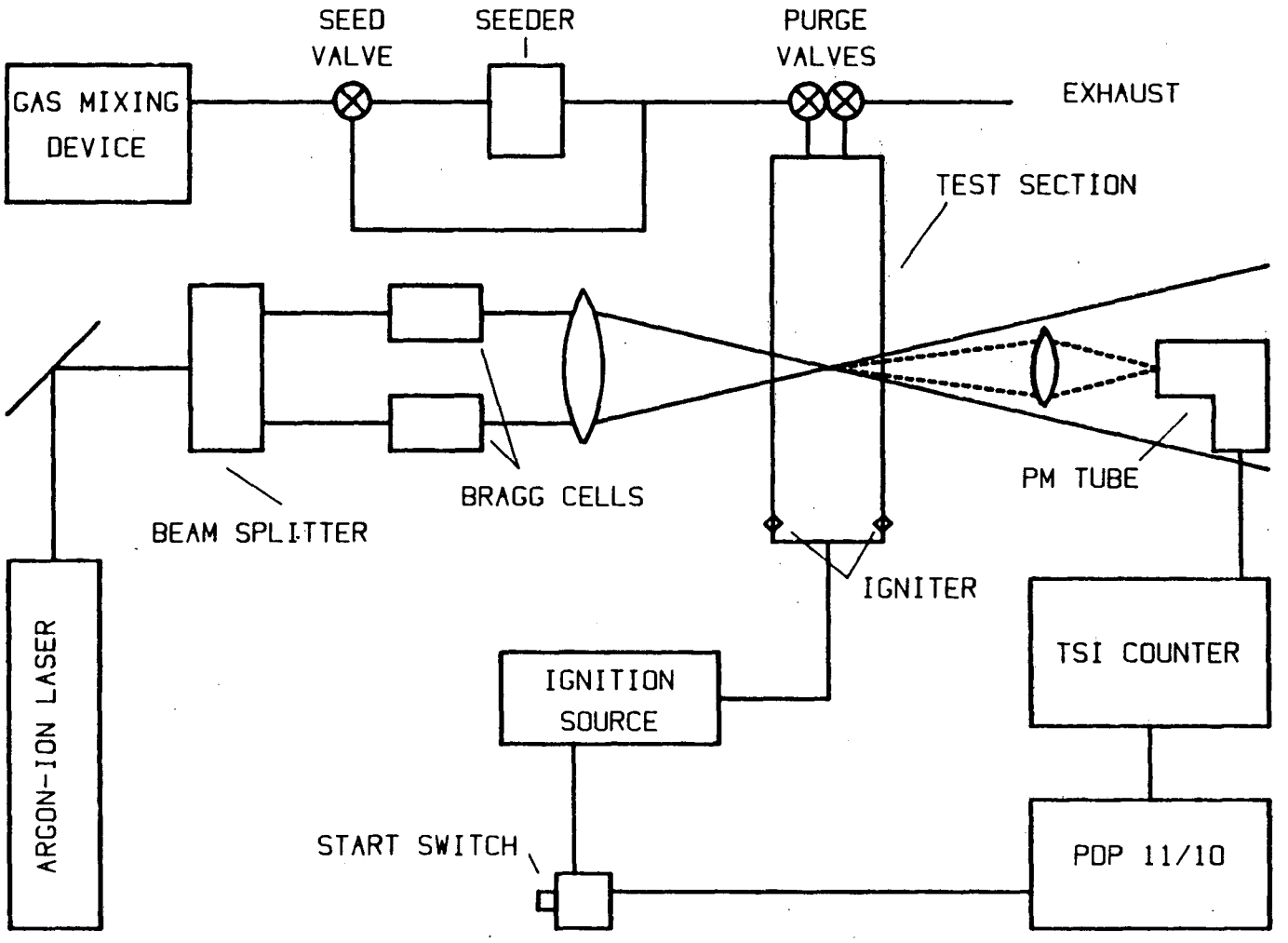

Figure 6-1. Schematic of experimental apparatus used to measure axial velocity of gas during closed tube combustion.

measure the axial component of velocity, V. The two beams are frequency shifted by Bragg cells to remove directional ambiguity. The differential frequency is 2 Mhz. The optical collection system includes a lens, filter and photomultiplier tube placed in the forward scatter direction. Doppler scattering sites are provided by 0.3 micrometer aluminum oxide particles introduced into the inlet methane/air flow by a spouted bed seeder. A TSI 1980A frequency counter (fixed exponent = 4, 8 cycles/burst, multiple validations/particle, 2% error, low filter = 100 khz, high filter = 10 Mhz) analyzes the Doppler signal. An analog to digital converter and a PDP 11/10 mini-computer digitize and record the analog output of the counter.

6.3 Methodology

The duct is purged with fresh mixture for a time sufficient for 20 complete changes of contents as before. The LDA seed is introduced only during the latter stages of the purging process to limit particle deposition on the chamber walls. After purging, all valves are closed and the gas motion is allowed to subside. The mixture is ignited when the counter output is consistent with zero velocity and a visual check of the movement of seed particles near the LDA probe volume verifies a nearly quiescent initial state.

The ignition source simultaneously initiates combustion and triggers the data acquisition system. The analog LDA output is digitized at 30 khz from t = 0 (the time of ignition) to t = 250 ms. Measurements are taken along the central axis of the

chamber at 10 mm increments from X = 20 mm to X = 140 mm, Figure 6-2. The measurement is repeated five times at each location to determine the run-to-run variations.

The high-speed schlieren movies presented in Chapter 4 determine the flame arrival at particular measurement locations. The movies are taken from two perpendicular planes (X-Y and X-Z) to expose the effect of two-point ignition. Schlieren sequences from these high-speed movies were presented in Figure 4-19.

6.4 Data reduction

The digitized counter output must be analyzed to extract the true validated velocity measurement. The extraction is required because the LDA counter validations occur at random intervals while the LDA output signal is sampled at a constant rate. An indication of a new validation and the critereon for extraction is that a recorded value differ from the preceding point by more than the expected uncertainty in the A/D converter. Data points showing exceedingly large deviations associated with noise are not selected. The digitized counter output and the extracted data from a typical experiment are compared in Figure 6-3.

A cubic spline smoothing routine based on the algorithm of Reinsch (1967) is used to fit the extracted data points. Figure 6-4 shows individual validated measurements (dots) and a smooth spline fit (solid). Also noted in the figure are three characteristic features of the velocity/time records which will be discussed later: the maximum velocity reached after ignition,

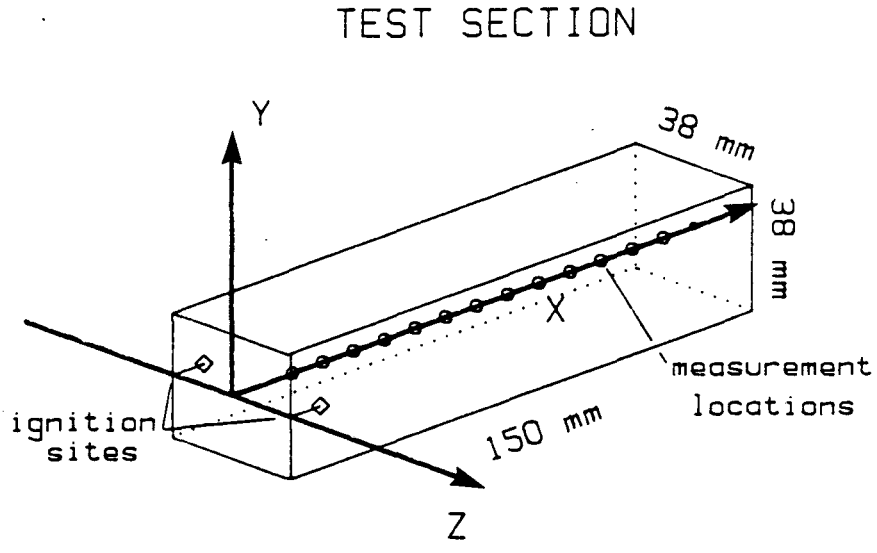

Figure 6-2. Coordinate layout of combustion vessel and the location of laser Doppler anemometer measurement points.

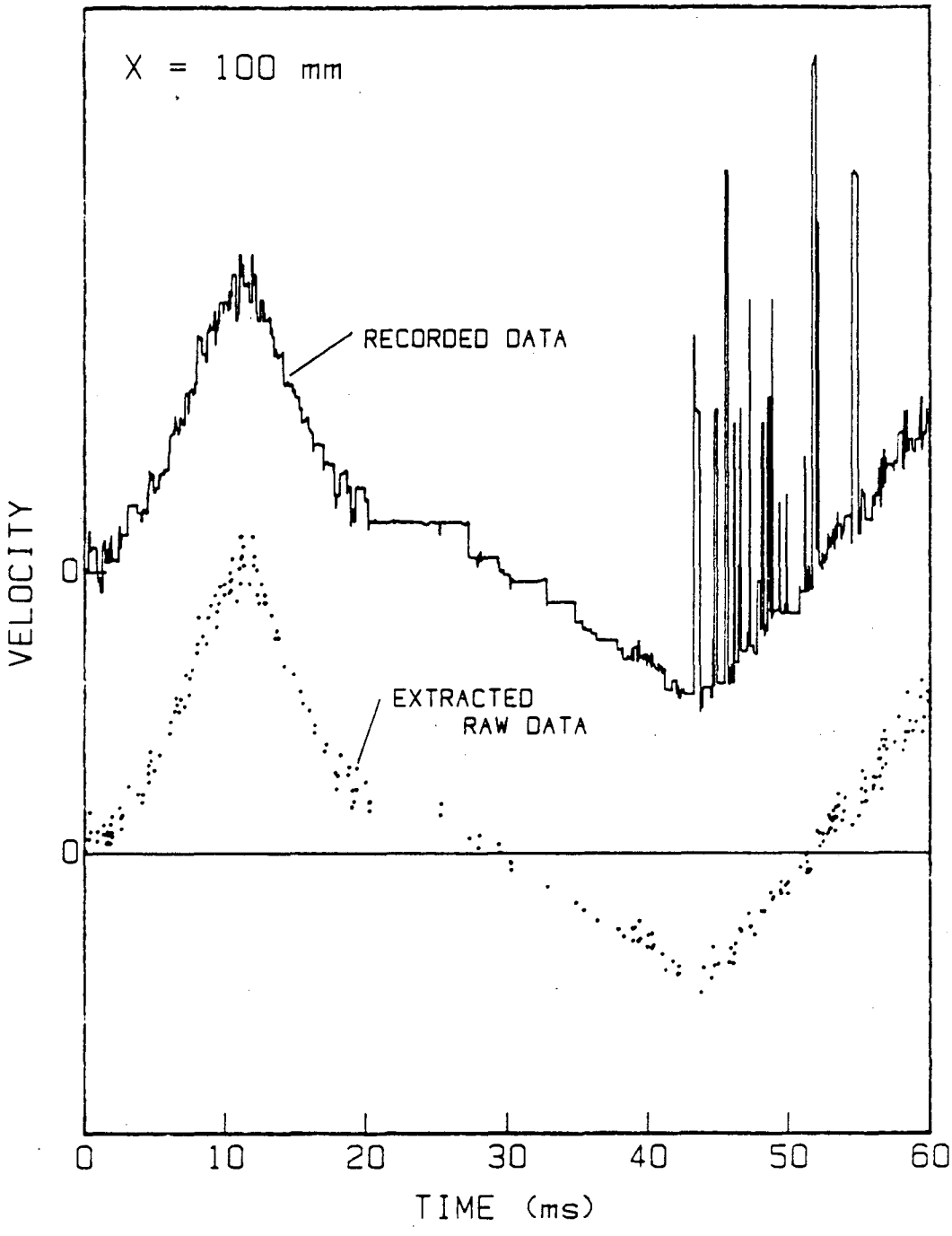

Figure 6-3. Comparison between the recorded digitized LDA signal and the extracted raw data points.

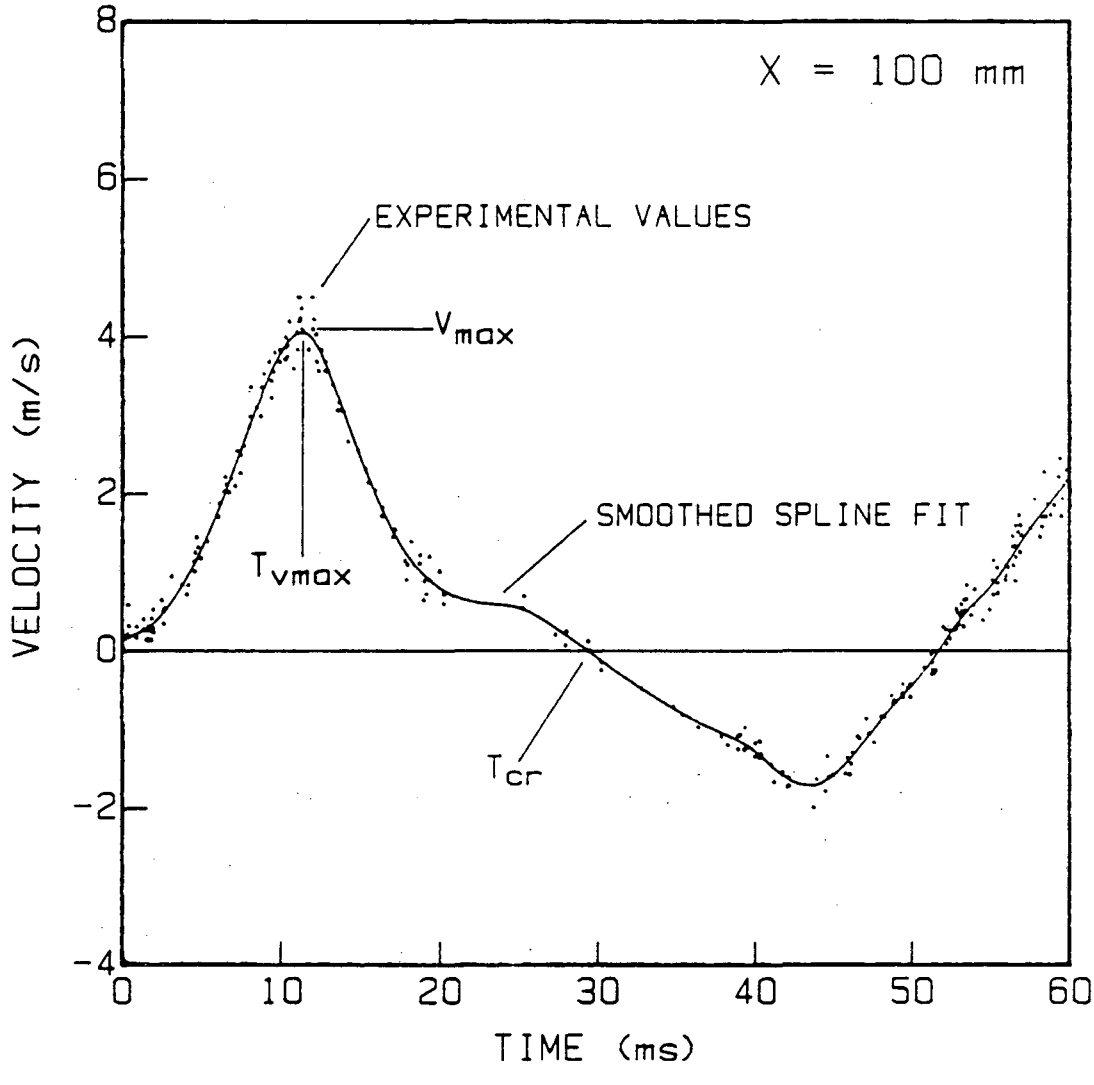

Figure 6-4. Comparison between the extracted raw data points and the smooth spline fit to these points. Also shown is the nomenclature used to describe the velocity curves. T_{vmax} is the time of maximum velocity. V_{max} is the maximum velocity. T_{cr} is the time that the velocity crosses zero.

V_{max}, the time at which this maximum occurs, T_{vmax}, and the time of the first velocity zero crossing, T_{cr}.

Each experiment produces a different spline fit. All fits for a single measurement location are averaged to produce a representative curve for that location, Figure 6-5a. The scatter in the smooth curves reproduces the run-to-run scatter of the raw data. The run-to-run scatter is represented by the standard deviation of the individual smooth curves about the representative average curve, Figure 6-5b. There is very little run-to-run variation for data taken at X > 80 mm. There is larger run-to-run variation for data taken at X < 80 mm, Figure 6-6, but all measurements are reproducible until some time after the first velocity zero crossing, T_{cr}. Typical uncertainties associated with the LDA technique are less than 1 percent of the measured velocity (Pitz, 1971). This uncertainty is insignificant compared to the run-to-run variability of the experiment.

High-speed schlieren movies provide flame trajectories at the centerline of the duct. The time of flame arrival is denoted T_f. Flame position, X_f, is taken as the flame location at the duct centerline. The centerline flame trajectories from both viewing directions (X-Y and X-Z) are shown in Figure 6-7. The discrepancy in the two trajectories for t < 15 ms is due to the two-point ignition. The X-Y movie shows two separate flame kernels growing toward the duct center and coalescing into a single front at t = 15 ms. The centerline flame position is not

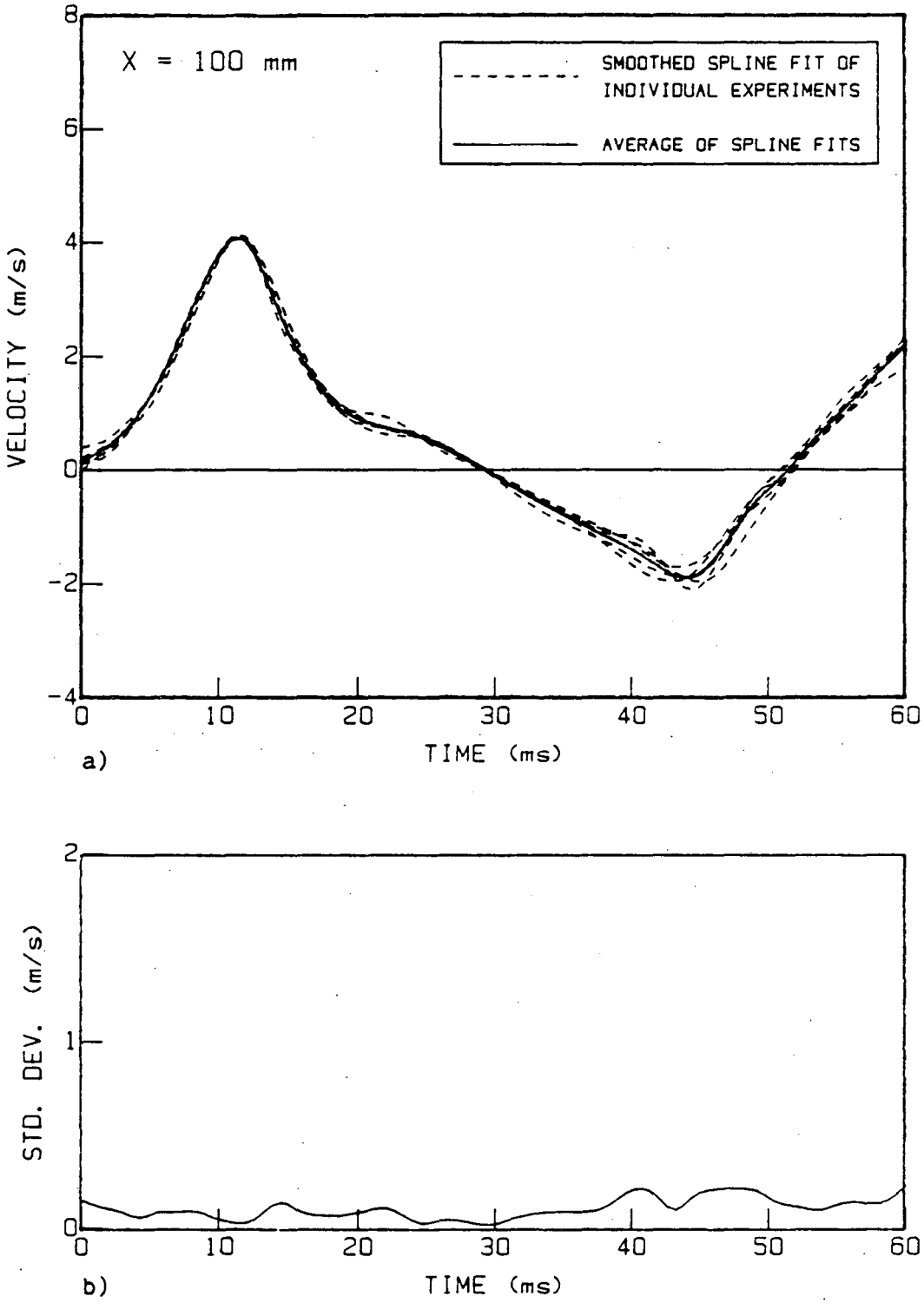

Figure 6-5. Comparison between smooth spline fits of individual experiments and the average of these fits. Result is typical of measurements taken for X > 70 mm.
a) Smooth splines and average
b) Standard deviation about the average

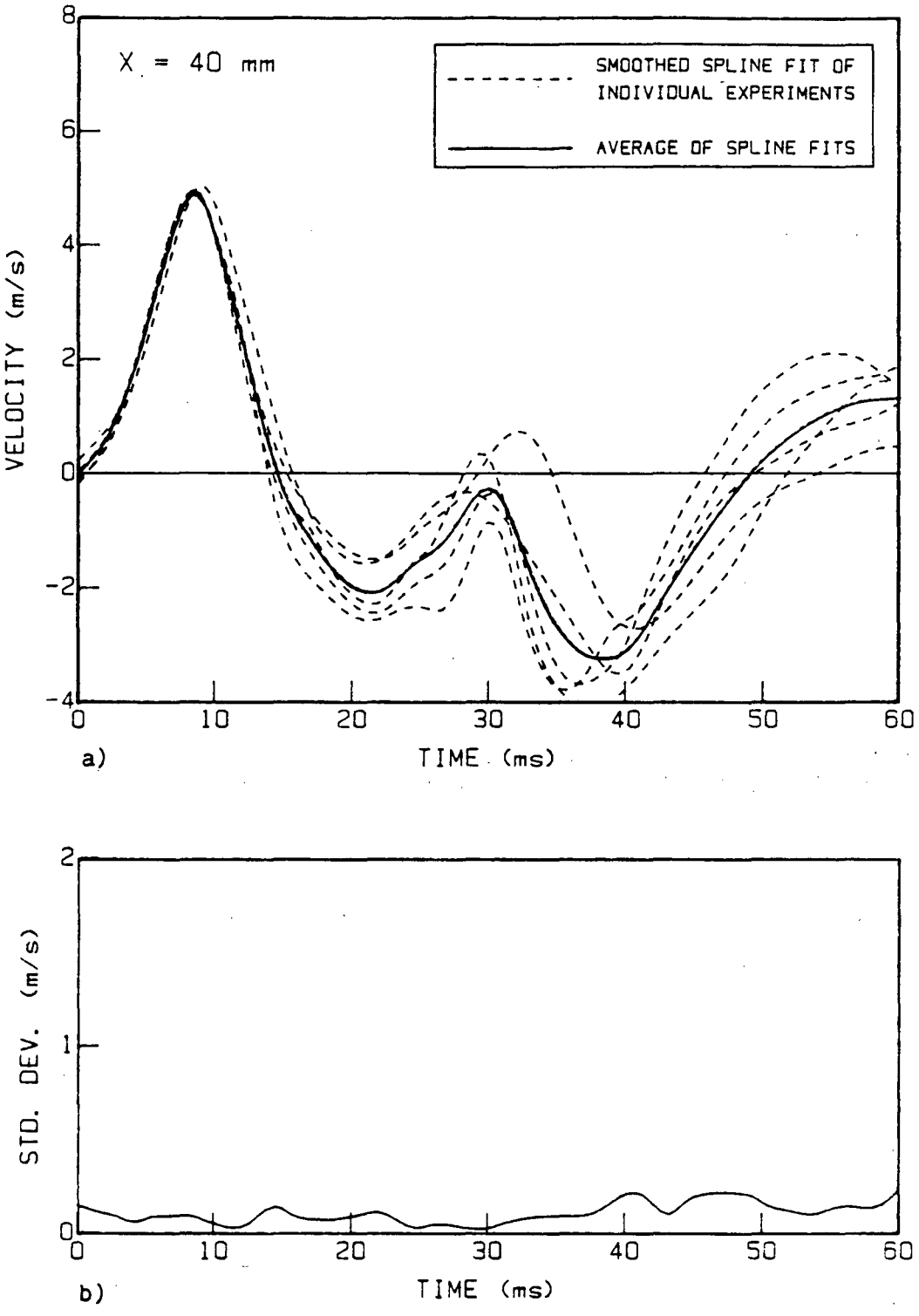

Figure 6-6. Comparison between smooth spline fits of individual experiments and the average of these fits. Result is typical for measurements taken for X < 70 mm.
a) Smooth splines and average
b) Standard deviation about the average

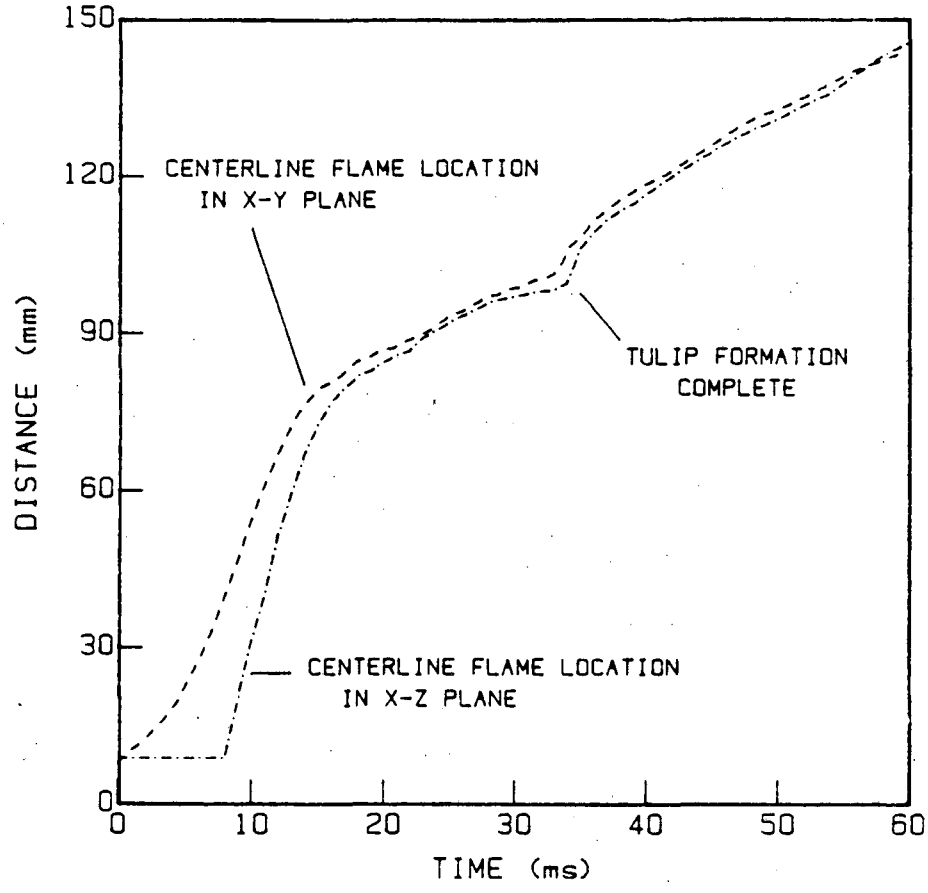

Figure 6-7. Centerline flame position recorded from high-speed schlieren movies. Flame position from two views (X-Y and X-Z) are shown.

well defined before the two flames join. The centerline flame position is always defined in the X-Z projection as only a single flame front can be distinguished.

The high degree of reproducibility in the LDA results and in the high-speed movies allows correlation of flame shape and position with the axial component of the centerline gas velocity.

6.5 Results

The flame displays three distinct stages of propagation: 1 - initiation, 2 - transition, 3 - "tulip". These stages were described in Chapter 2, section 1. For a particular combustion vessel, the three stages may be delineated in time (in the present case: 1 - $t < 15$ ms, 2 - 15 ms $< t <$ 20 ms, 3 - $t >$ 20 ms) or in space, by the axial location of the flame, X_f (in the present case: 1 - $X_f < 50$ mm, 2 - 50 mm $< X_f <$ 80 mm, 3 - $X_f >$ 80 mm). X_f is taken from the X-Z trajectory shown in Figure 6-7. The axial component of velocity during combustion at various measurement locations in a closed chamber, initiated from a two-point igniter, is shown in Figure 6-8. The velocity/time curves are separated into three groups to emphasize characteristic differences which are associated with the three stages of flame propagation. The results are grouped according to the whether the LDA measurement was taken at an X-location in the range (1), (2), or (3) above.

All velocity/time curves show a distinct initial peak in gas velocity. However, the maximum velocity, V_{max}, and the time that the maximum occurs, T_{vmax}, behave differently in the three

groups. Near the igniter (X < 50 mm), Figure 6-8a, V_{max} and T_{vmax} increase with X. Further V_{max} coincides with the arrival of the flame. In the central region of the chamber (60 mm < X < 80 mm), Figure 6-8b, both V_{max} and T_{vmax} are nearly constant. Far from the igniter (X > 90 mm), Figure 6-8c, V_{max} decreases with X, and T_{vmax} is constant. The relationship between T_{vmax} and T_f for different measurement locations is shown in Figure 6-9.

The initial peak in gas velocity corresponds to the rapid increase and decrease in flame area during the initiation and transition stages of flame propagation. The centerline flame velocity, V_f, as determined from the derivative of the X-Z flame trajectory, has a peak behavior similar to the gas velocity, Figure 6-10. The peaks are similar because the expanding burned gas accelerates both the flame and the unburned gas forward. The rate of expansion decreases when the flame quenches at the side walls of the combustion vessel, and both the flame and the unburned gas decelerate. After the velocity surge (t > 20 ms), the correlation between the flame velocity and the unburned gas velocity disappears. The "tulip" formation immediately follows the velocity surge.

The portions of the velocity/time curves which represent the burned gas motion (velocity after flame arrival) during the "tulip" period, Figure 6-8, have similar shape for all measurement locations. The curves are offset in time, but the

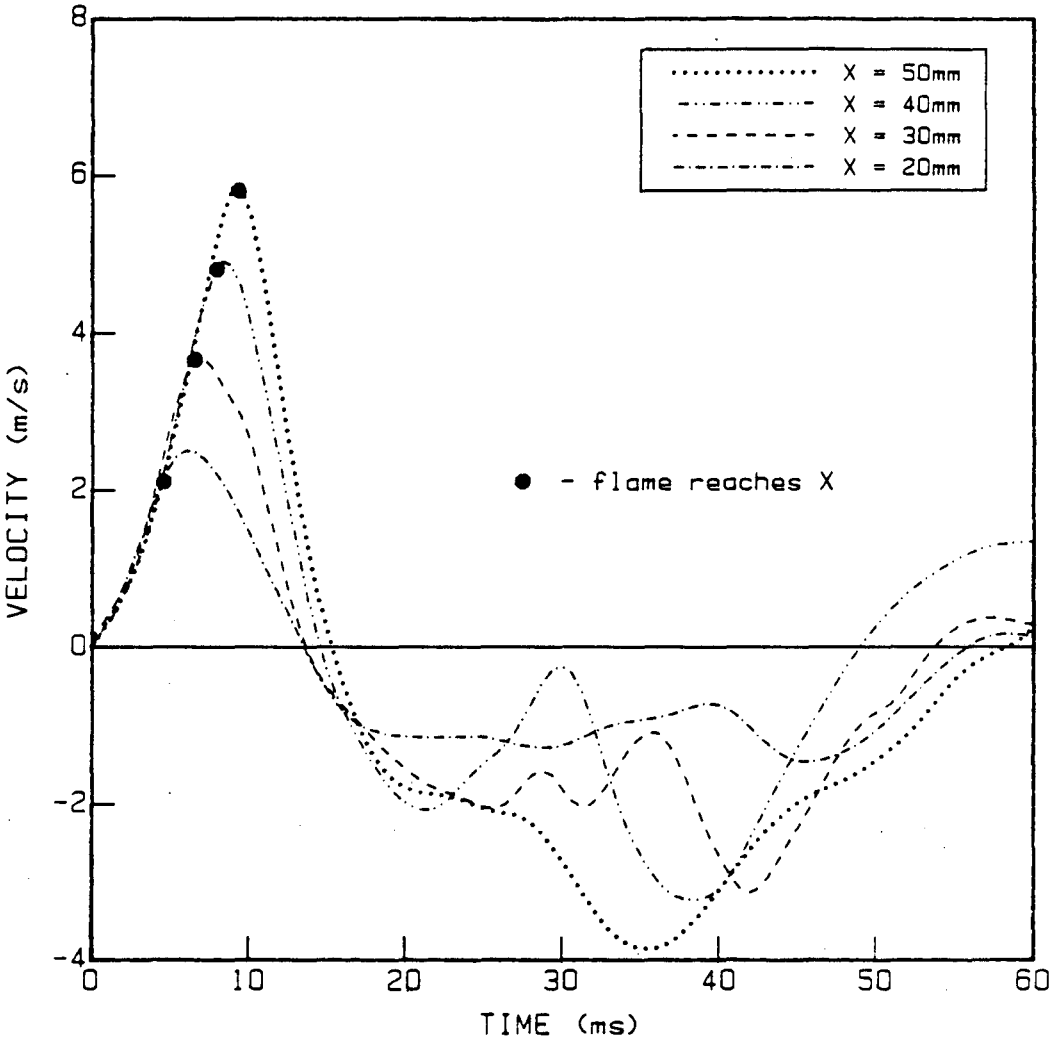

Figure 6-8a. Average axial centerline velocity histories for measurement locations near the igniter endwall.

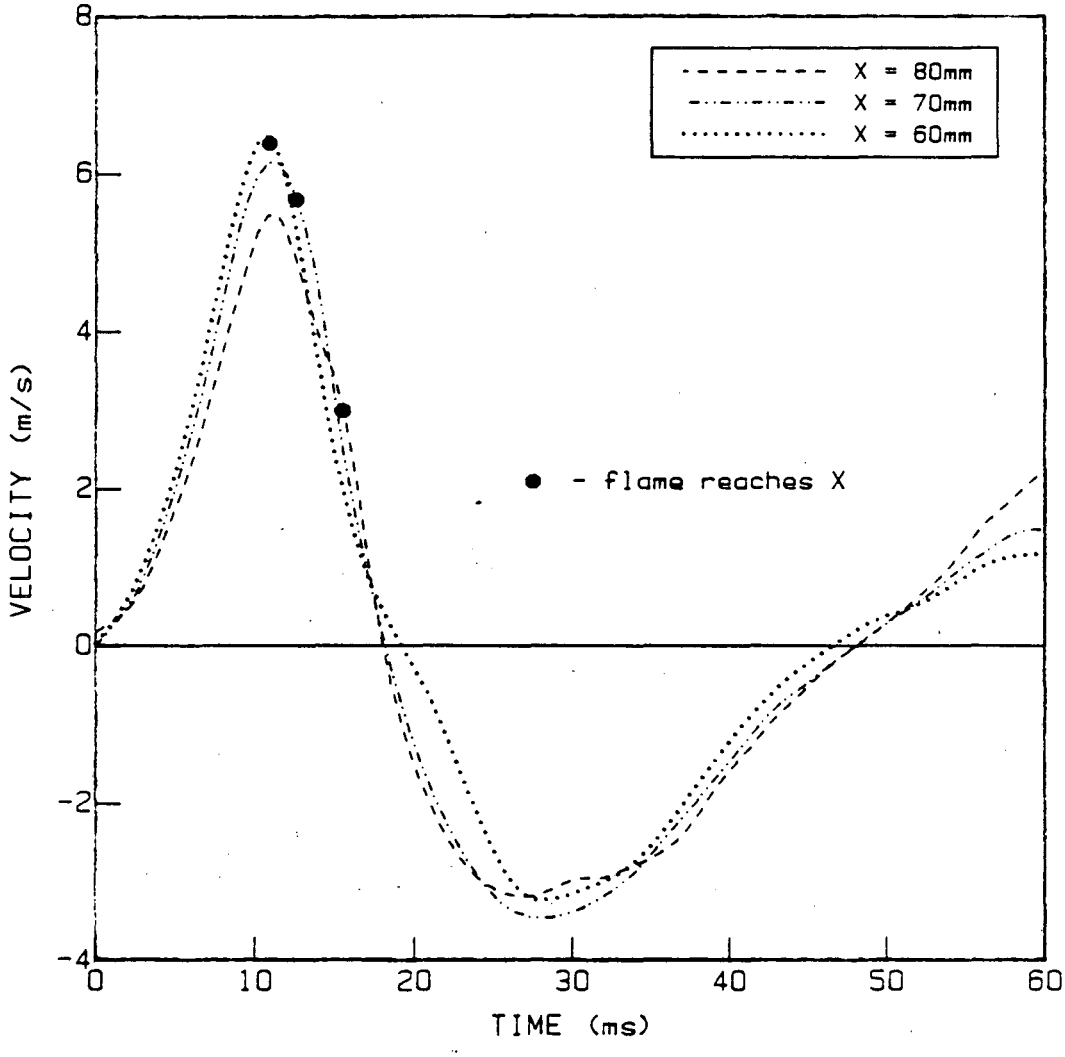

Figure 6-8b. Average axial centerline velocity histories for measurment locations midway between the igniter and the opposite endwall.

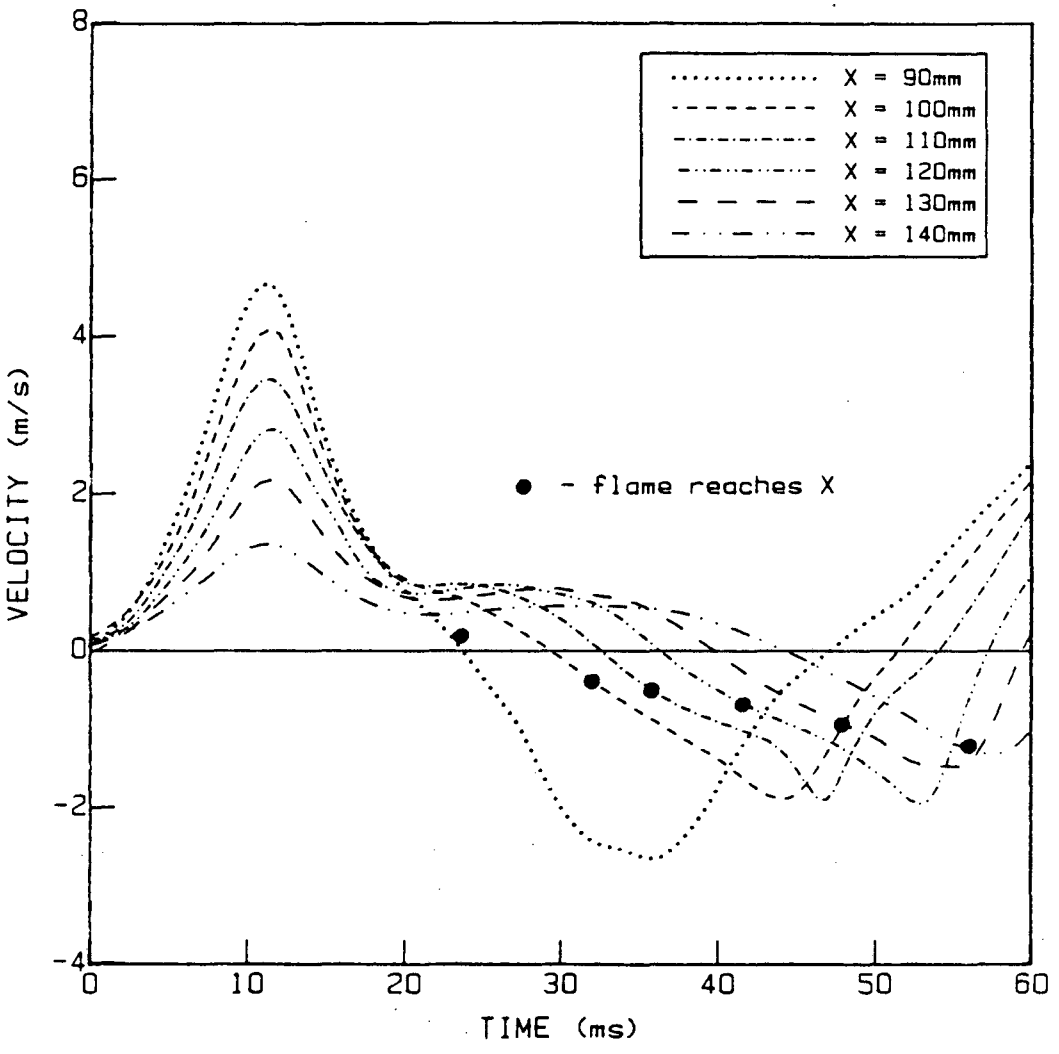

Figure 6-8c. Average axial centerline velocity histories for measurement locations far from the igniter endwall.

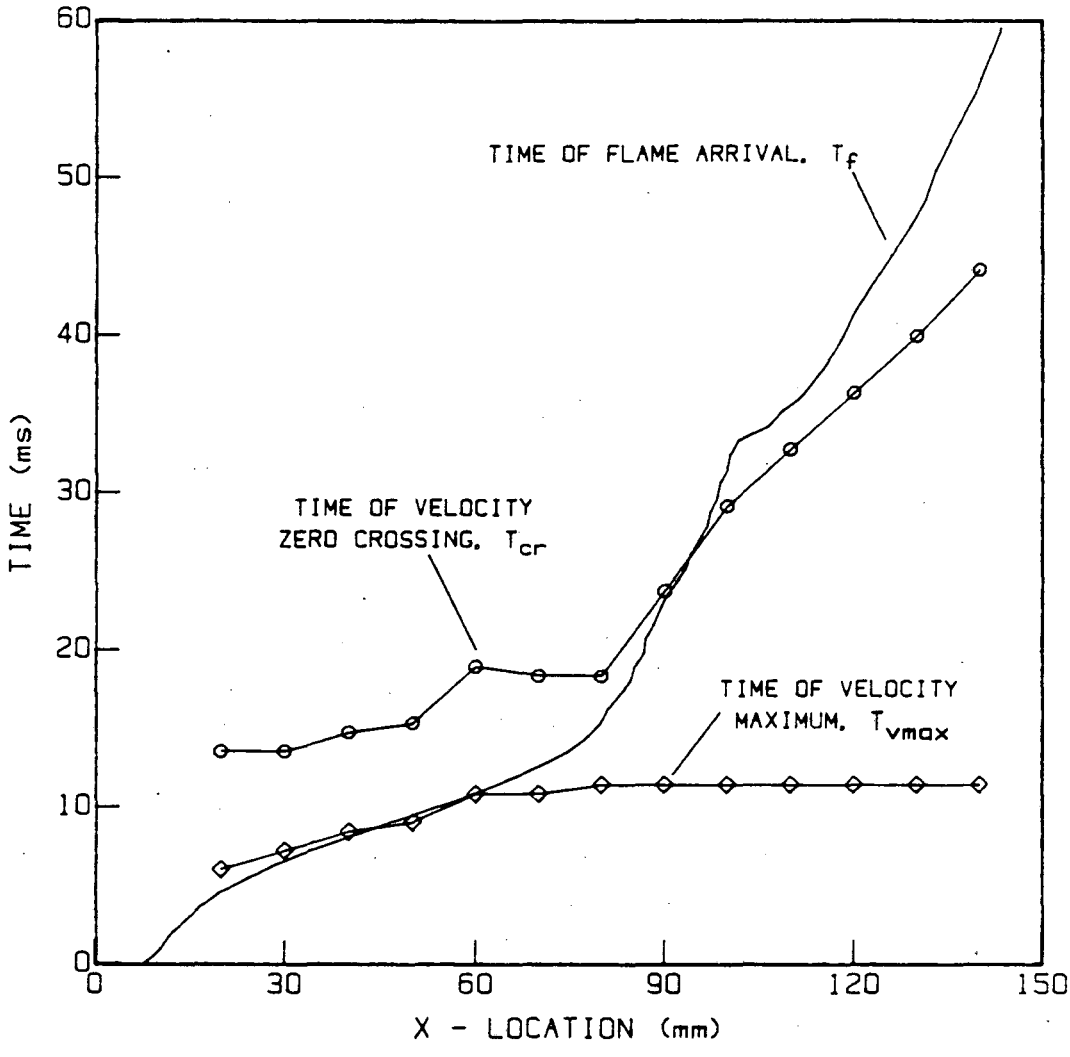

Figure 6-9. Relationship between the time of velocity zero crossing, the time of velocity maximum and the time of flame arrival.

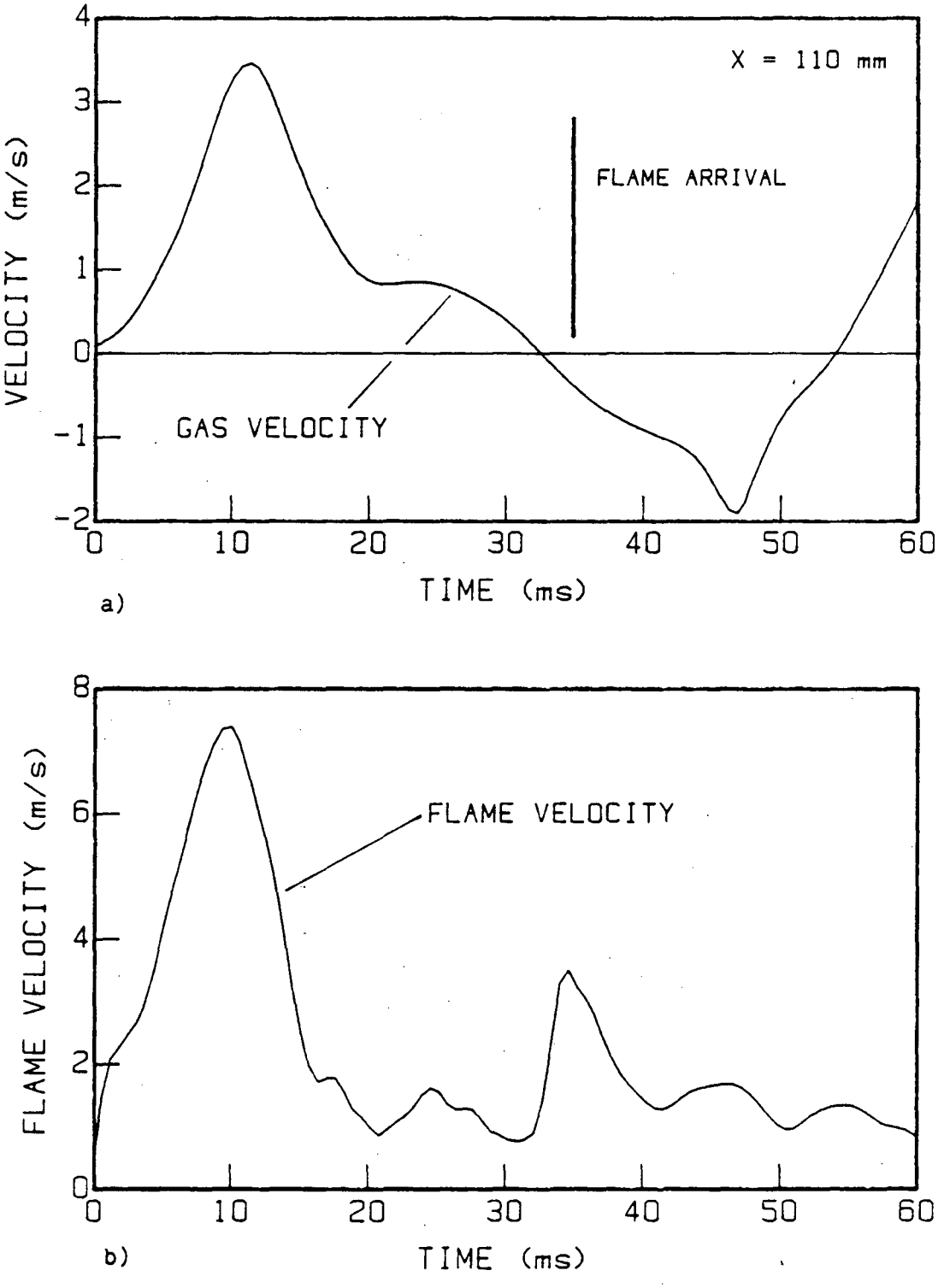

Figure 6-10. Comparison between measured axial centerline gas velocity history at a single representative measurement location and the centerline flame velocity.
a) Gas velocity at X = 110 mm
b) Flame velocity

similarity in shape suggests a nearly stationary unburned gas flow field relative to the flame front.

The relationship between the time of flame arrival, T_f, and the time of velocity zero crossing, T_{cr}, Figure 6-9, suggests a reverse flow ahead of the flame after the "tulip" forms. For X < 90 mm the flow ahead of the flame does not become negative until after the flame arrives. For X > 90 mm, however, the flow ahead of the flame becomes negative before the flame arrives. The time at which the flame reaches the transition point (X = 90 mm) corresponds approximately to the start of the "tulip" stage of flame propagation. The negative flow has been noted by other researchers using tracer flames (Ellis, 1928, Shimizu et al, 1984) and hanging aluminum strips (Leyer and Manson, 1971). The reverse flow supports the large scale flow explanation for the "tulip" formation, but the velocity profile inside the combustion vessel must be obtained to determine the extent of the reverse flow region.

The velocity/time measurements from different experiments are combined to give a time history of the centerline axial velocity profile. These profiles and the corresponding frames from one of the X-Y schlieren movies are shown in Figure 6-11. The length of the error bars in the velocity profiles indicate the standard deviation of the measurement as described in the data analysis section. The flame propagates from left to right, so the burned gas is to the left of the schlieren flame image and the unburned gas is to right of the schlieren flame image.

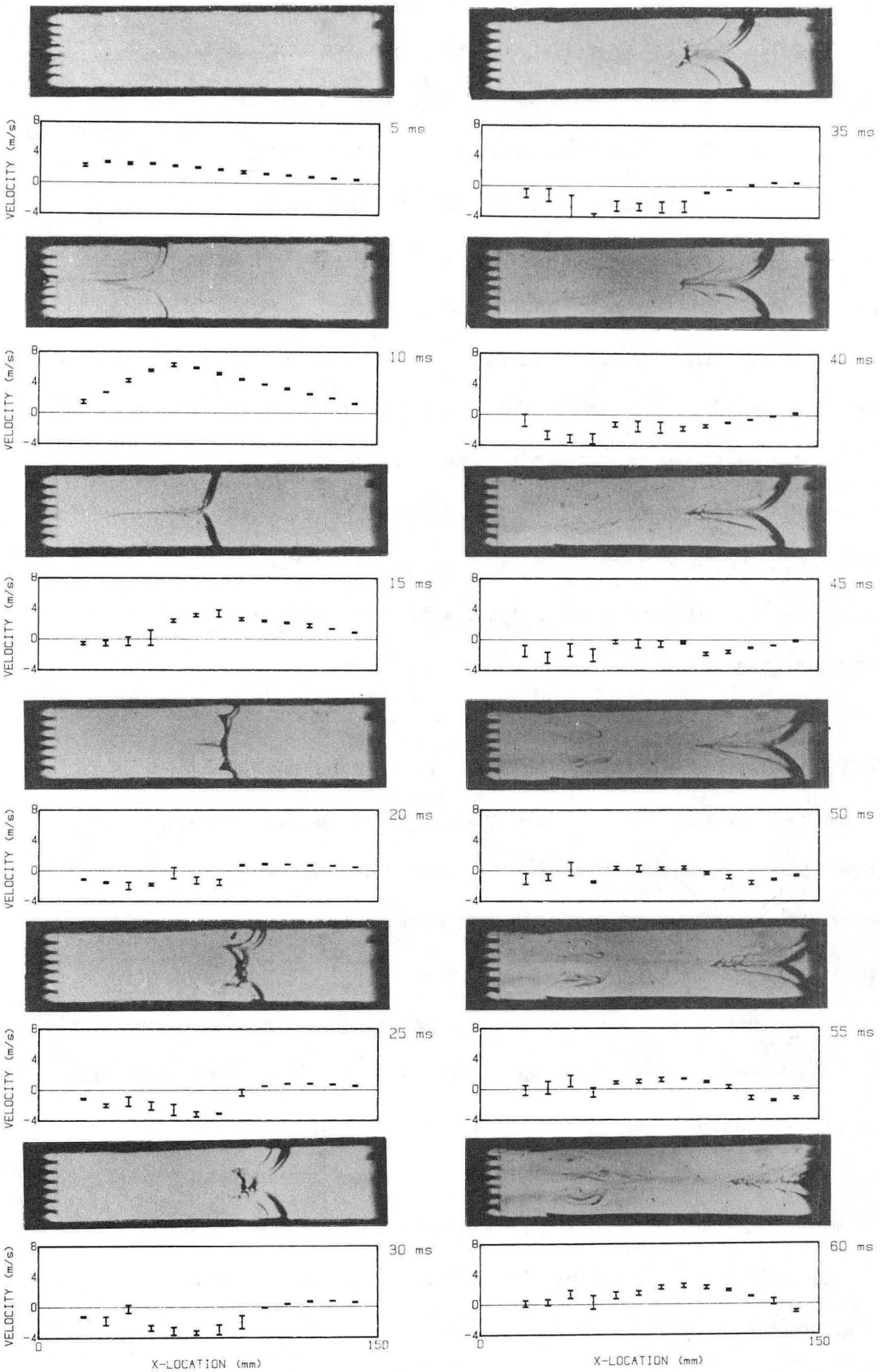

Figure 6-11. Comparison between the flame shape and axial centerline velocity profiles.

For the first 15 ms the unburned gas velocity decreases nearly linearly from a maximum at the flame to zero at the endwall. At 20 ms the unburned gas velocity drops to a small constant value (approximately 1 m/s) and the velocity just ahead of the flame becomes negative. Two cusps form in the flame at approximately t = 20 ms. As the cusps become more pronounced, and grow into the "tulip" flame, the unburned gas velocity within the cusp is negative, while the unburned gas velocity farther ahead of the flame remains positive. Therefore, the extent of the reverse flow, which was deduced from the velocity/time results above, is within the cusp only. This result suggests a localized circulation rather than a large scale reverse flow of unburned gas.

From 20 ms to 40 ms the unburned gas which is beyond the "tulip" maintains a small, approximately constant positive velocity, indicating that the transition to a full "tulip" flame does not noticeably influence the unburned gas velocity field ahead of the "tulip" cusp. The "tulip" shape is maintained for the remainder of the flame propagation. A flow reversal occurs in the burned gas beginning at approximately 45 ms. The reversal becomes more and more dominant from 45 ms to 60 ms and is likely to be caused by a leak out of the chamber end. The schlieren records reveal small vortices in the burned gas at about X = 50 mm for t > 40 ms. The vortices are accompanied by a small dip in the velocity results and an increase in the uncertainty of the measurements.

6.6 Summary

The results of the second set of experiments are summarized below:

1) The behavior of the axial component of velocity at the centerline of the chamber can be broken into three groups based on the axial distance of the measurement location from the igniter. The three groups correspond to the three stages of the flame behavior discussed earlier. The flame shape therefore correlates with the velocity in the chamber.

2) The time of velocity maximum, T_{vmax}, corresponds approximately to the time of maximum flame area. Near the igniter ($X < 60$ mm), the maximum velocity occurs coincident with the flame arrival because the flame area is continually increasing as it passes these measurement locations. Far from the igniter ($X > 60$ mm), T_{vmax} is independent of flame arrival ($T_{vmax} = 10$ ms) because the maximum flame area has occurred before the flame reaches the measurement locations far from the igniter.

3) Once the "tulip" is fully established ($t > 35$ ms) the burned gas velocity is steady when viewed from the frame of reference of the flame.

4) Before the "tulip" forms, the magnitude of the centerline axial component of velocity decreases approximately linearly from a maximum at the flame front to

near zero at the endwall. After the "tulip" forms the velocity is slightly negative within the flame cusp and has constant slightly positive value ahead of the flame. This result indicates a localized circulation within the cusp, but no large scale reverse flow of the unburned gas.

5) Two vortices appear in the burned gas after the "tulip" forms.

The second set of experiments shows that the "tulip" flame is not the result of a large scale reverse flow in the unburned gas. However, the close correlation between the flame shape and the velocity field, as well as the discovery of localized reverse flows supports the involvement of fluid mechanics in the "tulip" formation. A complete vector velocity mapping of the flow field generated during the flame propagation is necessary to further explore the dynamics of closed duct combustion generated flow. The complete vector velocity mapping is the subject of the next chapter.

CHAPTER 7

Complete Velocity Vector Map of Flow Field

7.1 Introduction

The previous experiment shows that the "tulip" flame is not caused by a large scale recirculation in the unburned gas ahead of the flame. However, because of the limited information available from a single component of velocity only along the duct centerline, the possible role of localized recirculations cannot be determined. The next set of experiments provides a more complete vector velocity map of the flow field generated during nonsteady flame propagation in a closed duct, and explores the role of localized recirculation zones in "tulip" flame formation.

7.2 Apparatus

The experimental apparatus, Figure 7-1, is similar to the apparatus described in Chapter 6. It consists of a constant volume combustion vessel, a pressure recording system, a laser Doppler anemometer (LDA), and a data acquisition microcomputer.

A plexiglas combustion vessel is again used, but this vessel is slightly longer (155 mm vs 150 mm) than the plexiglas chamber described previously. The length difference has no effect on the qualitative results and an insignificant effect on the velocity field. The flame starts from a single 3 mm spark gap located on the chamber axis approximately 10 mm from one endwall. Figure 7-2 shows the spark gap location, the direction convention adopted, and the coordinate layout of the combustion vessel.

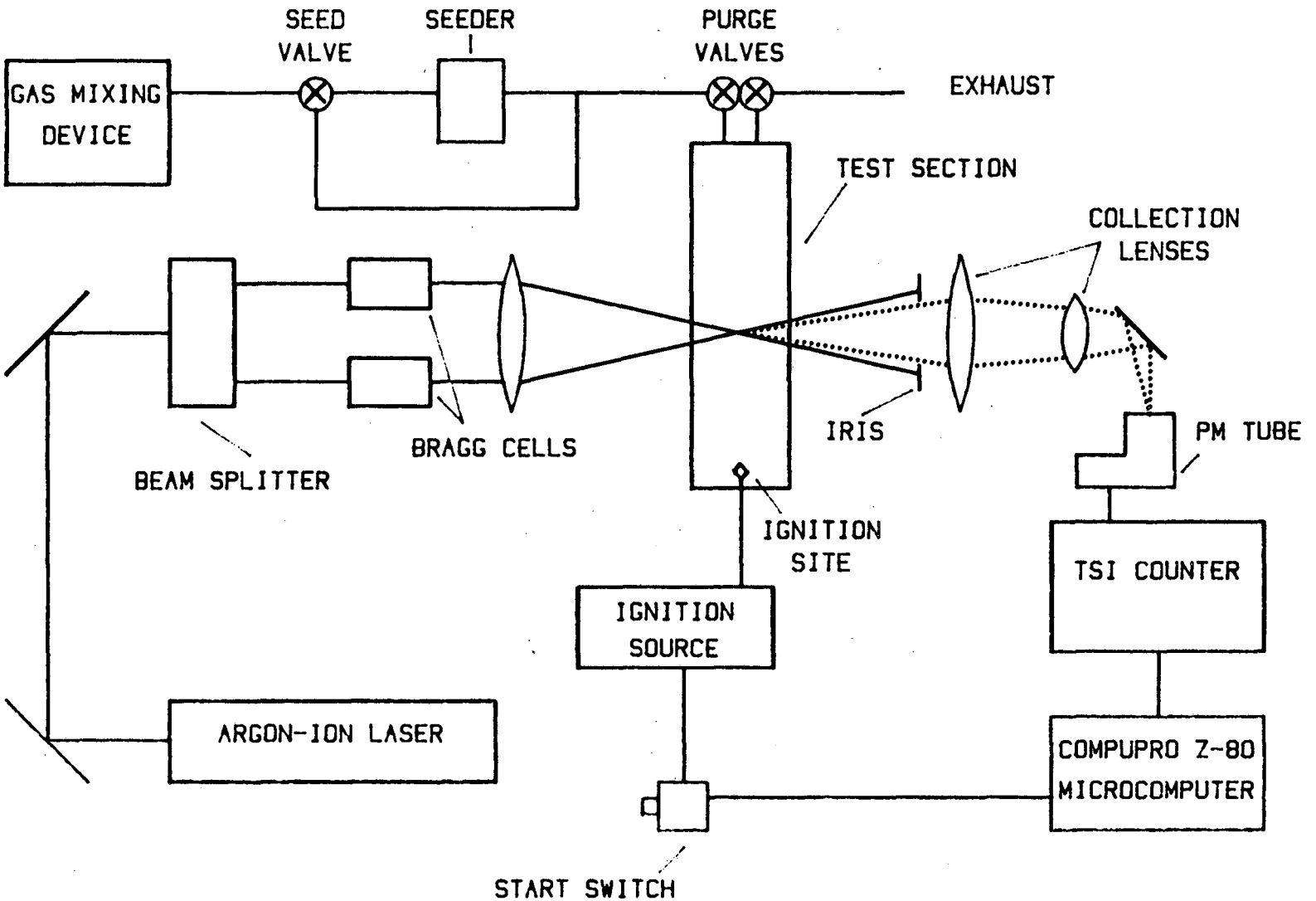

Figure 7-1. Schematic of experimental apparatus.

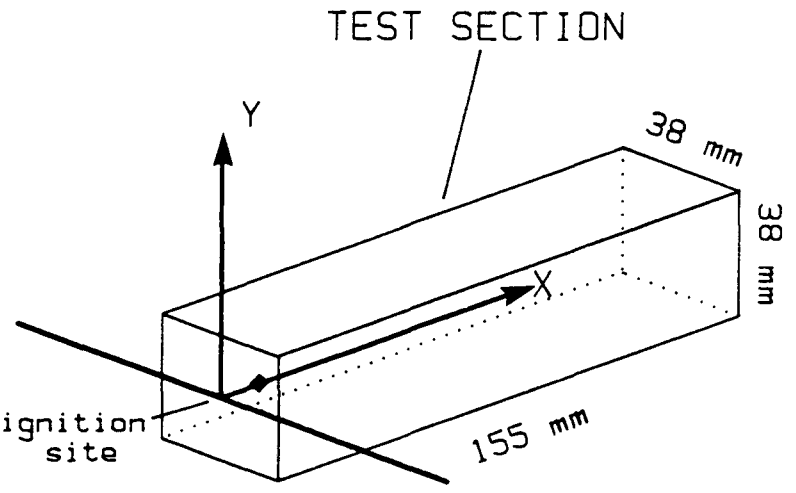

Figure 7-2. Coordinate layout of the combustion vessel showing the ignition location.

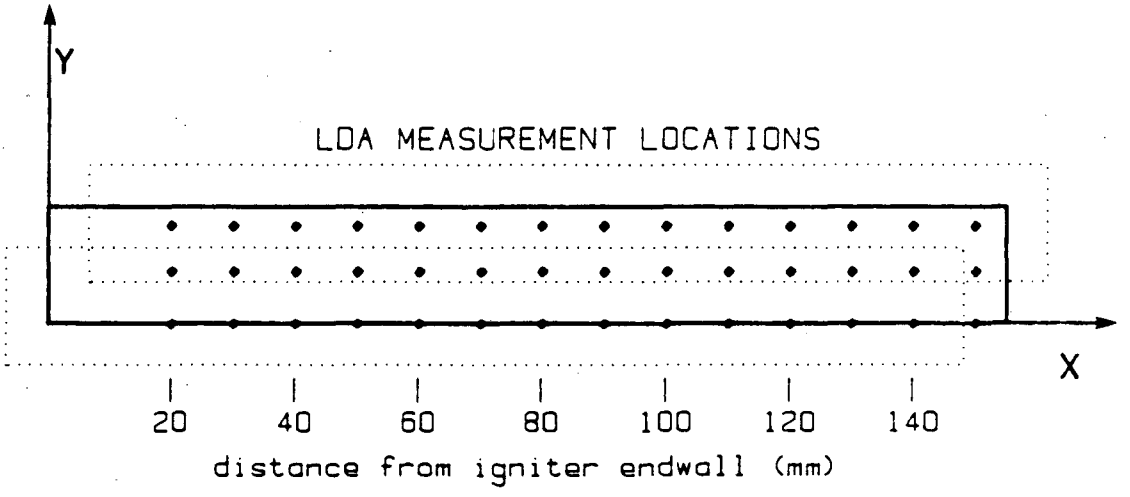

Figure 7-3. Matrix of LDA measurement locations.

The LDA operates in a standard forward scatter configuration. A 2 watt argon-ion laser, operated at 488 nm, provides the necessary coherent light. The laser power varies to optimize the LDA signal, but remains between 0.1 and 0.3 watt. The transmitting optics consist of a beam splitter of 50 mm fixed separation and a 295 mm focal length lens. Bragg cells differentially shift the resulting two beams to remove the directional ambiguity of the Doppler signal. The differential frequency is either 2 Mhz or 4 Mhz depending on the negative velocity expected. The transmitting optics rotate to measure either the radial (Y) or the axial (X) component of velocity. Aluminum oxide particles (approximately 1 micrometer), introduced into the inlet fuel/air flow by a spouted bed seeder, provide Doppler scattering sites. The collection optical system includes another 295 mm focal length lens, a secondary focusing lens, a plane mirror and a photomultiplier tube.

A TSI 1980A frequency counter analyzes the Doppler signal and outputs the validated velocity measurement to a microcomputer. The microcomputer (Compupro, 6 Mhz Z80 microprocessor) samples and stores the time of the measurement and the value of the velocity at a minimum frequency of approximately 15 kHz. The software used for the data acquisition is reproduced in Appendix I.

7.3 Methodology

The combustible gas is a stoichiometric mixture of methane and air as in the previous set of experiments. The combustion

vessel purging process is identical to that described in the previous chapter.

Ignition simultaneously initiates combustion and triggers the data acquisition microcomputer. Each experiment records one component of velocity at a fixed location from t = 0 (the time of ignition) to t = 150 ms. Axial and radial components of velocity are measured at 42 locations inside the combustion vessel, Figure 7-3. The combination of these two components gives a velocity vector history at each measurement location. Five repeated measurements of each component at each location helps establish the run-to-run variations. As mentioned in the previous chapter, the run-to-run variability (approximately 5 percent) is much larger than the uncertainty introduced by the LDA technique (less than 1 percent).

7.4 Data reduction

Figure 7-4 shows the raw axial velocity data at X = 100 mm and Y = 0 mm (the centerline). Five experiments are overlayed in the figure to indicate the run-to-run variability. The scatter of the data increases after the flame passes, but the variations are relatively small. The scatter in the raw velocity/time data shown in the figure is typical of all measurements. Averaging the data of all five runs in 0.5 ms windows and fitting the resulting average data with a smooth spline provides a curve representative of the velocity-time behavior at a single

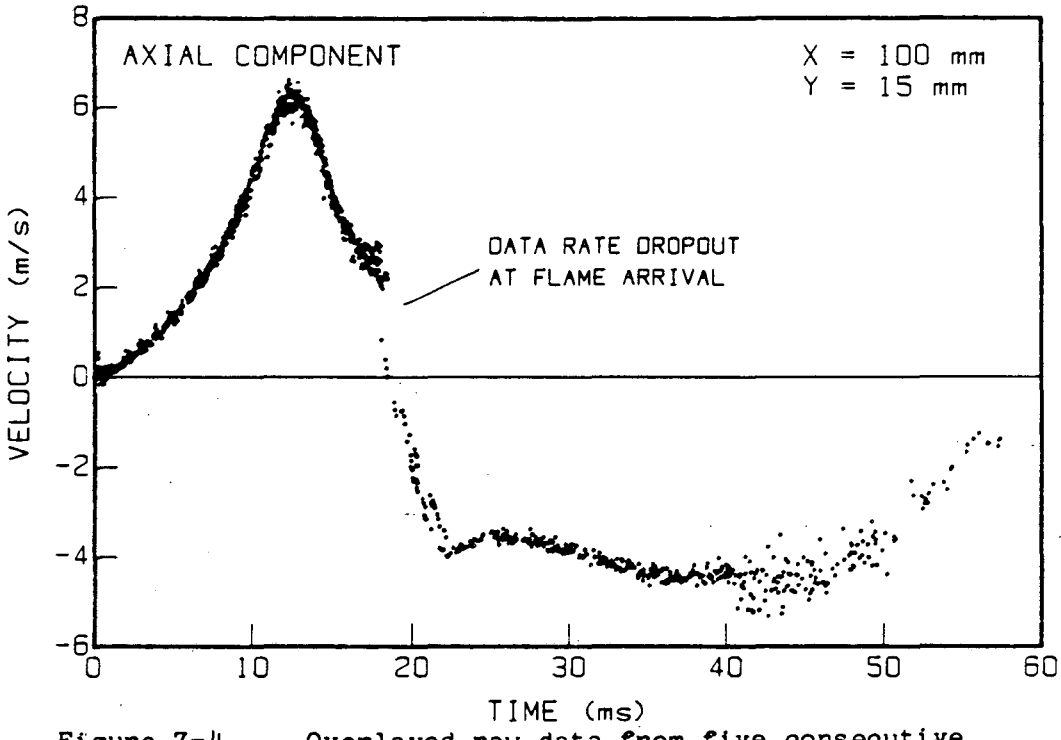

Figure 7-4. Overlayed raw data from five consecutive experiments.

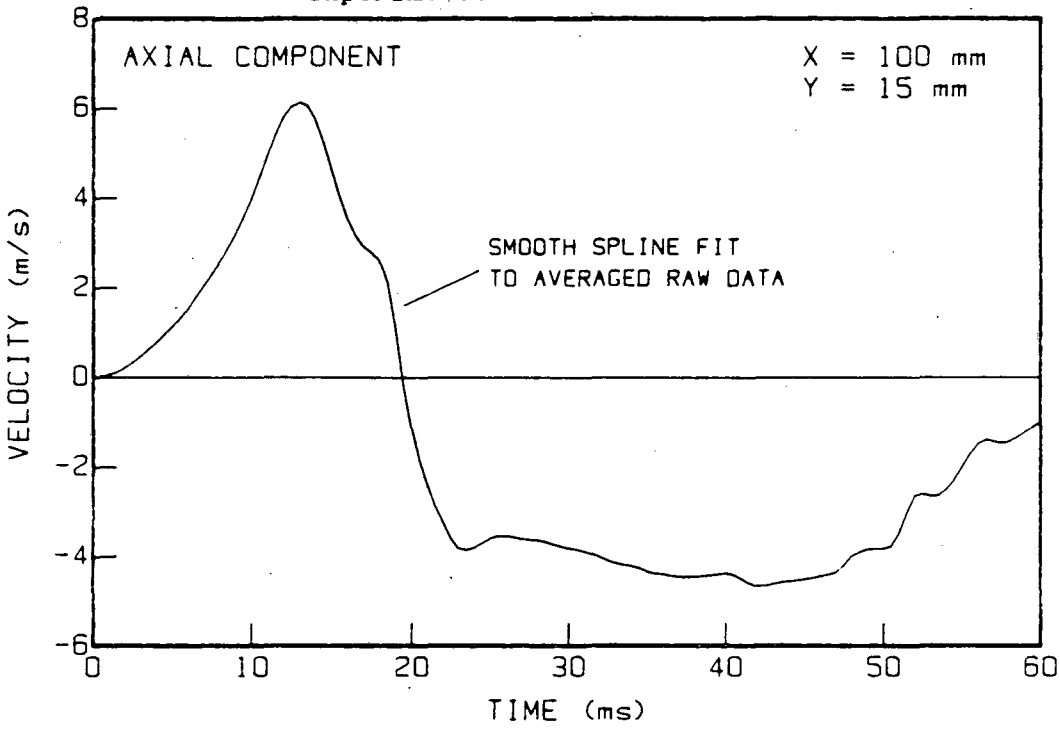

Figure 7-5. Smooth spline fit to the averaged raw data.

measurement point, Figure 7-5. All velocity/time information presented in this chapter is the smoothed average value.

7.5 Time of flame arrival

Noticeable LDA signal dropout accompanies the passage of the flame through the measurement volume, Figure 7-4. The time of signal dropout represents the time of flame arrival at the LDA measurement point because the dropout is due primarily to decreased particle density in the expanded burned gas. It has also been suggested (Witze, 1984) that the LDA seed particles agglomerate, providing large scattering sites in the unburned gas. When the flame arrives, the agglomerates are broken up and the LDA seed size drops below the detectability threshold of the Doppler system. The sensitivity of the laser Doppler anemometer to particle size has been discussed recently by Haghooie et al. (1984). The dropout was not apparent in the LDA results of Chapter 6 because the laser source was more powerful, and perhaps the dropout was somewhat obscured by the data reduction technique.

Fortuitously, the time of signal dropout provides an accurate measure of the time of flame arrival because the time of dropout is not subject to the line-of-sight integration uncertainty associated with schlieren measurements. There are, however, some uncertainties in the time of flame arrival data obtained by the dropout technique. These uncertainties arise from run-to-run variability in the flame shape. The flame trajectories based on the time of LDA signal dropout are shown in Figures 7-6a (near the wall, Y = 15 mm), 7-6b (near the mid-

radius, Y = 8 mm), and 7-6c (at the centerline, Y = 0 mm). Each data point represents the flame arrival time deduced from a single experiment. There are three sets of points and a kink in the flame trajectory at X = 95 mm because the flame actually reverses direction at this location. The reversal causes the LDA to measure in succession, unburned gas, burned gas as the flame passes, unburned gas a second time as the flame reverses, and finally burned gas again. The three sets of points represent the three flame passage times associated with this behavior. Figure 7-7 shows an approximate flame shape and position history computed from smooth splines fitted to the flame arrival data at each of the three radial positions. The approximate flame shape agrees well with high-speed schlieren cinematographic records of the flame propagation.

Interestingly, the flame propagation deduced from LDA signal dropout can be closely approximated by straight lines with an abrupt break in slope at approximately t = 15 ms, Figure 7-8. The break occurs as the flame encounters the side walls and begins to flatten during the early stages of the transition to "tulip". This result is in agreement with earlier observations of a transition period in the flame shape, the chamber pressure behavior, and the centerline velocity behavior.

7.6 Results

The axial component of velocity at the centerline of the combustion vessel during flame propagation initiated from a

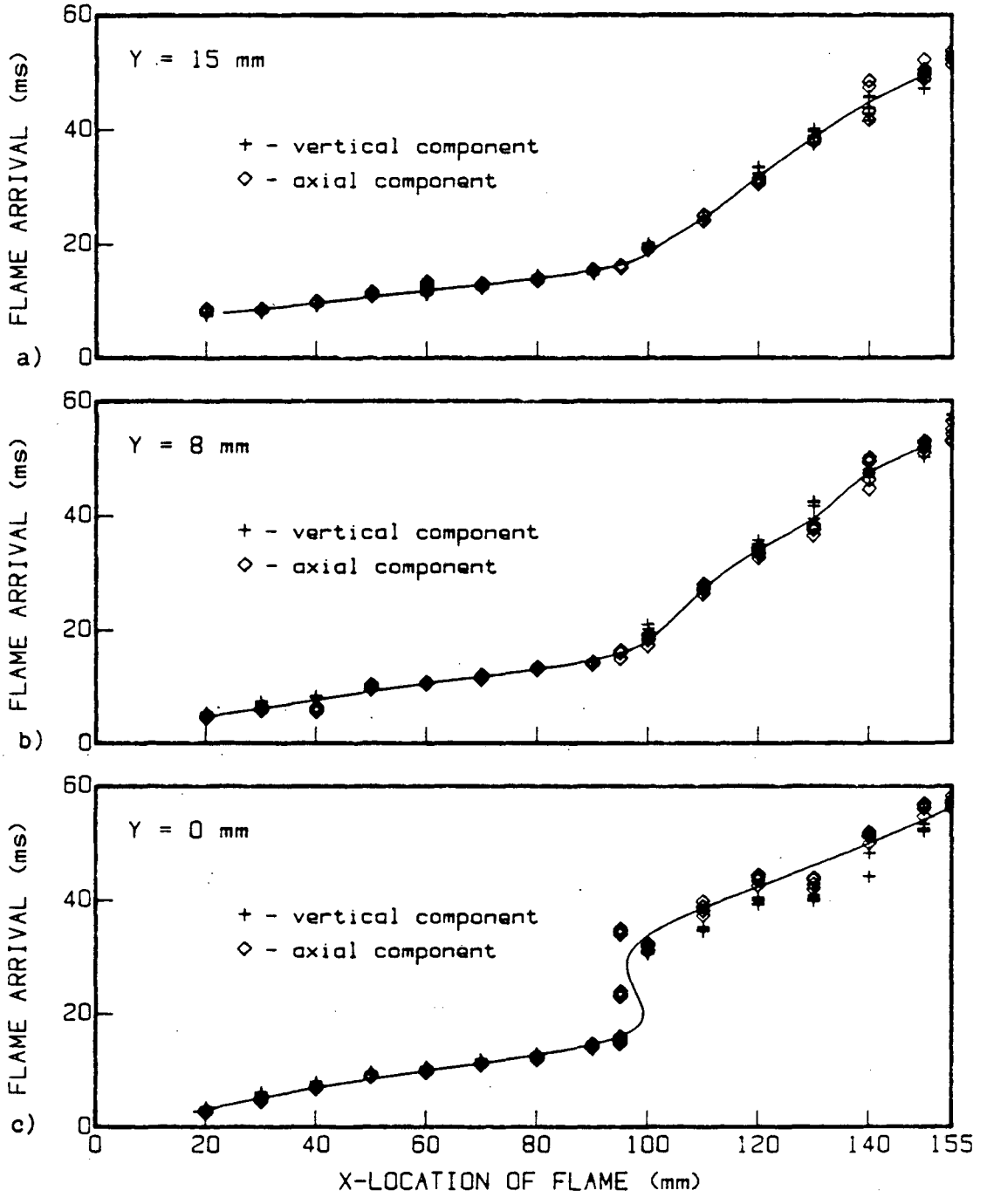

Figure 7-6. Flame arrival deduced from LDA dropout.
a) Near the sidewall (Y = 15 mm)
b) Half-radius location (Y = 8 mm)
c) At the centerline (Y = 0 mm)

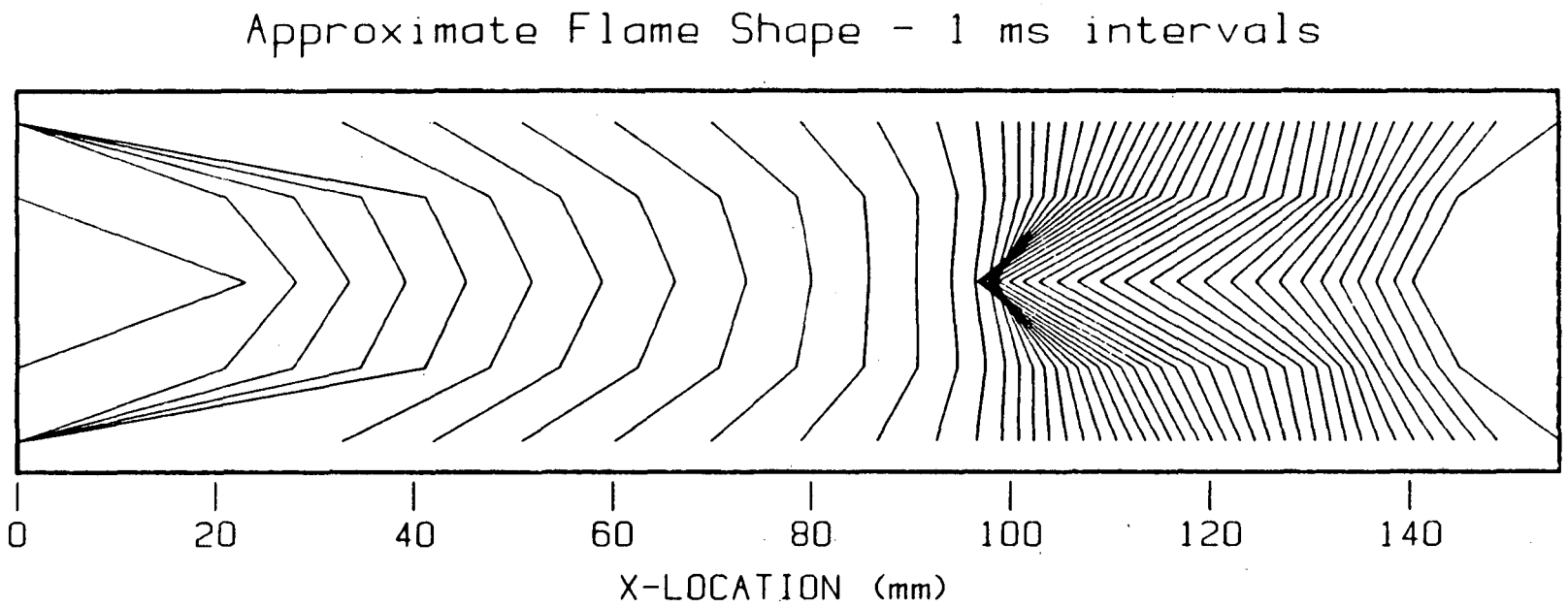

Figure 7-7. Flame shape history generated from flame arrival information.

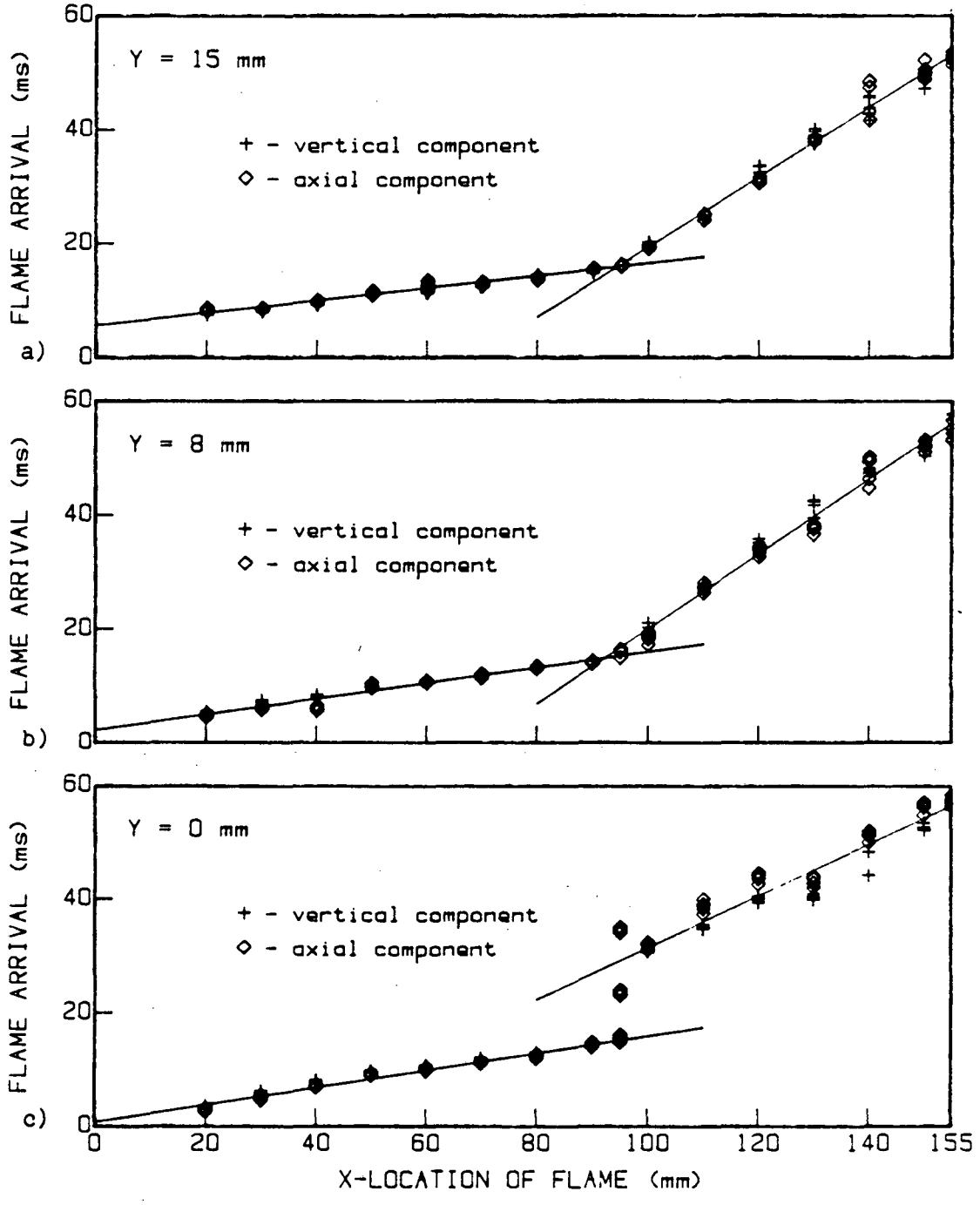

Figure 7-8. Nearly linear behavior of flame arrival data showing a sharp kink at the time of "tulip" formation.

single spark is shown in Figure 7-9. The results are divided into three groups as described in the results section of the previous experiments. The results are qualitatively similar to the LDA measurements obtained with the two-point igniter, and also agree with velocity measurements presented by other investigators (Starke and Roth, 1984, Shimizu et al., 1984).

In the group of measurements far from the igniter, Figure 7-9c (X > 90 mm), the time of velocity maximum is nearly constant, the maximum velocity decreases with increasing X, the flow becomes negative before the flame arrives, and the burned gas motion is approximately stationary when viewed from the frame of reference of the flame front. These results are the same as those reported for the two-point igniter in the previous chapter. The similarity in the two-point and single-point igniter velocity results is in accord with the schlieren observation of the insensitivity of the later flame propagation to igniter geometry.

In the group of measurements near the igniter, Figure 7-9a (X < 70 mm), the behavior is somewhat different from the velocity behavior with a two-point igniter. As in the two-point igniter results the velocity maximum increases with increasing X, and the velocity rise is terminated by the flame arrival. However, the single-point results show a sharp, almost discontinuous, drop in velocity as the flame passes, and then a gradual increase to a new peak velocity, which in some cases (X = 60 mm for example) is greater than the initial velocity peak. The difference is due to the early flame geometry. With a single point ignition a clearly

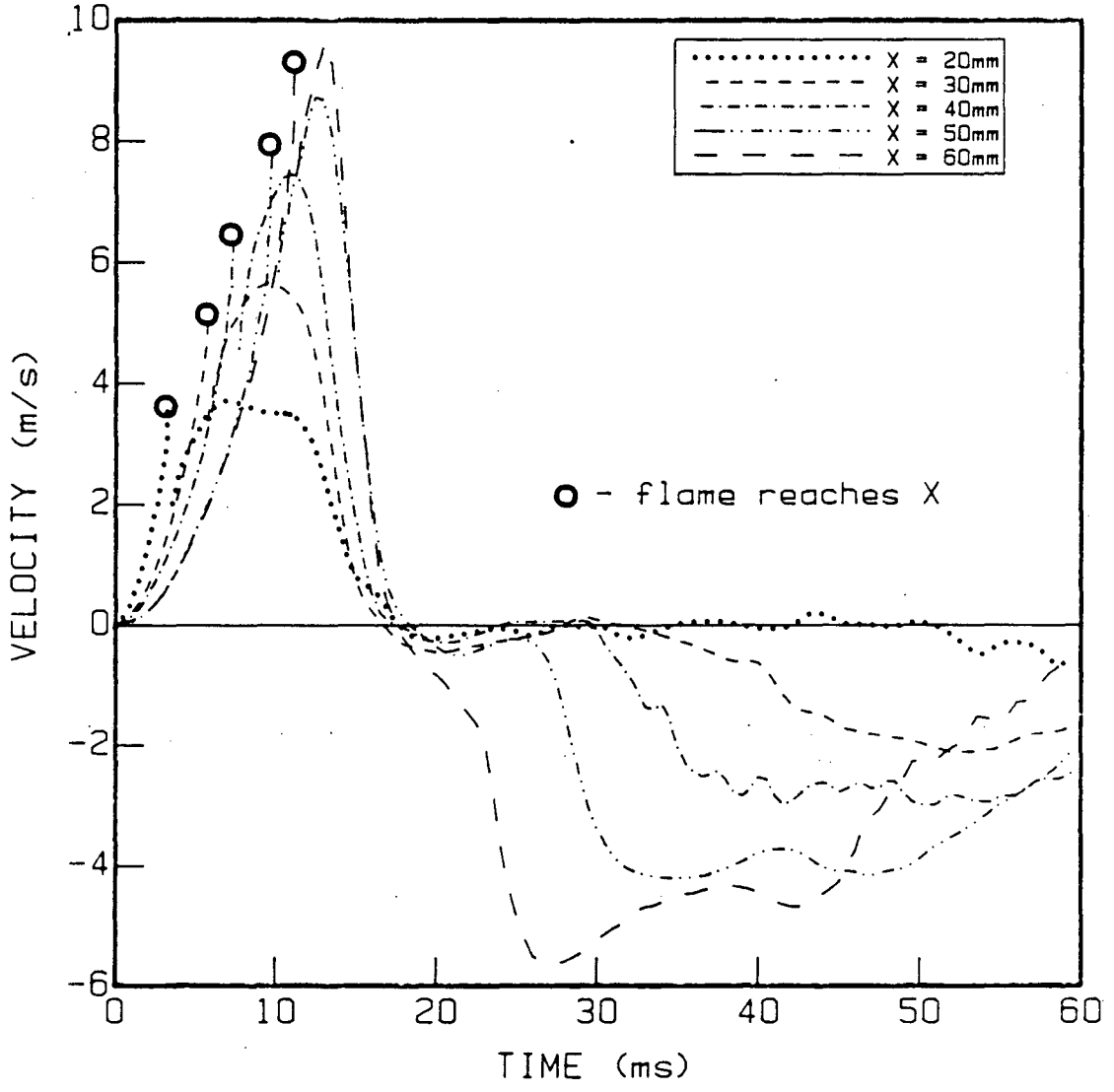

Figure 7-9a. Axial component of centerline velocity generated during combustion initiated by a single point igniter. Near the ignition endwall.

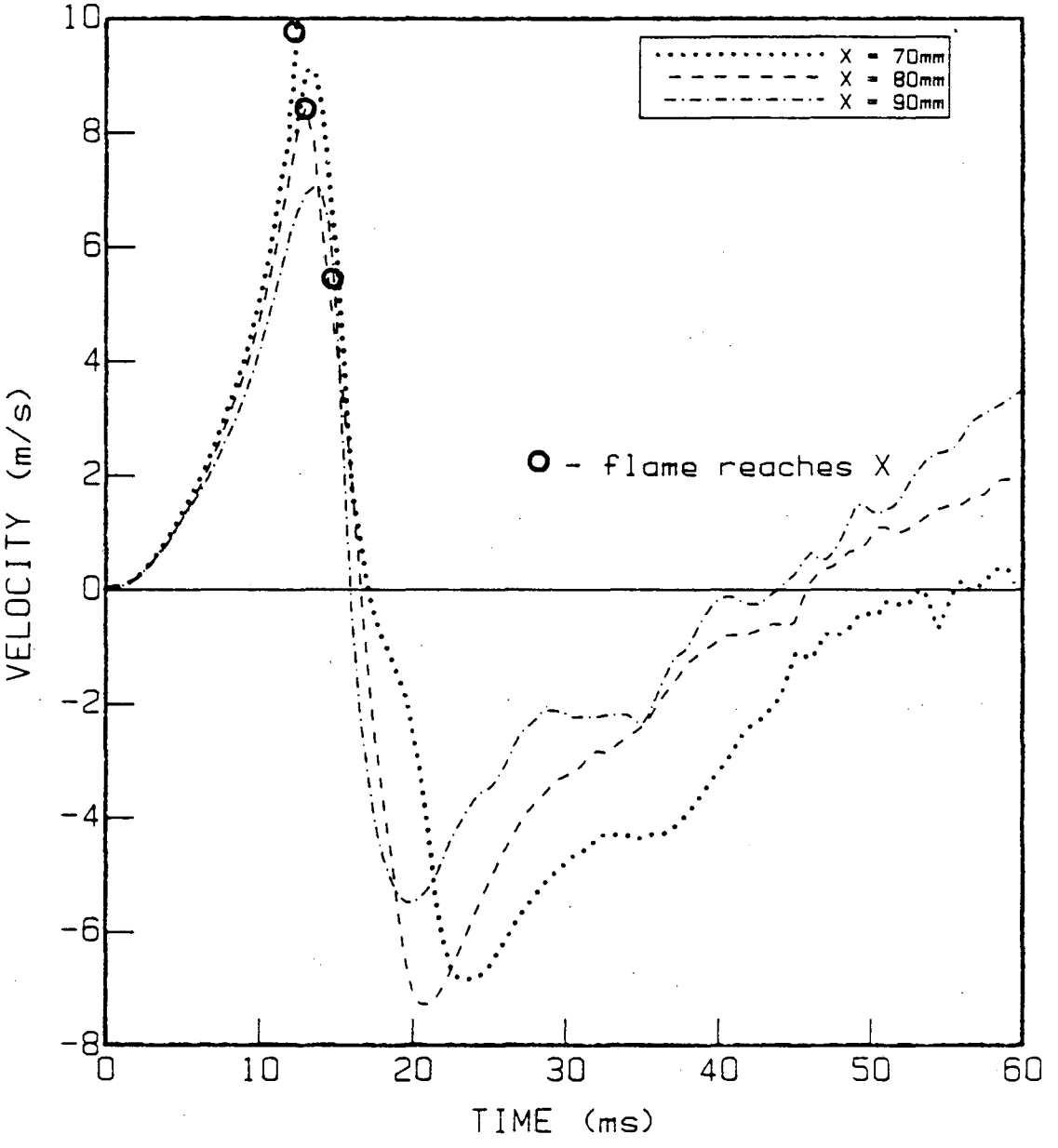

Figure 7-9b. Axial component of centerline velocity generated during combustion initiated by a single point igniter. X-location is midway between the endwalls of the combustion vessel.

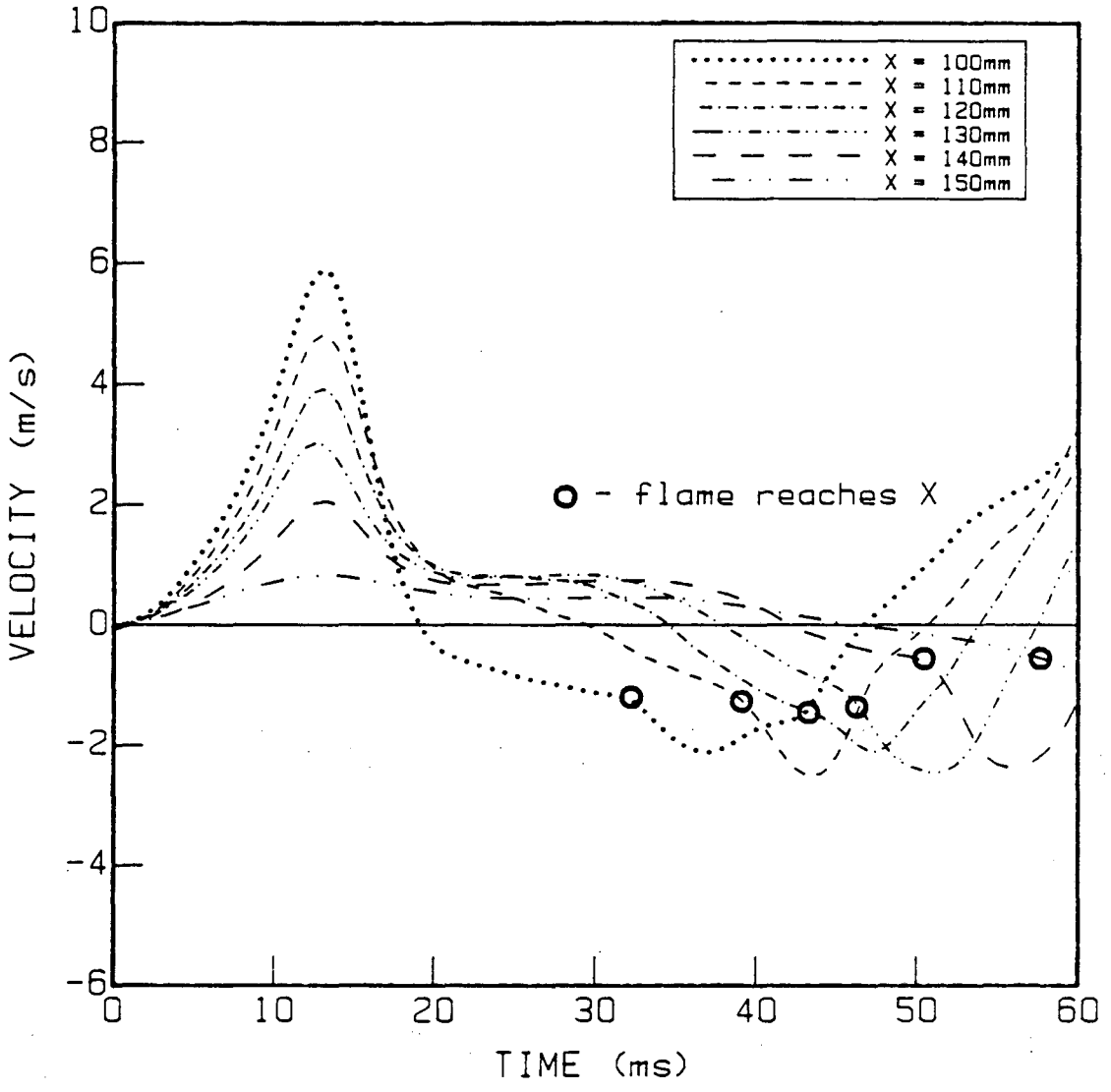

Figure 7-9c. Axial component of centerline velocity generated during combustion initiated by a single point igniter. Far from the igniter endwall.

defined flame front passes the measurement location. There is a discontinuous velocity change across the flame front, and this change is measured by the LDA. With the two-point igniter the flame front is a vee-shape, and is not clearly defined. Therefore a distinct discontinuity is not noticeable.

7.7 Velocity vector field

The velocity vector field is obtained by combining the velocity/time information of both velocity components at all of the measurement locations. An overview of the vector field appears in Figure 7-10 (vector scale: 1 mm = 2.5 m/s). The heavy line marks the flame location deduced from LDA signal dropout as described above. The vectors begin at the end marked by the dot. Positive axial flow is to the right. Positive radial flow is away from the centerline. The symmetry about the centerline of the duct is assumed, and the lower half of the velocity field is shown only to assist in vizualizing the flow. The symmetry was validated at various measurement locations. Slight deviations from symmetry by the flame occasionally causes the centerline velocity to appear double valued. This behavior is only an artifact of the symmetry assumption.

The information contained in the velocity vector field during the flame propagation is separated into sections. The sections follow the example of the velocity/time measurements and are divided in time by the three phases of flame propagation: 1) initiation ($t < 15$ ms), 2) transition (15 ms $< t <$ 20 ms), 3)

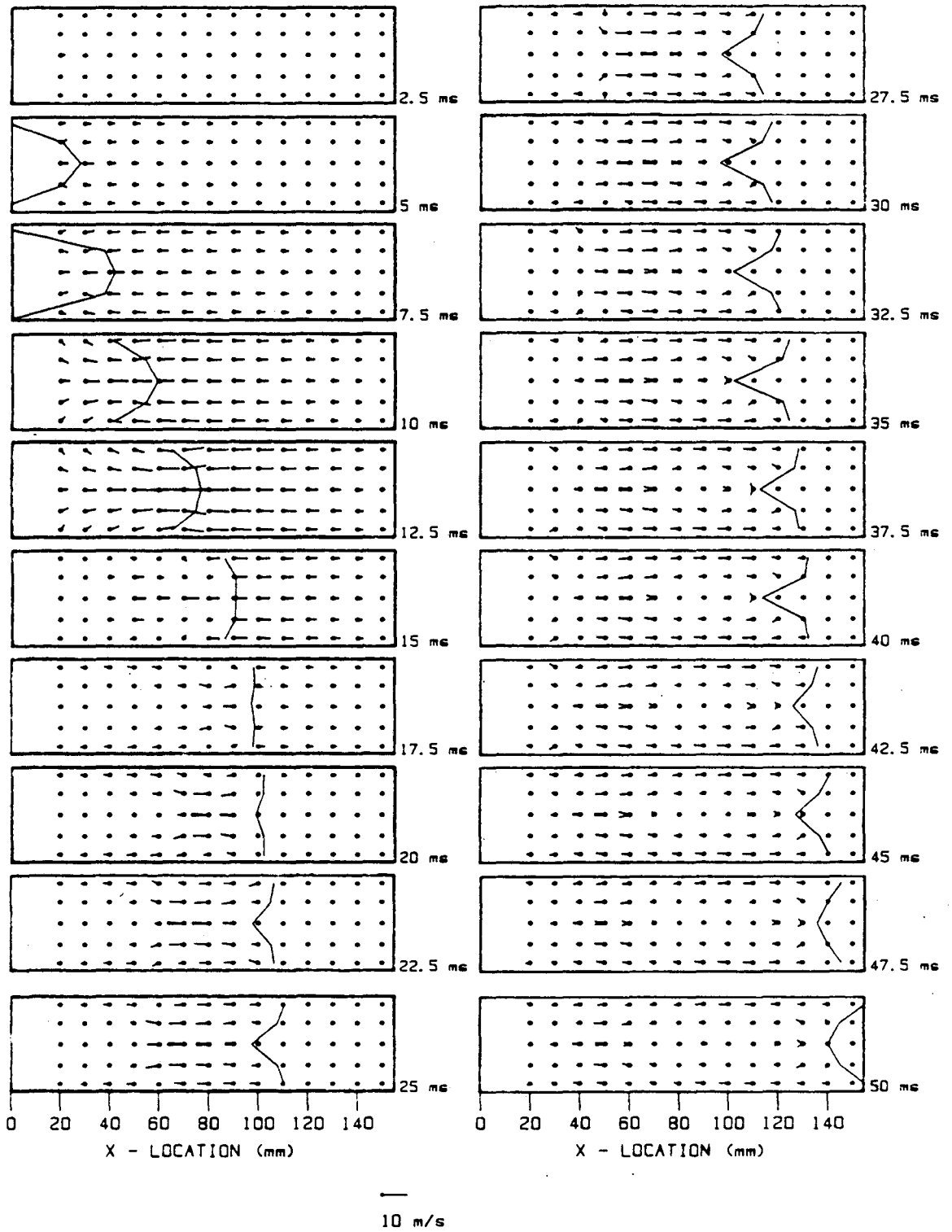

Figure 7-10. Overview at 2.5 ms intervals of the vector velocity field generated by combustion in a closed vessel. Vector scale : 1 mm = 2.5 m/s.

"tulip" (t > 20 ms). Within each section the location of the flame front divides the velocity field into burned and unburned gas.

7.7.1 Section 1 -- initiation phase:

The velocity field during the initiation phase of flame propagation is shown in Figure 7-11 (vector scale: 1 mm = 1.25 m/s). The entire flow field accelerates from zero velocity at the ignition to a maximum velocity just before the flame contacts the side walls. The flow in both the unburned gas and burned gas is positive during the initiation period.

Near the flame front the unburned gas is divergent, driven outward by the curved flame. When the flame passes, the flow becomes convergent as it is deflected toward the centerline of the vessel. This deflection of the flow is clearly shown in the radial component of velocity, Figure 7-12. The radial component of velocity is positive (toward the side walls) before the flame arrives, and is negative after the flame passes. The deflection appears to funnel the burned gas into the center of the duct, creating a large positive velocity there.

The unburned gas velocity more than one centimeter ahead of the flame front is uniform, with no radial dependence nor significant radial component of velocity. The magnitude of the axial unburned gas velocity decreases from a maximum near the flame to near zero at the endwall of the combustion vessel. The burned gas more than one centimeter behind the flame, however, retains the influence of the deflection caused by the flame

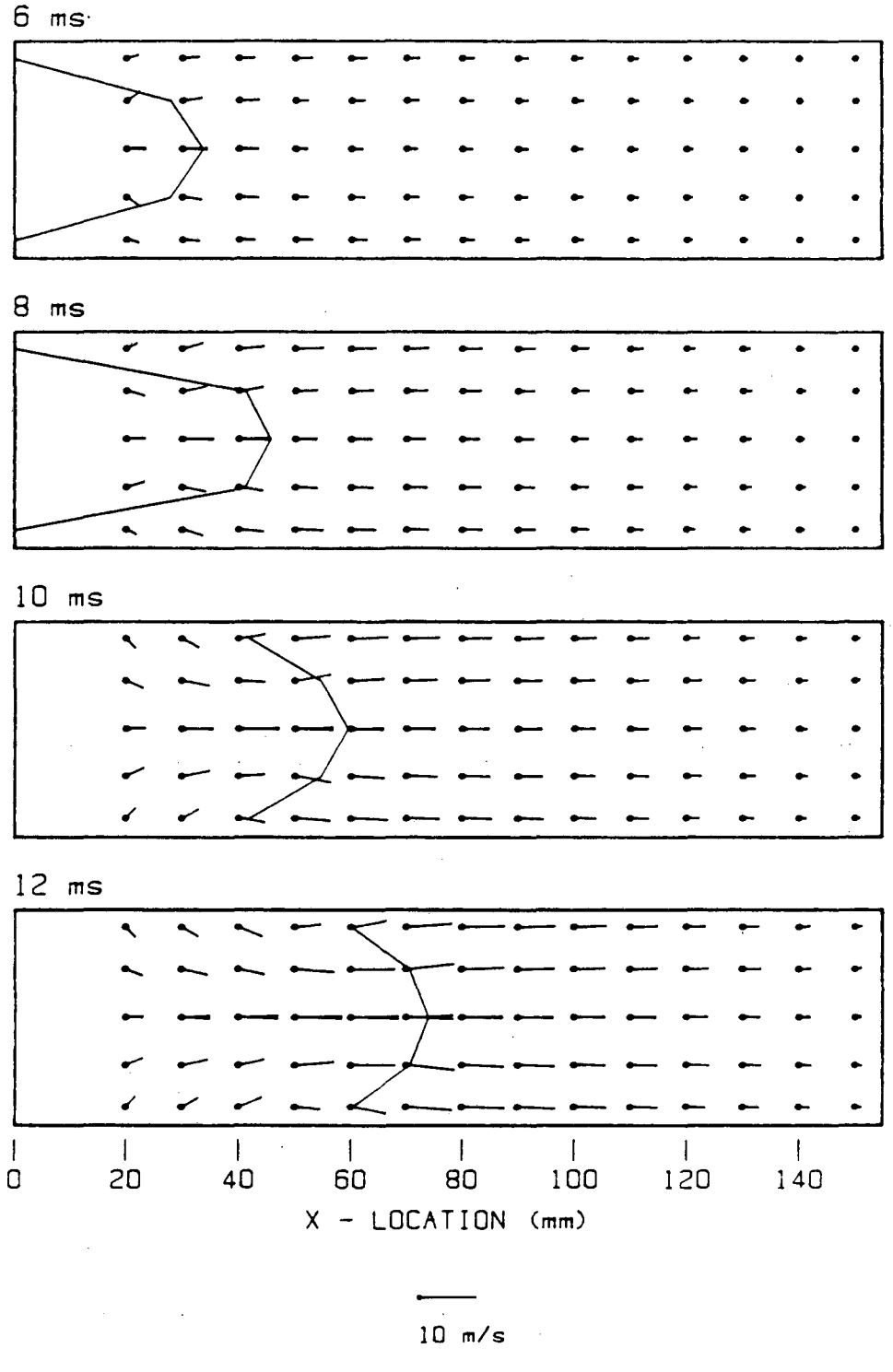

Figure 7-11. Close-up of vector field during the initiation phase of flame propagation. Vector scale: 1 mm = 1.25 m/s.

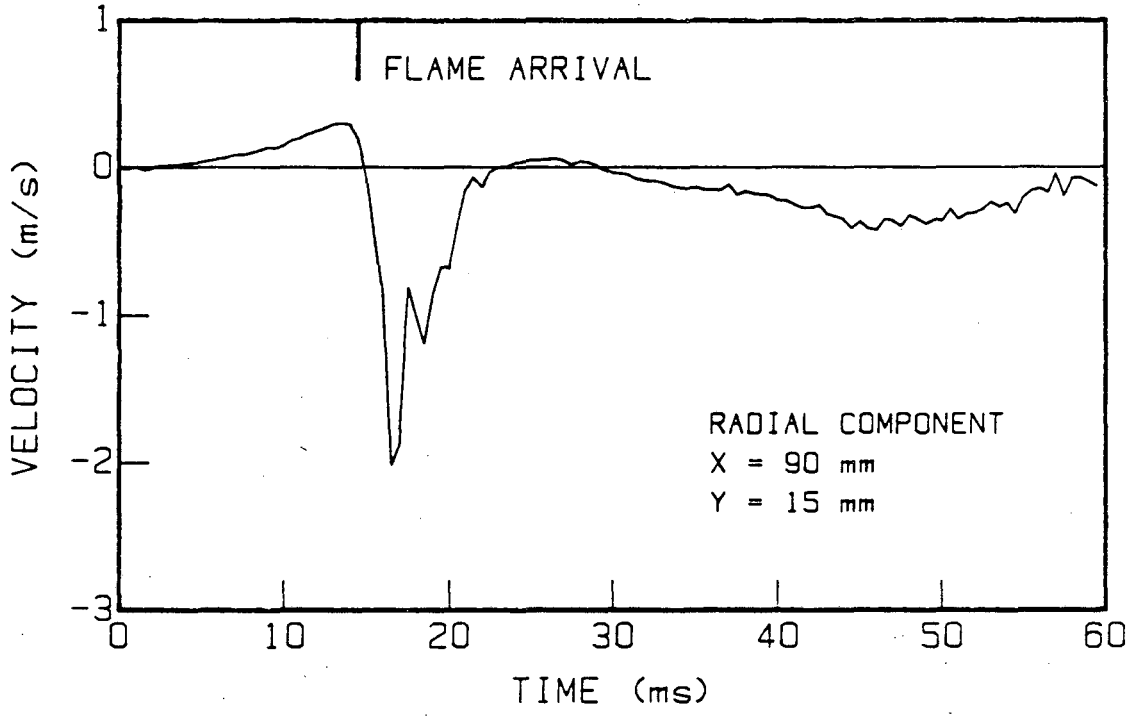

Figure 7-12. Deflection of flow by flame passage. The radial component of velocity changes sign when the flame arrives.

passage. Further, the burned gas velocity shows a radial dependence; near the wall, the velocity magnitude is smaller and the deflection toward the centerline is larger. Except at the centerline, the velocity shows a similar dependence on the axial coordinate. Near the igniter endwall the magnitude of the velocity is smaller and the deflection toward the centerline is greater. At the centerline, there is no deflection but the magnitude decreases in the direction toward the igniter.

The salient features of the velocity field during the initiation phase of the flame propagation are enumerated below:

1) The magnitude of the velocity field increases with increasing flame area, and the axial component of velocity is positive in both the burned and unburned gas.

2) The unburned gas flow, except very near the flame front, is one-dimensional. The burned gas motion is not one-dimensional anywhere in the combustion vessel.

3) The magnitude of velocity decreases from a maximum at the flame front to near zero at the endwall in both the burned and unburned gas. The deflection of the burned velocity vectors increase both toward the side walls and toward the igniter endwall of the combustion vessel.

7.7.2 Section 2 -- transition phase:

Although the transition phase has relatively long duration overall (10 ms), many features of the vector velocity field

change dramatically during the first few milliseconds. The vector velocity field is shown in Figure 7-13 (vector scale: 1 mm = 1.25 m/s).

During the transition phase the flame area decreases rapidly, as the flame is quenched by the side walls of the combustion vessel. At the same time the magnitude of the velocity vectors begins to decrease (t = 13.5 ms). The decrease in velocity magnitude is particularly noticeable in the unburned gas. The unburned gas velocity decreases until approximately t = 20 ms and then remains approximately constant for the duration of the transition phase. The one-dimensional nature of the unburned gas a short distance ahead of the flame front described above continues to prevail, however, the decrease in magnitude from a maximum at the flame front to near zero at the endwall is not apparent. The velocity is positive, almost entirely axial, and uniform in the unburned gas except very near the flame front.

In the burned gas, the non-uniformity in velocity increases. At the start of the transition localized regions of slight reverse flow near the side walls of the vessel appear. The reverse flow gradually grows into an envelope along the side walls and just behind the flame front. A central core of positive flow in the burned gas remains (t = 17.5 ms). The reverse flow in the burned gas becomes more and more pronounced, until the entire burned gas motion is negative. There is, however, a region of high velocity negative flow, distinctly separated from a region of low velocity negative flow. The point

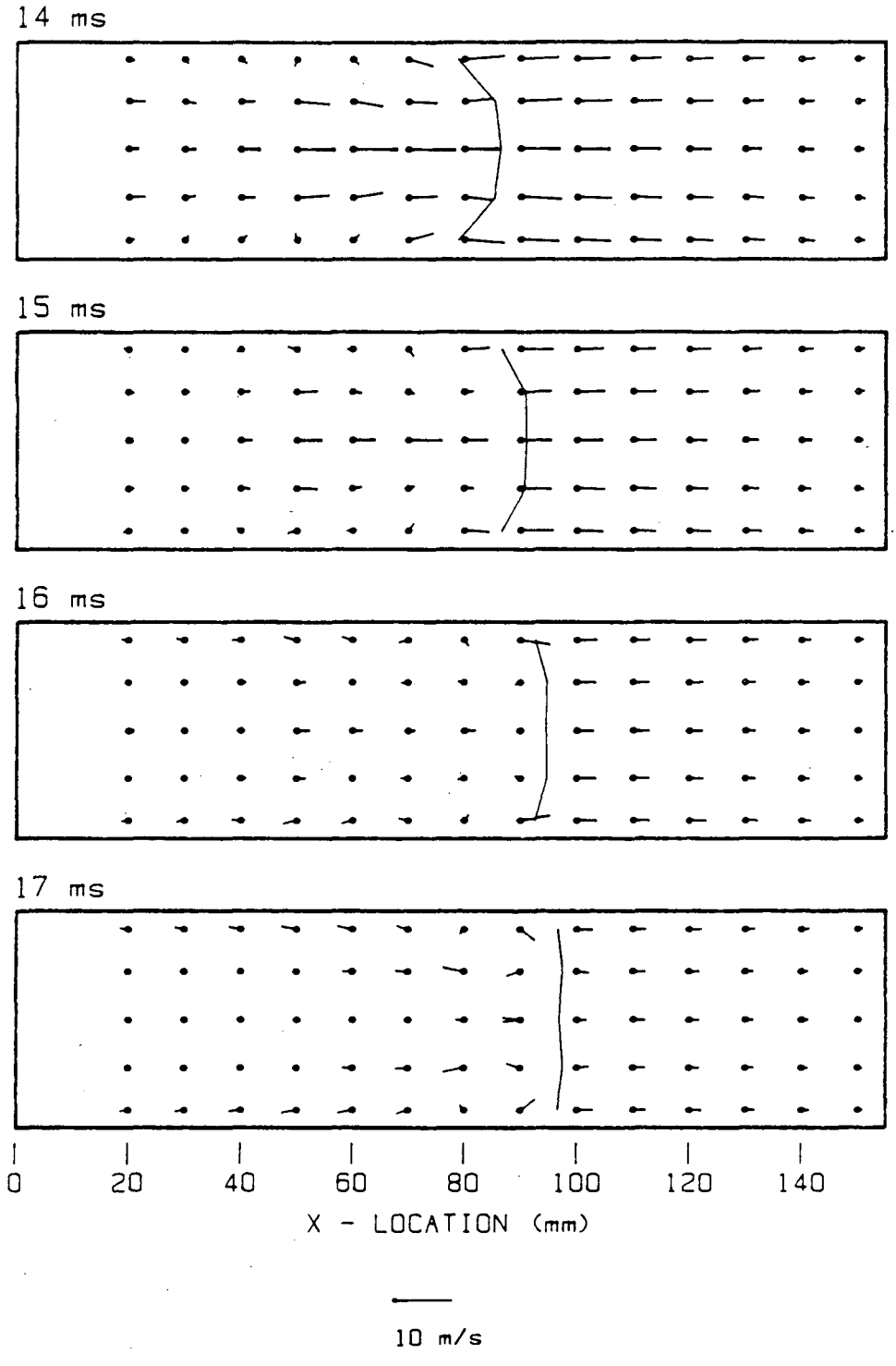

Figure 7-13a. Close-up of vector field during the transition phase of flame propagation. Vector scale 1 mm = 1.25 m/s. 14 ms $\leq$ t $\leq$ 17 ms.

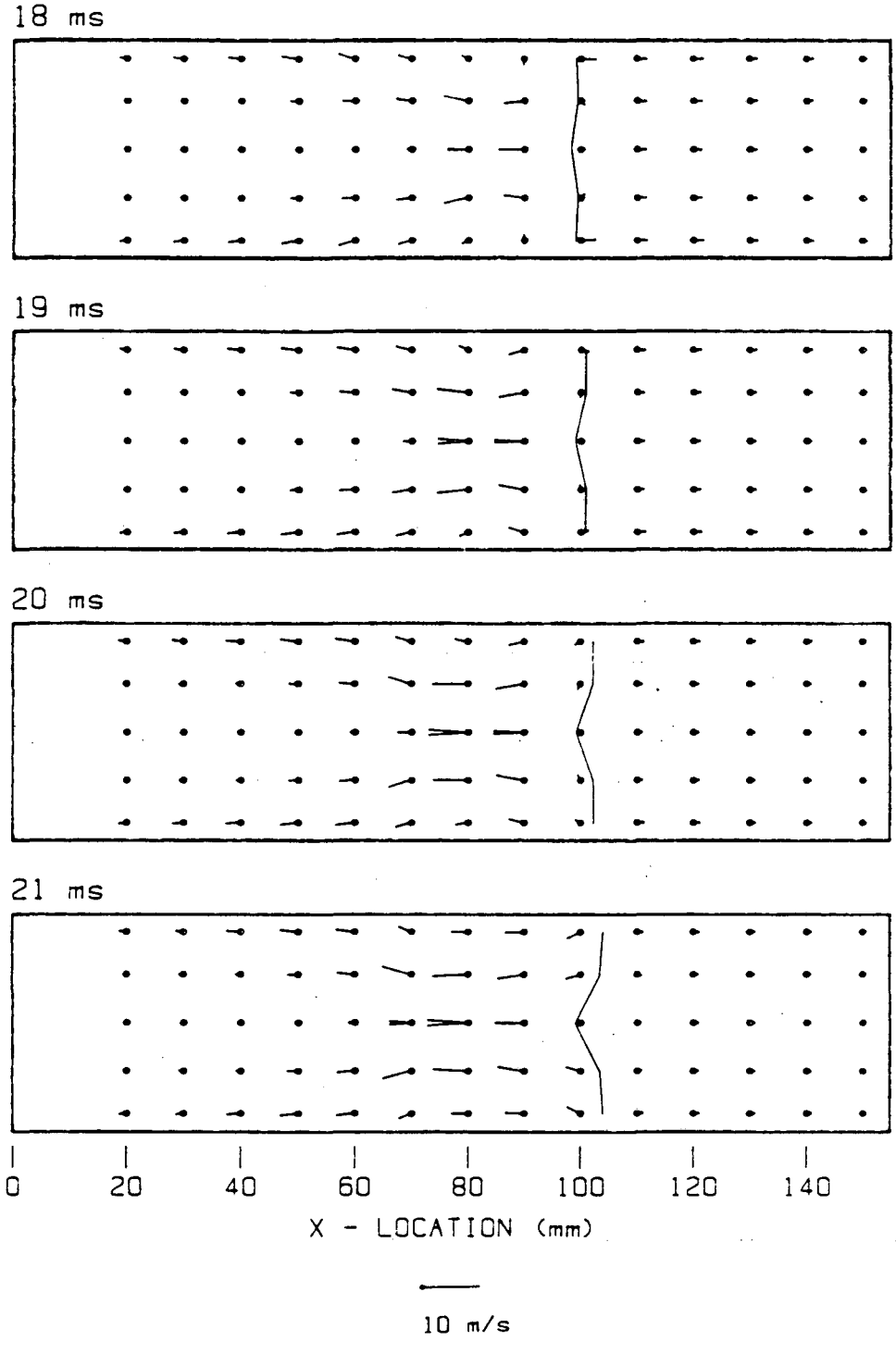

Figure 7-13b. Close-up of vector field during the transition phase of flame propagation. Vector scale: 1 mm = 1.25 m/s. 18 ms < t < 21 ms.

of separation, which started as the negative flow envelope, gradually moves back through the burned gas as the combustion proceeds.

The off-centerline unburned gas near the flame front is deflected toward the centerline as the "tulip" forms near the end of the transition phase. The unburned gas centerline velocity just within the flame cusp is slightly negative. The small reverse flow within the cusp of the "tulip" was also noted in the previous experimental results.

The burned gas near the flame front shows a strong rotational character. The velocity vectors near the flame front at t = 15 ms is shown in detail in Figure 7-14. Just behind the flame a distinct rotational structure is apparent. This structure marks the boundary of the reverse flow envelope mentioned above. Based on the cylindrical symmetry of the process the rotational structure is actually a planar view of a ring vortex behind the flame. As the "tulip" continues to form, the vortex moves back through the burned gas, and becomes the demarkation between the high velocity reverse flow region and the low velocity reverse flow region in the burned gas.

The salient features of the velocity vector field during the transition phase are enumerated below:

1) The magnitude of velocity everywhere decreases as the flame area decreases.

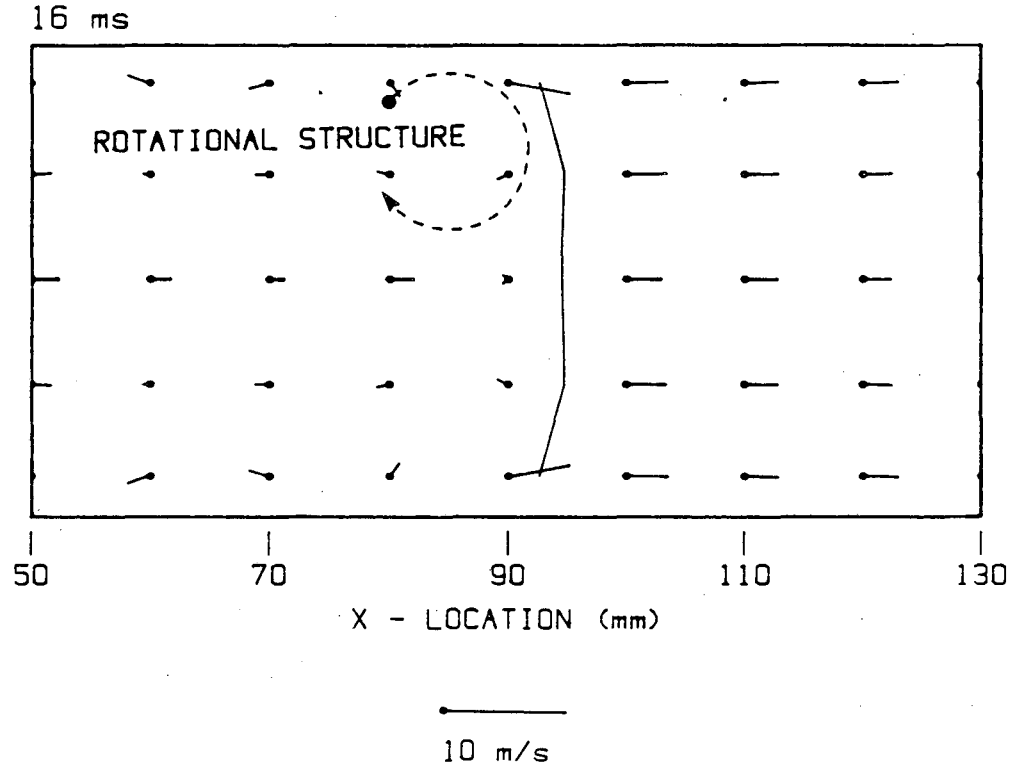

Figure 7-14. Close-up of vector field near the flame at the formation of the rotational structure. Vector scale: 1 mm = 0.625 m/s.

2) The unburned gas flow, except near the flame front, remains nearly one-dimensional, and at the end of the transition phase the unburned gas flow is nearly uniform as well.

3) The burned gas flow gradually changes from being positive everywhere, to exhibiting localized regions of reverse flow near the walls, to finally becoming negative everywhere.

4) In the unburned gas near the flame front, the off-centerline velocity is deflected toward the centerline as the "tulip" forms. The centerline velocity with the "tulip" cusp becomes negative.

5) A localized rotational region or ring vortex is formed just behind the flame as the "tulip" process begins. The vortex separates the burned gas into a high negative velocity region and low negative velocity region. The vortex moves back through the unburned gas as the flame progresses.

7.7.3 Section 3 -- "tulip" phase:

The "tulip" phase of flame propagation takes the longest time (approximately 25 ms). Although the flame must travel only the final one-third of the chamber, the unburned gas has been compressed so that the final one-third contains more than half of the initial combustible mass. The "tulip" phase is remarkably

stable. The velocity field during the "tulip" phase is shown in Figure 7-15 (velocity vector scale 1 mm = 1.25 m/s).

The unburned gas flow is nearly identical to the flow at the end of the transition phase. The flow is positive and uniform except near the flame front. Within the "tulip" cusp the flow is driven toward the duct centerline. This creates a stagnation point which results in a negative velocity just within the flame cusp and positive velocity ahead of it.

The burned gas flow is also similar to the burned gas motion at the end of the transition region. The fully formed "tulip", however, deflects the flow toward the side walls of the combustion vessel. The deflected fluid is then constrained by the walls and returned to nearly axial flow. As the "tulip" becomes more pronounced, the deflection creates a stagnation zone behind the cusp. The stagnation region is similar to the flame generated stagnation regions discussed by Zeldovich (1981), and is described in more detail in Chapter 9. Once the "tulip" is well established, the burned gas flow appears steady relative to the position of the flame. The steadiness was previously suggested by the axial velocity component measurements shown in Figure 7-9, but the vector field also appears steady. The remnants of the vortex created in the transition phase remain near the igniter, and continue to separate the burned gas into two regions. The regions are less distinct during the "tulip" phase because the magnitudes of velocity are lower.

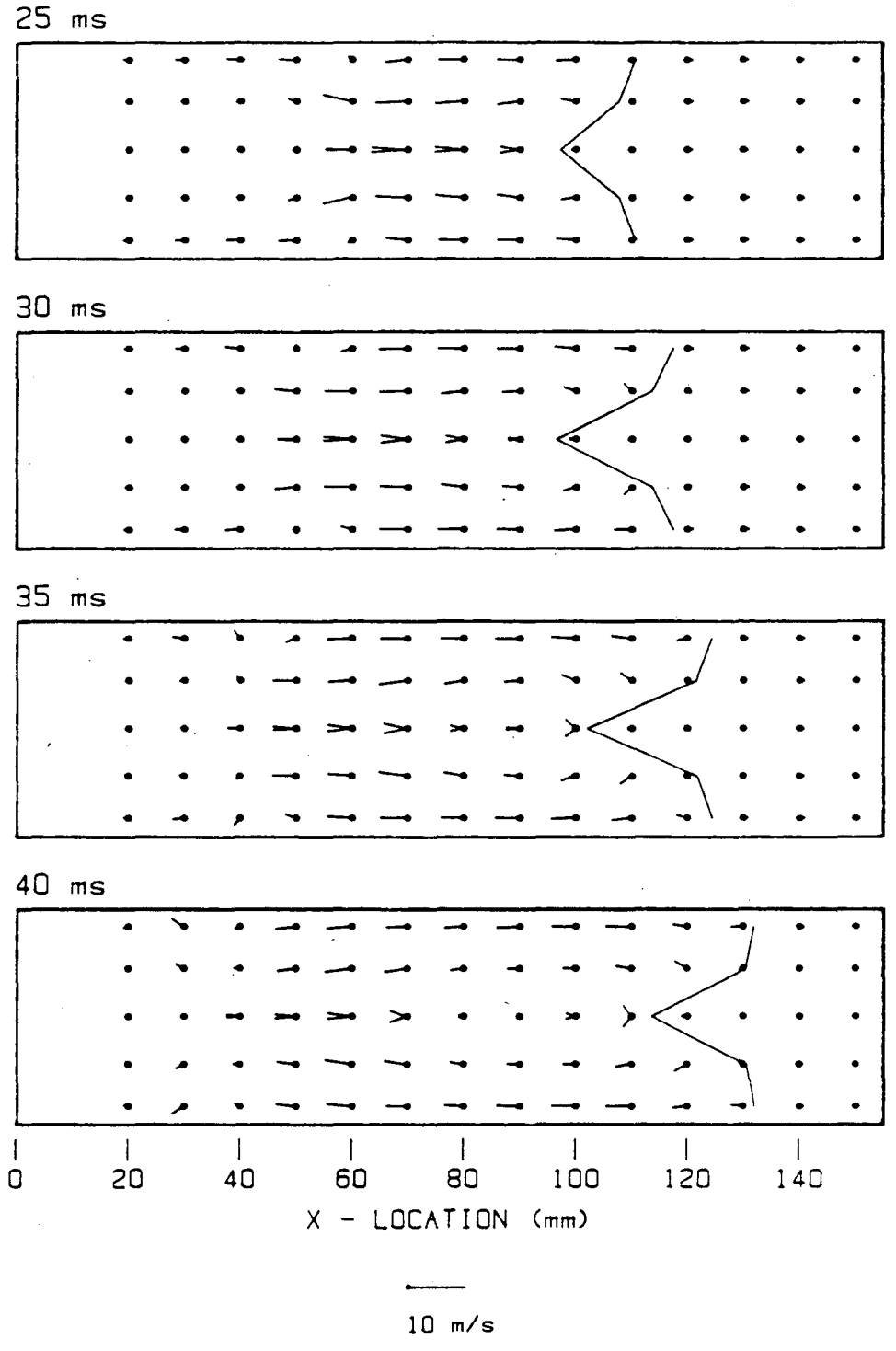

Figure 7-15. Close-up of vector field during the "tulip" phase. Vector scale: 1 mm = 1.25 m/s.

The salient features of the velocity vector field during the "tulip" phase are enumerated below:

1) The unburned gas, except near the "tulip" has small uniform positive velocity.

2) Near the "tulip" the small centerline reverse flow and off-centerline deflection, which began during the transition phase, are maintained.

3) The burned gas motion becomes steady relative to the flame front, except for the remnants of the vortex generated during the transition phase, which remain near the igniter endwall.

4) The "tulip" cusp causes a stagnation region behind its vertex, as the flame deflects the gas passing from the unburned to the burned side.

7.8 Discussion

The burned gas behavior is complex because the flame shape influences the flow in the burned gas. The deflection of flow by a flame sheet (Maxworthy, 1961, Strehlow, 1984), and the generation of vorticity by a curved flame (Hayes, 1953) are examples of this influence. The character of the burned gas flow field changes during the flame propagation because both the flame shape and the magnitude of the unburned gas velocity are not steady. Once the flame shape and the unburned flow become steady (approximately t = 30 ms), the burned gas flow field also becomes

steady (except for the remnants of the vortex generated earlier). The coupling of the burned gas fluid motion with the flame shape and the unburned gas flow makes quantitative discussion of the burned gas flow field difficult. A more complete discussion of the influence of the flame on the burned gas flow field is reserved for Chapter 9.

The unburned gas flow field, however, except within the flame cusp, does not appear sensitive to the flame shape. Further, the measured one-dimensional nature of the unburned gas flow encourages the use of one-dimensional modeling to determine the major influences in the flow generation. A one-dimensional model for the unburned gas motion, and its dependence on the flame front is presented in Chapter 8.

7.9 Summary

The important discoveries of this final set of experiments are:

1) The burned gas velocity field is much more complicated than the unburned gas velocity field. The burned gas motion depends both on the unburned gas motion and the flame shape, while the unburned gas is nearly one-dimensional.

2) The unburned gas velocity is positive everywhere and at all times except just within the "tulip" cusp. The negative velocity within the cusp is caused by a stagnation flow generated by the lobes of the "tulip" forcing unburned gas flow toward the centerline.

3) A transition in the velocity vector behavior accompanies the transition of the flame to its "tulip" shape. The burned gas flow changes direction from positive to negative, and the unburned gas flow dramatically decreases in magnitude.

4) A ring vortex is formed in the burned gas behind the flame at the end of the transition phase. The vortex remains intact and moves back through the burned gas as the propagation proceeds.

5) The "tulip" phase of propagation is very stable. The burned gas motion and the unburned gas motion during this phase appear steady when viewed from a frame of reference on the flame front.

The velocity vectors indicate many interesting features of fluid motion within a closed duct during nonsteady flame propagation. However, most of the dynamic in the flow occurs during the transition phase. The dynamic nature of the flow during this period is undoubtedly associated with the rapid change in flame area as the wall quench takes effect. The discussion presented in Chapter 5 links the flame area and the rate of pressure rise. A similar connection exists between the flame area and the fluid velocity. This connection is presented in the following chapter. Similarly, there are non-uniform and rotational features of the burned gas motion which appear during

the transition phase which correlate with the appearance of the "tulip" flame. The connection between the flame shape and the rotational motion of the burned gas is discussed in Chapter 9.

CHAPTER 8

One-dimensional Model for Unburned Gas Motion

8.1 Analytical discussion

There are two one-dimensional configurations for flame propagation in closed vessels. The first is the propagation of a flame in a spherical chamber, initiated by a centrally located spark. The single space dimension is the radius of the flame front, r. This configuration has been used extensively for the determination of laminar flame speeds (Bradley and Mitcheson, 1976, Rallis and Garforth, 1976). The second is the propagation of a planar flame in a tube, where the single space dimension the axial location of the flame front, X. A planar flame in tubes is not realized in practice, but most closely approximates the flame propagation associated with "tulip" flames.

The analysis relies primarily on the one-dimensional unsteady continuity equation. The unsteady continuity equation with a single space dimension in rectangular cartesian coordinates, Figure 8-1a, is,

$$(1/\rho)(\partial\rho/\partial t) + \partial V/\partial X = 0, \qquad (8.1a)$$

and in spherical coordinates, Figure 8-1b, is,

$$(1/\rho)(\partial\rho/\partial t) + \partial V/\partial r + 2V/r = 0 \qquad (8.1b)$$

where ρ is the density, t is the time, and V is the velocity. Assuming ρ a function of time only, except for a discontinuous change in density across the flame front (this assumption is

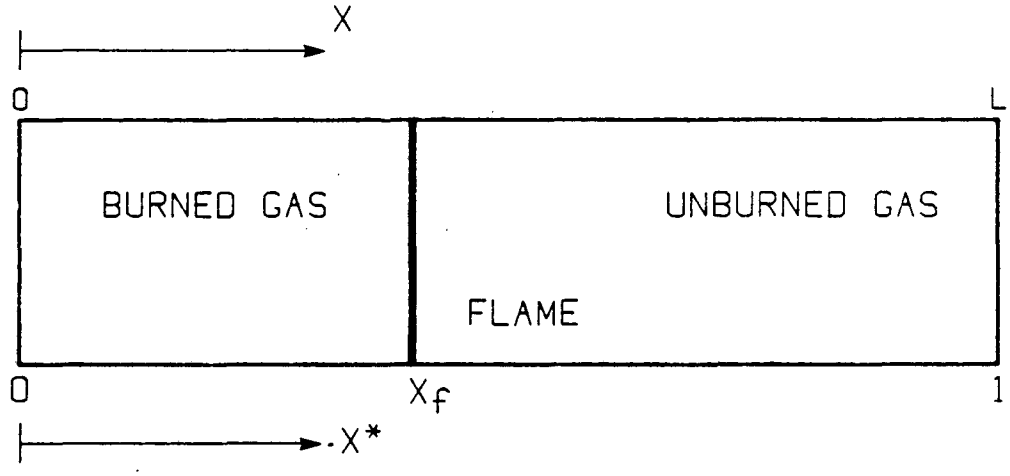

a)

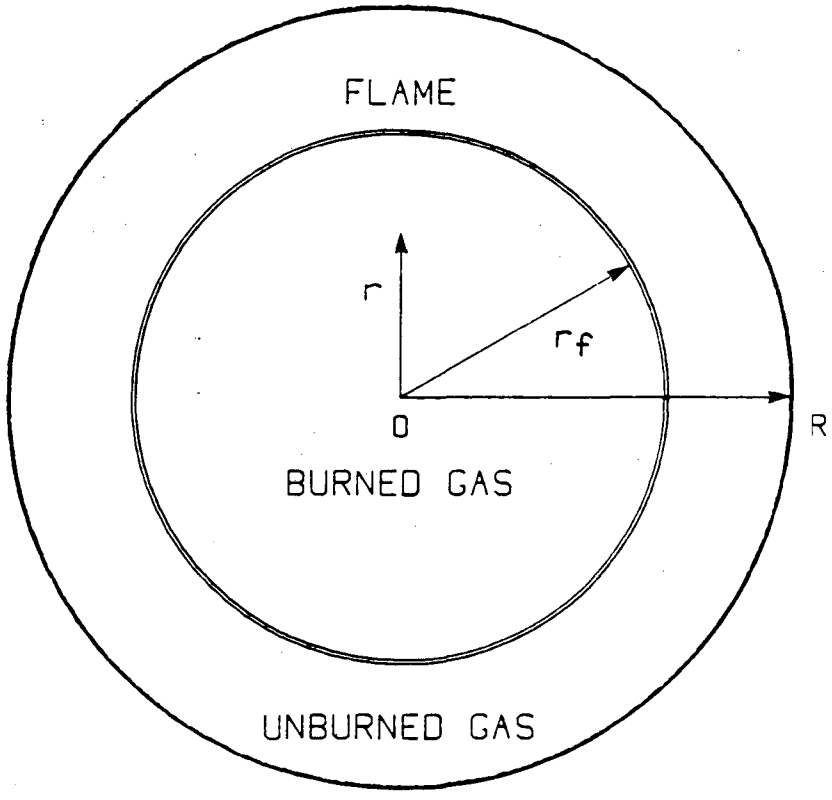

b)

Figure 8-1. Coordinate layout for one-dimensional analysis.
a) Planar one-dimensional
b) Spherical one-dimensional

described in Chapter 3), the continuity equations can be spatially integrated to within a function dependent only on time,

$$V(X,t) = (1/\rho)(d\rho/dt)X + g1(t) \qquad (8.2a)$$

and

$$V(r,t) = (1/3)(1/\rho)(d\rho/dt)(1/r^2 - r) + g2(t), \qquad (8.2b)$$

where g1(t) and g2(t) are functions depending only on time, and are determined from the boundary conditions. Equations 8.2 apply in both the burned and unburned fluid but cannot be applied across the flame boundary. Consequently, the solution of the above equations is different in the burned and unburned gas. The boundary conditions for the planar case are,

unburned gas: V = 0 at X = L, where L is tube endwall

burned gas: V = 0 at X = 0, the igniter endwall

and for the spherical case the boundary conditions are,

unburned gas: V = 0 at r = R, with R the vessel radius

burned gas: V - finite at r = 0, the vessel center

Imposing the above boundary conditions produces one-dimensional velocity profiles in the two geometric configurations. For the planar case the solutions are,

unburned ($X > X_f$): $V(X,t) = (1/\rho)(d\rho/dt)(L - X)$ (8.3a)

burned ($X < X_f$): $V(X,t) = -(1/\rho)(d\rho/dt)X$

and for the spherical case the solutions are,

unburned ($r > r_f$):

$$V(r,t) = (1/3)(1/\rho)(d\rho/dt)((R^3/r^2) - r) \qquad (8.3b)$$

burned ($r < r_f$): $\quad V(r,t) = -(1/3)(1/\rho)(d\rho/dt)r$

The specification of the velocity field is completed by the velocity jump condition at the flame. The velocity jump is required to maintain mass continuity through the flame,

$$\rho_b S_b = \rho_u S_u, \qquad (8.4)$$

or

$$S_b = \sigma S_u, \qquad (8.5)$$

where S is the velocity relative to the flame front, Figure 8-2a, σ is the expansion ratio of the mixture (ρ_u/ρ_b), and the subscripts b and u represent burned and unburned gas respectively. The velocity jump from the unburned gas velocity, S_u, to the burned gas velocity, S_b, is then,

$$\Delta V = S_u - S_b = (\sigma - 1)S_u. \qquad (8.6)$$

When the frame of reference becomes the fixed laboratory coordinates, Figure 8-2b, the jump condition still applies, but there is a convective component which is added to the jump velocity. The jump condition affects only the component of velocity normal to the flame front.

The character of the solutions at a fixed time in the two geometric configurations are shown in Figure 8-3. The magnitude

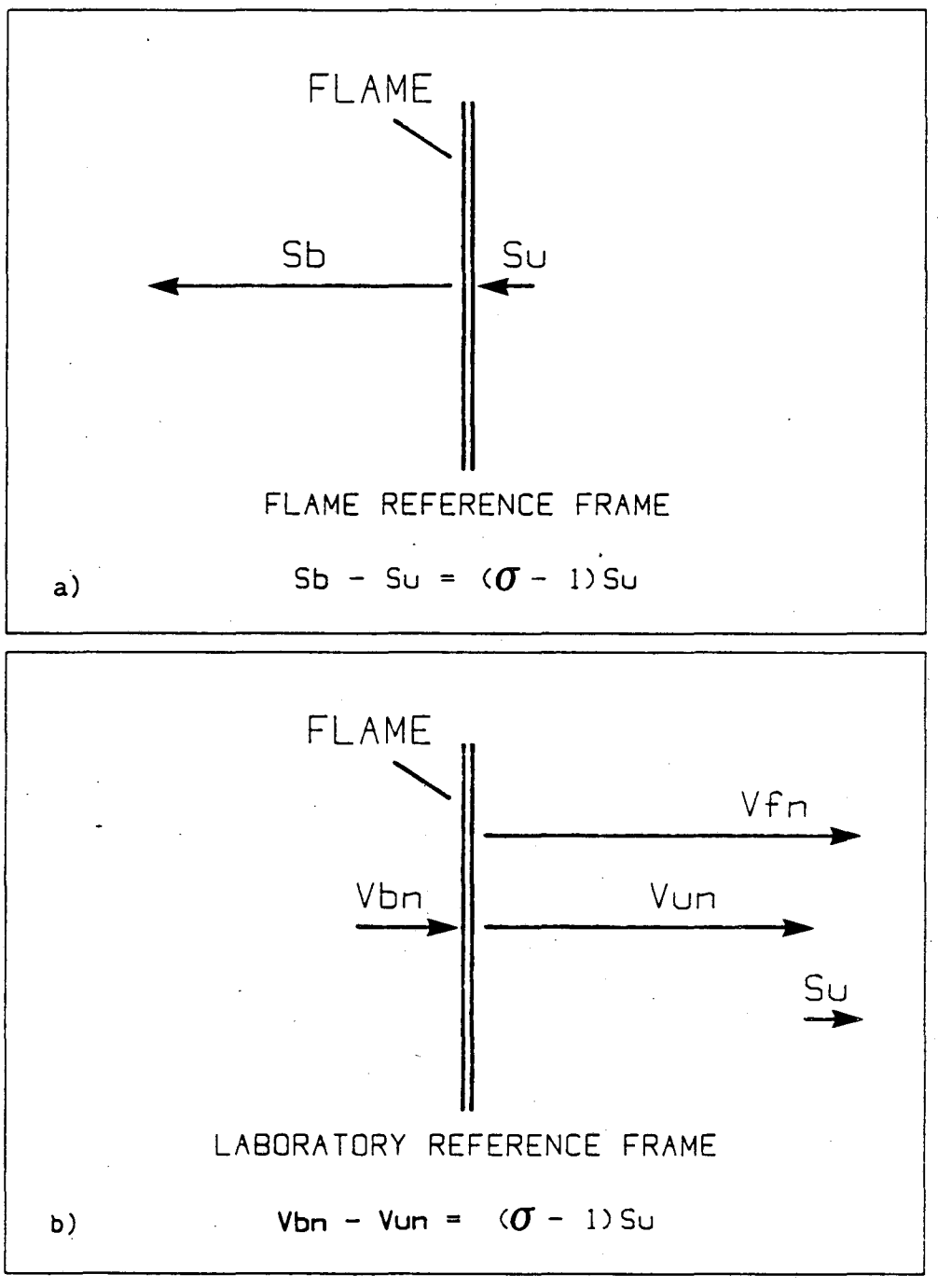

Figure 8-2. Velocity jump at the flame front.
a) Flame reference frame
b) Laboratory reference frame

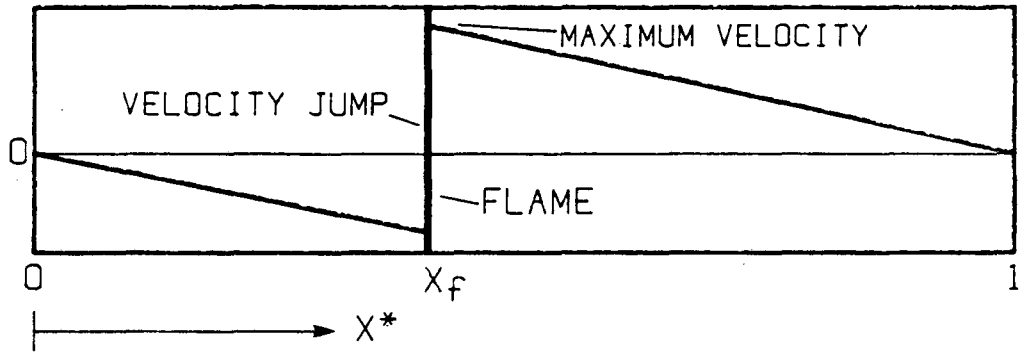

a)

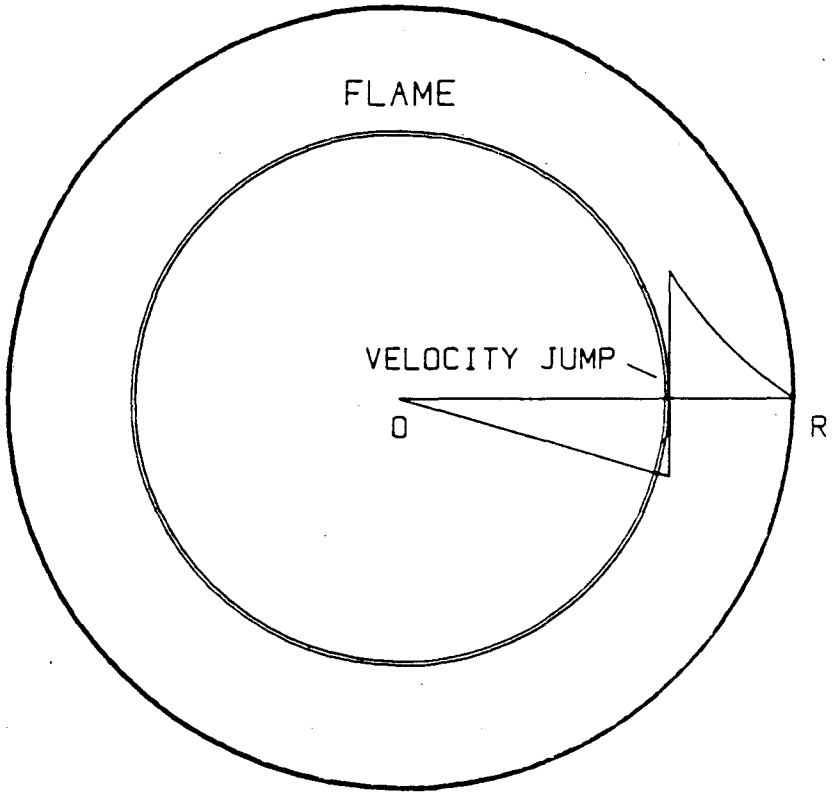

b)

Figure 8-3. Form of the one-dimensional solutions.
a) Planar one-dimensional
b) Spherical one-dimensional

of the solution depends on the $(1/\rho)(d\rho/dt)$ term. The planar solution, Figure 8-3a, shows a linear decrease in the unburned gas velocity from a maximum at the flame front to zero at the endwall. The burned gas velocity profile is also linear increasing from a negative maximum at the flame front to zero at the igniter endwall. The spherical solution is linear from the center of the vessel to the flame front and then an inverse r^2 dependence is added in the unburned gas. The solution is compared to the numerical results of Bradley and Mitcheson (1976) and Rallis and Garforth (1976) in Figure 8-4. Unfortunately, there is very little experimental evidence of the velocity field generated during flame propagation in a spherical vessel, but the available results agree with the numerical references mentioned above.

The density can be replaced with pressure to determine the value of the $(1/\rho)(d\rho/dt)$ term in the unburned gas, by making the assumption of isentropic compression of the unburned gas,

$$p = \text{const}(\rho^{\gamma}) \tag{8.7}$$

and differentiating,

$$(1/\gamma p)(dp/dt) = (1/\rho)(d\rho/dt). \tag{8.8}$$

After substituting (8.8) into the appropriate velocity profile solution, the one-dimensional gas velocity field can be determined from the pressure/time record of the closed volume combustion process alone.

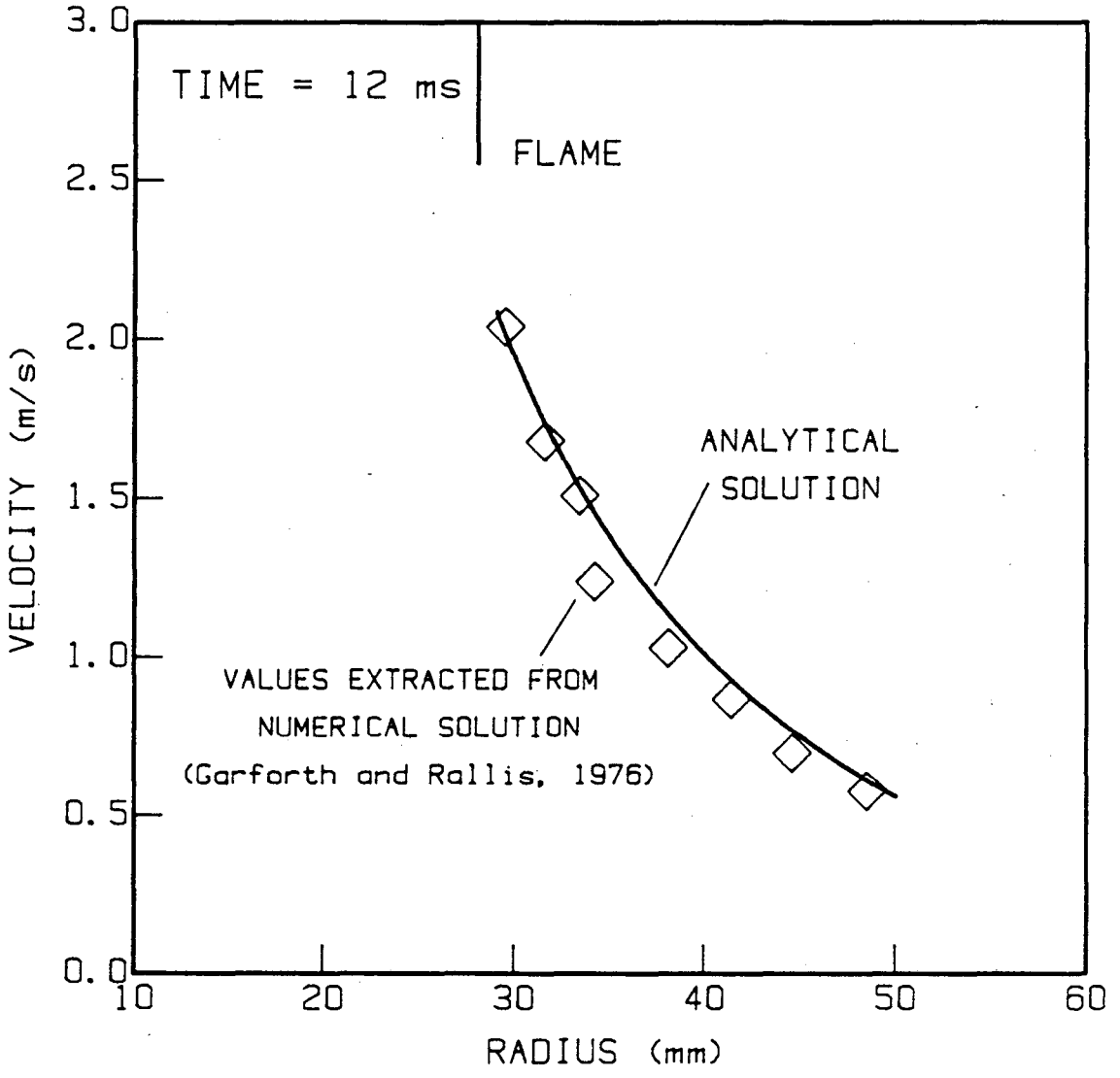

Figure 8-4. Comparison of analytic solution of fluid velocity in constant volume spherical vessel to the velocity extracted from particle trajectories in the numerical solution of Garforth and Rallis (1976).

8.2 Comparison of experiment to one-dimensional model

A stable planar flame can be realized only in very slow burning mixtures (Clavin, 1985). These mixtures cannot be ignited by a spark, and consequently are difficult to generate in closed vessels. Furthermore, very slow burning mixtures are subject to large buoyancy effects (see Chapter 4 ethylene/air flame with equivalence ratio = 0.6). The one-dimensional planar solution is, therefore, only an approximation to the tube combustion presented in this work. The approximation is particularly poor in the burned gas because the flow deflection caused by the flame front (Chapter 9) produces large non-uniformities in the burned gas flow field. The non-uniformity of the burned gas is evident from the velocity vector maps presented in the preceeding chapter. Interestingly, however, despite the non-planar flame shape, the unburned gas velocity field appears from the experimental results to be nearly one-dimensional. Figure 8-5 shows the axial component of velocity/time behavior of the unburned gas at a fixed X location but at different radial locations. The velocity is nearly identical in all cases until the flame arrives. The lack of dependence of the axial component of velocity with radial location was also reported by Starke and Roth (1984). Figure 8-6 shows the radial component of velocity at two X locations and three Y locations. In all cases, the radial component is negligibly small until the flame arrives. At the centerline the radial velocity is negligible at all times because of the symmetry constraint. These results suggest that,

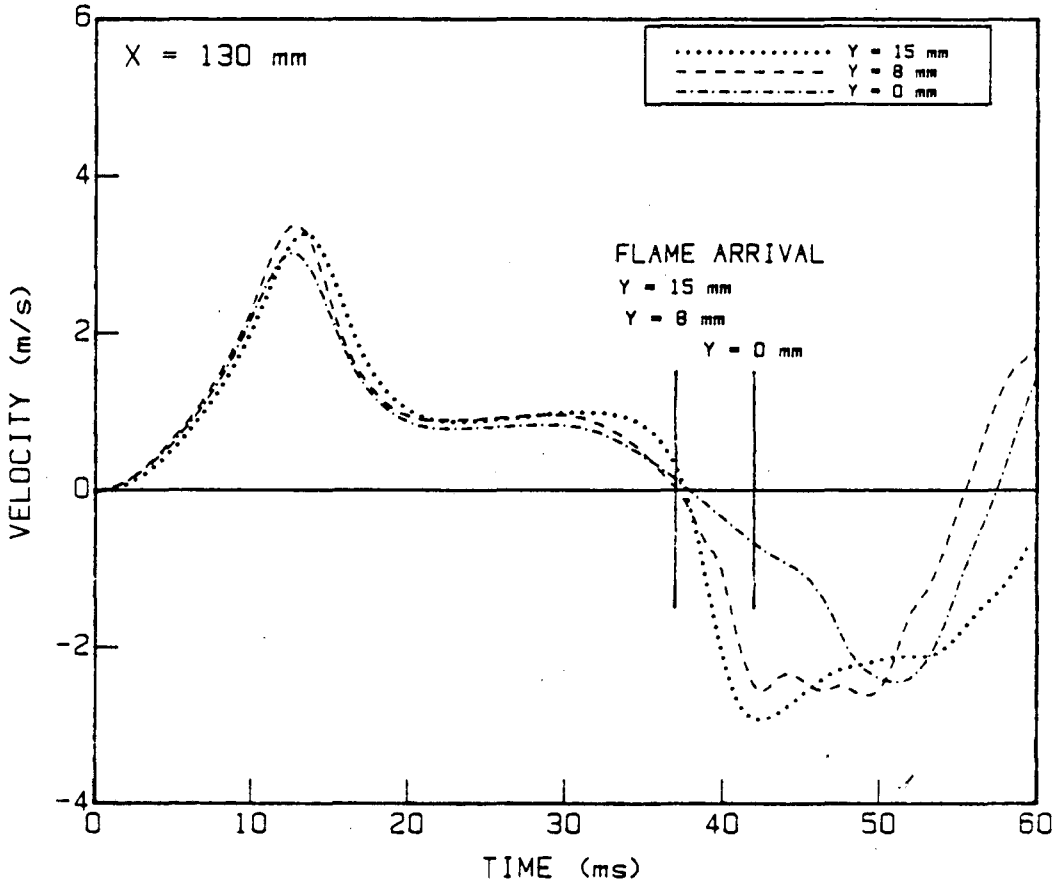

Figure 8-5. Axial component of velocity at three radial locations. The curves are very similar until the flame arrives.

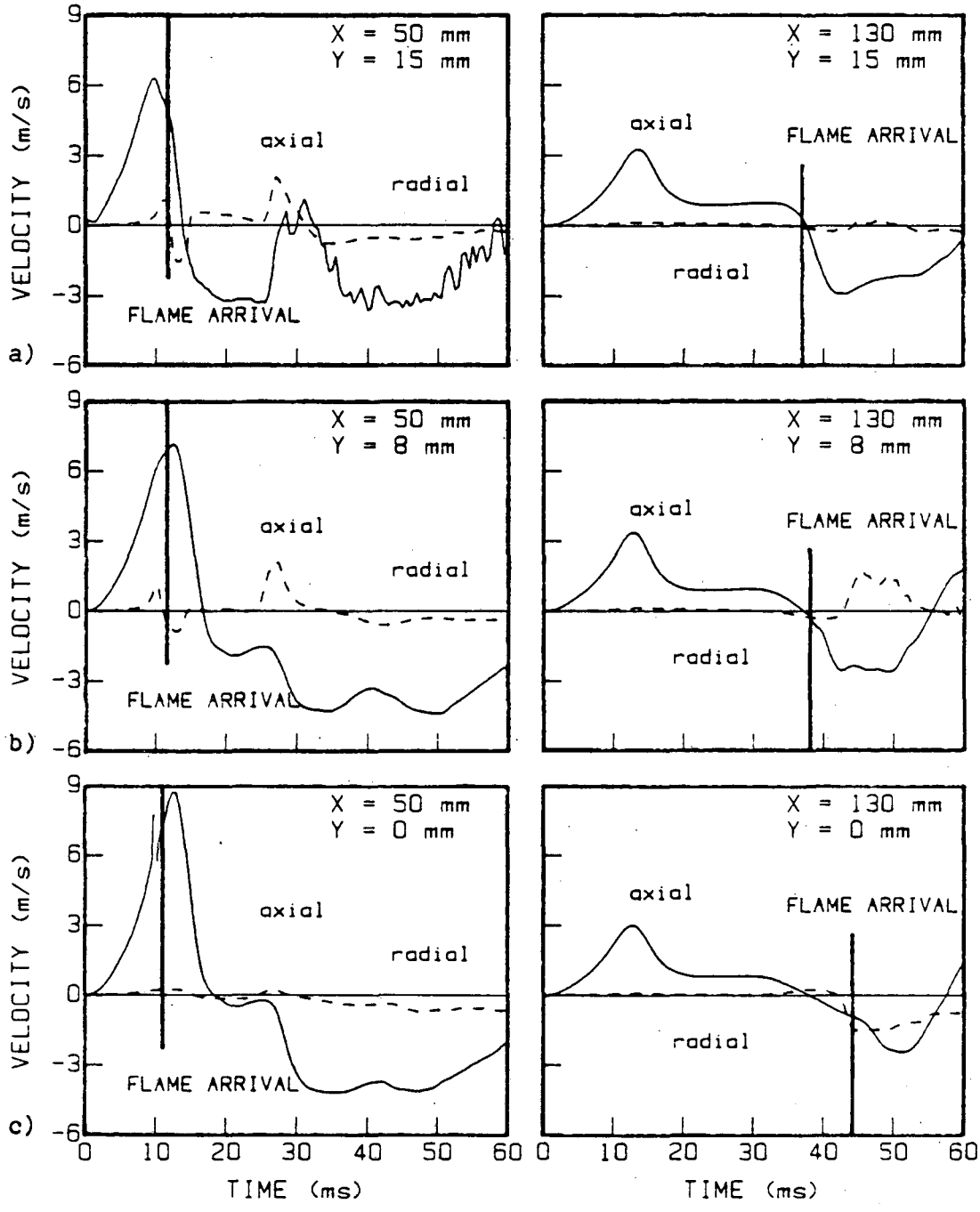

Figure 8-6. Axial and radial component of velocity at several measurement locations. In all cases, the radial component is insignificant until the flame arrives.
a) Y = 15 mm
b) Y = 8 mm
c) Y = 0 mm

contrary to the burned gas motion, the unburned gas is not noticeably affected by specific changes in flame shape, and is therefore a good candidate for analysis by the one-dimensional model described above.

The planar one-dimensional solution for the unburned gas, with the density replaced by pressure is,

$$V(X,t) = (1/\gamma p)(dp/dt)(L - X). \qquad (8.9)$$

This equation contains two pieces of information:

1) The velocity decreases linearly from a maximum at the flame front to zero at the endwall.

2) The velocity magnitude can be related to the pressure and rate of pressure rise during the combustion.

Agreement between the experimental results and the linearity prediction (1) is very good, Figure 8-7. The figure shows the axial component of the centerline velocity in the unburned gas at several times during the combustion. Figures 8-4 and 8-5 show that the axial component of the centerline velocity is representative of the entire unburned gas flow. The velocity increases until approximately 12.5 ms, Figure 8-6a, and then decreases, Figure 8-6b. The velocity magnitude remains linearly decreasing with X throughout the velocity increase and decrease. The measured velocity does not go to zero at the endwall due to leaks out of the chamber end. The velocity at the endwall, obtained by extrapolation, provides an estimate of the leak loss

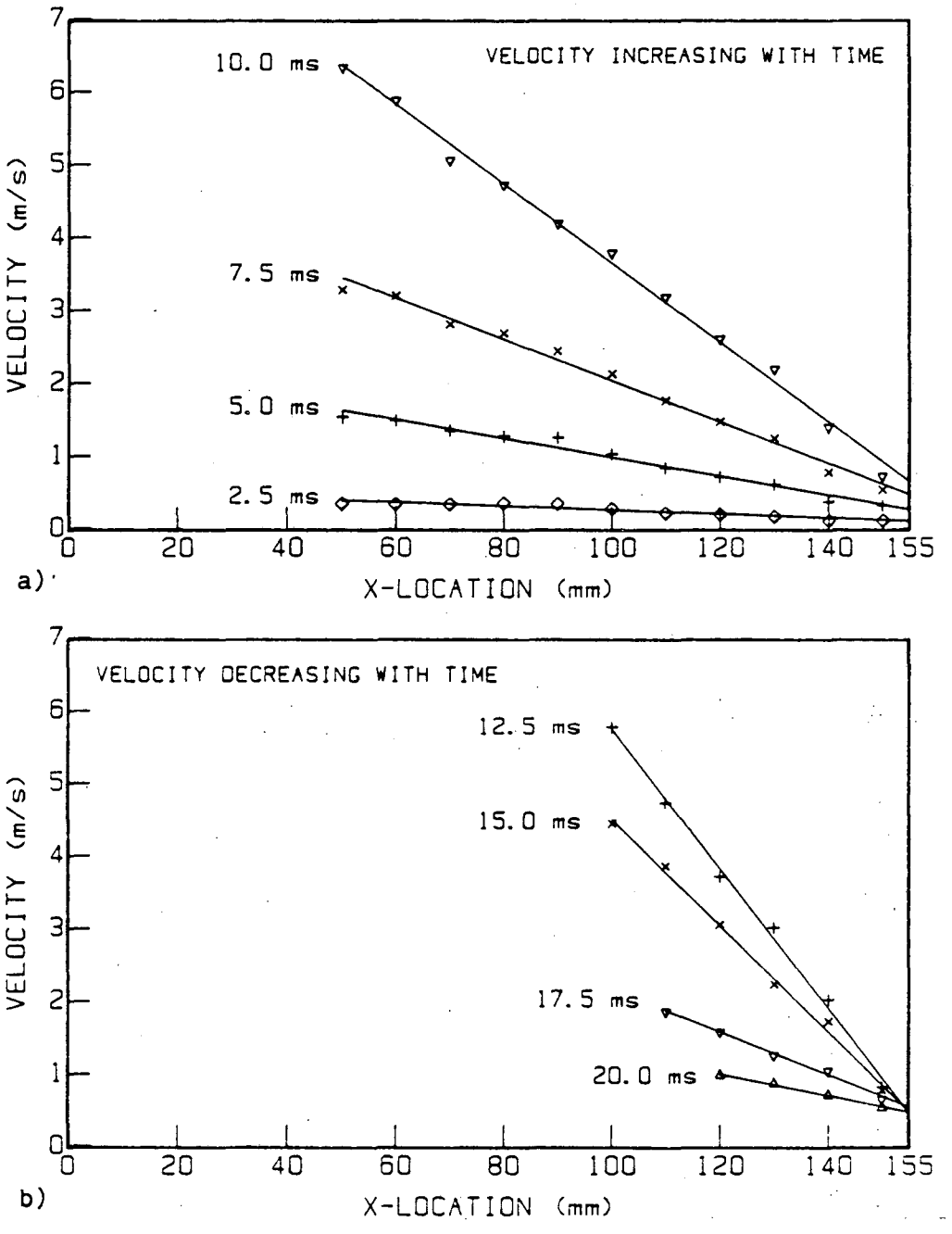

Figure 8-7. Axial component of unburned gas velocity showing linear decrease from the flame to the endwall.
a) $t < 11$ ms
b) $t > 11$ ms

from the chamber. The fraction of gas lost during the combustion is,

$$(m_l/m_o) = (\rho_{av}/\rho_o)V_{av}T_c/L \qquad (8.10)$$

where m_l is the mass loss through leaks, m_o is the initial mass in the combustion vessel, (ρ_{av}/ρ_o) is the ratio of the average leaking gas density to the initial gas density (approximately 2), L is the duct length (155 mm), V_{av} is the average extrapolated endwall velocity (approximately 0.4 m/s), and T_c is the total combustion time (approximately 50 ms). Equation (8.10) predicts that approximately 30 percent of the initial mass leaks out of the vessel. Most of the leaking gas escapes through the open inlet and exhaust ports located in the endwall.

The recorded pressure during the single point ignition combustion process, Figure 8-8, shows the effect of heat losses and leak losses from combustion vessel. At approximately t = 15 ms, the drop in pressure due to these losses is actually greater than the increase in pressure from the combustion process. It is difficult to separate the heat loss from the leak loss, but previous heat transfer work in a similar combustion vessel (Woodard et al., 1981), indicates that heat loss accounts for less than 20 percent of the difference between the measured pressure and the expected adiabatic pressure. Equation (8.9) uses the pressure information to predict the unburned gas velocity. Figure 8-9 compares the predicted velocity at X = 130 mm (dashed line) and the measured axial velocity (solid line)

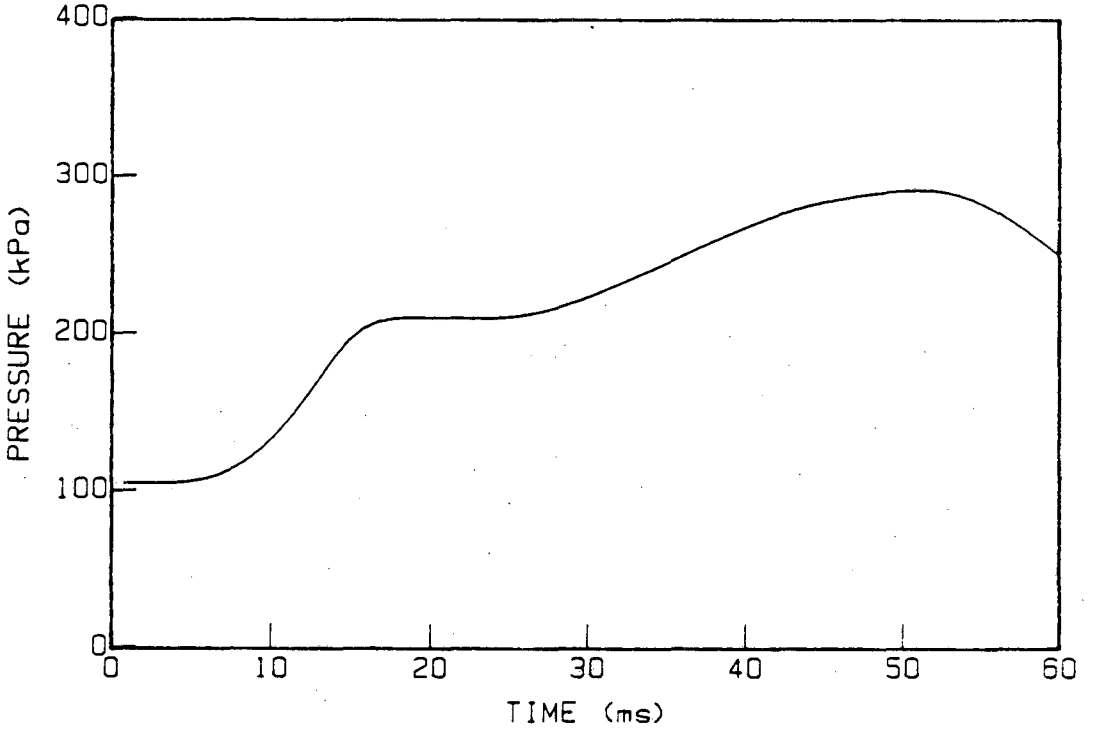

Figure 8-8. Pressure/time history of combustion initiated by a single point igniter in a plexiglas combustion vessel with leaks.

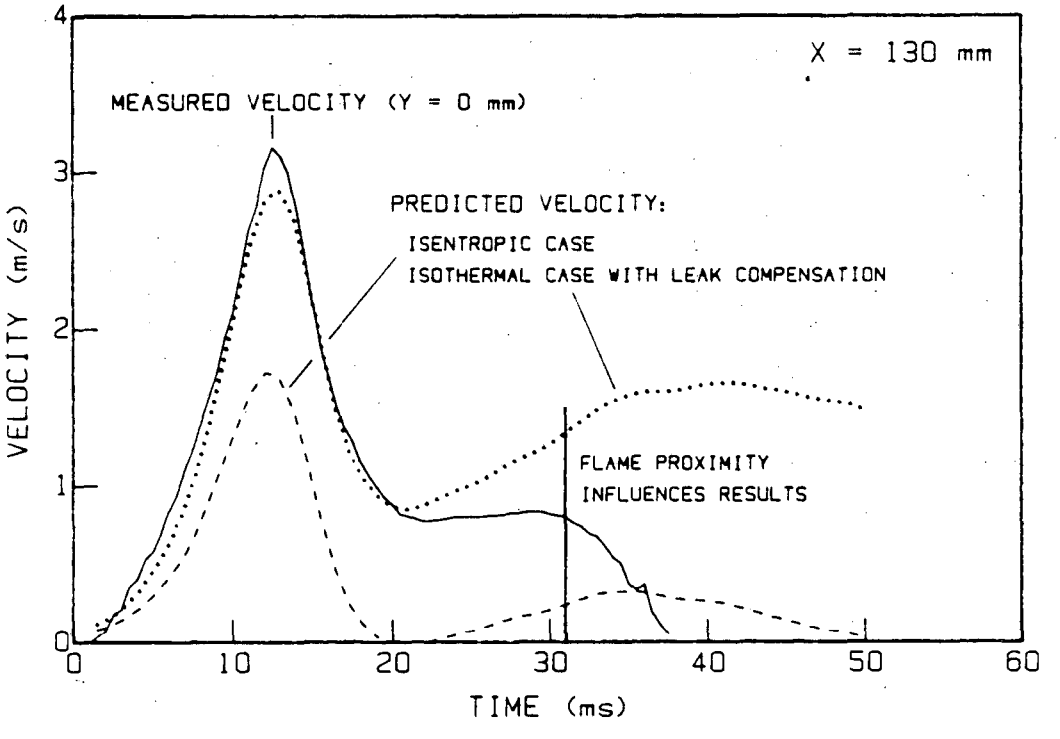

Figure 8-9. Comparison of measured axial component of velocity to the predicted value from one-dimensional models.

at the same location. Both curves have a velocity peak near t = 13 ms, but the measured velocity magnitude is much higher than the predicted velocity. The discrepancy arises from the inappropriate model assumptions of isentropic compression and zero velocity at the boundary. The magnitude of the leak from the combustion vessel gives a non-zero velocity at the endwall (X = L), and suggests an isothermal compression assumption for converting the density in equation (8.1) to the pressure in equation (8.9). With these new assumptions, equation (8.9) becomes,

$$V = (1/p)(dp/dt)(L - X) + V(L,t). \qquad (8.11)$$

Figure 8-9 also shows a comparison of the predicted velocity from equation (8.11) at X = 130 mm (dotted line) to the measured axial velocity at the same location (solid line). For simplicity, the prediction assumes that the endwall velocity, V(L,t), is linearly related to the pressure. The modified predicted velocity and the measured velocity are approximately equal until the flame influence begins to affect the measured velocity (approximately t = 35 ms).

8.3 Flame area relationship to fluid velocity

Chapter 5 showed the relationship between the flame area and the pressure inside a closed combustion vessel. The above discussion relates the pressure inside the vessel to the gas velocity. It is apparent, therefore, that the flame area is related to the gas velocity. The expression relating the flame

area to the pressure and rate of pressure rise from Chapter 5 is,

$$a_f = [(m_o/\rho_o)(1/(p_f - p_o))S_u](p/p_o)^{(-1/\gamma)}(dp/dt) \qquad (8.12)$$

The flame area can be related to the one-dimensional velocity in the following way. The expression for mass burning rate obtained in Chapter 5 is,

$$dm/dt = \rho_o(p/p_o)^{(1/\gamma)}S_u a_f. \qquad (8.13)$$

Noting that $\rho_o = m_o/(a_c L)$, where a_c is the cross-sectional area of the chamber and L is the length of the chamber, and introducing $P = p/p_o$ and $A_f = a_f/a_c$, (8.13) becomes,

$$(1/m_o)(dm/dt) = (A_f S_u/L)(P)^{(1/\gamma)}. \qquad (8.14)$$

Another expression for mass burning rate comes again from Chapter 5,

$$(1/m_o)(dm/dt) = (1/(p_f - p_o))(dp/dt) \qquad (8.15)$$

Equating (8.14) and (8.15) and solving for dP/dt,

$$dP/dt = (P_f - 1)(S_u A_f/L)(P)^{(1/\gamma)}. \qquad (8.16)$$

Replacing dp/dt in (8.8) above, an expression relating the velocity in the unburned gas to the flame area is,

$$V(X^*,t) = (1/\gamma)(P_f - 1)(P)^{((1/\gamma) - 1)}(A_f S_u)(1 - X^*), \qquad (8.17)$$

where $X^* = X/L$. A similar analysis using the isothermal compression assumption and the leak velocity leads to a slightly

different relationship between flame area and velocity,

$$V(X^*,t) = (P_f - 1)A_f S_u(1 - X^*) + V(1,t) \qquad (8.18)$$

In both cases the velocity is linearly dependent on the flame area. All of the unburned gas velocity measurements show a velocity surge early in the combustion process ($t < 20$ ms), Figure 8-10. The equivalence of equations (8.9) and (8.17) indicates that the instantaneous flame area is the primary factor involved in the early velocity peak.

The flame shape history, deduced from LDA dropout (Chapter 7) and high-speed schlieren movies (Chapter 4), shows that the maximum flame area coincides approximately with the maximum in the unburned gas velocity. Further, the decrease in unburned gas velocity following this maximum is accompanied by a rapid decrease in flame area. Unfortunately, the precise flame area is difficult to determine from schlieren or LDA dropout measurements. The schlieren only gives a line-of sight integrated image and hence some assumption must be made as to the three-dimensional structure of the flame front. The assumption used by Smith (1977) and Steinert et al. (1982) was that a flame initiated by a line igniter remains two-dimensional for the duration of the combustion process. The flame area, therefore, is the length of the schlieren image of the flame multiplied by the viewing depth of the chamber. Smith estimated a possible error of 100 percent with this technique due to flame curvature near the vessel walls. As shown in the schlieren sequences

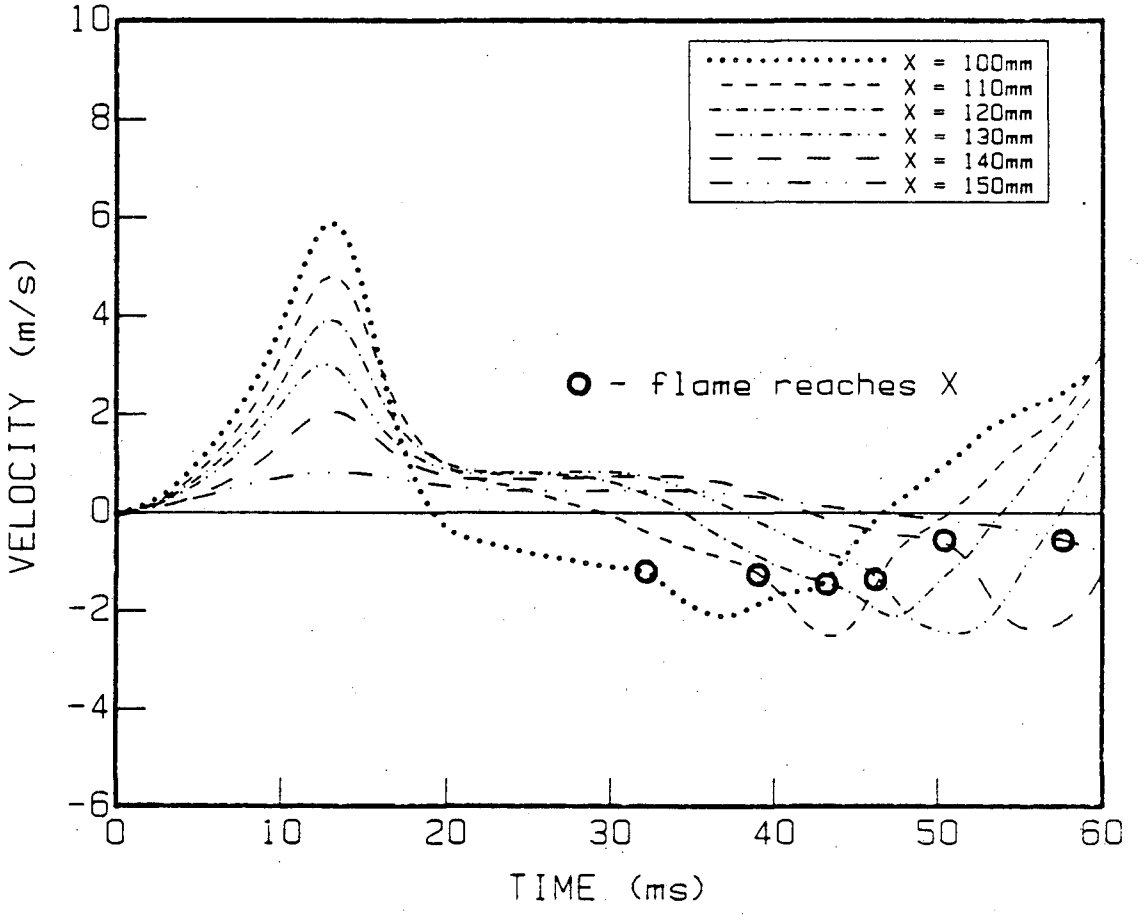

Figure 8-10. Axial component of velocity at the centerline (Y = 0 mm) for various measurement locations.

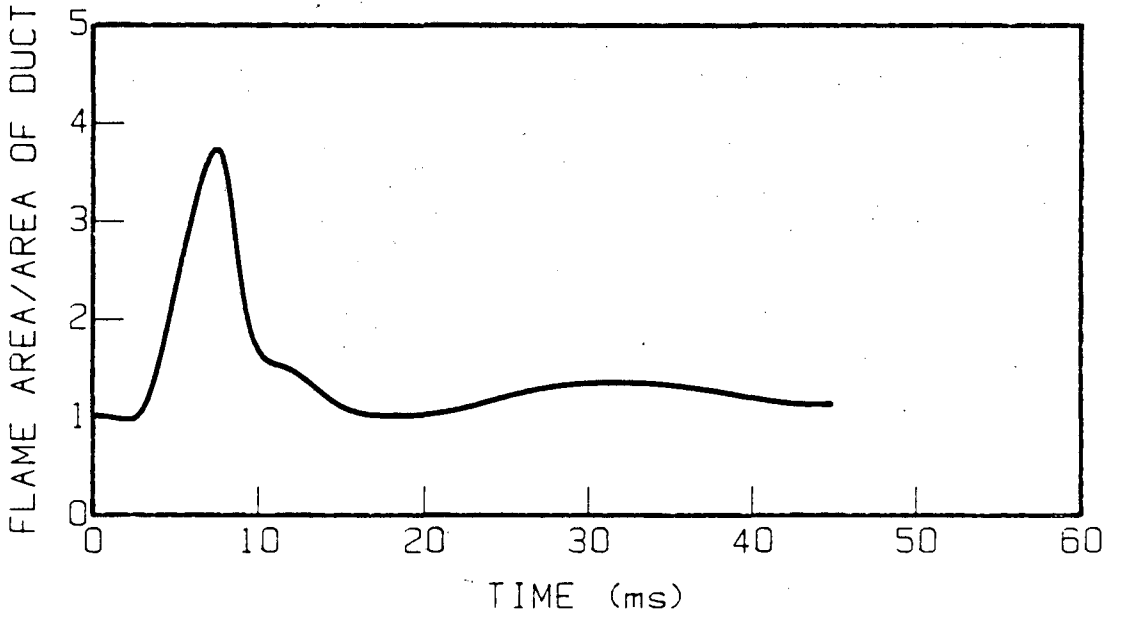

Figure 8-11. Flame area determined from flame trajectory information normalized by the cross-sectional area of the combustion vessel.

presented in Chapter 4, however, the two-dimensional assumption for the later flame is not accurate, as the "tulip" shape is nearly cylindrically symmetric. Small scale wrinkling of the flame front also causes errors in the flame area determination. The flame is assumed smooth, and any deviations from smoothness will not be accurately accounted for. It appears, therefore, that the errors in flame area from the schlieren technique are likely to be somewhat higher than estimated by Smith.

The time of flame arrival from LDA dropout, Chapter 7, can also be used to reconstruct the flame shape history, Figure 7-7, and therefore determine the flame area. Unfortunately, this flame area determination technique is also rife with uncertainties. There are uncertainties about the flame location in the corners of the duct and very near the duct sidewalls, as the LDA was never used in these locations. The wrinkling uncertainty in the schlieren method is also a problem in the LDA technique because the reconstruction of the flame front assumes a smooth, cylindrically symmetric surface. Despite the large uncertainties, however, some indication of the relationship between the flame area and the velocity field can be obtained from the LDA determined flame shape. Conversion of the approximate flame shape lines, Figure 7-7, into surfaces of revolution about the duct axis, provides a rough estimate of the flame area variation with time. The approximate flame area/time curve, Figure 8-11, shows a definite peak early in the combustion. The peak occurs earlier than the measured velocity

peak, because of the large inaccuracies in the flame area determination described above.

8.4 Summary of one-dimensional analysis

The accuracy of the one-dimensional model suggests that the expanding burned gas uniformly compresses the unburned gas. The area of the flame affects the rate of compression of the unburned gas, but the particular flame shape does not affect the predominantly one-dimensional nature of the unburned gas velocity field. The larger the flame area, the more rapidly unburned gas is converted to burned gas, and the more rapid is the burned gas expansion process which compresses the unburned gas. The velocity of the unburned gas is simply the motion of this gas as it is being compressed.

The burned gas velocity field is not one-dimensional because the flame deflects the flow as it passes from the unburned to the burned side. The next chapter discusses the flow deflection by a flame and the consequent circulations in the burned gas.

CHAPTER 9

Deflection of Flow by a Flame Front

9.1 Introduction

The discussion in the previous chapter, and the experimental results, clearly link the flame area and the general magnitude of the velocity field. In the burned gas, however, the flow is rotational and not one-dimensional. Both the flame shape and the unburned gas flow are important influences in the burned gas motion. The following discussion describes this relationship and how both regions of vorticity and regions of stagnation are generated in the burned gas.

9.2 Analytical discussion

Interpretation of the velocity field is simplified by adopting the flame sheet model, Chapter 3, for the closed tube flame. The flame is assumed to be an infinitely thin interface where unburned gas is instantaneously and irreversibly converted to high temperature burned gas. With this assumption, classical deflagration analysis predicts deflection of the flow as it passes through the flame sheet from the unburned to the burned side. The analysis appears in combustion texts (Strehlow, 1984) and in the earlier literature (Tsien, 1951, Gross and Esch, 1954, Uberoi, 1959, Maxworthy, 1961).

The component of gas velocity parallel to the flame front is continuous across the front. The component of gas velocity perpendicular to the reaction front, however, changes

discontinuously across the flame as the unburned mixture is converted to higher temperature, lower density burned gas. This discontinuous velocity change was described in Chapter 8 and is shown in Figure 9-1,

$$S_b = \sigma S_u, \tag{9.1}$$

where S represents the normal velocity relative to the flame sheet, subscripts b and u refer to the burned and unburned gas respectively, and σ is the density ratio ρ_u/ρ_b (also referred to as the expansion ratio). S_u is the fundamental flame speed of the mixture. The discontinuous normal velocity change, determined in Chapter 8, is,

$$\Delta V = S_b - S_u = (\sigma - 1)S_u. \tag{9.2}$$

The velocity jump is $(\sigma - 1)S_u$ even if the frame of reference is the fixed laboratory frame.

When the the flame sheet approaches obliquely the unburned gas flow the discontinuous change in the velocity component perpendicular to the flame causes a deflection of the flow direction across the flame, Figure 9-2. V_f is the flame velocity in the laboratory reference frame. V is the magnitude of the vector velocity of the gas, with the subscripts u and b denoting unburned and burned gas as before. The additional subscript n refers to the normal component. The angle of incidence between the upstream flow and the flame sheet is denoted θ_i. The deflected angle, θ_d, is the angle between the

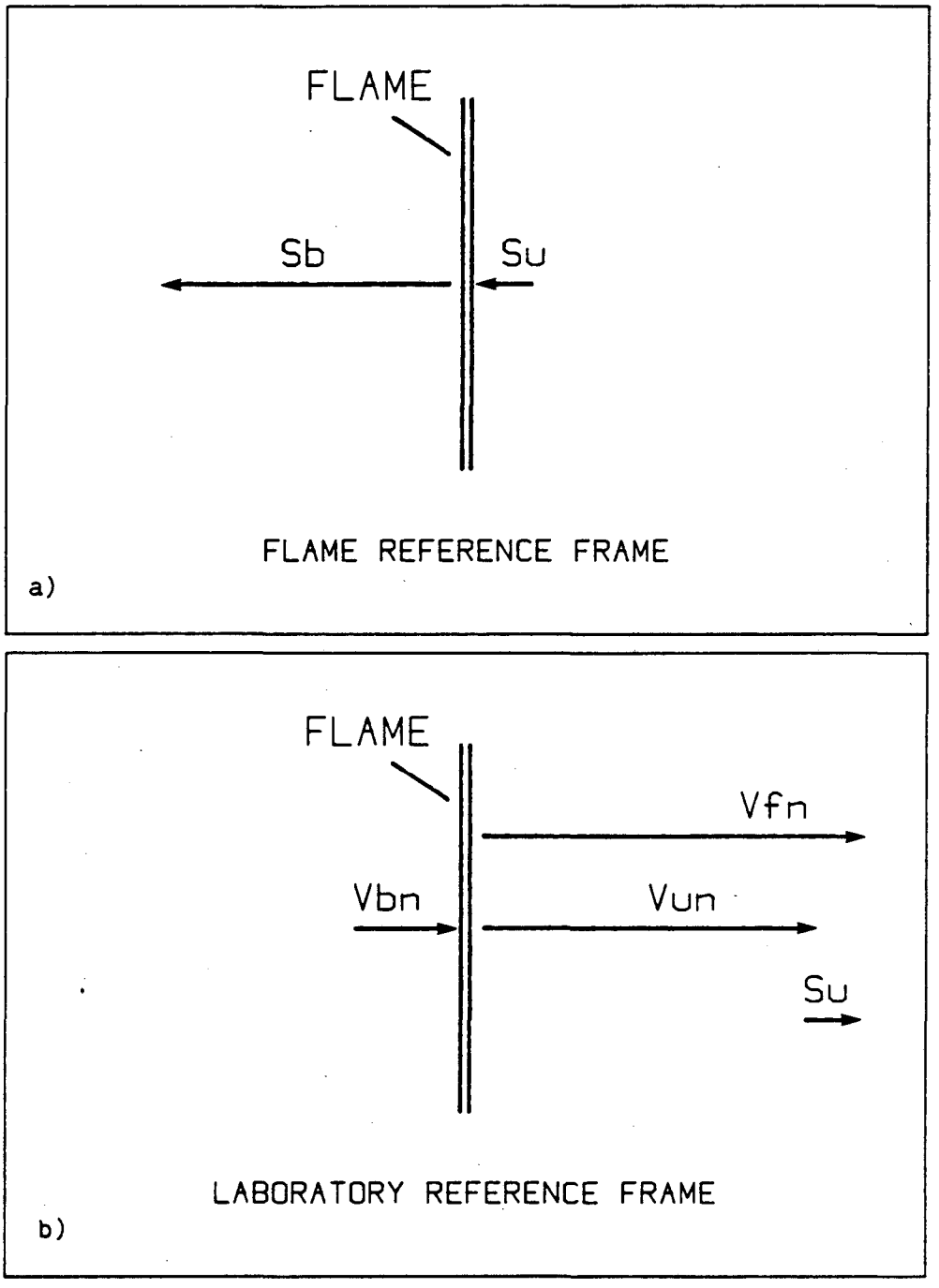

Figure 9-1. Velocity jump at the flame interface.
a) Flame reference frame
b) Laboratory reference frame

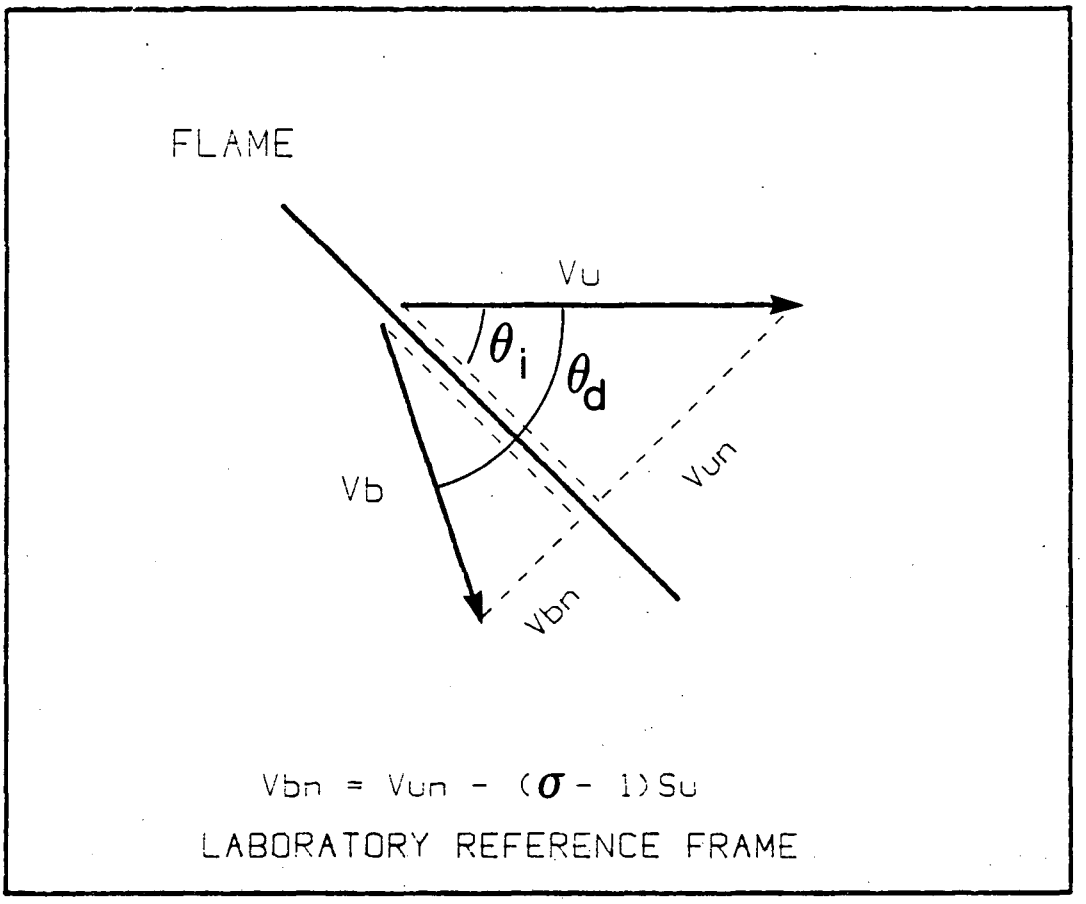

Figure 9-2. Schematic of flow deflection caused by a flame sheet oblique to the incoming flow.

unburned gas velocity vector and the burned gas velocity vector. Simple geometric and algebraic considerations produce the following relationships between the unburned gas flow speed, V_u, the angle of incidence, θ_i, the deflected angle, θ_d, and the burned gas flow, V_b:

$$\theta_d = \theta_i + \arctan\left(\frac{V_u\sin(\theta_i) - (\sigma - 1)Su}{V_u\cos(\theta_i)}\right)$$

$$V_b = \sqrt{(V_u\cos(\theta_i)^2+(V_u\sin(\theta_i)-(\sigma-1)S_u)^2)}$$

When θ_d is greater than 90 degrees the burned gas velocity is negative in the laboratory reference frame. The above relationship between θ_i, θ_b, V_u, and V_b explains the dependence of the burned gas motion on both the flame shape, which enters the above expression as θ_i, and the unburned gas motion, which enters the expression as V_u.

Because of the dependence of the burned gas velocity on the incident angle, a curved flame front will produce vorticity in the burned gas. The variation of burned gas velocity with θ_i creates a velocity gradient in the burned gas. This gradient represents vorticity. A precise mathematical description of vorticity generation by a curved flame surface can be found in Hayes (1953). The results of the mathematical description are equivalent to the heuristic description above.

9.3 Comparison to experimental results

Particle track photographs of steady flow through a bunsen burner flame (Lewis and Von Elbe, 1943) and flow through steady flames in open channels (Uberoi, 1959) show clearly the deflection behavior described in the previous section. Maxworthy (1961) showed, however, that the measured deflection rarely approached the theoretically predicted deflection. He attributed the discrepancy to tangential diffusion. Because of the difficulty in using particle track methods in nonsteady combustion situations, the deflection phenomenon is not well documented in flame propagation in closed tubes and ducts. Fortunately, the LDA results presented in previous chapters can demonstrate three attributes of flame affected burned gas motion in closed vessels. The first is the discontinuous change in the normal velocity ($V_{bn} - V_{un}$) across the flame front. The second is the deflection of flow across a flame front oblique to the incident flow. The third is the generation vorticity and regions of circulation in the burned gas.

The measured discontinuous velocity change across the flame appears in the axial component of the centerline velocity/time curves measurement locations near the igniter, Figure 9-3. The flame is nearly symmetric as it passes these locations, Figure 9-4, and consequently it approximates a plane flame front for these measurement points. The discontinuous velocity change as the flame passes is approximately equal at all measurement locations, Figure 9-5, and is approximately equal to the predicted value for

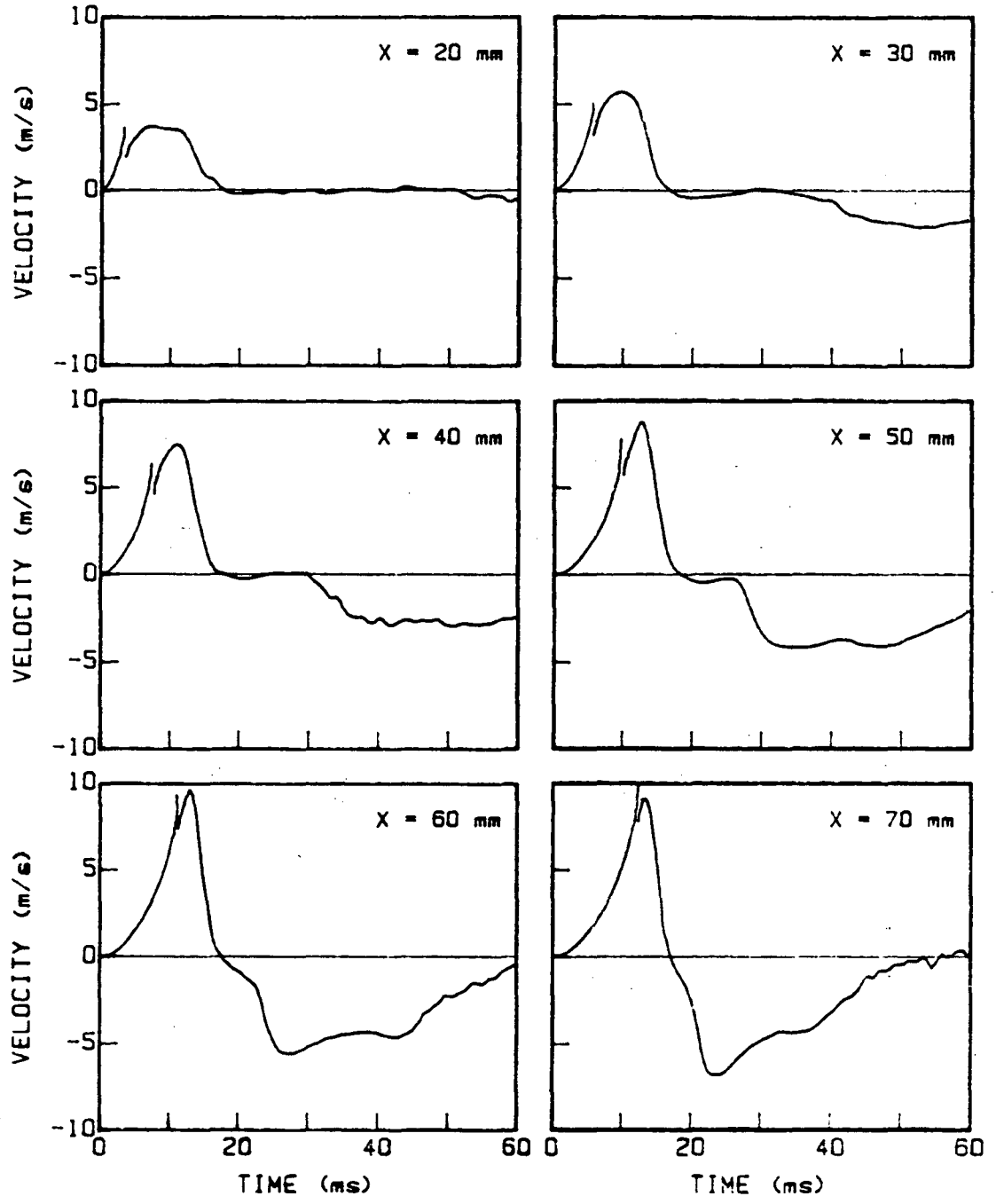

Figure 9-3. Axial component of the centerline (Y = 0 mm) velocity near the igniter (X < 80 mm) showing a distinct velocity jump at flame arrival.

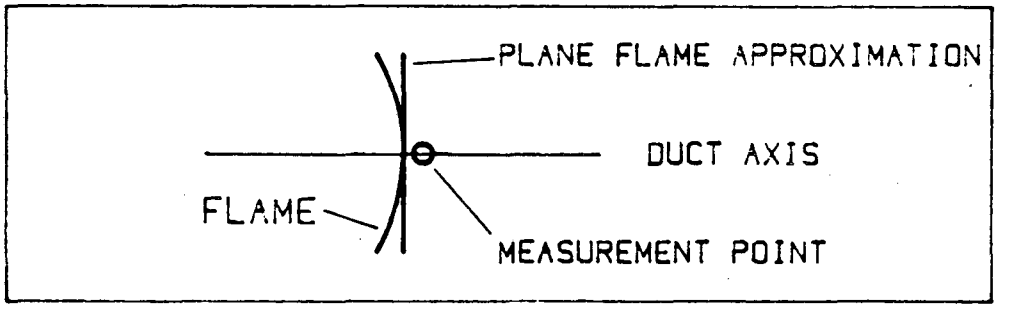

Figure 9-4. Plane flame approximation at the centerline of the combustion vessel when the flame is symmetric and convex toward the unburned gas.

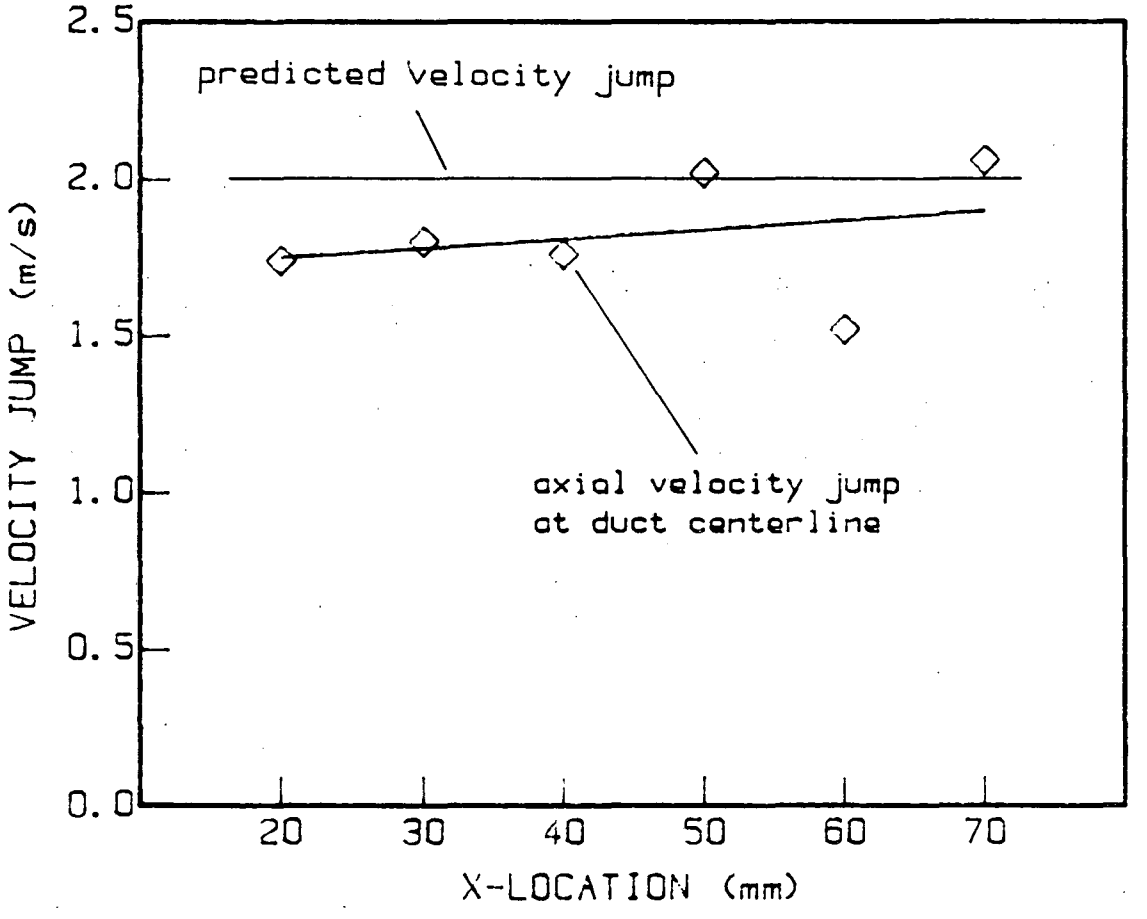

Figure 9-5. Comparison of measured velocity jump of the axial component of the centerline velocities to the predicted value.

stoichiometric methane/air mixtures ($\Delta V \approx 2.0$ m/s: $\sigma \approx 6.75$, $S_u \approx 0.35$ m/s, $\Delta V = (\sigma - 1)S_u$). The values of the expansion ratio and the laminar flame speed actually change during the combustion process, but the small pressure rise during the initiation phase insures that the changes are not significant (σ varies between 6.82 and 6.66 during this period, and S_u is nearly constant). The measured velocity is lower than the predicted value partly because of slight deviations from symmetry by the flame front, and more importantly because the LDA particles are unable to follow faithfully the flow during the extremely rapid velocity jump across the flame. Haghgooie et al. (1984) have indicated substantial lag between particle velocity and gas velocity during rapid acceleration. The agreement is relatively good between the measured and predicted velocity jump despite the particle lag problem. The tangential diffusion problem observed by Maxworthy (1961) does not appear during the short duration closed tube combustion event. The velocity jump is not apparent in axial component centerline velocity/time curves at measurement locations far from the igniter, Figure 7-9c, because the "tulip" cusp voids the planar flame front assumption.

The deflection of gas flow by a flame front was shown diagramatically in Figure 9-2. The measured velocity vector field shows approximately the same behavior, Figure 9-6. The figure shows the velocity vector field near the flame and the approximate flame location at a fixed time during the combustion. The comparison of the deflection to the predicted deflection can

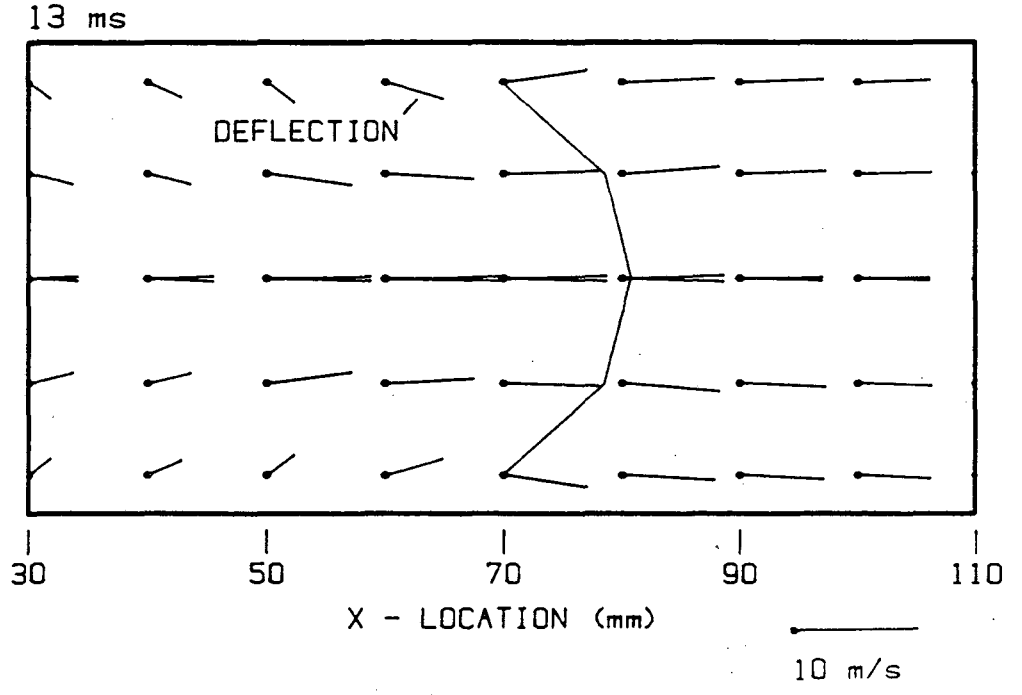

Figure 9-6. Measured velocity deflection early in the transition phase as the flame passes. Vector scale: 1 mm = 0.625 m/s. Time = 13 ms.

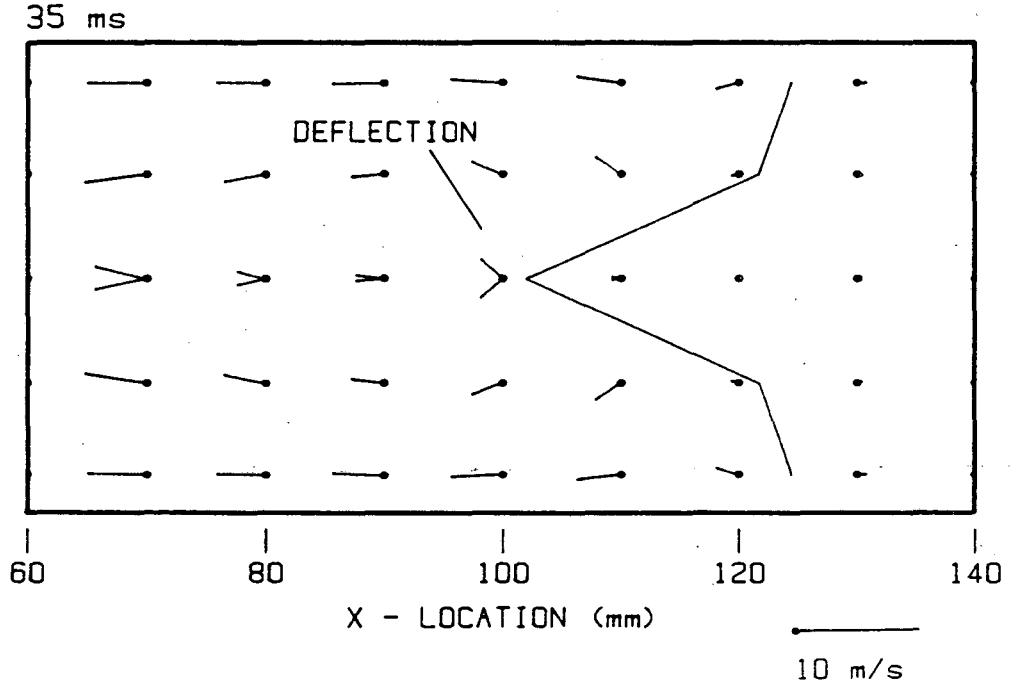

Figure 9-7. Measured velocity deflection during the "tulip" phase as the flame passes. Vector scale: 1 mm = 0.625 m/s. Time = 35 ms.

be only qualitative because quantitative comparison requires the accurate determination of θ_i, the angle of incidence of the unburned gas flow. Unfortunately, the flame angle is not well known. The arrival of the flame can be relatively well deduced by LDA signal dropout, but the slope of the flame requires a finer measurement grid. In fact, if flame wrinkling occurs, as suggested by the schlieren movies, there is little likelihood that even a fine grid of measurement points will supply sufficient information because the run-to-run variations will obscure the flame angle. The difficulty in quantitative comparison between the predicted and measured flow deflection has also been encountered and discussed by Cheng and Ng (1983). The deflection of the burned gas by the flame after the "tulip" forms is shown in Figure 9-7. In this case the deflection is away from the centerline of the duct, generating a stagnation zone similar to the stagnation zone in the wake of a solid body. A stagnation zone formed near the wall by a flame convex toward the unburned gas has been discussed by Uberoi (1959) and Zeldovich (1981). The stagnation zone generated by the "tulip" cusp has the same origin as the wall stagnation zone. If the convex flame is cut in half along the axis, and then joined at the walls, Figure 9-8, the similarity between the two cases is apparent.

The consequence of the flow deflection described in the preceeding paragraph is the creation of vortical motion in the burned gas. The generation of circulation is shown schematically in Figure 9-9. The unburned gas velocity, V_u, is assumed

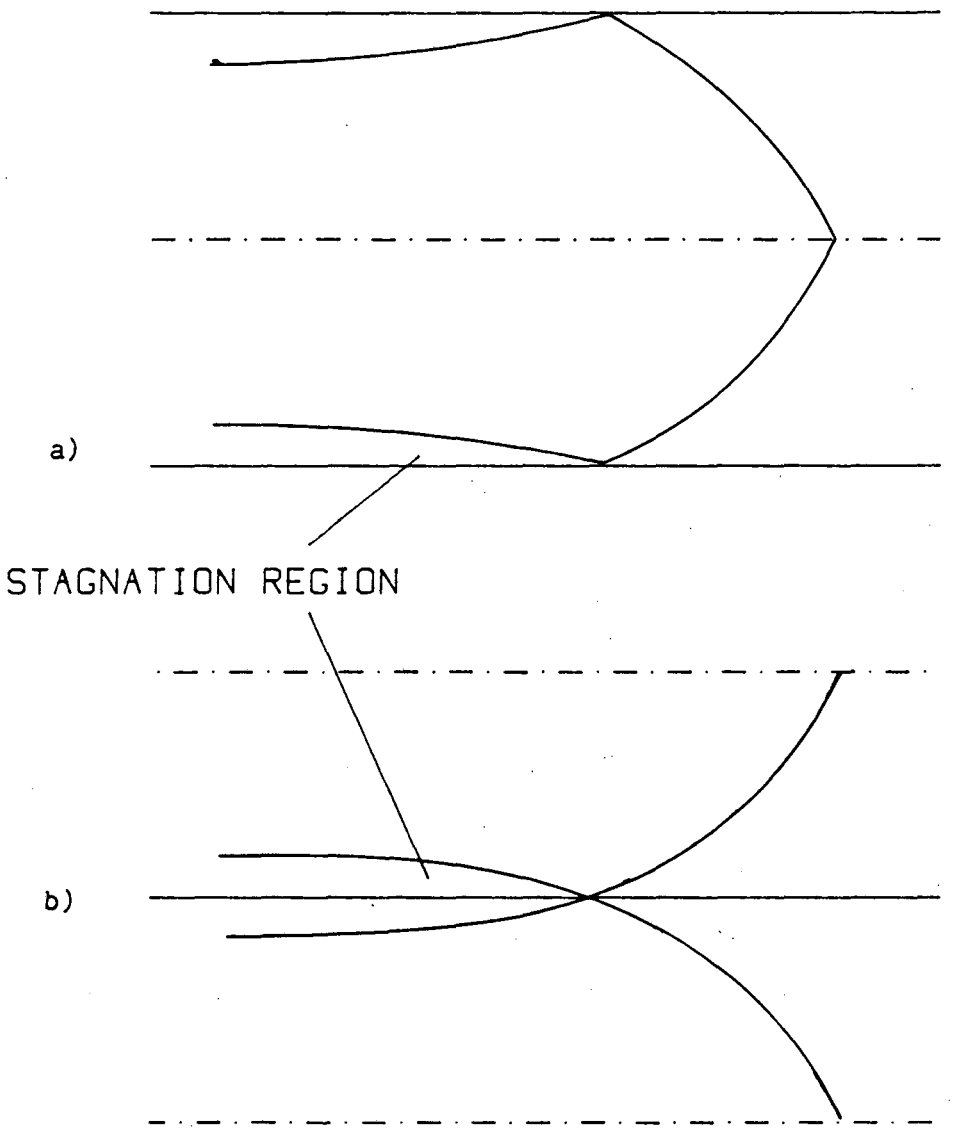

Figure 9-8. Schematic showing similarity between stagnation region discussed by Uberoi (1959) and Zeldovich (1981) and the stagnation region behind the "tulip" cusp.
a) Stagnation zone of Uberoi (1959)
b) Stagnation zone behind "tulip"

constant and parallel. The burned gas velocity is not constant or parallel because θ_i varies along the flame front. The LDA measurements show a vortex structure behind the flame as the "tulip" forms which is similar to the predicted circulation, Figure 9-10. The vortex rotates clockwise, and was also noted in the high-speed schlieren movies. The vortex generated as the "tulip" forms does not dissipate but retains its integrity and moves back through the burned gas. Evidence of this feature of the burned gas vortex appears clearly in the radial velocity component at off-centerline measurement points (Y = 8 mm and Y = 15 mm), Figure 9-11. The time scale calculation of viscous diffusion time reported in Chapter 3 suggests that the vortex does not have time to diffuse because of the short combustion duration.

9.4 Summary

The analysis and measurements presented above indicate that both the flame shape and the unburned gas motion affect the burned gas flow structure. In particular the flame causes a velocity jump, flow deflection, and regions of circulation in the burned gas. The obvious regions of circulation in the burned gas appear just as the "tulip" forms. The next chapter proposes a causal relationship between the vortex generated as the flame quenches and the "tulip" formation.

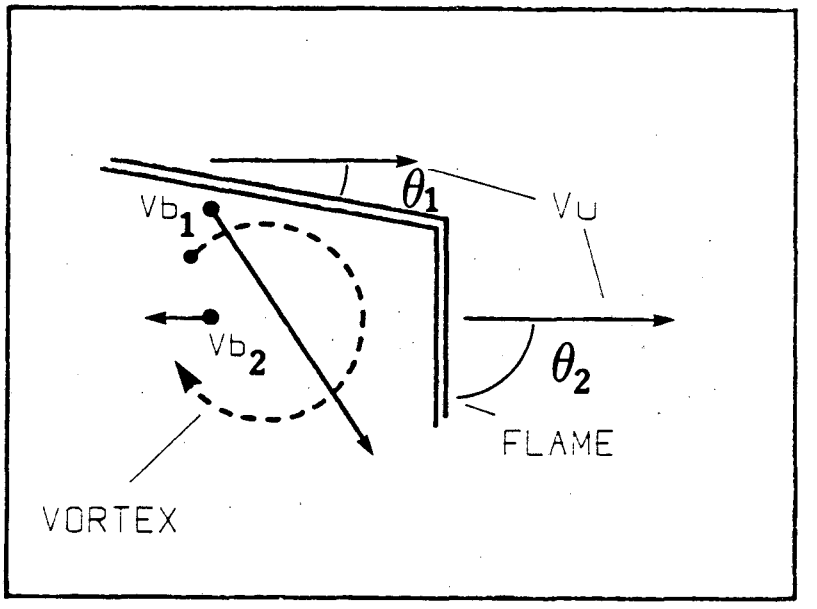

Figure 9-9. Schematic showing generation of regions of circulation by a curved flame front.

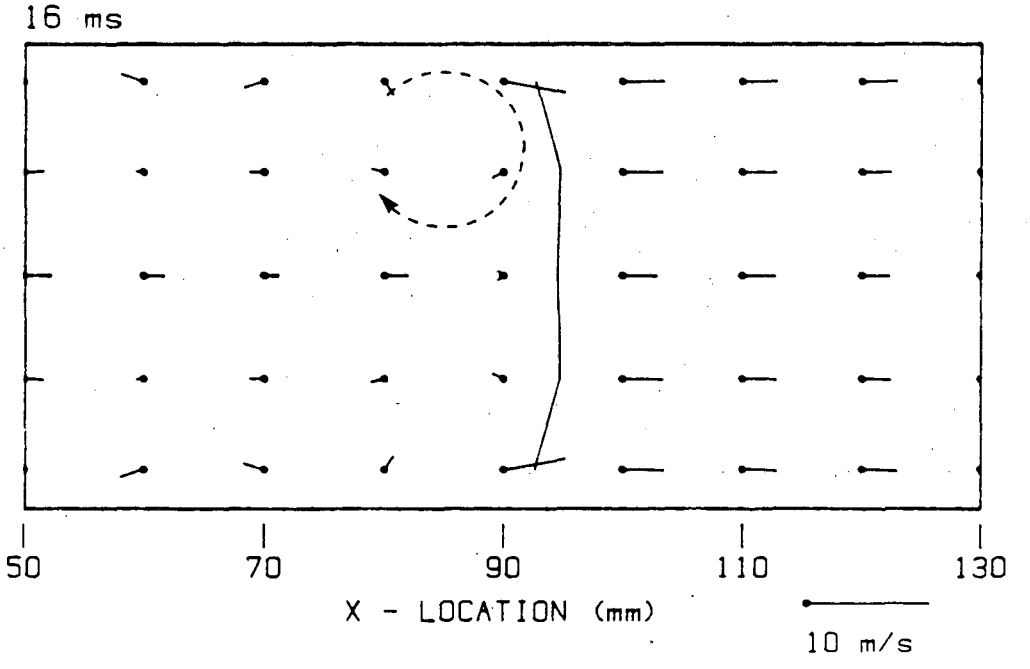

Figure 9-10. Measured velocity field showing vortical structure generated behind the flame during the transition phase. Velocity scale: 1 mm = 0.625 m/s. Time = 16 ms.

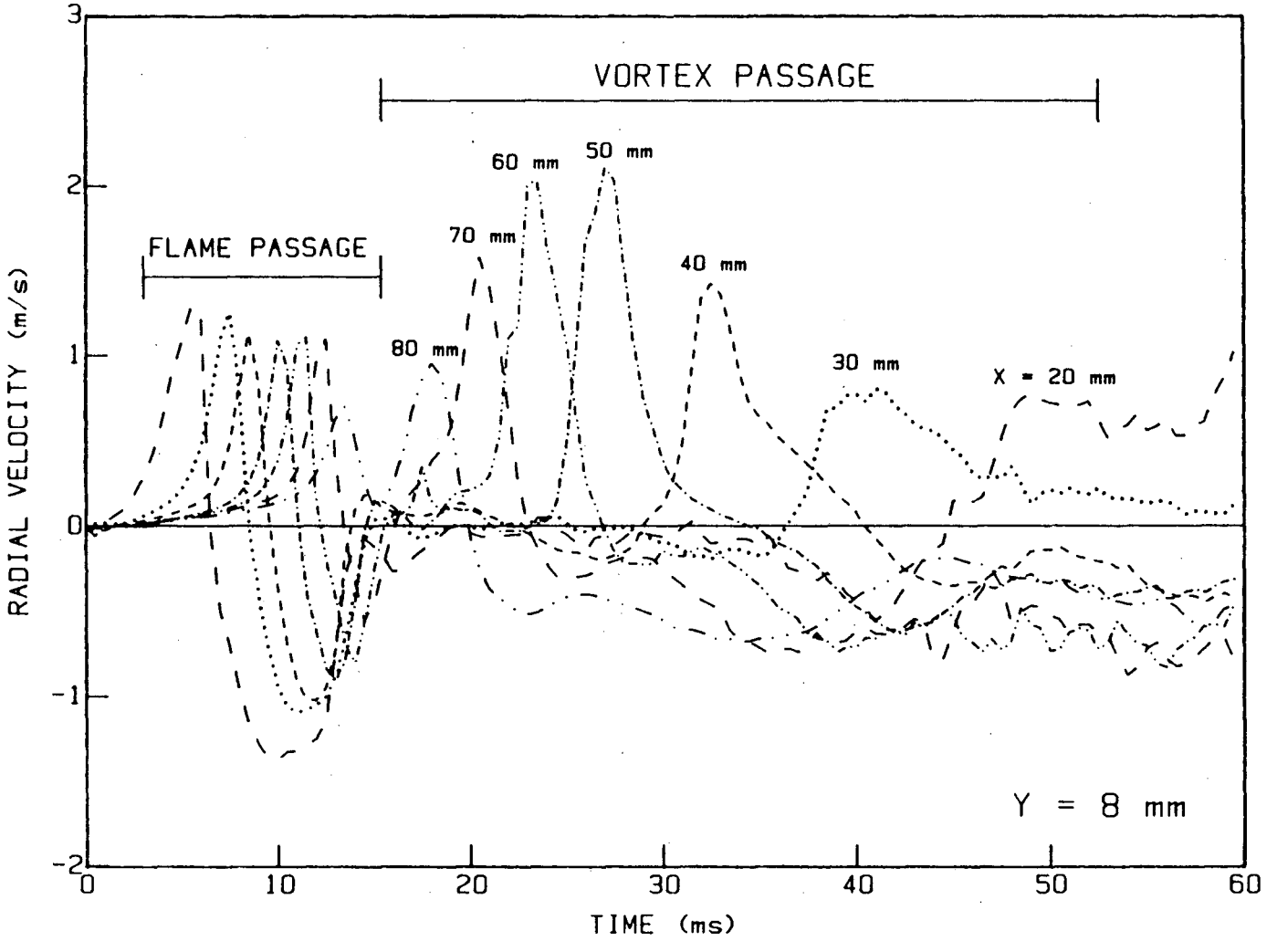

Figure 9-11. Radial velocity component near the igniter at the mid-radius position (Y = 8 mm) showing the passage of first the flame and then the vortex.

CHAPTER 10

A Fluid Mechanical Explanation for the "Tulip" Flame

10.1 Introduction

The explanations for the "tulip" formation appearing in the literature (Chapter 2) are based on qualitative observations of closed tube flame propagation. The LDA measurements of the velocity field during the combustion (Chapters 6 and 7) represent new quantitative information about the flame induced flow which can help determine the "tulip" mechanism. This chapter uses the velocity data to support a new fluid mechanical explanation for the "tulip" flame formation. The new explanation appears more likely than those proposed in the literature.

10.2 Discussion of proposed "tulip" explanations

Two explanations for the "tulip" flame presented in Chapter 2 suggest that an instability phenomenon is responsible for the "tulip" cusp. One proposal involves a cellular instability and the other involves a Taylor (1950) instability.

It is unlikely that the "tulip" cusp is one cell of a cellular instability because this instability is sensitive to fuel type and equivalence ratio (for a review of the cellular instability see Sivashinsky, 1983). Experiments show that the "tulip" formation does not depend strongly on fuel type or equivalence ratio. Further, the schlieren movies show small scale structure on the larger "tulip" cusp. These small scale structures are likely to be associated with the cellular

instability because they are influenced by fuel type and equivalence ratio. The small structures indicate that the fundamental cell size of the instability is much smaller than the dimension of the "tulip" cusp.

It is also unlikely that the "tulip" forms as a manifestation of a Taylor (1950) instability. Studies by Markstein (1964) show that the response of a flame front to accelerations by shock waves and pressure waves is different than is observed in the formation of the "tulip" flame. After passage of a shock, the flame quickly becomes turbulent. Furthermore, the shock induced turbulence appears on the flame surface very rapidly (less than 1 ms after the shock passage) while the "tulip" cusp grows smoothly over a longer time period (approximately 10 ms). There is a pressure wave generated when the flame quenches at the sidewalls of the vessel. This pressure wave begins the vibratory phase of flame propagation (Guenoche, 1964, Starke and Roth, 1982) discussed earlier (Chapter 1), but it does not appear to modify the flame shape significantly.

The "tulip" formation is much more reproducible than most instability phenomenon, and velocity measurements indicate that the "tulip" forms on a time scale comparable to the convective flow time scale. This suggests that the "tulip" cusp is fluid mechanical in origin. Of the proposed explanations for the "tulip" flame (Chapter 2), only one is fluid mechanical. This explanation suggests that a large scale recirculation in the unburned gas is responsible for the "tulip" formation. The

velocity measurements conclusively show, however, that no large scale unburned gas recirculation exists.

10.3 New explanation for the "tulip" flame formation

The formation of the "tulip" begins with the partial flame quench at the side walls. The quench occurs from the natural burning behavior of the flame. The time of flame quench in stoichimetric methane/air flames is nearly independent of the chamber length, Figure 4-11. The burn to the sidewalls is therefore approximately independent of the chamber length, and the quench is a natural consequence of this burning process. Four events accompany the flame quench at the vessel sidewalls:

1) dp/dt decreases dramatically -- This is explained by the relationship between the rate of pressure rise and the instantaneous flame area, Chapter 5.

2) unburned gas velocity decreases -- This is explained by the relationship between the unburned gas velocity and the instantaneous flame area, Chapter 8.

3) burned gas velocity reverses direction -- This is a consequence of 2) above and the velocity jump condition at the flame, Chapter 8. The velocity jump is constant across the flame. If the unburned gas velocity decreases to a value below the velocity jump, then the burned gas velocity must be negative.

4) the flame shape changes -- As the extended portions of the flame are quenched, only the flatter dome portion approximately parallel to the chamber endwalls remains.

The above events, except for 1), are evident in the vector velocity field during the transition phase, Figure 7-12.

The experimental velocity field results and the deflection analysis (Chapter 9) indicate a vortex just behind the flame as the quench occurs. Just before the quench the flame is nearly parallel to the sidewall, while in the center of the duct the flame is nearly parallel with the endwall. This strong curvature generates a vortex behind the flame. Immediately following the generation of this vortex the flame burns out at the side walls and the vortex is then sitting behind a nearly planar front, Figure 10-1. Furthermore, the flame and flow field come to a near standstill because the flame area has dropped so drastically. Consequently, the vortex sits in close proximity behind the flame for an extended period of time. After the flame quench occurs the vortex, the nearly planar flame shape, and the unburned gas motion are not compatible because the vortex requires a curved flame front. The flow field and flame shape must change to accommodate the new conditions. The change occurs very rapidly, and appears as flame curvature associated with the onset of the "tulip" cusp. In effect, the burned gas vortex grabs the flame and unburned gas and curves them into a "tulip". Once the cusp begins, the natural burning behavior extends the "tulip" and then maintains this shape. Numerical support for the

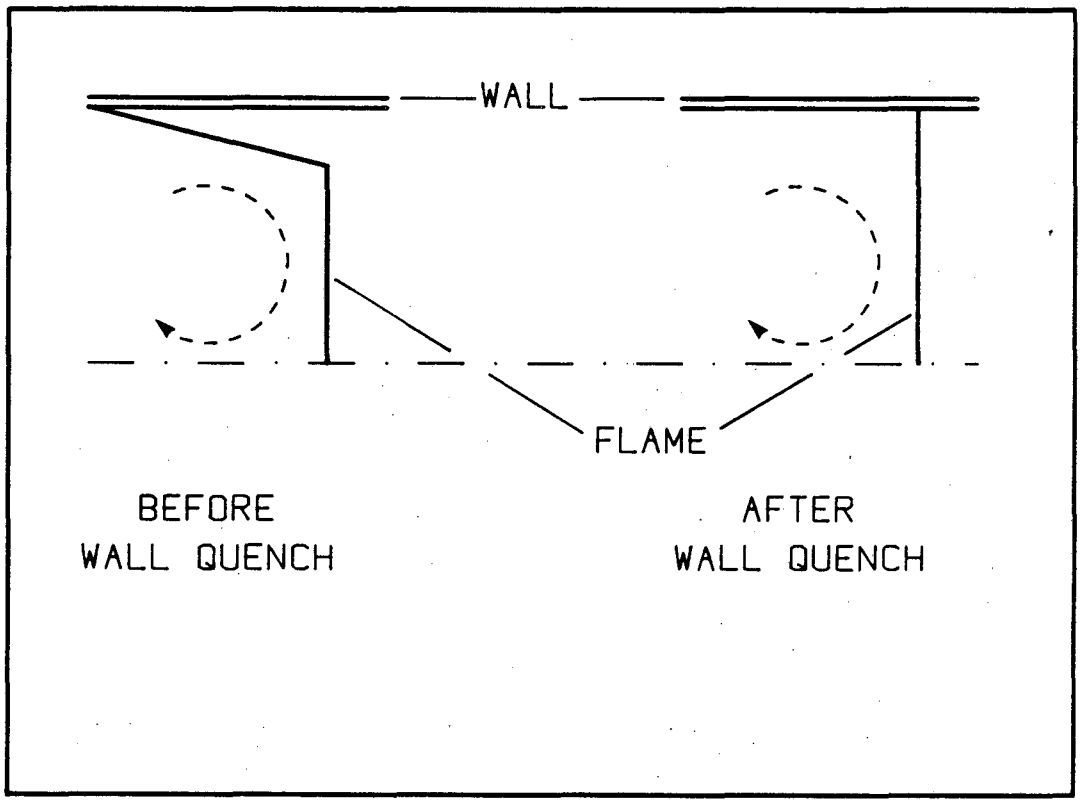

Figure 10-1. Schematic showing behavior of flame and flow field at the time of wall quench.

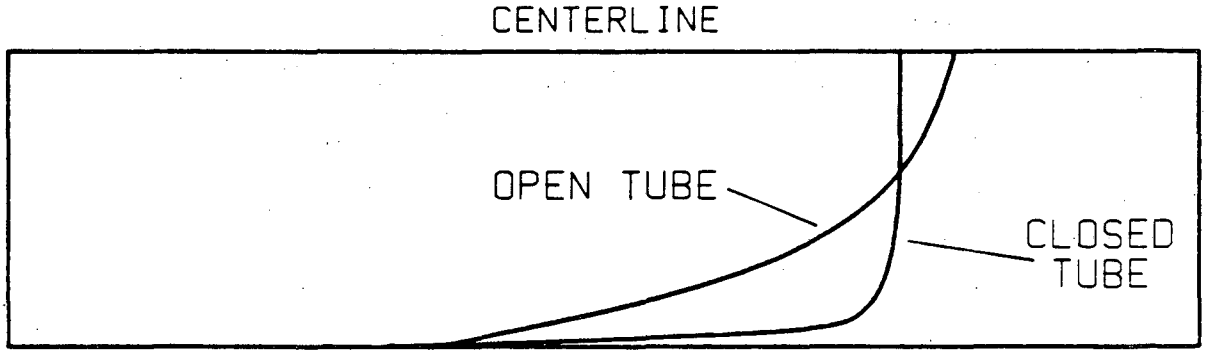

Figure 10-2. Schematic showing difference between flame shape during combustion in open tubes and flame shape during combustion in closed tubes.

vortex caused "tulip" flame has been obtained by Hsiao (1985). He demonstrated that a vortex in the burned gas behind a planar flame front will cause the flame to "tulip". As the flame area increases during the "tulip" phase, the vortex is swept downstream and no longer affects the flame front. The burned gas vortex coupled with the sudden change in flame shape as the wall quench occurs is responsible for the "tulip" flame formation.

10.4 Discussion of new "tulip" explanation

Flames propagating in tubes open at one or both ends do not demonstrate the "tulip" effect. Two differences between the closed and open tube case are suggested as the reason for this lack of "tulip" flames in open tubes. First, the closed end changes the fluid dynamics such that the closed tube flame is much more blunt when the wall quench occurs than is the open tube flame, Figure 10-2. Consequently, the flame quench in a closed tube generates stronger vortical burned gas motion than it generates in an open tube. The second difference concerns the proximity of the vortex to the flame sheet. In an open tube the vortex is quickly driven far from the flame by the burned gas expansion, while in the closed tube the vortex remains near the flame for a significant time. The effect of the vortex diminishes rapidly with distance, which suggests that the open tube vortex has considerably less effect on the unburned gas and flame than does the closed tube vortex.

When the flame curvature is localized extremely near the wall, as in the blunt flame of Figure 10-2, and in the top view of the line ignited methane/air flame, Figure 4-17, the vortex is also confined near the wall. Therefore, the "tulip" process begins as a small cusp near the wall which then grows toward the center of the chamber. This behavior is clearly shown in Figure 4-17.

The wall quench is much less pronounced in short chambers (Figures 4-6 and 4-7) and consequently the vortex generation is significantly reduced. The reduced circulation prevents the "tulip" from forming in these smaller chambers.

The open exhaust valve case, Figure 4-20, and the non-planar endwall case, Figure 4-21, indicate little effect of these conditions on the "tulip" formation. This result is expected because neither of these conditions affect significantly the burned gas vortex.

10.5 The time resolution difficulty

The onset of the "tulip" flame occurs simultaneously with the quench of the flame at the sidewalls of the combustion vessel. At this moment the flame flattens, the rate of pressure rise, dp/dt, decreases dramatically, the unburned gas velocity drops to a small nearly constant value, and the burned gas velocity changes from being predominantly positive to entirely negative. All of these phenomena occur in a very short time (approximately 3 ms). Unfortunately, the repeatability in time of the flame behavior is also approximately 3 ms, which limits

the time resolution of the experimental results. Consequently the causal relationship between the flame quench, decrease in dp/dt, drop in unburned gas velocity, and reversal in burned gas motion cannot be explored precisely using the current data. Furthermore, the proposed mechanisms for the "tulip" flame formation from Chapter 2, which involve a sudden occurrence at or near the time of flame quench (spontaneous instability, Taylor-Markstein instability) cannot be conclusively eliminated based on the experimental results of the previous chapters. However, the new fluid mechanical explanation for the "tulip" flame is more likely based on the experimental results. The new explanation accounts for all of the observed phenomenon.

10.6 Summary

The features of the flow field associated with the formation of the "tulip" shape occur during the transition period of the combustion process (from t = 15 ms to t = 20 ms). These features appear to be caused by the rapid change in the flame area due to wall quench. The reduced flame area decreases the overall velocity of the unburned gas flow and the flame propagation rate. The flame area decrease is also accompanied by a change in flame shape that generates a strong circulation in the burned gas near the flame. This circulation, or vortex, affects both the flame shape and the unburned gas, causing the flame to propagate more quickly at the walls than at the center. The ultimate effect of the different flame propagation rates is the "tulip" formation.

CHAPTER 11

Summary of Flame Propagation in Closed Ducts

11.1 Introduction

The interaction between a laminar premixed flame and its self-generated flow has been experimentally studied in a closed duct. Laser Doppler anemometry measurements provide a complete vector velocity map of the flow field during the constant volume flame propagation. High-speed schlieren movies are used to observe changes in flame shape and position. The experimental results suggest that the combustion process is a strong contributor to the flow field, and that there is a dynamic coupling between the flame and the burned gas motion. The understanding of the dynamic nature of the flame interface and its influence on the flow field in the simple duct geometry is applicable to more complex combustion environments.

11.2 Conclusions

A combination of experimental results and simple analytical models lead to the following conclusions concerning the flow field generated by nonsteady flame propagation in a closed rectangular duct:

1) Unburned gas motion (Chapters 7 and 8) -- The unburned gas, except in a region very near the flame front, is unaffected by changes in the flame shape. Expanding burned gas behind the flame front uniformly compresses the unburned gas. The compression appears as a nearly one-dimensional

flow in the velocity measurements. The measured unburned gas velocity decreases linearly from a maximum at the flame front to near zero at the endwall. A one-dimensional analysis of a uniformly compressed gas predicts this linear velocity behavior.

2) Velocity jump at the flame (Chapters 7 and 9) -- The density of the gas inside the combustion vessel changes discontinuously across the flame front. The component of gas velocity normal to the flame front must also change discontinuously at the flame interface in order to maintain a continuity of mass flux through the flame. If the velocity of the unburned gas is not normal to the flame sheet, the velocity jump condition causes a deflection of the gas flow as it passes through the flame. When the flame is curved, the deflection generates vorticity in the burned gas. Velocity measurements clearly show a jump in the gas velocity at the flame front and the resulting flow deflection. Both the velocity measurements and high-speed schlieren movies show evidence of vortical structures in the burned gas.

3) The wall quench phenomenon (Chapters 4,5,6,and 7) -- The onset of a large flame cusp, or "tulip" shape, occurs when part of the flame is quenched by the sidewalls of the combustion vessel. The following events also coincide with the time of wall quench: 1 - the rate of pressure rise,

dp/dt, decreases rapidly, 2 - the flame shape changes dramatically, 3 - the magnitude of the unburned gas velocity decreases, 4 - the burned gas flow changes direction (from positive to negative), 5 - a ring vortex appears behind the flame in the burned gas. All of these events (except 5) occur because the reduced combustion rate after the wall quench significantly decreases the flame area. The burned gas vortex is caused by flow deflection from the strongly curved flame shape just prior to the wall quench.

4) The "tulip" flame formation (Chapter 10) -- As the flame quenches at the sidewalls of the combustion vessel, the flame shape changes from a curved front to a nearly planar one. However, just prior to the quench, a vortex which is compatible with a curved flame front forms in the burned gas. The post-quench planar flame front is not compatible with the vortex and the flame and flow field quickly adjust to new compatible conditions. These new conditions include the modification of the flow field such that a cusp forms in the planar flame front. This cusp then grows into the "tulip" flame. The vortex mechanism is more likely than previously suggested explanations for the "tulip" flame phenomenon.

11.3 Future work

Experimental investigations of the flow field generated by flame propagation in closed ducts of different lengths would help

support the proposed vortex mechanism for the "tulip" flame. Numerical simulations of the flame propagation would also be useful for further exploration of the flame/flow interaction.

REFERENCES

Andrews, G.E., Bradley, D. (1972). "Determination of Burning Velocities: A Critical Review." Combustion and Flame, 19, 275-288.

Ball, G. (1951). "Two-Dimensional Flame in a Laminar Flow Channel." Combustion Project Report. Harvard University, July.

Barr, P.K. (1984). "Simulation of Flame Propagation Through Vorticity Regions Using the Discrete Vortex Method." Sandia National Laboratory Report No. SAND84-8715. Presented at the Symposium on Fluid Dynamics, University of Illinois at Urbana-Champaign, April.

Barr, P.K. (1985). Personal communication. Sandia National Laboratory, Livermore, CA.

Bradley, D., Mitcheson, A. (1976). "Mathematical Solutions for Explosions in Spherical Vessels." Combustion and Flame, 26, 201-217.

Cattolica, R.J., Vosen, S.R. (1984). "Two-Dimensional Fluorescence Imaging of a Flame-Vortex Interaction." AIAA Paper No. AIAA-84-1799. Presented at the 19th Thermophysics Conference, June 25-28, Snowmass, CO.

Cheng, R.K., Ng, T.T. (1983). "Velocity Statistics in Premixed Turbulent Flames." Combustion and Flame, 52, 2, 185-202.

Cho, K-K, Jeung, I-S. (1983). "Application of Laser Doppler Velocimetry to Flame Propagation Studies." Society of Photo-Optical Instrumentation Engineers volume 398- Industrial Applications of Laser Technology.

Chorin, A.J. (1980). "Flame Advection and Propagation Algorithms." Journal of Computational Physics, 35, 1-11.

Chu, B-T. (1952). "On the Generation of Pressure Waves at a Plane Flame Front." Fourth Symposium (International) on Combustion. Williams and Wilkins, Baltimore, 603-612.

Clavin, P. (1985). "Dynamic Behavior of Premixed Flame Fronts in Laminar and Turbulent Flows." Progress in Energy and Combustion Science. To appear.

Cloutman, L.D. (1982). Personal communication. Los Alamos National Laboratory, Theoretical Division, Los Alamos, NM.

Cloutman, L.D., Dukowicz, J.K., Ramshaw, J.K., Amsden, A.A. (1982). "CONCHAS-SPRAY: A Computer Code for Reactive Flows with Fuel Sprays." Los Alamos Report No. LA-9294-MS.

Coward, H.F., Hartwell, F.J. (1932). "Studies in the Mechanism of Flame Movement. Part I. The Uniform Movement of Flame in Mixtures of Methane and Air, in Relation to Tube Diameter." Journal of the Chemical Society, London, 1932:2, 1996-2004.

Coward H.F., Payman, W. (1937). "Problems in Flame Propagation." Chemical Reviews, 21, 359-366.

Darrieus, G. (1938). "Propagation d'un front de flamme: essai de theorie des vitesses anomales de deflagration par developpment spontane de la turbulence." Unpublished manuscript of paper presented at La Technique Moderne, 1938, and Le Congres de Mechanique Appliquee, Paris, 1945.

de Soete, G.G. (1981). "Measurement of Initial Flame Speed by Laser Tomography." First Specialists Meeting (International) of the Combustion Institute, Bordeaux, France, July, 20-24.

Dunn-Rankin, D., Cheng, R.K., Sawyer, R.F. (1984). "LDA Study of Non-Steady Flame Propagation in a Constant Volume Duct." Second International Symposium on the Applications of Laser Doppler Anemometry to Fluid Mechanics. July 2-4, Lisbon, Portugal.

Dunn-Rankin, D., Sawyer, R.F. (1983). "Combustion of Lean Mixtures Under Simulated Internal Combustion Engine Conditions." Western States Section/The Combustion Institute Paper No. 83-53. Also Lawrence Berkeley Laboratory Report No. LBL-16745.

Edwards, C.F., Oppenheim, A.K. (1983). "A Comparative Study of Plasma Ignition Systems." Society of Automotive Engineers Paper No. 830479.

Egerton, A.C., Saunders, O.A., Lefebvre, A.H., Moore, N.P.W. (1953). "Some Observations by Schlieren Technique of the Propagation of Flames in a Closed Vessel." Fourth Symposium (International) on Combustion. Williams and Wilkins, Baltimore, 496-402.

Ellis, O.C. de C., Wheeler, R.V. (1928). Explosions in Closed Cylinders. Part III. The Manner of Movement of Flame." Journal of the Chemical Society, London, 1928:2, 3215-3218.

Ellis, O.C. de C., Robinson, H. (1925). "A New Method of Flame Analysis." Journal of the Chemical Society, 127, 760-764.

Ellis, O.C. de C., Wheeler, R.V. (1925). "The Movement of Flame in Closed Vessels." Journal of the Chemical Society, 127, 764-767.

Ellis, O.C. de C. (1928). "Flame Movement in Gaseous Explosive Mixtures (Part 7)." Fuel; a journal of fuel science, 7, 11, 502-508.

Fristrom, R.M., Westenberg, A.A. (1965). Flame Structure. McGraw Hill, New York.

Garforth, A.M., Rallis, C.J. (1976). "Gas Movement During Flame Propagation in a Constant Volume Bomb." Acta Astronautica, 3, 879-888.

Gerstein, M., Levine, O., Wong, E.L. (1951). "Flame Propagation. II. The Determination of Fundamental Burning Velocities of Hydrocarbons by a Revised Tube Method." Journal of the American Chemical Society, 73, 418-422.

Ghoniem, A.F., Chorin, A.J., Oppenheim, A.K. (1982). "Numerical Modeling of Turbulent Flow in a Combustion Tunnel." Philosophical Transactions of the Royal Society, London, A304, 303-325.

Glassman, I. (1977). Combustion. Academic Press, New York.

Gross, R.A., Esch, R. (1954). "Low-Speed Combustion Aerodynamics." Jet Propulsion, 24, 95-101.

Guenoche, H. (1964). "Flame Propagation in Tubes and Closed Vessels." Non-Steady Flame Propagation, G.H. Markstein editor, Pergamon Press, New York, 107-176.

Guenoche, H., Jouy, M. (1953). "Changes in the Shape of Flames Propagating in Tubes." Fourth Symposium (International) on Combustion. Williams and Wilkins, Baltimore. 403-406.

Guenoche, H., Jouy, M. (1954). "L'utilisation de la methode du tube pour la mesure des vitesses de deflagration." Rev. Inst. Franc. Petrole, IX, 10, Octobre, 562-572.

Guenoche, H., Manson, N., Mannot, G. (1948). "L'influence des conditions aux limites longitudinales sur la propagation des deflagrations dans les tubes cylindriques lisses." Academie des Sciences - Comptes Rendus, 226, 163-164.

Haghgooie, M., Kent, J.C., Tabaczynski, R.J. (1984). "A Method for LDA and Seed Generator System Checkout Using Seed Particle Velocity Lag Measurements in Accelerating Flow." Ninth Symposium on Turbulence, University of Missouri-Rolla, October 1-3.

Haward, Sastry, (1917). "The Uniform Movement of Flame in Mixtures of Acetylene and Air." Journal of the Chemical Society - Transactions, 111, 841-843.

Hayes, W.D. (1957). "The Vorticity Jump Across a Gasdynamic Discontinuity." Journal of Fluid Mechanics, 2, 595-600.

Hopkinson, B. (1906). "Explosions in Coal-Gas and Air." Proceedings of the Royal Society, Series A, 77, 387-413.

Hsiao, C.-C. (1985). "Numerical Modeling of Aerodynamic Features in Premixed Turbulent Combustion." PhD Thesis, College of Engineering, University of California, Berkeley.

Jost, Croft, (1946). Explosion and Combustion Processes in Gases, McGraw Hill Co., New York.

Kirkby, W.A., Wheeler, R.V. (1928). "Explosions in Closed Cylinders. Part I. Methane-Air Explosions in a Long Cylinder. Part II. The Effect of the Length of the Cylinder." Journal of the Chemical Society, London, 1928:2, 3203-3215.

Laderman, A.J., Urtiew, P.A., Oppenheim, A.K. (1963). "On the Generation of a Shock Wave by Flame in an Explosive Gas." Ninth Symposium (International) on Combustion. Academic Press, New York, 265-274.

Landau, L.D. (1944). "On the Theory of Slow Combustion." Acta Physicochim. URSS, 19, 77-85.

Lee, J.H.S., Knystautas, R., Chan, C., Barr, P.K., Grcar, J.F., Ashurst, W.T. (1983). "Turbulent Flame Acceleration: Mechanisms and Computer Modeling." Presented at the International Meeting on Light-Water Reactor Severe Accident Evaluation, Cambridge, MA, August 28 - September 1, Paper 9.8. Also Sandia National Laboratory Report No. SAND83-8655.

Lewis, B., Von Elbe, G. (1943). "Stability and Structure of Burner Flames." Journal of Chemical Physics, 11, 75-97.

Lewis, B., Von Elbe, G. (1961). Combustion, Flames and Explosions of Gases. Second Edition, Academic Press, New York.

Leyer, J.-C., Manson, N. (1971). "Development of Vibratory Flame Propagation in Short Closed Tubes and Vessels." Thirteenth Symposium (International) on Combustion. The Combustion Institute, Pittsburgh, 551-558.

Linnet, J.W. (1953). "Methods of Measuring Burning Velocities." Fourth Symposium (International) on Combustion, Williams and Wilkins, Baltimore, 20-35.

Linnet, J.W., Hoare, M.F. (1949). "Burning Velocities in Ethylene-Air-Nitrogen Mixtures." Third Symposium on Combustion and Flame and Explosion Phenomenon. Williams and Wilkins, Baltimore, 195-204.

Liou, T.M., Santavicca, D.A. (1982). "Cycle Resolved LDV Measurements in a Motored IC Engine." Proceedings, 103rd Winter Annual Meeting of ASME, Phoenix, AZ.

Mallard, E., LeChatlier, H. (1883). "Reserches Experimentales et Theoriques sur la Combustion des Melanges Gazeux Explosifs." Annals des Mines. Memoires, 8, series 4, 274-568.

Markstein, G.H. (1951). "Experimental and Theoretical Studies of Flame Front Stability." Journal of the Aeronautical Sciences, 18, 199-209.

Markstein, G.H. (1953). "Instability Phenomenon in Combustion Waves." Fourth Symposium (International) on Combustion. Williams and Wilkins, Baltimore, 44-59.

Markstein, G.H. (1957). "A Shock Tube Study of Flame Front-Pressure Wave Interaction." Sixth Symposium (International) on Combustion. Reinhold, New York, 387-398.

Markstein, G.H. (1964). "Theory of Flame Propagation." Non-Steady Flame Propagation, G.H. Markstein editor, Pergamon Press, New York, 5-12.

Markstein, G.H. (1964). "Perturbation Analysis of Stability and Response of Plane Flame Fronts." Non-Steady Flame Propagation, G.H. Markstein editor, Pergamon Press, New York, 17-73.

Markstein, G.H. (1964). "Experimental Studies of Flame-Front Instability." Non-Steady Flame Propagation, G.H. Markstein editor, Pergamon Press, New York, 75-103.

Mason, W., Wheeler, R.V. (1919). "The Propagation of Flame in Mixtures of Acetylene and Air." Journal of the American Chemical Society, 115, 578-587.

Maxworthy, T. (1961). "Discontinuity Properties of Laminar Flames." The Physics of Fluids, 4, 5, 558-564.

Maxworthy, T. (1962). "Flame Propagation in Tubes." The Physics of Fluids, 5, 4, 407-417.

Michelson, D.M., Sivashinsky, G.I. (1977). "Nonlinear Analysis of Hydrodynamic Instability of Laminar Flames -II. Numerical Experiments." Acta Astronautica, 4, 1207-1221.

Morse, A.P., Whitelaw, J.H., Yianneskis, M. (1979). "Measurements by Laser Doppler Anemometry in Motored Piston Assemblies." Journal of Fluids Engineering, 101, 208.

Oppenheim, A.K., Laderman, A.J., Urtiew, P.A. (1962). "Onset of Retonation." Combustion and Flame, 6, 193-197.

Pelce, P., Clavin, P. (1982). "Influence of Hydrodynamics and Diffusion upon the Stability Limits of Laminar Premixed Flames." Journal of Fluid Mechanics, 124, 219.

Pitz, R.W. (1981). "An Experimental Study of Combustion: The Turbulent Stucture of a Reacting Shear Layer Formed at a Rearward Facing Step." PhD Thesis, College of Engineering, University of California, Berkeley.

Popov, V.A. (1959). "On the Pre-Detonation Period of Flame Propagation." Seventh Symposium (International) on Combustion. Butterworths Scientific Publications, London, 799-806.

Predvoditelev, A.S. (1952). "Theoretical Examination of Vibratory Movement of the Flame Front in Closed Vessels." Fourth Symposium (International) on Combustion. Baltimore, 779-782.

Rallis, C.J., Garforth, A.M. (1980). "The Determination of Laminar Burning Velocity." Progress in Energy and Combustion Science, 6, 303-329.

Salamandra, G.D., Bazhenova, T.V., Naboko, I.M. (1959). "Formation of Detonation Wave during Combustion of Gas in Combustion Tube." Seventh Symposium (International) on Combustion. Butterworths Scientific Publications, London, 851-855

Schmidt, E.H.W., Steinicke, H., Neubert, U. (1952). "Flame and Schlieren Photographs of Combustion Waves in Tubes." Fourth Symposium (International) on Combustion. Williams and Wilkins, Baltimore, 658-666.

Searby, G., Sabathier, F., Clavin, P., Boyer, L. (1983). "Hydrodynamical Coupling Between the Motionof a Flame Front and the Upstream Gas Flow." Physical Review Letters, 51, 16, 1450-1453.

Shimizu, S., Sakai, S. (1982). "Temperature Distributions and their Histories of Burnt Gas in a Closed Combustion Chamber." Japan Society of Automotive Engineers Review, March, 21-29.

Shimizu, S., Wakai, K., Shinji, S. (1983). "Combustion Processes and the State of Gases in a Divided Chamber." Proceedings of the 2nd International Pacific Conference on Automotive Engineering, Paper No. 830865, Tokyo, 57-67.

Simon, D.M. (1951). "Flame Propagation. III. Theoretical Consideration of the Burning Velocities of Hydrocarbons." Journal of the American Chemical Society, 73, 422-425.

Sivashinsky, G.I. (1976). "On a Distorted Flame Front as a Hydrodynamic Discontinuity." Acta Astronautica, 3, 889-918.

Sivashinsky, G.I. (1977). "Hydrodynamic Theory of Flame Propagation in an Enclosed Volume." Acta Astronautica, 6, 631-645.

Sivashinsky, G.I. (1977). "Nonlinear Analysis of Hydrodynamic Instability of Laminar Flames -I. Derivation of Basic Equations." Acta Astronautica, 4, 1177-1206.

Sivashinsky, G.I. (1983). "Instabilities, Pattern Formation and Turbulence in Flames." Annual Review of Fluid Mechanics, 15, 179-199.

Smith, O.I. (1977). "Lean Limit Combustion in an Expanding Chamber." Lawrence Berkeley Laboratory Report No. LBL-6851, PhD Thesis, College of Engineering, University of California, Berkeley.

Starke, R., Roth, P. (1984). "LDA - Measurements in Cylindrical Vessel Explosions." Second International Symposium on Applications of Laser Doppler Anemometry to Fluid Mechanics. July 2-4, Lisbon, Portugal.

Steinert, W.J., Dunn-Rankin, D., Sawyer, R.F. (1982). "Influence of Chamber Length and Equivalence Ratio on Flame Propagation in a Constant Volume Duct." Western States Section/The Combustion Institute Paper No. 82-52 and Lawrence Berkeley Laboratory Report No. LBL-14965.

Strehlow, R.A. (1984). Combustion Fundamentals. McGraw Hill, New York.

Taylor, G.I. (1950). "The Instability of Liquid Surfaces when Accelerated in a Direction Perpendicular to their Planes. I." Proceedings of the Royal Society of London, series A, 201, 192-196.

Tsien, H.S. (1951). "Influence of Flame Front on the Flow Field." Journal of Applied Mechanics, 18, 188-194.

Uberoi, M.S. (1959). "Flow Field of a Flame in a Channel." The Physics of Fluids, 2, 1, 72-78.

Urtiew, P.A., Oppenheim, A.K. (1966). "Experimental Observations of the Transition to Detonation in an Explosive Gas." Proceedings of the Royal Society, series A, 295, 13-28.

Urtiew, P.A., Oppenheim, A.K. (1968). "Transverse Flame-Shock Interactions in an Explosive Gas." Proceedings of the Royal Society, series A, 304, 379-385.

Wakai, K., Shimizu, S. (1984). "Behavior of the Flame in a Closed Chamber." Proceedings of the Japanese Society of Mechanical Engineers. Paper No. 840-14 (October), 87-89.

Wakai, K., Shimizu, S., Hibino, Y. (1984). "Concave Flame Front in a Constant Volume Chamber." Proceedings of the 22nd Japanese Symposium on Combustion. November, 148-150. In Japanese

Weinberg, F.J. (1963). Optics of Flames. Butterworths, London.

Wheatley, P.J. (1950). "The Propagation of Flames in Tubes." Fuel, 29; 80-83.

Williams, F.A. (1965). Combustion Theory. Addison-Wesley, Reading, MA.

Witze, P.O. (1984). Personal communication. Sandia National Laboratory, Livermore, CA.

Witze, P.O., Martin, J.K., Borgnakke, C. (1983). "Conditionally-Sampled Velocity and Turbulence Measurements in a Spark Ignition Engine." Combustion Science and Technology, 36, 301-317. Also Sandia National Laboratory Report SAND83-8794.

Witze, P.O., Vilchis, F.R. (1981). "Stroboscopic Laser Shadowgraph Study of the Effect of Swirl on Homogeneous Combustion in a Spark Ignition Engine." SAE Transactions. Paper No. 810226, 90, 979.

Woodard, J.B., Hirvo, D.H., Greif, R., Sawyer, R.F. (1981). "Wall Heat Transfer and Flame Propagation in a Constant Volume Duct." Western States Section/The Combustion Institute Paper No. 81-51 and Lawrence Berkeley Laboratory Report No. LBL-13021.

Yip, T.W.G., Strehlow, R.A., Ormsbee, A.I. (1984). "An Experimental Investigation of Two Dimensional Flame-Vortex Interactions." Twentieth Symposium (International) on Combustion, The Combustion Institute, Pittsburgh.

Yuan, S.-L., (1985). Personal communication. Department of Mechanical Engineering, University of California, Berkeley.

Zeldovich, Ya.B. (1981). "Structure and Stability of Steady Laminar Flame at Moderately Large Reynolds Numbers." Combustion and Flame, 40, 225-234.

Zeldovich, Ya.B., Istratov, A.G., Kidin, N.I., Librovich, V.B. (1980). "Flame Propagation in Tubes: Hydrodynamics and Stability." Combustion Science and Technology, 24, 1-13.

APPENDIX I

Data Acquisition Software

The following program is written in Pascal and compiled using Borland International's TurboPascal compiler. The program runs on a Compupro S-100 buss computer with 64K of memory. The computer uses a Z-80 microprocessor running at 6 MHz. The timer circuit is located on a System Support I card. Parallel I/O is handled by an Interfacer II board. The parallel I/O board is interfaced to the TSI 1980A counter of the LDA system. The program is separated into five subsections:

Stdio.p - standard definitions

Stdio.pas - standard input/output routines

Getdat.p - definitions not contained in stdio.p

Getdat.inc - library routines for the data acquisition

Getdat.pas - the main program

The subsections are all included at compile time.

STDIO.P

This file contains definitions and type assignments used throughout the main body of the program.

```
const
     DEFSYM = '@';          { symbol representing default value }
     MAXCMD = 70;           { maximum command line length }
     MAXLEN = 255;
     MAXNAME = 15;          { maximum length of file name }
     NULL = 0;
     EPS = 1.0E-10;
     NEWLINE = 10;          { ASCII value }
type
     name = string[MAXNAME];
```

```
     index = integer;
     sentence = string[MAXLEN];
     filvar = text;
     str80 = string[80];
     str65 = string[65];
     str15 = string[15];
     str14 = string[14];
     str8 = string[8];
     str5 = string[5];
     str3 = string[3];
     character = -1..127;              { ASCII, plus ENDFILE }
     UPASCII = set of 'A'..'Z';
var
     Cmdline :string[MAXCMD] absolute $81;
     in1,out1,in2,out2,infile,outfile :name;
     stdin,stdout,F1,F2,Fin,Fout :filvar;
```

STDIO.PAS

This file contains standard input/output and general purpose functions and procedures used throughout the main program. These routines are not specific to this main program and are useful in other software as well.

```
{ Aye -- see if user answered yes }
function Aye: boolean;
var
   c :char;
begin
   write(' Answer: ');
   readln(c);
   Aye := (c in ['y', 'Y'])
end;                                 { end of Aye function }


{ Exist- checks if a file is on disk }
function Exist(file1 :name) :boolean;
var
     F :filvar;
begin
     if (file1 <> 'CON:') then begin
        Assign(F,file1);
        {$I-}
        Reset(F);
        {$I+}
```

```
        if IOresult <> 0 then
             Exist := false
        else
             Exist := true;
     end
     else Exist := true;
end;


{ Fclose -- close a file forcing a ^Z to end file }
procedure Fclose(var filnum :filvar; filname :name);
begin
     if (filname <> 'CON:') then begin;
         write(filnum,^Z);
         Close(filnum);
     end;
end;


{ Fopen -- open a file for either read or write I/O }
procedure Fopen( var F :filvar; filename :name; itype :char);
begin
     Assign(F,filename);
     if (itype in ['r','R']) then
         Reset(F)
     else if (itype in ['w','W']) then
         Rewrite(F);
end;


{ Nay -- see if user answered no }
function Nay: boolean;
var
    c :char;
begin
   write(' Answer: ');
   readln(c);
   Nay := c in ['n', 'N']
end;


{ readint - prompts for integer input.  The present value of the
            variable replaces DEFSYM in the prompt string }
procedure readint(var x :integer; msg :str80);
var
    i :integer;

begin
    for i := 1 to Length(msg) do
        if (msg[i] <> DEFSYM) then
            write(msg[i])
        else
```

```
            write(x);
    readln(x);
end;


{ readreal - prompts for real input.  The present value of the
             variable replaces DEFSYM in the prompt string }
procedure readreal(var x :real; msg :str80);
var
    i :integer;

begin
    for i := 1 to Length(msg) do
        if (msg[i] <> DEFSYM) then
            write(msg[i])
        else
            write(x:4:4);
    readln(x);
end;


{ readstr - prompts for string input.  The present value of the
            variable replaces DEFSYM in the prompt string }
procedure readstr(var strvar :str15; msg :str65);
var
    i :integer;
    oldstr :str15;

begin
    oldstr := strvar;
    for i := 1 to Length(msg) do
        if (msg[i] <> DEFSYM) then
            write(msg[i])
        else
            write(strvar);
    readln(strvar);
    if(strvar = '') then strvar := oldstr;
end;


{ stdopen - opens an input and output file pair }
procedure stdopen(var filin,filout :filvar;
                  var namein,nameout :name);
begin
     readstr(namein,'Input filename (@): ');
     readstr(nameout,'Output filename (@): ');
     Fopen(filin,namein,'r');
     Fopen(filout,nameout,'w');
end;
```

GETDAT.P

This routine gives mnemonic names to various hardware addresses and limiting values. The global variables, known throughout the remainder of the program are also defined here. These definitions are specific to the hardware (Interfacer II parallel I/O board and System Support board) and to the hardware configuration (the base address of the S-100 boards).

```
{ Name constants for convenience }

const

    CK0MD3 = $36;           { Set clock zero to mode 3 }
    CK1MD4 = $78;           { Set clock 1 to mode 4 }
    CK1HI = $7F;            { Set clock 1 initial high byte }
    CK1LO = $FF;            { Set clock 1 initial low byte }
    CK1RD = $40;            { Buffered read of clock 1 }
    CLK0 = $54;             { Port address for clock 0 of 8253 }
    CLK1 = $55;             { Port address for clock 1 of 8253 }
    CLKFREQ = 2;            { Base 8253 clock frequency in MHz }
    CLKSTAT = $57;          { Mode port address for 8253 }
    CPUCLK = 6;             { Cpu clock rate in MHz }
    CYCLETIME = 0.060;      { Time for one data grab cycle (ms) }
    DELCYCLES = 15;         { Tcycles for stabilizing delay loop }
    DROMSK = $1;            { Data ready port zero mask }
    FACTOR = 10;            { Factor for time output (1000 = ms) }
    FFACT = 1000;           { Controls freq output (1E6 = khz) }
    FREQVEL = 2.89;         { Converts freq to vel in mm/s }
    HOLD = $40;             { Hold real time clock for read }
    HRS1 = $04;             { Address of hours ones digit }
    HRS10 = $05;            { Address of hours tens digit }
    INHIBIT = $00;          { Inhibit on,  00000000 }
    LOFOUR = $0F;           { Lower 4 bit mask }
    MAXCOUNT = 32767;       { Maximum value of clocks }
    MAXDAT = 2000;          { Maximum number of data points }
    MAXROW = 20;            { Maximum number of plot rows }
    MILLI = 1000;           { Conversion of micro to milli }
    MINDAT = 10;            { Minimum number of data points }
    MIN1 = $02;             { Address of minutes ones digit }
    MIN10 = $03;            { Address of minutes tens digit }
    NUMCOL = 70;            { Number of columns on screen plot }
    NOINHIBIT = $FF;        { Inhibit off, 11111111 }
    NUMROW = 19;            { Number of rows on screen plot }
    PLTCHR = '*';           { Plot character for screen plot }
```

```
    PP0 = $04;              { Port address for parallel port 0 }
    PP1 = $05;              { Port address for parallel port 1 }
    PP2 = $06;              { Port address for parallel port 2 }
    PPSTAT = $07;           { Status port address of para ports }
    RDHOLD = $50;           { Read with hold }
    REALCLK = $5A;          { Port address of real time clock }
    SEC1 = $00;             { Address of seconds ones digit }
    SEC10 = $01;            { Address of seconds tens digit }
    SHIFT = 2000;           { Shift frequency }
    UPFOUR = $F0;           { Upper 4 bit mask }

{ Variable type definitions that are not in STDIO.P }

type
    alldat = record time :integer; lodat,hidat :byte end;
    datarray = array[1..MAXDAT] of alldat;


{ global variables known to entire program }

var
    timres :integer;              { time resolution of data run }
    ttime :real;                  { total time of experiment    }
    cycles :integer;              { # cycles/burst from TSI box }
    date :string[8];              { date of experiment          }
    watch :string[8];             { time of experiment          }
    name1 :string[10];            { primary name of data file   }
    dataout :str14;               { output filename             }
    axial,radial : integer;       { measurement location (mm)   }
    phi :real;                    { equivalence ratio           }
    fuel :string[15];             { fuel being used             }
    loopnum :integer;             { # runs in present set       }
    once :boolean;                { for default time setting    }
```

GETDAT.INC

This section of the program contains general service routines used by the main program. These routines include the set-up and help functions, as well as the post processing routines which plot the data on the screen for a quick preview or store the data for later manipulation.

```
{ twopow - calculates a power of two }
function twopow(value :integer) :real;
```

```
var
    final :real;
    flip :boolean;
    i :index;

begin
     final := 1;
     if (value < 0) then flip := true else flip := false;
     if (value = 0) then
         twopow := 1
     else
         for i := 1 to Abs(value) do
             final := final * 2;
     if(flip) then final := 1/final;
     twopow := final;
end;



{ clkget - reads the clock to assure the proper time is set }
procedure clkget(var digit: byte; address :byte);
begin
     Port[REALCLK] := address + RDHOLD;
     digit := Port[REALCLK + 1];
end;


{ realtime - reads the real time clock }
function realtime :str8;
var
     time :string[8];
     hh1,hh10,mm1,mm10,ss1,ss10 :byte;

begin

     time := '';
     clkget(hh10,HRS10);
     clkget(hh1,HRS1);
     clkget(mm10,MIN10);
     clkget(mm1,MIN1);
     clkget(ss10,SEC10);
     clkget(ss1,SEC1);
     Port[REALCLK] := NULL;

     time := time + Chr(hh10 - $08 + $30) + Chr(hh1 + $30)
              + ':' + Chr(mm10 + $30) + Chr(mm1 + $30)
              + ':' + Chr(ss10 + $30) + Chr(ss1 + $30);

     realtime := time;
end;
```

```
{ name2 - returns the character representation
          of the data file extension }
function name2(loopnum :integer) :str3;
var
    temp :string[3];
    hunds,tens,ones :byte;
begin
     temp := '';
     hunds := loopnum div 100 + $30;
     tens := (loopnum - ((hunds - $30) * 100)) div 10 + $30;
     ones := loopnum mod 10 + $30;
     temp := temp + Chr(hunds) + Chr(tens) + Chr(ones);
     name2 := temp;
end;



{ convert - converts the LDA counter output to real values }
procedure convert(intime,counts,lobyte,hibyte :integer;
                  var rtime,vel,intfreq :integer);
var
    expon,mant :integer;
    hitemp,lotemp :byte;
    freq :real;

begin                { strip out exponent and mantissa }

    hitemp := 256 - hibyte - 1;          { invert hibyte bits }
    lotemp := 256 - lobyte -1;           { invert lobyte bits }

    expon := hitemp div 16;
    mant := ((hitemp mod 16) shl 8) + lotemp;

                     { convert to real values }

    rtime :=Round(intime - counts);
    freq := ((FFACT/twopow(expon-2)/mant) * cycles * 1000);
    vel := Round(FREQVEL * (freq - SHIFT));
    intfreq := Round(freq);

end;



{ plot - plots the data for low resolution perusal }
procedure plot(intime,numdat :integer; var x :datarray;
               var maxvel,minvel :integer);
var
     ch :char;
     ob,rtime,vel,intfreq,i,j,row,col :integer;
```

```
begin
  repeat
    write(' maximum velocity (',maxvel,'): ');readln(maxvel);
    write(' minimum velocity (',minvel,'); ');readln(minvel);
              { draw box around data }
    ob := 0;

    Clrscr;

    for i := 2 to (NUMROW - 1) do begin
         GotoXY(1,i); write('|');
         GotoXY(NUMCOL,i); write('|');
    end;
    for i := 2 to (NUMCOL - 1) do begin
         GotoXY(i,1); write('-');
         GotoXY(i,NUMROW); write('-');
    end;
    GotoXY(1,1); write('+');
    GotoXY(NUMCOL,1); write('+');
    GotoXY(1,NUMROW); write('+');
    GotoXY(NUMCOL,NUMROW); write('+');

              { plot the data }

    for i := 1 to numdat do begin
         convert(intime,x[i].time,x[i].lodat,
                        x[i].hidat,rtime,vel,intfreq);
         row := NUMROW - Round(((NUMROW-1)/(maxvel - minvel))*
                                        (vel-minvel));
         col := Round((NUMCOL/intime)*rtime) + 1;
         if ((row <= NUMROW) and (row > 0) and
                              (col <= NUMCOL) and (col > 0))
         then begin
              GotoXY(col,row); write(PLTCHR);
              end
         else ob := ob + 1;
    end;

    GoToXY(1,(NUMROW + 2));
    writeln('velocity full scale is ',minvel:6,' to ',maxvel:6);
    writeln('time full scale is 0 to ',ttime:6:0,' ms');
    writeln('data points out of bounds: ',ob);

    writeln; write('Rescale velocity ? ');readln(ch);
  until(not(ch in ['y','Y']));
end;


{ help - print help list of commands }
procedure help;
begin
  writeln;
```

```
  writeln('Legal commands:');
  writeln;
  writeln('c - change the header values and cycles per burst');
  writeln('f - change the filename and extension number');
  writeln('h - print the help list');
  writeln('l - list the data on the screen');
  writeln('p - plot the data on the screen');
  writeln('q - quit');
  writeln('r - change the run duration of experiment');
  writeln('s - take a data sample');
  writeln('w - write the data to the disk');
  writeln;
end;


{ getfile - changes the primary output name }
procedure getfile;
begin
     write('primary output name (',name1,'): ');
     readln(dataout);
     if(dataout <> '') then  name1 := dataout;
     write('initial file extension number (',loopnum,'): ');
     readln(loopnum);
     dataout := name1 + '.' + name2(loopnum);
end;



{ store - stores the data on disk or lists it on the screen }
procedure store(var Fvar :filvar; numdat,intime :integer;
                        var x :datarray);
var
     intfreq,rtime,vel,i :integer;

begin
     watch := realtime;
     Fopen(Fvar,dataout,'w');
     writeln(Fvar,'# date = ',date,'  time = ',watch);
     writeln(Fvar,'# filename = ',dataout);
     writeln(Fvar,'# fuel = ',fuel,
                  '  equivalence ratio = ',phi:4:1);
     writeln(Fvar,'# time resolution (micro) = ',timres);
     writeln(Fvar,'# total time (ms) = ',ttime:8:3);
     writeln(Fvar,'# number of data points = ',numdat);
     writeln(Fvar,'# axial = ',axial:5,'  radial = ',radial:5);
     writeln(Fvar,'#');
     writeln(Fvar,'#',
    ' time (timres units)   frequency (kHz)   velocity (mm/s)')
     writeln(Fvar,'#');

               { data portion of output file }
```

```
      if (numdat > 0) then
         for i := 1 to numdat do begin
             convert(intime,x[i].time,x[i].lodat,x[i].hidat,
                           rtime,vel,intfreq);
             writeln(Fvar,rtime:13,intfreq:20,vel:20);
             end;
      Close(Fvar);
      if(dataout <> 'CON:') then begin
           writeln('Output filename: ',dataout);
           writeln;
           loopnum := loopnum + 1;
      end;
end;


{ change - changes the data file header information }
procedure change;
begin
    readint(cycles,'number of cycles/burst (@): ');
    writeln;
    readint(axial,'axial position (@): ');
    readint(radial,'radial position (@): ');
    readstr(fuel,'fuel (@): ');
    readreal(phi,'equivalence ratio (@): ');
    writeln;
end;
```

GETDAT.PAS

This file contains the procedures which are used in the actual run sequence of the main program. The four routines listed at the top of the program contain all of the ancillary definitions and routines.

```
{$I stdio.p}                { standard header definitions }
{$I stdio.pas}              { standard I/O routines }
{$I getdat.p}               { constant definitions etc. }
{$I getdat.inc}             { common routines }


      { ********** MAIN PROGRAM PROCEDURES *********** }
```

```
{ init - initializes the necessary varibles and ports }
procedure init(var intime,waitlength :integer);
var
    clktime :integer;
    maxres :integer;

begin


              { clock initialization section }

  if (once) then begin                              { for default }
    writeln;
    readreal(ttime,'total time of event in milliseconds (@): ');
  end;

            { calculate minimum clock resolution possible }

    timres := Trunc(ttime * (MILLI/MAXCOUNT) + 0.9999);

            { check if resolution larger than allowed }

    maxres := Trunc(((CYCLETIME * (MAXDAT/MINDAT)) * MILLI) +
                                                        0.9999);
    if (timres > maxres) then begin
        ttime := (maxres/MILLI) * MAXCOUNT;
        writeln('*** total time too large--set to maximum = ',
                                                    ttime:3:3);
        timres := maxres;
    end;
    writeln('*** time resolution = ',timres,' microseconds');
    writeln;

            { determine number of main clock counts required }

    intime := Round((ttime/timres) * MILLI);

      { convert resolution in time to resolution
                                  in counts for driving clock }

    clktime := Round(timres*CLKFREQ);    { timres in counts }
    Port[CLKSTAT] := CK0MD3;             { clock0 to square wave }
    Port[CLK0] := clktime mod 256;       { wave period of clock0 }
    Port[CLK0] := clktime div 256;       { load high byte }
    Port[PP0] := NOINHIBIT;              { counter inhibit off }

   { compute the stabilizing delay required for clock to settle }

    waitlength := Round(timres * CPUCLK/DELCYCLES) - 1;

end; { init }
```

```
{ default- sets the default values of the globals }
procedure default(var intime,waitlength,numdat :integer);
begin
     numdat := 0;                    { number of data points taken }
     ttime := 150;                   { total time of run in msec }

     writeln('time of event = ',ttime:0:0,' milliseconds');

     once := false;
     init(intime,waitlength);        { initialize clocks and ports }
     once := true;

                          { header information }

     cycles := 8;                { number of cycles on TSI counter }
     fuel := 'CH4';              { fuel type }
     phi := 1.0;                 { equivalence ratio }
     axial := 0;                 { position coordinate }
     radial := 0;                { position coordinate }
     name1 := 'data';            { base name of data files }
     loopnum := 1;               { starting number of data files }

           { form data file name from base and extension }

     dataout := name1 + '.' + name2(loopnum);

end;



{ ready - does dummy reads to clear the data ready
                                        and informs user of start }
procedure ready;
var
    test :byte;

begin
    test := Port[PP0];
    test := Port[PP1];
    test := Port[PP2];

    writeln;
    writeln('**** WAITING FOR START PULSE ****');
    writeln;

end; { ready }



{grab- assembly loop to take the data quickly }
```

```
procedure grab(var x :datarray; intime,waitlength :integer);
begin
     inline(              { wait for start pulse          }

     $DB/$07/             {START:   IN      PPSTAT        }
     $E6/$10/             {         ANI     STARTBIT      }
     $CA/*-5/             {         JZ      START         }

                          { clear old data                }

     $DB/$04/             {          IN     PP0           }
     $DB/$05/             {          IN     PP1           }
     $DB/$06/             {          IN     PP2           }

                          { initialize clock to total time }

     $3E/$78/             {         MVI     A,CK1MD4      }
     $D3/$57/             {         OUT     CLKSTAT       }
     $2A/intime/          {         LHLD    INTIME        }
     $7D/                 {         MOV     A,L ;least sig }
     $D3/$55/             {         OUT     CLK1          }
     $7C/                 {         MOV     A,H ;most sig  }
     $D3/$55/             {         OUT     CLK1          }

                          { let clock stabilize           }

     $2A/waitlength/      {         LHLD    WAITLENGTH    }
     $2B/                 {DELAY:   DCX     H             }
     $7C/                 {         MOV     A,H           }
     $B5/                 {         ORA     L             }
     $C2/*-4/             {         JNZ     DELAY         }

                          { load address of main array    }

     $2A/x/               {         LHLD    X             }
     $01/MAXDAT/          {         LXI     B,MAXDAT      }

                          { read the clock                }

     $3E/$40/             {WAIT:    MVI     A,CK1RD       }
     $D3/$57/             {         OUT     CLKSTAT       }
     $DB/$55/             {         IN      CLK1          }
     $5F/                 {         MOV     E,A ;least sig }
     $DB/$55/             {         IN      CLK1          }
     $57/                 {         MOV     D,A ;most sig  }

                          { check for timeout             }

     $B7/                 {         ORA     A             }
     $FA/*+38/            {         JM      TIMEOUT       }

                          { check for data ready          }
```

```
        $DB/$07/            {          IN      PPSTAT          }
        $E6/$01/            {          ANI     DROMSK          }
        $CA/*-19/           {          JZ      WAIT            }

                            { subscript out of bounds check    }

        $0B/                {          DCX     B               }
        $78/                {          MOV     A,B             }
        $B1/                {          ORA     C               }
        $CA/*+25/           {          JZ      TIMEOUT         }

                            { store the time and lda data      }

        $3E/$00/            {          MVI     A,INHIBIT       }
        $D3/$04/            {          OUT     PP0             }

        $73/                {          MOV     M,E ;least sig  }
        $23/                {          INX     H               }
        $72/                {          MOV     M,D ;most sig   }
        $23/                {          INX     H               }

        $DB/$04/            {          IN      PP0             }
        $77/                {          MOV     M,A             }
        $23/                {          INX     H               }
        $DB/$05/            {          IN      PP1             }
        $77/                {          MOV     M,A             }
        $23/                {          INX     H               }

        $3E/$FF/            {          MVI     A,NOINHIBIT     }
        $D3/$04/            {          OUT     PP0             }

        $C3/*-48/           {          JMP     WAIT            }

                            { end the file with all zeros      }

        $36/$00/            {TIMEOUT:  MVI     M,NULL          }
        $23/                {          INX     H               }
        $36/$00/            {          MVI     M,NULL          }
        $23/                {          INX     H               }
        $36/$00/            {          MVI     M,NULL          }
        $23/                {          INX     H               }
        $36/$00/            {          MVI     M,NULL          }
        $23);               {          INX     H               }

end;


{ stats - computes the end of run statistics }
procedure stats(var numdat :integer;
```

```
                    intime :integer; var x :datarray);
var
     oldtime,delt :integer;
     meandelt,maxdelt,lastime,stall :real;

begin
     numdat := 1;
     oldtime := intime;
     maxdelt := 0;                    { defaults }
     meandelt := 0;
     delt := 0; stall := 0; lastime := 0;

     while(x[numdat].time <> 0) do begin
        delt := oldtime - x[numdat].time;
        if(delt > maxdelt) then maxdelt := delt;
        meandelt := meandelt + delt;
        oldtime := x[numdat].time;
        numdat := numdat + 1;
     end;
     numdat := numdat - 1;

               { convert to real time }

     maxdelt := maxdelt * timres;
     if(numdat > 1) then begin
          meandelt := (meandelt/numdat) * timres;
          stall := intime;
          stall := (stall - x[1].time) * timres;
          lastime := (intime - x[numdat].time) * (timres/MILLI);
     end;

               { output the end of run statistics }

     writeln; writeln(' *** end of run statistics *** ');
     writeln;
     writeln('*** number of data points accepted          ',
                                                  numdat:6);
     writeln('*** average time between points in microsec ',
                                                  meandelt:6:0);
     writeln('*** maximum time between points in microsec ',
                                                  maxdelt:6:0);
     writeln('*** time of last valid datum (ms)           ',
                                                  lastime:3:3);
     writeln('*** time of first valid datum (mics)        ',
                                                  stall:6:0);
     writeln;

end;


                    {*** Main Program ***}
```

```
var
    ch :char;
    waitlength : integer;       { clock stabilizing delay }
    maxvel,minvel :integer;     { velocity scale for plot }
    i :integer;
    intime: integer;            { number of counts on slow clock }
    numdat :integer;            { number of data points }
    x :datarray;                { primary data array }
    Fvar :filvar;

begin
    maxvel := 10000; minvel := -10000;          { default }
    ClrScr;
    writeln;writeln;writeln;writeln;
    writeln('*** DATA ACQUISITION PROGRAM FOR LDA SYSTEM ***');
    writeln;
    write('Todays date (mm/dd/yy): ');readln(date);
    if(date = '') then date := '00/00/00';
    writeln;writeln;
    default(intime,waitlength,numdat);
    repeat
        write('? ');readln(ch);
        if (ch in ['c','C']) then
           change;
        if (ch in ['w','W']) then begin
           dataout := name1 + '.' + name2(loopnum);
           store(Fvar,numdat,intime,x);
           end;
        if (ch in ['f','F']) then
           getfile;
        if (ch in ['h','H']) then
           help;
        if (ch in ['l','L']) then begin
           dataout := 'CON:';
           store(Fvar,numdat,intime,x);
           end;
        if ((ch in ['p','P']) and (numdat > 0)) then
           plot(intime,numdat,x,maxvel,minvel);
        if (ch in ['r','R']) then
           init(intime,waitlength);
        if (ch in ['s','S']) then begin
           ready;
           grab(x,intime,waitlength);
           stats(numdat,intime,x);
           end;
    until(ch in ['q','Q']);
end.
```

LAWRENCE BERKELEY LABORATORY
TECHNICAL INFORMATION DEPARTMENT
UNIVERSITY OF CALIFORNIA
BERKELEY, CALIFORNIA 94720